ParisTech
INSTITUT DES SCIENCES ET TECHNOLOGIES
PARIS INSTITUTE OF TECHNOLOGY

TELECOM ParisTech

Doctorat ParisTech

T H È S E

pour obtenir le grade de docteur délivré par

TELECOM ParisTech

Spécialité « Communication et Electronique »

présentée et soutenue publiquement par

Sebastian WAGNER

le 13 Octobre 2011

Techniques de Transmission et de Réception MU-MIMO pour la Génération Suivante de Standards de Télécommunications Cellulaires

Directeur de thèse : **Dirk T. M. SLOCK**
Co-encadrement de la thèse : **Stefania SESIA**

Jury

M. Philippe LOUBATON, Professeur, LIGM, Université Paris-Est	Rapporteur
M. Giuseppe CAIRE, Professeur, Department of Electrical Engineering, USC Viterbi	Rapporteur
M. David GESBERT, Professeur, Mobile Communications, Eurecom	Examinateur
M. Mérouane DEBBAH, Professeur, Alcatel Lucent Chair on Flexible Radio, Supélec	Examinateur
M. Xavier MESTRE, Docteur, Radio communications, CTTC	Examinateur
M. Fabrizio TOMATIS, M.Sc., Leader Algorithm Team, ST-Ericsson	Invité

TELECOM ParisTech
école de l'Institut Télécom - membre de ParisTech

THÈSE

ParisTech
INSTITUT DES SCIENCES ET TECHNOLOGIES
PARIS INSTITUTE OF TECHNOLOGY

TELECOM ParisTech

Dissertation ParisTech

T H E S I S

In partial fulfillment of the requirements for the degree of doctor of philosophy from

TELECOM ParisTech

Specialization: Communication and Electronics

presented and publicly defended by

Sebastian WAGNER

the 13th of October 2011

MU-MIMO Transmission and Reception Techniques for the Next Generation of Cellular Wireless Standards (LTE-A)

Thesis Supervisor: **Dirk T. M. SLOCK**
Thesis Co-advisor: **Stefania SESIA**

THÈSE

Committee

Mr. Philippe LOUBATON, Professor, LIGM, Université Paris-Est	Reviewer
Mr. Giuseppe CAIRE, Professor, Department of Electrical Engineering, USC Viterbi	Reviewer
Mr. David GESBERT, Professor, Mobile Communications, Eurecom	Examiner
Mr. Mérouane DEBBAH, Professor, Alcatel Lucent Chair on Flexible Radio, Supélec	Examiner
Mr. Xavier MESTRE, Ph.D., Radio communications, CTTC	Examiner
Mr. Fabrizio TOMATIS, M.S., Leader Algorithm Team, ST-Ericsson	Invitee

TELECOM ParisTech
école de l'Institut Télécom - membre de ParisTech

Résumé

Pour satisfaire la demande en constante augmentation de haut débit, les techniques de transmission multi antennes (MIMO) ont été largement adoptées dans les normes de communications mobiles les plus récentes, puisqu'elles promettent une augmentation linéaire de capacité en fonction du nombre d'antennes. Cependant, pour tirer profit de ce gain potentiel de capacité, le canal de propagation doit être bien conditionné et les interférences doivent être efficacement atténuées. Il est bien connu que les transmissions simultanées sur plusieurs récepteurs spatialement dispersés créent un canal avec une capacité plus élevée que la transmission à un seul récepteur, ceci étant dû à l'augmentation de la diversité spatiale. Le second schéma de transmission est appelé MIMO mono-utilisateur, tandis que le premier est généralement appelé MIMO multi-utilisateurs (MU) et est le sujet de cette thèse. En MU-MIMO, les signaux sont précodés de façon à minimiser l'interférence au niveau des récepteurs. Les techniques efficaces de précodage exigent la connaissance de l'état du canal descendant qui est habituellement disponible uniquement au niveau des récepteurs. Par conséquent, l'état du canal descendant doit être mis à la disposition de l'émetteur grâce aux informations en retour des récepteurs sur un canal de débit limité, résultant en des informations plus ou moins précises sur l'état de canal à l'émetteur (CSIT).

Dans cette thèse, nous étudions les systèmes MU, où chaque récepteur dispose d'une unique antenne appelés MU-MISO. Nous nous concentrons sur les techniques de précodage linéaire, car elles offrent un bon compromis entre performance et complexité. Plus précisément, nous considérons un précodage linéaire optimal (la maximisation de la somme pondérée des débits), précodage par filtre adapté, précodage de forçage à zéro (ZF), un précodage ZF régularisé et un modèle pratique appelé CUBF, où la matrice de précodage est unitaire avec des entrées de module constant. A cause du canal de propagation aléatoire, il est difficile d'avoir un aperçu du comportement du système, qui est nécessaire pour résoudre des problèmes importants tels que la quantité optimale des informations de *feedback*. Typiquement, le rapport signal sur interférence plus bruit (SINR) aléatoire peut être borné par une quantité déterministe considérant le comportement du système en moyenne et un schéma de précodage spécifique. Cependant, une autre façon de rendre le SINR indépendant des réalisations de canal est de supposer que le nombre d'antennes d'émission M et de récepteurs K est grand alors que leur rapport reste borné. Cette hypothèse est motivée par la norme LTE-A actuelle qui suppose déjà jusqu'à huit antennes d'émission. Dans cette thèse, nous développons un cadre général et consistent pour l'étude des techniques de précodage linéaire dans les grands systèmes MU-MISO dans une large gamme d'environnements de canal de propagation et de connaissance imparfaite du canal à l'émetteur. Nous fournissons les outils nécessaires à partir de la théorie des matrices aléatoires de grandes dimensions pour obtenir des *équivalents déterministes* du SINR aléatoire, c'est à dire, des approximations du SINR indépendantes des réalisations de canal qui sont presque surement exactes lorsque $M, K \to \infty$. Ces approximations du SINR peuvent être appliquées pour résoudre une variété de problèmes pratiques d'optimisation dont plusieurs sont

présentés dans ce travail. Les résultats des simulations montrent que ce sont des solutions proches de l'optimal même pour les systèmes de petite dimension. Notre cadre constitue la base pour l'étude des systèmes plus complexes tels que MU-MIMO et multi-cellules MU-MIMO et pour explorer de nouvelles voies pour l'analyse des systèmes avec *feedback* limité.

Abstract

To satisfy the ever increasing demand for high data rates, multiple antenna transmission techniques have been widely adopted in recent mobile communication standards since they promise a linear capacity increase in the number of antennas. However, to leverage this potential capacity gains, the propagation channel has to be well-conditioned and the interference has to be efficiently mitigated. It is well-known that simultaneous transmissions to multiple spatially scattered receivers create a channel with higher capacity than transmission to a single receiver due to the increased spatial diversity. The latter transmission scheme is called single-user MIMO, while the former scheme is usually referred to as multi-user MIMO and is the topic of this dissertation. In MU-MIMO, the signals are precoded such that the interference at the receivers is minimized. Efficient precoding techniques require knowledge of the downlink channel state which is typically only available at the receivers. Therefore, the downlink channel state has to be made available to the transmitter through feedback from the receivers over a limited rate channel resulting in more or less accurate channel state information at the transmitter (CSIT).

In this thesis, we study MU systems where each receiver has a single antenna, called MU-MISO. We focus on linear precoding techniques, since they offer a good performance/complexity trade-off. More precisely, we consider optimal (maximizing the weighted sum rate) linear precoding, matched-filter precoding, zero-forcing (ZF) precoding, regularized ZF precoding and a practical scheme coined CUBF, where the precoding matrix is unitary with constant modulus entries. Due to the random propagation channel it is difficult to gain insight into the system behavior which is necessary to solve important problems such as the optimal amount of feedback. Typically, the random signal-to-interference plus noise ratio (SINR) can be bounded by a deterministic quantity considering the average system behavior and a specific precoding scheme. However, another way to render the SINR independent of the channel realizations is to assume that the number of transmit antennas M and receivers K is *large* while their ratio remains bounded. This assumption is well motivated since the current LTE-A standard already defines up to eight transmit antennas. In this dissertation, we develop a general and consistent framework for the study of linear precoding techniques in large MU-MISO systems under a wide range of channel propagation environments and imperfect CSIT. We provide the necessary tools from large dimensional random matrix theory to derive *deterministic equivalents* of the random SINR, i.e., SINR approximations independent of the channel realizations that are almost surely exact as $M, K \to \infty$. These SINR approximations can be applied to solve a variety of practical optimization problems of which several are presented in this work. Simulation results show that these solutions are close-to-optimal even for small system dimensions. Our framework forms the basis for the study of more complex systems like MU-MIMO and multi-cell MU-MIMO and opens up new ways to analyze limited feedback systems.

Acknowledgements

My decision to endeavour in a PhD was the result of an interesting six-month internship and subsequent diploma thesis at NXP Semiconductors in Sophia Antipolis while being a student at Technische Universitäet Dresden. During this year as an intern, I had the pleasure to work in the algorithm development team offering a vibrant, inspiring and challenging environment. As a result, the team leader Fabrizio Tomatis encountered little resistance in convincing me to consider a PhD within the company. Therefore, I would first like to thank all my colleagues, especially Fabrizio Tomatis and my advisors Andrea Ancora and Stefania Sesia. Fortunately I was not alone working toward my PhD, I had the great pleasure of sharing this fate with my fellow PhD students and colleagues Sébastien Aubert and Romain Couillet. Our small "PhD Group" (which included some of our other colleagues and interns) was very effective in sharing ideas and reviewing each others' works. We also created a little award called "The Geek of the Week" for which the recipient had to come up with a particular "geeky" application, usually a piece of code facilitating the everyday life of a PhD student. I would like to give special thanks to my good friend Romain Couillet from whom I learned a lot and who never grew tired in explaining complicated mathematics to me. He not only patiently reviewed my papers but also shared my fondness for nature and we spent uncountable weekends hiking and canyoning in the French riviera.

I would like to thank my fellow PhD students at EURECOM as well, in particular Rizwan Ghaffar and Paul de Kerret for their kindness and support. Further north, my thanks go to the members of Supélec Gif-sur-Yvette, first and foremost to Professor Mérouane Debbah whose ideas and engagement greatly contributed to the success of my thesis. Furthermore, my thanks go to Jakob Hoydis, who relentlessly engaged in constructive discussions and whose comments were always of great help. My gratitude goes also to Feten Zmerli who is my inexhaustible source of joy and spicy food.

Finally, I would like to express my deep gratitude for my PhD advisor Dirk Slock. He always found time to listen to the problems and to discuss my work. His experience, expertise and rigorous inquiry significantly improved my understanding of the subject matter.

Contents

List of Tables

List of Figures

Abbreviations

Acronym	Description
AWGN	Additive White Gaussian Noise
BC	Broadcast Channel
CDMA	Code-Division Multiple Access
CQI	Channel Quality Indicator
CSI	Channel State Information
CSIR	Channel State Information at Receiver
CSIT	Channel State Information at Transmitter
CUBF	Constrained Unitary Beamforming
DPC	Dirty-Paper Coding
e.s.d.	Empirical Spectral Distribution
FDD	Frequency-Division Duplex
i.i.d.	Independent Identical Distributed
LHS	Left-Hand Side
l.s.d.	Limiting Spectral Distribution
LTE	Long Term Evolution
MF	Matched Filter
MIL	Matrix Inversion Lemma
MIMO	Multiple-Input Multiple-Output
MISO	Multiple-Input Single-Output
MMSE	Minimum Mean Square Error
MSE	Mean Square Error
MU	Multi-User
PAPR	Peak-to-Average Power Ratio
RF	Radio Frequency
RMT	Random Matrix Theory
RVQ	Random Vector Quantization
RZF	Regularized Zero Forcing
SINR	Signal-to-Interference plus Noise Ratio
SNR	Signal-to-Noise Ratio
SU	Single-User
TDD	Time-Division Duplex
WSR	Weighted Sum Rate
ZF	Zero Forcing

Notation

Symbol	Description
$\mathbf{A}$	Matrix $\mathbf{A}$ (boldface upper-case letter)
$\mathbf{a}$	Vector $\mathbf{a}$ (boldface lower-case letter)
a	Scalar a (lower-case letter)
$(\cdot)^{\mathsf{T}}$	Transpose operator
$(\cdot)^{\mathsf{H}}$	Conjugate transpose operator
$\mathrm{tr}(\cdot)$	Trace operator
$E[\cdot]$	Expectation operator
$\mathbf{I}_N$	$N \times N$ identity matrix
$\mathbf{0}$	zero matrix or vector
$\log(\cdot)$	Natural logarithm
$\mathbb{R}$	Set of real numbers
$\mathbb{C}$	Set of complex numbers
$\mathbf{i}$	$\mathbf{i} = \sqrt{-1}$
$\Im(z)$	imaginary part of $z \in \mathbb{C}$
$\Re(z)$	real part of $z \in \mathbb{C}$
$\mathrm{diag}(a_1, a_2, \ldots, a_N)$	$N \times N$ diagonal matrix with $a_1, \ldots, a_N$ on the main diagonal
$\lambda_{\min}(\mathbf{A})$	Minimum eigenvalue of Hermitian matrix $\mathbf{A}$
$\lambda_{\max}(\mathbf{A})$	Maximum eigenvalue of Hermitian matrix $\mathbf{A}$
$\|\mathbf{A}\|$	Spectral norm of Hermitian $\mathbf{A}$ or $\|\mathbf{A}\| = \lambda_{\max}(\mathbf{A})$
$\|z\|$	Absolute value of $z \in \mathbb{C}$
$\mathbf{x} \sim \mathcal{CN}(\bar{\mathbf{x}}, \mathbf{R}_{\mathbf{xx}})$	$\mathbf{x}$ is Gaussian distributed with mean $\bar{\mathbf{x}}$ and covariance $\mathbf{R}_{\mathbf{xx}}$
$\min(a, b)$	minimum, $\min(a, b) = a$ if $a < b$ and $\min(a, b) = b$ is $b < a$
$\max(a, b)$	maximum, $\max(a, b) = a$ if $a > b$ and $\max(a, b) = b$ is $b > a$
$\|\mathbf{x}\|_2$	Euclidean norm $\sqrt{\mathbf{x}^{\mathsf{H}}\mathbf{x}}$
$\mathrm{Supp}(F)$	Support of a distribution function F with density f, $\mathrm{Supp}(F)$ is the closure of the set $\{x \in \mathbb{R}, f(x) > 0\}$
$\Rightarrow$	Convergence in distribution
$(a, b) = \{x \in \mathbb{R} \mid a < x < b\}$	Interval excluding the endpoints a and b
$[a, b] = \{x \in \mathbb{R} \mid a \leq x \leq b\}$	Interval including the endpoints a and b

Synthèse du Manuscrit

« Techniques de Transmission et de Réception MU-MIMO pour la Génération Suivante de Standards de Télécommunications Cellulaires »

1 Introduction et Modèle du Système

Cette section situe ce travail dans son contexte des télécommunications mobiles et présente l'état de l'art sur le sujet traité dans cette thèse. Ensuite, le modèle de transmission ainsi que le modèle de canal sont expliqués.

1.1 Introduction

Le travail originel de Foschini [1] et Telatar [2] a révélé que la capacité d'un canal point-à-point (mono-utilisateurs (SU)) à entrées et sorties multiples (MIMO) peut potentiellement augmenter linéairement avec le nombre d'antennes. Cependant, les implémentations pratiques ont démontré rapidement que dans la plupart des environnements de propagation le gain de capacité escompté du SU-MIMO est irréalisable en raison de la corrélation entre antennes et des composantes de lien direct du canal [3]. Dans un scenario multi-utilisateur, le problème inhérent à la transmission SU-MIMO peut être largement surmonté par l'exploitation de la diversité multi-utilisateur (MU), i.e., le partage de la dimension spatiale, non seulement entre les antennes du récepteur, mais entre les utilisateurs (de manière non-coopérative). Le canal sous-jacent pour la transmission de MU-MIMO est dénommé le canal MIMO broadcast (BC) ou canal descendant multi-utilisateur. Bien que beaucoup plus robuste à la corrélation du canal, le MIMO-BC souffre de l'interférence entre utilisateurs au niveau des récepteurs. Cette interférence ne peut pas être efficacement annulée du fait que les récepteurs n'ont aucune connaissance des canaux interférents, et encore moins de l'alphabet symbole interférent. Par conséquent, transmettre aux récepteurs séparément dans l'espace présente l'inconvénient de créer un niveau d'interférence accru au niveau de ces mêmes récepteurs. Pour remédier à cet inconvénient, l'annulation de l'interférence est déplacée vers l'émetteur. Idéalement, l'émetteur peut précoder le signal de telle sorte que l'interférence au niveau des récepteurs est complètement absente. Toutefois, pour ce faire, l'émetteur né-

cessite une connaissance parfaite *a priori* de la voie descendante, qui dans la pratique, est impossible à obtenir. Le problème de l'acquisition de l'information sur l'état du canal à l'émetteur (CSIT) est traité plus tard.

Dans le cas d'une connaissance parfaite du canal (CSIT parfait), il a été prouvé que le codage du *dirty-paper* (DPC) [4] est une stratégie de précodage atteignant la capacité de la MIMO-BC [5–9]. Toutefois, le précodeur DPC est non-linéaire et à ce jour trop complexe pour être mis en œuvre efficacement en pratique. Il a été démontré dans [5, 10–12] que les précodeurs linéaires sous-optimaux peuvent atteindre une grande partie de la région de capacité du BC tout en offrant une faible complexité de calcul. Ainsi, beaucoup de recherches ont mis l'accent récemment sur les stratégies de précodage linéaire.

En général, le précodeur linéaire qui maximise la capacité du BC n'a pas de forme explicite. Plusieurs algorithmes itératifs ont été proposés dans [13–15] mais aucune convergence globale n'a été prouvée. Ces algorithmes itératifs ont une grande complexité de calcul qui motive le recours aux filtres linéaires sous-optimaux en transmission en imposant plus de structure dans la conception de ces filtres. Une technique simple consiste à précoder par l'inverse du canal. Ce schéma est appelé inversion du canal ou forçage à zéro (ZF) [5, 10, 16].

Bien qu'il est légitime que le travail [10, 13, 14, 17] assume une CSIT parfaite pour déterminer théoriquement des performances optimales, cette hypothèse est intenable dans la pratique. En outre, c'est une hypothèse particulièrement forte, vu que la performance de toutes les stratégies de précodages sont crucialement dépendante de la CSIT. Dans les systèmes pratiques, l'émetteur doit acquérir les informations sur l'état du canal (CSI) de la voie descendante par le *feedback* de signalisation de la liaison montante. Etant donné que dans la pratique le temps de cohérence du canal (i.e. le temps ou le canal est a peu près constant) est fini, l'information sur l'état du canal instantané est intrinsèquement incomplète. Pour cette raison, beaucoup de recherches ont été menées afin de comprendre l'impact de la CSIT imparfaite sur le comportement du système, voir [18] pour une étude récente.

Dans cette thèse, nous considérons un émetteur équipé de M antennes et K utilisateurs avec une seule antenne, i.e. un système MU entrées multiples, sorties unique (MISO), sous un précodage linéaire et une CSIT imparfaite. En particulier, nous étudions le précodeur linéaire optimal (la maximisation de la somme pondérée des débits) proposé dans [13], précodage par filtre adapté (MF), précodage de forçage à zéro (ZF), un précodage ZF régularisé (RZF). Notre modèle de canal prend en compte une corrélation par utilisateur, i.e. le vecteur du canal $\mathbf{h}_k \in \mathbb{C}^M$ de l'utilisateur k ($k = 1, \ldots, K$) satisfait $E[\mathbf{h}_k \mathbf{h}_k^{\mathsf{H}}] = \mathbf{\Theta}_k$. En outre, nous considérons une CSIT imparfaite qui est modélisée comme une somme pondérée du canal et du bruit. Pour obtenir des aperçus sur le comportement du système, on approxime le rapport signal sur interférence plus bruit (SINR) par une quantité déterministe.

La nouveauté de cette thèse réside dans l'approche du système *large* à estimer les performances du système par une quantité déterministe. Plus précisément, nous estimons le SINR γ_k de l'utilisateur k par un *équivalent déterministe* $\bar{\gamma}_k$ tel que $\gamma_k - \bar{\gamma}_k \to 0$ presque sûrement, lorsque les dimensions du système M et

K tendent vers l'infini avec un rapport borné $0 < \lim_{M\to\infty} \sup_M \frac{M}{K} = \beta < \infty$. Par conséquent, $\bar{\gamma}_k$ devient plus précis quand M, K augmente. Pour calculer $\bar{\gamma}_k$, nous appliquons les outils du domaine bien établi de la théorie des matrices aléatoires à grandes dimensions [19, 20]. La théorie des matrices aléatoires (RMT) étudie le comportement spectral (la plupart du temps les valeurs propres) des matrices de grandes dimensions. Pour certaines matrices, la distribution empirique spectrale (e.s.d.) converge vers une distribution limite spectrale (l.s.d.), presque sûrement, si les dimensions tendent vers l'infini avec un rapport borné. Si une telle convergence n'existe pas, on peut toutefois trouver des équivalents déterministes de certaines fonctionnelles de l'e.s.d. , qui sont des approximations exactes lorsque les dimensions sont asymptotiquement grandes, presque sûrement. Des travaux antérieurs ont considéré l'approximation du SINR basée sur des *bornes* de la moyenne (par rapport aux canaux aléatoires $\mathbf{h}_k$) du SINR. L'équivalent déterministe $\bar{\gamma}_K$ n'est pas une borne, mais une approximation *fine*, presque sûrement, pour M, K asymptotiquement larges. En outre, les outils de la RMT nous permettent de considérer des modèles de canaux avancés comme le modèle de corrélation par utilisateur, qui sont généralement très difficiles à étudier précisément pour des dimensions finies. Étonnamment, $\bar{\gamma}_K$ est très précis, même pour un système de petite dimension, par exemple, $M = K = 16$. Actuellement, la norme 3GPP LTE définit déjà jusqu'à 8 antennes d'émission motivant d'autant plus l'application d'approximations de grands systèmes pour caractériser la performance des systèmes de communication sans fil. Dans cette thèse, nous proposons un cadre cohérent pour l'étude des techniques de précodage linéaire duquel nous tirerons des équivalents déterministes pour chacun des précodeurs linéaires considérés.

Ensuite, nous appliquons ces approximations du SINR à divers problèmes d'optimisation pratiques. En particulier, nous calculons le terme de régularisation optimale du précodeur RZF, qui, selon les hypothèses de corrélation, est explicite ou est la solution d'une équation implicite. En outre, pour les canaux non corrélés, nous trouvons une solution en forme fermée pour le nombre optimal d'utilisateurs par antenne d'émission dans le cas de précodage ZF. De plus, pour un précodage MF, ZF et RZF, nous évaluons la stratégie optimale de l'allocation de puissance pour des qualités inégales de CSIT des utilisateurs. Dans ce cas, le schéma d'allocation de puissance optimale est la solution de l'algorithme classique *water-filling*. Nous considérons par ailleurs des systèmes pratiques de *feedback* limité, où la CSIT est obtenue soit par une signalisation de symboles pilotes par les utilisateurs ou soit par envoi de signaux de *feedback* du canal quantifié. La signalisation de pilotes est appropriée dans des systèmes duplex à division de temps (TDD), où les canaux montants et descendants sont supposés réciproques. Dans ce système TDD, nous dérivons la quantité optimale de l'apprentissage du canal si une transmission cohérente de données et l'apprentissage du canal se produisent dans le même intervalle de cohérence du canal. De même, dans les systèmes employant un *feedback* de la quantification du canal, généralement dans les systèmes duplex à division de fréquence (FDD), nous calculons l'ordre de grandeur de la quantité de *feedback* nécessaire pour atteindre un gain optimal de multiplexage sous l'hypothèse de la quantification

vectorielle aléatoire (RVQ). En outre, nous comparons les *feedback* RVQ aux *feedback* analogiques, où le canal est renvoyé par modulation de la porteuse. En plus du précodage optimal, MF, ZF et précodage RZF, nous considérons un système pratique de précodage, appelé « constrained unitary beamforming (CUBF) », où la matrice de précodage est unitaire avec des éléments du module constant. Toutes les normes actuelles 3GPP définissent des dictionnaires contenant des matrices CUBF pour le mode MU-MIMO. Puisque les vecteurs de précodage sont orthogonaux, chaque utilisateur peut calculer son SINR d'une manière exacte sans connaissance des vecteurs de précodage interférents. Ce SINR précis sert à calculer l'indicateur de qualité de canal (CQI), qui permet à son tour à la station de base d'améliorer l'ordonnancement d'utilisateur ainsi que d'appliquer la modulation et le schéma de codage corrects. La propriété des entrées du module constant a l'avantage de ne pas augmenter le facteur de crête (PAPR) (« peak-to-average power ratio ») et permet donc aux amplificateurs de puissance de radio-fréquence (RF) de fonctionner efficacement. Cependant, il est trop compliqué de trouver une approximation du SINR, pour un précodage CUBF, utilisant l'analyse des systèmes larges. Par conséquent, nous appliquons la théorie des matrices complexes de Hadamard pour paramétrer et optimiser les matrices CUBF. L'algorithme d'optimisation qui en résulte fournit une borne supérieure sur la performance des dictionnaires finis utilisés dans les systèmes pratiques.

1.2 État de l'Art

Les auteurs de [22] ont été les premiers à effectuer une analyse des systèmes larges avec $M, K \to \infty$ et un rapport fini pour un précodage linéaire inventant ainsi la notion de « channel hardening ». En particulier, ils ont considéré un précodage ZF, appelé inversion de canal (CI), pour $M > K$ et ont montré que pour des canaux gaussiens indépendants et identiquement distribués (i.i.d.) le SINR converge vers $\rho(\beta - 1)$, où ρ est le SNR, indépendamment de la stratégie de normalisation de puissance appliquée. Ils calculent également la charge du système $\bar{\beta}^\star$ maximisant la somme des débits pour un M donné. Leurs résultats sont un cas particulier de notre analyse en Section 3.3 et en Section 4.2. Les auteurs dans [22] concluent en montrant que, pour $\beta > 1$, le précodage ZF atteint le taux de croissance linéaire (par rapport à K) de la somme des débits. Le travail dans [10] étend l'analyse dans [22] au cas $M = K$ et montre que la somme des débits de ZF est constante dans M quand $M \to \infty$, c'est-à-dire que la croissance linéaire de la somme des débits est perdue à cause des grandes fluctuations des valeurs propres de la matrice du canal. Les auteurs dans [10] contrent ce problème en introduisant un terme de régularisation α dans l'inverse de la matrice du canal. Sous l'hypothèse que M, K sont larges et pour toute distribution de canal invariante par rotation, [10] dérive le terme de régularisation $\alpha = \bar{\alpha}^\star = 1/(\beta\rho)$ qui maximise le SINR. Notez ici que dans [10] les auteurs n'appliquent pas les outils classiques de la RMT à grandes dimensions pour obtenir leurs résultats, mais plutôt ils trouvent la solution en appliquant diverses espérances et approximations. Dans cette thèse, le précodeur RZF de [10] est

dénommé précodeur de « channel distortion-unaware » RZF (RZF-CDU), car sa conception suppose une CSIT parfaite, bien que la CSIT disponible est erronée ou déformée. Il a été observé dans [10] que le précodeur RZF-CDU est très similaire au filtre d'émission dérivé sous un critère de minimisation de l'erreur quadratique (MMSE) [17] et les deux deviennent identiques quand M et K deviennent asymptotiquement grands. De même, nous allons observer des similitudes entre RZF et des filtres MMSE lors de la considération d'une CSIT imparfaite. Le précodeur RZF dans [10] a été étendu dans [23] pour tenir compte des *feedback* de quantification du canal sous hypothèse de quantification vectorielle aléatoire (RVQ). Les auteurs de [23] n'ont pas appliqué les outils de la RMT à grandes dimensions, mais utilisent les mêmes techniques que dans [10] et obtiennent des résultats différents pour le paramètre de régularisation optimale et pour le SINR par rapport à nos résultats dans la Section 4.4.

Le premier travail appliquant des outils de la RMT à grandes dimensions pour calculer le SINR asymptotique sous les précodages ZF et RZF pour les canaux corrélés était présenté dans [24]. Cependant, dans [24], le paramètre de régularisation du précodeur considéré RZF a été fixé de sorte à satisfaire la contrainte totale de puissance moyenne. Un travail similaire [25] a été publié plus tard, où les auteurs ont considéré le précodeur RZF dans [10] et ont calculé le SINR asymptotique pour les canaux gaussiens non corrélés. En outre, ils ont évalué le paramètre de régularisation asymptotiquement optimal $\bar{\alpha}^\star = 1/(\beta\rho)$, déjà calculé dans [10], ce qui est un cas particulier de celui calculé dans la Section 4.1. Un autre travail [26] reproduisant nos résultats, a remarqué que le paramètre de régularisation optimal dans [10, 25] est indépendant de la corrélation lorsque la corrélation est identique pour tous les utilisateurs.

En ce qui concerne le précodeur MF, le SINR asymptotique pour les canaux de transmission avec une corrélation commune sous une CSIT parfaite ont été établi dans [27]. Récemment, un équivalent déterministe du SINR sous un précodage MF et une contamination des séquences pilote dans les systèmes multicellulaires des systèmes a été calculé dans [28].

En ce qui concerne le précodeur linéaire optimal, les résultats suivants sont disponibles. Dans la limite des systèmes larges et pour les canaux avec entrées i.i.d., les corrélations croisées entre les canaux des utilisateurs, et par conséquent, les SINRs des utilisateurs, sont identiques. Il a été démontré dans [29] que dans ce cas symétrique et pour des variances de bruit égales, le précodeur maximisant le SINR est de forme fermée et coïncide avec le précodeur RZF. Récemment, les auteurs de [30] ont affirmé qu'effectivement la structure du précodeur RZF apparaît comme la solution optimale pour un précodage linéaire quand $M, K \to \infty$. Cette optimalité asymptotique motive une analyse détaillée du précodeur RZF pour les systèmes de dimensions larges. Un algorithme itératif pour calculer le précodeur linéaire qui maximise la somme pondérée des débits (WSR) a été proposé dans [13]. Dans la Section 3.3, nous allons procéder à une analyse des systèmes larges de cet algorithme sous une CSIT parfaite. Cependant, bien que la structure RZF émerge pour la maximisation de la somme des débits et corrélation commune sous certaines hypothèses, nous ne sommes pas en mesure de prouver que l'approximation proposée pour le SINR à l'itération j est en effet

un équivalent déterministe pour le précodeur proposé dans [13]. Néanmoins, les simulations montrent que l'approximation proposée est exacte.

1.3 Modèle du Système

Dans cette section nous décrivons le modèle de transmission ainsi que le modèle de canal.

Modèle de Transmission

Considérons un canal MISO *broadcast* composé d'un émetteur central équipé avec M antennes et K récepteurs mono-antenne non-coopératifs. Nous supposons $M \geq K$ et une transmisson en bande étroite. Le signal y_k reçu par l'utilisateur k s'écrit à chaque instant

$$y_k = \mathbf{h}_k^{\mathsf{H}}\mathbf{x} + n_k, \quad k = 1, 2, \ldots, K,$$

où $\mathbf{h}_k \in \mathbb{C}^M$ est le canal aléatoire du émetteur à utilisateur k, $\mathbf{x} \in \mathbb{C}^M$ est le vecteur transmis et les termes de bruit $n_k \sim \mathcal{CN}(0, \sigma^2)$ sont indépendants. Nous supposons que le canal $\mathbf{h}_k$ évolue suivant un modèle *block-fading*, c'est-à-dire, le canal est constant à chaque instant mais varie *indépendamment* d'un instant à l'autre.

Le vecteur transmis $\mathbf{x}$ est une combinaison linéaire des symboles indépendant des utilisateurs s_k et s'écrit

$$\mathbf{x} = \sum_{k=1}^{K} \sqrt{p_k}\mathbf{g}_k s_k,$$

où $\mathbf{g}_k \in \mathbb{C}^M$ et $p_k \geq 0$ sont les vecteurs de précodage et la puissance du signal de l'utilisateur k respectivement. Ensuite, nous supposons que l'utilisateur k a une connaissance parfaite du canal $\mathbf{h}_k$ et du canal effectif $\mathbf{h}_k^{\mathsf{H}}\mathbf{g}_k$. Une estimation de $\mathbf{h}_k^{\mathsf{H}}\mathbf{g}_k$ peut être obtenue par un apprentissage dédié en précodant le signal de l'utilisateur k par $\mathbf{g}_k$. Les vecteurs de précodage sont normalisés pour satisfaire la contrainte de puissance totale moyenne

$$E[\|\mathbf{x}\|^2] = \mathrm{tr}(\mathbf{P}\mathbf{G}^{\mathsf{H}}\mathbf{G}) \leq P, \tag{1}$$

où $\mathbf{G} \triangleq [\mathbf{g}_1, \mathbf{g}_2, \ldots, \mathbf{g}_K] \in \mathbb{C}^{M \times K}$ est la matrice de précodage, $\mathbf{P} = \mathrm{diag}(p_1, \ldots, p_K)$ est la matrice de puissance et P est la puissance d'émission totale. Un diagramme à blocs du système MU-MISO est présenté en Figure 1.

Soit $\rho \triangleq P/\sigma^2$ le SNR. Sous la contrainte $s_k \sim \mathcal{CN}(0, 1)$ et une détection mono-utilisateur avec connaissance du canal parfaite à la réception, le SINR γ_k de l'utilisateur k est défini par

$$\gamma_k = \frac{p_k |\mathbf{h}_k^{\mathsf{H}}\mathbf{g}_k|^2}{\sum_{j=1, j\neq k}^{K} p_j |\mathbf{h}_k^{\mathsf{H}}\mathbf{g}_j|^2 + \sigma^2}. \tag{2}$$

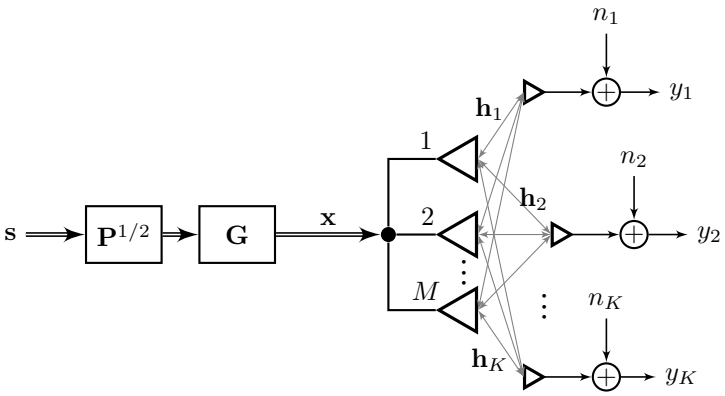

FIGURE 1: Diagramme à blocs du système MU-MISO avec transmisson en bande étroite.

Le débit R_k de l'utilisateur k est donné par

$$R_k = \log\left(1 + \gamma_k\right) \tag{3}$$

et la somme des débits R_{sum} définie par

$$R_{\text{sum}} = \sum_{k=1}^{K} R_k. \tag{4}$$

Alors que l'opérateur du réseau est souvent interessé par la capacité du système en moyenne, nous utilisons la plupart du temps les débits moyens $E[R_k]$, $E[R_{\text{wsum}}]$ et $E[R_{\text{sum}}]$, où l'espérance $E[\cdot]$ est prise sur les canaux aléatoires $\mathbf{h}_k$.

Modèle de Canal

Chaque canal $\mathbf{h}_k$ de l'utilisateur k s'écrit de la façon suivante

$$\mathbf{h}_k = \sqrt{M}\boldsymbol{\Theta}_k^{1/2}\mathbf{z}_k, \tag{5}$$

où $\boldsymbol{\Theta}_k$ est la matrice de corrélation de l'utilisateur k et $\mathbf{z}_k$ a des entrées i.i.d. de moyenne nulle et de variance $1/M$. Les matrices de corrélation varient lentement par rapport au temps de cohérence du canal et alors sont supposées parfaitement connues à l'émetteur, alors que le récepteur k a seulement connaissance de $\boldsymbol{\Theta}_k$. Ensuite, l'émetteur dispose seulement d'une estimée imparfaite $\hat{\mathbf{h}}_k$ du vrai canal $\mathbf{h}_k$ modélisé comme [38–41]

$$\hat{\mathbf{h}}_k = \sqrt{M}\boldsymbol{\Theta}_k^{1/2}\left(\sqrt{1-\tau_k^2}\mathbf{z}_k + \tau_k\mathbf{q}_k\right) = \sqrt{M}\boldsymbol{\Theta}_k^{1/2}\hat{\mathbf{z}}_k, \tag{6}$$

où $\hat{\mathbf{z}}_k = \sqrt{1-\tau_k^2}\mathbf{z}_k + \tau_k\mathbf{q}_k$, $\mathbf{q}_k$ a des entrées i.i.d. de moyenne nulle et de variance $1/M$, indépendantes de $\mathbf{z}_k$ et n_k. Le paramètre $\tau_k \in [0,1]$ indique la précision ou

qualité de l'estimée de canal $\hat{\mathbf{h}}_k$, c'est-à-dire, $\tau_k = 0$ correspond a CSIT parfaite alors que pour $\tau_k = 1$ la CSIT est complètement decorrélée du vrai canal.

2 Présuppositions mathématiques : Théorie des Matrices Aléatoires

Cette section met en place les outils nécessaires pour analyser le MISO BC à grandes dimensions avec précodage linéaire et corrélation par utilisateur.

2.1 Introduction et Outils

La théorie des matrices aléatoires (RMT) est un domaine très bien étudié en mathématique. Entre autre, la RMT consiste à étudier le comportement des valeurs propres des matrices hermitiennes. En l'occurrence Marčenko et Pastur ont prouvé que la distribution empirique des valeurs propres (e.s.d.) $F^{\mathbf{B}_N}$ d'une matrice hermitienne $\mathbf{B}_N \in \mathbb{C}^{N\times N}$ définie par

$$\mathbf{B}_N = \frac{1}{n}\sum_{i=1}^{n} \mathbf{x}_i \mathbf{x}_i^{\mathsf{H}}, \tag{7}$$

où $\mathbf{x}_i \in \mathbb{C}^N$ a des entrées indépendantes et identiquement distribués (i.i.d.) de moyenne nulle, de variance 1, converge vers une distribution limite des valeurs propres (l.s.d.) F qui est *déterministe* quand $n, N \to \infty$ avec rapport N/n borné. La l.s.d. F est appelée *la loi de Marčenko-Pastur* [49]. Il est beaucoup plus favorable de travailler avec la l.s.d. plutôt qu'avec la fonction de la densité jointe de probabilité (p.d.f.) des valeurs propres calculée dans [45–48].

Dans le domaine des télécommunications mobiles et en particulier dans notre système, le canal $\mathbf{H} \triangleq [\mathbf{h}_1, \mathbf{h}_2, \ldots, \mathbf{h}_K]^{\mathsf{H}} \in \mathbb{C}^{K\times M}$ est modélisé comme aléatoire (5). Notamment, dans l'analyse de précodage linéaire en Section 3 nous retrouvons des termes de la forme de $m_{F^{\mathbf{B}_N}}(z) \triangleq \frac{1}{N}\mathrm{tr}(\mathbf{B}_N - z\mathbf{I}_M)^{-1}$, $z \in \mathbb{C}\setminus\mathbb{R}^+$, qui est la *transformée de Stieltjes* de l'e.s.d. de la matrice hermitienne $\mathbf{B}_N$. La transformée de Stieltjes est définie en Définition 2.1 et est un outil essentiel en RMT, car il est très difficile de démontrer directement que l'e.s.d. $F^{\mathbf{B}_N}$ converge vers une l.s.d. F. Au lieu de cela, il est souvent beaucoup plus facile d'évaluer la limite $m_F(z)$ de la transformée de Stieltjes $m_{F^{\mathbf{B}_N}}(z)$, où il est démontré dans [51, Theorem B.9] que F est la l.s.d. de $F^{\mathbf{B}_N}$. Par conséquent, démontrer la convergence de $m_{F^{\mathbf{B}_N}}$ vers m_F est équivalent à démontrer la convergence de $F^{\mathbf{B}_N}$ vers F. Il est beaucoup plus simple de travailler avec la transformée de Stieltjes, qui laisse à disposition des outils comme le lemme d'inversion matriciel (MIL), l'identité de résolvante (Lemma F.2) ou le lemme de trace (F.3) qui rendent la démonstration de convergence beaucoup plus facile. Les conditions sous lesquelles m_F est une transformée de Stieltjes sont données dans Proposition 2.1.

Un autre outil important en télécommunication mobile est la *transformée de Shannon* $\mathcal{V}_F(z) \triangleq \log\det(\mathbf{I}_N + z\mathbf{B}_N)$, $z\in\mathbb{R}^+$, introduite dans [20]. La transformée de Shannon est proportionelle (avec un facteur N) à la capacité d'un canal MIMO mono-utilisateur.

Tout en sachant que l'e.s.d. $F^{\mathbf{B}_N}$ converge vers une l.s.d. F si $\mathbf{B}_N$ est définie selon (7), souvent la convergence n'est pas garantie pour des modèles de matrice

$\mathbf{B}_N$ plus sophistiqués. Néanmoins, même si la transformée de Stieltjes de $F^{\mathbf{B}_N}$ ne converge pas vers m_F, elle peut pourtant être approximée par une variable déterministe m_{F_N} telle que $m_{F^{\mathbf{B}_N}} - m_{F_N} \overset{N\to\infty}{\longrightarrow} 0$, presque sûrement, où $m_{F_N}\ \forall N$ est la transformée de Stieltjes de la fonction de distribution F_N telle que $F^{\mathbf{B}_N} - F_N \Rightarrow 0$, presque sûrement. La variable m_{F_N} est appelée *équivalent déterministe* et est définie en Définition 2.3.

Dans ce qui suit, nous démontrons le théorème principal qui offre un équivalent déterministe m_{F_N} de la transformée de Stieltjes $m_{F^{\mathbf{B}_N}}$ où $\mathbf{B}_N$ est aléatoire avec profil de variance généralisé. Le théorème élargit les résultats dans [31, 53] mais la démonstration repose fortement sure des techniques appliquées dans [31, 53].

Ensuite, nous simplifions la notation et écrivons $m_{\mathbf{X}} \triangleq m_{F^{\mathbf{X}}}$ et $\bar{m}_{\mathbf{X}} = m_{F_N}$.

2.2 Équivalent Déterministe de la Transformée de Stieltjes des Matrices avec Profil de Variance Généralisé

Théorème 1. *Considérons la matrice $\mathbf{B}_N = \mathbf{X}_N^{\mathsf{H}}\mathbf{X}_N + \mathbf{S}_N$, où $\mathbf{S}_N \in \mathbb{C}^{N\times N}$ est hermitienne définie positive et $\mathbf{X}_N \in \mathbb{C}^{n\times N}$ est aléatoire. La colonne i de $\mathbf{X}_N^{\mathsf{H}}$ est $\mathbf{x}_i = \mathbf{\Psi}_i\mathbf{y}_i$, où les entrées de $\mathbf{y}_i \in \mathbb{C}^{r_i}$ sont indépendantes et identiquement distribuées de moyenne nulle, de variance $1/N$ et ayant un moment d'ordre huit d'ordre $O\left(\frac{1}{N^4}\right)$. Les matrices $\mathbf{\Psi}_i \in \mathbb{C}^{N\times r_i}$ sont déterministes. En outre, soit $\mathbf{\Theta}_i = \mathbf{\Psi}_i\mathbf{\Psi}_i^{\mathsf{H}} \in \mathbb{C}^{N\times N}$ et $\mathbf{Q}_N \in \mathbb{C}^{N\times N}$ déterministe. Supposons que $\limsup_{N\to\infty}\sup_{1\le i\le n}\|\mathbf{\Theta}_i\| < \infty$ et $\mathbf{Q}_N$ de norme spectrale uniformément bornée. Soit*

$$m_{\mathbf{B}_N,\mathbf{Q}_N}(z) \triangleq \frac{1}{N}\mathrm{tr}\mathbf{Q}_N\left(\mathbf{B}_N - z\mathbf{I}_N\right)^{-1}. \tag{8}$$

Alors, pour $z\in\mathbb{C}\setminus\mathbb{R}^+$, lorsque n, N deviennent grands avec les rapports $\beta_{N,i} \triangleq N/r_i$ et $\beta_N \triangleq N/n$ tels que $0 < \liminf_N \beta_N \le \limsup_N \beta_N < \infty$ et $0 < \liminf_N \beta_{N,i} \le \limsup_N \beta_{N,i} < \infty$, nous avons

$$m_{\mathbf{B}_N,\mathbf{Q}_N}(z) - \bar{m}_{\mathbf{B}_N,\mathbf{Q}_N}(z) \overset{N\to\infty}{\longrightarrow} 0, \tag{9}$$

presque sûrement, où $\bar{m}_{\mathbf{B}_N,\mathbf{Q}_N}(z)$ vérifie

$$\bar{m}_{\mathbf{B}_N,\mathbf{Q}_N}(z) = \frac{1}{N}\mathrm{tr}\mathbf{Q}_N\left(\frac{1}{N}\sum_{j=1}^{n}\frac{\mathbf{\Theta}_j}{1+e_{N,j}(z)} + \mathbf{S}_N - z\mathbf{I}_N\right)^{-1} \tag{10}$$

et $e_{N,1}(z), \ldots, e_{N,n}(z)$ sont les uniques solutions positives de

$$e_{N,i}(z) = \frac{1}{N}\mathrm{tr}\mathbf{\Theta}_i\left(\frac{1}{N}\sum_{j=1}^{n}\frac{\mathbf{\Theta}_j}{1+e_{N,j}(z)} + \mathbf{S}_N - z\mathbf{I}_N\right)^{-1}. \tag{11}$$

Démonstration de Théorème 1. La démonstration se trouve en Section 2.2. □

Proposition 1 (Convergence de l'algorithme du point fixe)**.** *Soit* $z \in \mathbb{C} \setminus \mathbb{R}^+$ *et* $\{e_{N,i}^{(k)}(z)\}$ *(*$k \geq 0$*) une série définie par* $e_{N,i}^{(0)}(z) = -\frac{1}{z}$ *et*

$$e_{N,i}^{(k)}(z) = \frac{1}{N}\mathrm{tr}\boldsymbol{\Theta}_i \left(\frac{1}{N}\sum_{j=1}^{n} \frac{\boldsymbol{\Theta}_j}{1 + e_{N,j}^{(k-1)}(z)} + \mathbf{S}_N - z\mathbf{I}_N \right)^{-1} \tag{12}$$

pour $k > 0$*. Alors,* $\lim_{k\to\infty} e_{N,i}^{(k)}(z) = e_{N,i}(z)$ *définie dans* (2.10) *pour* $i \in \{1, 2, \ldots, n\}$.

Théorème 1 met à disposition une approximation déterministe $\bar{m}_{\mathbf{B}_N,\mathbf{Q}_N}(z)$ de la variable aléatoire $m_{\mathbf{B}_N,\mathbf{Q}_N}(z)$ qui devient de plus en plus exacte lorsque N augmente et est une fonction de n équations implicites couplées.

2.3 Équivalent Déterministe de la Transformée de Shannon des Matrices avec Profil de Variance Généralisé

Alors même que nous n'appliquons pas ce résultat dans cette thèse, une application récente au sujet de précodage aléatoire se trouve dans [56]. Le théorème suivant est original et élargit les résultats dans [31, 53].

Théorème 2. *Soit* $x > 0$ *et* $\mathbf{S}_N$ *de norme spectrale uniformément bornée. Sous les conditions de Théorème 1, considérons la transformée de Shannon de la matrice* $\mathbf{B}_N$ *comme* $\mathcal{V}_{\mathbf{B}_N}(x) \triangleq \frac{1}{N}\log\det(\mathbf{I}_N + x\mathbf{B}_N)$*. Alors,*

$$E\,\mathcal{V}_{\mathbf{B}_N}(x) - \bar{\mathcal{V}}_{\mathbf{B}_N}(x) \overset{N\to\infty}{\longrightarrow} 0, \tag{13}$$

avec $\bar{\mathcal{V}}_{\mathbf{B}_N}(x)$ *définie par*

$$\begin{aligned}\bar{\mathcal{V}}_{\mathbf{B}_N}(x) = \frac{1}{N}\log\det\left(\mathbf{I}_N + x\left[\mathbf{S}_N + \frac{1}{N}\sum_{j=1}^{n}\frac{\boldsymbol{\Theta}_i}{1 + e_{N,j}(-1/x)}\right]\right) \\ + \frac{1}{N}\sum_{j=1}^{n}\log\left[1 + e_{N,j}(-1/x)\right] - \frac{1}{N}\sum_{j=1}^{n}\frac{e_{N,j}(-1/x)}{1 + e_{N,j}(-1/x)},\end{aligned} \tag{14}$$

où les variables $e_{N,1}(-1/x), \ldots, e_{N,n}(-1/x)$ *sont les uniques solutions positives de* (2.10) *avec* $z = -1/x$*.*

Démonstration de Théorème 2.2. La démonstration se trouve en Section 2.3. □

3 MISO BC avec Précodage Linéaire : Une Analyse des Systèmes à Grandes Dimensions

Dans cette section, nous considérons le MISO-BC avec les techniques de précodage linéaire suivantes : précodage par filtre adapté (MF), précodage linéaire optimal (la maximisation de la somme pondérée des débits), précodage de forçage à zéro régularisé (RZF) et précodage de forçage à zéro (ZF). Nous supposons que le système est *large* dans le sens que le nombre d'utilisateurs K et le nombre d'antennes d'émission M deviennent grands avec rapport $M/K \to \beta < \infty$. Sous cette hypothèse, nous proposons des équivalents déterministes $\bar{\gamma}_k$ du SINR aléatoire γ_k de utilisateur k pour chaque technique de précodage. Dans cette synthèse du manuscrit, nous nous concentrons sur les précodeurs RZF et ZF. Les techniques de précodage MF et précodage linéaire optimal sont traitées en Section 3.2 et Section 3.3 respectivement.

3.1 Introduction

Pour obtenir une connaissance plus approfondie du comportement du système, il est nécessaire de déterminer la dépendance fondamentale de la mesure de performance du système sur les paramètres pertinents (par exemple, le SNR, la CSIT, la corrélation,...) du même système. Cette dépendance n'est pas explicite à cause du canal aléatoire. Par conséquent, il est difficile de prédire comment un changement d'un paramètre altérera la performance du système. Pour accomplir cela, nous pouvons considérer la performance du système en moyenne et l'approximer ou la borner par une variable *déterministe*, qui ensuite prédit comment un paramètre altérera la performance du système en moyenne. La dérivation de bornes exactes devient extrêmement compliquée pour des modèles de canal avancés comme le modèle de corrélation par utilisateur. Néanmoins, une autre possibilité pour approximer la performance du système consiste à supposer que les dimensions du système, c'est-à-dire le nombre d'utilisateurs K et le nombre d'antennes d'émission M, sont grandes mais que leur rapport M/K reste borné. Sous cette hypothèse, nous pouvons recourir aux outils avancés de la RMT pour calculer un *équivalent déterministe* $\bar{\gamma}_k$ tel que $\gamma_k - \bar{\gamma}_k \overset{M\to\infty}{\longrightarrow} 0$ presque sûrement. Pour le modèle de canal avec corrélation par utilisateur (ou profil de variance généralisé) quelques outils importants ont été mis en place dans la section précédente. Dans cette section, nous appliquons ces outils pour évaluer $\bar{\gamma}_k$ pour chaque technique de précodage consideré. Comme résultat, nous obtenons des approximations du SINR (ou du débit par utilisateur) qui sont asymptotiquement exactes (presque sûrement) et qui dépendent des paramètres de système importants d'une façon *déterministe*. Les résultats dans cette section mettent à disposition des outils qui peuvent être appliqués pour résoudre une multitude des problèmes pratiques, ce qui est le sujet de Section 4.

Hypothèses techniques

Nous avons besoin de quelques hypothèses techniques qui sont nécessaires pour l'analyse à grandes dimensions.

Hypothèse 1. *Toutes les matrices de corrélation $\mathbf{\Theta}_k$ sont uniformément bornées sur M,*

$$\limsup_{M\to\infty} \sup_{1\leq k\leq K} \|\mathbf{\Theta}_k\| < \infty. \tag{15}$$

Ensuite, nous avons besoin de l'hypothèse suivante sur la matrice d'allocation de puissance $\mathbf{P}$.

Hypothèse 2. *La puissance $p_{\max} = \max(p_1, \ldots, p_K)$ est de l'ordre $O(1/K)$,*

$$\|\mathbf{P}\| = O(1/K). \tag{16}$$

Hypothèse 3. *La matrice $\frac{1}{M}\hat{\mathbf{H}}^{\mathsf{H}}\hat{\mathbf{H}}$ est de norme spectrale uniformément bornée sur M avec probabilité 1, c'est-à-dire,*

$$\limsup_{M\to\infty} \|\frac{1}{M}\hat{\mathbf{H}}^{\mathsf{H}}\hat{\mathbf{H}}\| < \infty, \tag{17}$$

avec probabilité 1.

Remarque 1. *Hypothèse 3 est vraie si $\sup_K |\{\mathbf{\Theta}_k : k = 1, 2, \ldots, K\}| < \infty$, où $|\mathcal{A}|$ est la cardinalité de l'ensemble $\mathcal{A}$. C'est-à-dire $\{\mathbf{\Theta}_k\}$ fait partie d'une famille finie [57]. Dans la pratique nous travaillons typiquement avec un nombre fini de $\mathbf{\Theta}_k$. Par example, considérons le modèle de canal pour des systèmes MIMO de la norme 3GPP LTE [59], où les matrices de corrélation $\mathbf{\Theta}_k$ comprennent seulement trois matrices différentes correspondant aux corrélations faible, moyenne et forte. En outre, si $\mathbf{\Theta}_k = \mathbf{\Theta}$ $\forall k$, alors l'Hypothèse 3 est vraie, car $\frac{1}{M}\|\hat{\mathbf{H}}^{\mathsf{H}}\hat{\mathbf{H}}\| \leq \|\mathbf{\Theta}\|\|\mathbf{Z}^{\mathsf{H}}\mathbf{Z}\|$, où $\mathbf{Z} = [\mathbf{z}_1, \ldots, \mathbf{z}_K]^{\mathsf{H}}$ et les deux matrices $\|\mathbf{\Theta}\|$ et $\|\mathbf{Z}^{\mathsf{H}}\mathbf{Z}\|$ sont uniformément bornées sur M pour tout M large avec probabilité 1, [60].*

Dans ce qui suit, nous déduisons des *équivalents déterministes* du SINR aléatoire pour toutes techniques de précodage linéaire considérées.

3.2 Précodage de Forçage à Zéro Régularisé

Considérons la matrice de précodage de forçage à zéro régularisé

$$\mathbf{G}_{\text{rzf}} = \xi_{\text{rzf}} \left(\hat{\mathbf{H}}^{\mathsf{H}}\hat{\mathbf{H}} + M\alpha\mathbf{I}_M\right)^{-1} \hat{\mathbf{H}}^{\mathsf{H}}, \tag{18}$$

où $\hat{\mathbf{H}} \triangleq [\hat{\mathbf{h}}_1, \hat{\mathbf{h}}_2, \ldots, \hat{\mathbf{h}}_K]^{\mathsf{H}} \in \mathbb{C}^{K\times M}$ est l'estimée de la matrice de canal à l'émetteur, ξ_{rzf} est une constante de normalisation pour satisfaire la contrainte de puissance (1) et $\alpha > 0$ est le paramètre de régularisation. Ici, α est multipliée par M pour assurer que α lui-même converge vers une constante lorsque $M \to \infty$.

De la contrainte de puissance (1), nous obtenons ξ^2_{rzf}

$$\xi^2_{\text{rzf}} = \frac{P}{\text{tr}\mathbf{P}\hat{\mathbf{H}}(\hat{\mathbf{H}}^{\mathsf{H}}\hat{\mathbf{H}} + M\alpha\mathbf{I}_M)^{-2}\hat{\mathbf{H}}^{\mathsf{H}}} = \frac{P}{\Psi_{\text{rzf}}},$$

où $\Psi_{\text{rzf}} \triangleq \text{tr}\mathbf{P}\hat{\mathbf{H}}(\hat{\mathbf{H}}^{\mathsf{H}}\hat{\mathbf{H}} + M\alpha\mathbf{I}_M)^{-2}\hat{\mathbf{H}}^{\mathsf{H}}$. Soit $\hat{\mathbf{W}} \triangleq (\hat{\mathbf{H}}^{\mathsf{H}}\hat{\mathbf{H}} + M\alpha\mathbf{I}_M)^{-1}$, le SINR (2) de l'utilisateur k avec précodage RZF s'écrit

$$\gamma_{k,\text{rzf}} = \frac{p_k|\mathbf{h}_k^{\mathsf{H}}\hat{\mathbf{W}}\hat{\mathbf{h}}_k|^2}{\mathbf{h}_k^{\mathsf{H}}\hat{\mathbf{W}}\hat{\mathbf{H}}_{[k]}^{\mathsf{H}}\mathbf{P}_{[k]}\hat{\mathbf{H}}_{[k]}\hat{\mathbf{W}}\mathbf{h}_k + \frac{\Psi_{\text{rzf}}}{\rho}}, \tag{19}$$

où $\hat{\mathbf{H}}_{[k]} \triangleq [\hat{\mathbf{h}}_1, \ldots, \hat{\mathbf{h}}_{k-1}, \hat{\mathbf{h}}_{k+1}, \ldots, \hat{\mathbf{h}}_K]^{\mathsf{H}} \in \mathbb{C}^{K-1\times M}$ et $\mathbf{P}_{[k]} \triangleq \text{diag}(p_1, \ldots, p_{k-1}, p_{k+1}, \ldots, p_K)$.

Le théorème suivant offre une approximation déterministe $\bar{\gamma}_{k,\text{rzf}}$ de $\gamma_{k,\text{rzf}}$ définie dans (19), qui devient de plus en plus exacte lorsque $M, K \to \infty$.

Théorème 3. *En supposant que les hypothèses 1, 2 et 3 sont vraies et soit $\alpha > 0$ et soit $\gamma_{k,\text{rzf}}$ le SINR de l'utilisateur k défini dans* (19)*. Alors*

$$\gamma_{k,\text{rzf}} - \bar{\gamma}_{k,\text{rzf}} \overset{M\to\infty}{\longrightarrow} 0,$$

presque sûrement, où $\bar{\gamma}_{k,\text{rzf}}$ s'écrit

$$\bar{\gamma}_{k,\text{rzf}} = \frac{p_k(1-\tau_k^2)e_k^2}{\bar{\Upsilon}_{k,\text{rzf}}(1-\tau_k^2[1-(1+e_k)^2]) + \frac{\bar{\Psi}_{\text{rzf}}}{\rho}(1+e_k)^2}, \tag{20}$$

où les $e_1, \ldots, e_K$ sont les uniques solutions positives de

$$e_i = \frac{1}{M}\text{tr}\mathbf{\Theta}_i\mathbf{T}$$
$$\mathbf{T} = \left(\frac{1}{M}\sum_{j=1}^{K}\frac{\mathbf{\Theta}_j}{1+e_j} + \alpha\mathbf{I}_M\right)^{-1}$$

et $\bar{\Psi}_{\text{rzf}}$ et $\bar{\Upsilon}_{k,\text{rzf}}$ s'écrivent

$$\bar{\Psi}_{\text{rzf}} = \frac{1}{M}\sum_{j=1}^{K}\frac{p_j e'_j}{(1+e_j)^2},$$
$$\bar{\Upsilon}_{k,\text{rzf}} = \frac{1}{M}\sum_{j=1,j\neq k}^{K}\frac{p_j e'_{j,k}}{(1+e_j)^2}.$$

Soit $\mathbf{e}' = [e'_1, \ldots, e'_K]^{\mathsf{T}}$ et $\mathbf{e}'_k = [e'_{1,k}, \ldots, e'_{K,k}]^{\mathsf{T}}$, qui vérifient

$$\mathbf{e}' = (\mathbf{I}_K - \mathbf{J})^{-1}\mathbf{v},$$
$$\mathbf{e}'_k = (\mathbf{I}_K - \mathbf{J})^{-1}\mathbf{v}_k,$$

où $\mathbf{J}$, $\mathbf{v}$ *et* $\mathbf{v}_k$ *s'écrivent*

$$[\mathbf{J}]_{ij} = \frac{\frac{1}{M}\mathrm{tr}\boldsymbol{\Theta}_i\mathbf{T}\boldsymbol{\Theta}_j\mathbf{T}}{M(1+e_j)^2},$$
$$\mathbf{v} = \left[\frac{1}{M}\mathrm{tr}\boldsymbol{\Theta}_1\mathbf{T}^2, \ldots, \frac{1}{M}\mathrm{tr}\boldsymbol{\Theta}_K\mathbf{T}^2\right]^{\mathsf{T}},$$
$$\mathbf{v}_k = \left[\frac{1}{M}\mathrm{tr}\boldsymbol{\Theta}_1\mathbf{T}\boldsymbol{\Theta}_k\mathbf{T}, \ldots, \frac{1}{M}\mathrm{tr}\boldsymbol{\Theta}_K\mathbf{T}\boldsymbol{\Theta}_k\mathbf{T}\right]^{\mathsf{T}}.$$

Démonstration de Théorème 3. La démonstration se trouve en Section 3.4. □

Corollaire 1. *En supposant que les hypothèses 1, 2 sont vraies et soit* $\alpha > 0$ *et* $\boldsymbol{\Theta}_k = \boldsymbol{\Theta}$ $\forall k$*, alors* $\bar{\gamma}_{k,\mathrm{rzf}}$ *s'écrit*

$$\bar{\gamma}_{k,\mathrm{rzf}} = \frac{p_k}{P/K}\frac{e\ (1-\tau_k^2)\left[e_{22}+\alpha\beta(1+e)^2e_{12}\right]}{e_{22}(1-p_k/P)\left[1-\tau_k^2(1-(1+e)^2)\right]+\frac{1}{\rho}(1+e)^2e_{12}}, \tag{21}$$

où e *est la unique solution positive de*

$$e = \frac{1}{M}\mathrm{tr}\boldsymbol{\Theta}\mathbf{T} \tag{22}$$
$$\mathbf{T} = \left(\frac{\boldsymbol{\Theta}/\beta}{1+e}+\alpha\mathbf{I}_M\right)^{-1} \tag{23}$$

et e_{ij} *s'écrit*

$$e_{ij} = \frac{1}{(1+e)^j}\frac{1}{M}\mathrm{tr}\boldsymbol{\Theta}^i\mathbf{T}^j. \tag{24}$$

Dans cette thèse, nous considérons deux techniques de précodage RZF différentes. La première correspond au précodage dans [10], où $\alpha = \frac{1}{\beta\rho}$ et est optimale (α maximise de la somme des débits) lorsque la corrélation est la même pour chaque utilisateur (corrélation identique) et CSIT parfaite quand M, K sont larges [10, 25, 26]. Ce précodage est appelé RZF « *channel distortion unaware* » (RZF-CDU). Le deuxième précodage maximise la somme des débits pour corrélation identique et CSIT *imparfaite* et est calculé en Section 4.1. Ce précodage est appelé RZF « *channel distortion aware* » (RZF-CDA).

Un autre cas spécial de précodage RZF est le précodage ZF, où le le paramètre de régularisation est zéro.

3.3 Précodage de Forçage à Zéro

Pour $\alpha = 0$, la matrice de précodage RZF dans (18) devient la matrice de précodage ZF $\mathbf{G}_{\mathrm{zf}}$ et s'écrit

$$\mathbf{G}_{\mathrm{zf}} = \xi_{\mathrm{zf}}\hat{\mathbf{H}}^{\mathsf{H}}\left(\hat{\mathbf{H}}\hat{\mathbf{H}}^{\mathsf{H}}\right)^{-1},$$

où ξ_{zf} est une constante de normalisation pour satisfaire la contrainte de puissance (1) et s'écrit

$$\xi_{\text{zf}}^2 = \frac{P}{\text{tr}\mathbf{P}(\hat{\mathbf{H}}\hat{\mathbf{H}}^{\mathsf{H}})^{-1}} = \frac{P}{\Psi_{\text{zf}}},$$

où $\Psi_{\text{zf}} \triangleq \text{tr}\mathbf{P}(\hat{\mathbf{H}}\hat{\mathbf{H}}^{\mathsf{H}})^{-1}$. Soit $\hat{\bar{\mathbf{W}}} \triangleq \hat{\mathbf{H}}^{\mathsf{H}}(\hat{\mathbf{H}}\hat{\mathbf{H}}^{\mathsf{H}})^{-2}\hat{\mathbf{H}}$, le SINR (2) de l'utilisateur k avec précodage ZF s'écrit

$$\gamma_{k,\text{zf}} = \frac{p_k|\mathbf{h}_k^{\mathsf{H}}\hat{\bar{\mathbf{W}}}\hat{\mathbf{h}}_k|^2}{\mathbf{h}_k^{\mathsf{H}}\hat{\bar{\mathbf{W}}}\hat{\mathbf{H}}_{[k]}^{\mathsf{H}}\mathbf{P}_{[k]}\hat{\mathbf{H}}_{[k]}\hat{\bar{\mathbf{W}}}\mathbf{h}_k + \frac{\Psi_{\text{zf}}}{\rho}}. \tag{25}$$

Pour obtenir un équivalent déterministe du SINR (25), il est nécessaire d'assurer que la valeur propre minimale de $\hat{\mathbf{H}}\hat{\mathbf{H}}^{\mathsf{H}}$ est bornée en dehors de zéro pour tout M large, presque sûrement. Comme expliqué dans [10], pour $M = K$, la valeur propre minimale de la l.s.d. de $\hat{\mathbf{H}}\hat{\mathbf{H}}^{\mathsf{H}}$ contient zéro. Alors, $\|(\hat{\mathbf{H}}\hat{\mathbf{H}}^{\mathsf{H}})^{-1}\|$ n'est pas bornée sur M et un équivalent déterministe de $\gamma_{k,\text{zf}}$ n'existe pas. Alors, nous avons besoin de l'hypothèse suivante.

Hypothèse 4. *Il existe $\varepsilon > 0$ tel que, pour tout M large, nous avons que $\lambda_{\min}(\frac{1}{M}\hat{\mathbf{H}}\hat{\mathbf{H}}^{\mathsf{H}}) > \varepsilon$ avec probabilité 1.*

Remarque 2. *Si $\mathbf{\Theta}_k = \mathbf{\Theta}$ $\forall k$ et $\lambda_{\min}(\mathbf{\Theta}) > \varepsilon > 0$ (i.e. contrairement au Théorème 3, $\mathbf{\Theta}$ doit être inversible), pour tout M, alors l'Hypothèse 4 est vraie si $\beta > 1$. En effet, pour $\beta > 1$, de [60], il existe $\zeta > 0$ telle que, pour tout M large, $\lambda_{\min}(\hat{\mathbf{Z}}\hat{\mathbf{Z}}^{\mathsf{H}}) > \zeta$, où $\hat{\mathbf{Z}} = [\hat{\mathbf{z}}_1, \ldots, \hat{\mathbf{z}}_K]^{\mathsf{H}}$, avec probabilité 1. Alors, pour tout M large, $\lambda_{\min}(\frac{1}{M}\hat{\mathbf{H}}\hat{\mathbf{H}}^{\mathsf{H}}) \geq \lambda_{\min}(\hat{\mathbf{Z}}\hat{\mathbf{Z}}^{\mathsf{H}})\lambda_{\min}(\mathbf{\Theta}) > \zeta\varepsilon > 0$ presque sûrement.*

Un équivalent déterministe $\bar{\gamma}_{k,\text{zf}}$ de $\gamma_{k,\text{zf}}$ est donné dans le théorème suivant.

Théorème 4. *En supposant que les hypothèses 3.1, 3.2, 3.4, 3.5 et 3.6 sont vraies et soit $\gamma_{k,\text{zf}}$ le SINR de l'utilisateur k défini dans* (25)*. Alors*

$$\gamma_{k,\text{zf}} - \bar{\gamma}_{k,\text{zf}} \overset{M\to\infty}{\longrightarrow} 0, \tag{26}$$

presque sûrement, où $\bar{\gamma}_{k,\text{zf}}$ s'écrit

$$\bar{\gamma}_{k,\text{zf}} = p_k \frac{1-\tau_k^2}{\tau_k^2\bar{\Upsilon}_{k,\text{zf}} + \frac{\bar{\Psi}_{\text{zf}}}{\rho}}, \tag{27}$$

où $\bar{\Psi}_{\text{zf}}$ et $\bar{\Upsilon}_{k,\text{zf}}$ s'écrivent

$$\bar{\Psi}_{\text{zf}} = \frac{1}{M}\sum_{j=1}^{K}\frac{p_j}{\underline{e}_j},$$

$$\bar{\Upsilon}_{k,\text{zf}} = \frac{1}{M}\sum_{j=1,j\neq k}^{K} p_j\frac{\underline{e}'_{j,k}}{\underline{e}_j^2}. \tag{28}$$

Les fonctions $\underline{e}_1, \ldots, \underline{e}_K$ *sont les unique solutions positives de*

$$\underline{e}_i = \frac{1}{M}\mathrm{tr}\boldsymbol{\Theta}_i\underline{\mathbf{T}} \tag{29}$$

$$\underline{\mathbf{T}} = \left(\frac{1}{M}\sum_{j=1}^{K}\frac{\boldsymbol{\Theta}_j}{\underline{e}_j} + \mathbf{I}_M\right)^{-1}. \tag{30}$$

En outre, soit $\underline{\mathbf{e}}'_k = [\underline{e}'_{1,k}, \ldots, \underline{e}'_{K,k}]^{\mathsf{T}}$*, qui vérifie*

$$\underline{\mathbf{e}}'_k = (\mathbf{I}_K - \underline{\mathbf{J}})^{-1}\,\underline{\mathbf{v}}_k, \tag{31}$$

où $\underline{\mathbf{J}}$ *et* $\underline{\mathbf{v}}_k$ *s'écrivent*

$$[\underline{\mathbf{J}}]_{ij} = \frac{\frac{1}{M}\mathrm{tr}\boldsymbol{\Theta}_i\underline{\mathbf{T}}\boldsymbol{\Theta}_j\underline{\mathbf{T}}}{M\,\underline{e}_j^2},$$

$$\underline{\mathbf{v}}_k = \left[\frac{1}{M}\mathrm{tr}\boldsymbol{\Theta}_1\underline{\mathbf{T}}\boldsymbol{\Theta}_k\underline{\mathbf{T}}, \ldots, \frac{1}{M}\mathrm{tr}\boldsymbol{\Theta}_K\underline{\mathbf{T}}\boldsymbol{\Theta}_k\underline{\mathbf{T}}\right]^{\mathsf{T}}.$$

Démonstration de Théorème 4. La démonstration se trouve en Appendice C. □

3.4 Approximations du Débit

Une approximation $\hat{R}_{\mathrm{sum}}$ de la somme des débits ergodique R_{sum} peut être obtenue en remplaçant le SINR instantané (c'est-à-dire, sans moyenner sur la distribution de canal) γ_k avec son approximation à grandes dimensions $\bar{\gamma}_k$,

$$\hat{R}_{\mathrm{sum}} = \sum_{k=1}^{K}\log\left(1+\bar{\gamma}_k\right). \tag{32}$$

3.5 Résultats Numériques

Nous vérifions les résultats dans le Théorème 3 et le Théorème 4 en comparant la somme des débits ergodique (4), obtenue par simulations numériques des canaux i.i.d. « Rayleigh block-fading », à l'approximation à grandes dimensions $\hat{R}_{\mathrm{sum}}$, pour des systèmes de dimensions finies et une allocation de puissance uniforme $\mathbf{P} = \frac{1}{K}\mathbf{I}_K$.

La corrélation $\boldsymbol{\Theta}_k$ du canal de l'utilisateur k est modélisée comme dans [63]. Les ondes percutent le récepteur k uniformément avec un angle θ compris entre $\theta_{k,\min}$ et $\theta_{k,\max}$. Soit d_{ij} la distance entre l'antenne d'émission i et j, la corrélation s'écrit

$$[\boldsymbol{\Theta}_k]_{ij} = \frac{1}{\theta_{k,\max}-\theta_{k,\min}}\int_{\theta_{k,\min}}^{\theta_{k,\max}} e^{\,\mathrm{i}\frac{2\pi}{\lambda}d_{ij}\cos(\theta)}d\theta, \tag{33}$$

où λ est la longueur d'onde du signal. Les utilisateurs sont supposés uniformément distribués autour d'émetteur dans un angle $\varphi_k = 2\pi k/K$ et comme un exemple simple, nous choisissons $\theta_{k,\min} = -\pi$ et $\theta_{k,\max} = \varphi_k - \pi$. Remarquez que pour des petites valeurs de $\theta_{k,\max} - \theta_{k,\min}$ (dans notre exemple pour des petites valeurs de k), le signal correspondant à l'utilisateur k est fortement corrélé car les signaux arrivent d'un angle très fin. Par conséquent, le modèle de corrélation (33) donne des matrices de rang déficient pour quelques utilisateurs. L'émetteur est équipé avec une ligne uniforme d'antennes (ULA). Pour assurer que $\|\mathbf{\Theta}_k\|$ est bornée pour M large, nous supposons que la distance entre antennes adjacentes est indépendante de M, c'est-à-dire la longueur de l'ULA augmente avec M.

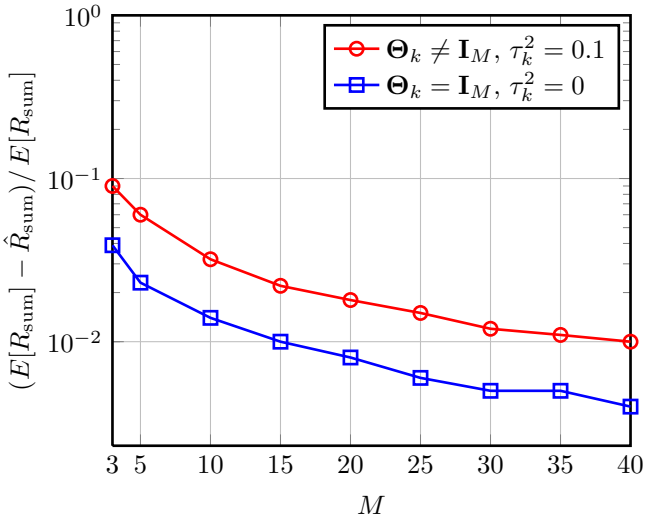

FIGURE 2: RZF-CDU, $(E[R_{\text{sum}}] - \hat{R}_{\text{sum}})/\, E[R_{\text{sum}}]$ en fonction de M pour un SNR fix de $\rho = 10$ dB avec $M = K$, $\alpha = 1/\rho$.

Les résultats de simulation représentés dans Figure 2 montent l'erreur absolue de la somme des débits approximé $\hat{R}_{\text{sum}}$ comparé à la somme des débits ergodique $E[R_{\text{sum}}]$, moyennés sur 10 000 réalisations de canal indépendantes. La notation « $\mathbf{\Theta}_k \neq \mathbf{I}_M$ » indique que $\mathbf{\Theta}_k$ est modélisée selon (33) avec $d_{ij}/\lambda = 0.5$. De la Figure 2, nous observons que la somme des débits approximé $\hat{R}_{\text{sum}}$ devient de plus en plus exacte quand M augmente.

Figures 3 et 4 comparent la somme des débits ergodique à l'approximation déterministe (32) pour les précodeurs RZF et ZF respectivement. Les barres d'erreur indiquent l'écart type des simulations numériques. Nous observons que l'approximation est environ de l'ordre d'une fois l'écart type. De la Figure 3, pour CSIT imparfaite ($\tau_k^2 = 0.1$), la somme des débits se dégrade à fort SNR parce que le paramètre de régularisation α ne considère pas les τ_k^2 et la matrice $\hat{\mathbf{H}}^{\mathsf{H}}\hat{\mathbf{H}} + M\alpha\mathbf{I}_M$ donc le précodeur RZF devient mal conditionné. Figure 4 montre

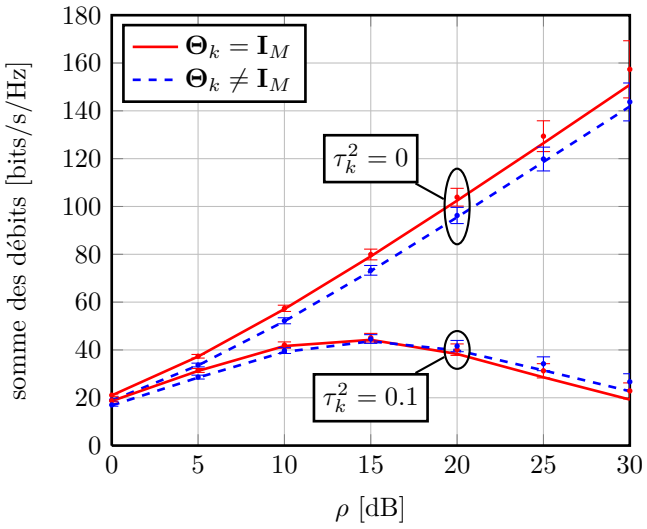

FIGURE 3: RZF-CDU, la somme des débits en fonction de SNR avec $M = K = 30$ et $\alpha = 1/\rho$, les résultats de simulation sont indiqués par des cercles avec l'écart type.

que, pour $M > K$, la somme des débits ne se dégrade pas à fort SNR, car la CSIT $\hat{\mathbf{H}}$ est beaucoup mieux conditionnée. La régularisation optimale est étudiée en Section 4.1. De plus, nous observons que dans Figure 3 l'approximation déterministe devient moins exacte pour fort SNR. La raison est que dans les calculs du SINR approximé, nous appliquons Théorème 1 pour $z = -\alpha = -1/\rho$ et donc les bornes dans Proposition 2.3 (Chapitre 2 Section 2.2.1) sont proportionnelles au SNR. Alors, pour augmenter la précision du SINR approximé, des dimensions plus larges sont nécessaires.

Nous concluons que les approximations déterministes dans Théorème 3 et Théorème 4 sont précises même pour des dimensions petites et donc peuvent être appliquées aux problèmes pratiques discutés dans la section suivante.

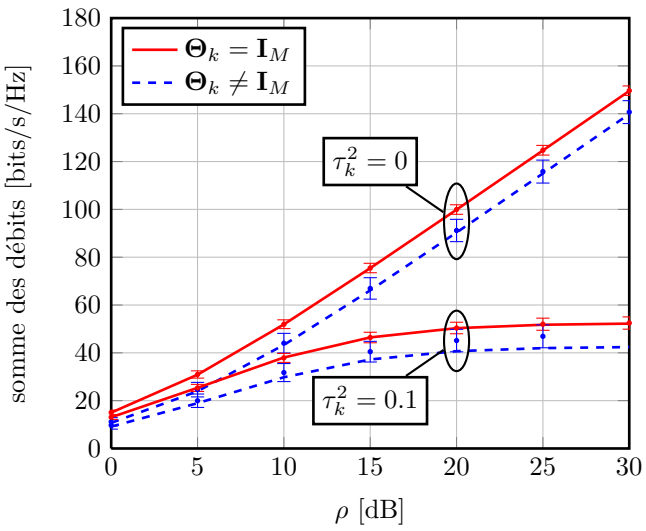

FIGURE 4: ZF, la somme des débits en fonction de SNR avec $M = 30$, $K = 15$, les résultats de simulation sont indiqués par des cercles avec l'écart type.

4 MISO BC à Grandes Dimensions et Précodage Linéaire : Applications

Cette section présente différentes applications de l'approximation du SINR proposée dans la section précédente. Ces applications montrent que les approximations pour des systèmes larges mènent à des résultats profonds qui se révèlent proches de l'optimum même pour des dimensions petites. Remarquez que les applications aux systèmes TDD/FDD à grandes dimensions sont présentées dans les Section 4.3 et 4.4 dans Chapitre 4.

4.1 Régularisation Optimale

Le paramètre de régularisation $\bar{\alpha}^\star$ qui maximise (32) est défini comme

$$\bar{\alpha}^\star = \arg\max_{\alpha>0} \sum_{k=1}^{K} \log\left(1+\bar{\gamma}_{k,\mathrm{rzf}}\right). \tag{34}$$

Généralement, le problème (34) est non-convexe en α et la solution doit être calculer numériquement par une recherche exhaustive mono-dimensionnelle.

Nous considérons le cas de corrélation identique $\mathbf{\Theta}_k = \mathbf{\Theta}\ \forall k$ et supposons que la distorsion τ_k^2 de la CSIT $\hat{\mathbf{h}}_k$ est également identique parmi les utilisateurs, car leurs canaux sont statistiquement équivalents. Dans ces conditions, $\mathbf{P} = \frac{1}{K}\mathbf{I}_K$ maximise (32) et l'optimisation (34) a la solution suivante.

Proposition 2. *Soit $\mathbf{\Theta}_k = \mathbf{\Theta}$, $0 \le \tau_k = \tau < 1\ \forall k$ et $p_k = P/K\ \forall k$. Le SINR approximé $\bar{\gamma}_{k,\mathrm{rzf}}$ de l'utilisateur k pour précodage RZF est maximiseé pour un paramètre de régularisation $\alpha \triangleq \bar{\alpha}^\star$, qui est une solution positive de la fonction implicite*

$$\bar{\alpha}^\star = \frac{\left[1+\nu(\bar{\alpha}^\star)+\tau^2\rho\frac{e_{22}(\bar{\alpha}^\star)}{e_{12}(\bar{\alpha}^\star)}\right]\frac{1}{\beta\rho}}{(1-\tau^2)[1+\nu(\bar{\alpha}^\star)]+\tau^2\nu(\bar{\alpha}^\star)[1+e(\bar{\alpha}^\star)]^2} \tag{35}$$

où $e(\alpha)$ est définie dans (22) *et $\nu(\alpha)$ s'écrit*

$$\nu(\alpha) = \frac{1}{(1+e)e_{22}}\frac{e_{13}}{e_{12}}\left[\frac{e_{22}}{e_{12}} - \frac{e_{23}}{e_{13}}\right] \tag{36}$$

avec e_{ij} définie dans (24).

Démonstration de la Proposition 2. La démonstration se trouve en Appendice D. □

En cas de CSIT parfaite ($\tau^2 = 0$), Proposition 2 se simplifie et nous obtenons la solution bien-connue $\bar{\alpha}^\star = \frac{1}{\beta\rho}$, qui a été calculée précédemment dans [10, 25, 27]. Comme mentionné dans [10], pour *M grand*, le précodeur RZF-CDA est identique au précodeur MMSE dans [17, 64]. Les auteurs dans [27] ont montré que, en cas de CSIT parfaite, $\bar{\alpha}^\star$ est indépendant de la corrélation $\mathbf{\Theta}$. Par contre, en cas de CSIT *imparfaite* ($\tau^2 \neq 0$), le paramètre de régularisation (35) dépend

de la corrélation au travers des paramètres $e(\alpha)$ et $e_{ij}(\alpha)$. Pour des canaux decorrélés ($\mathbf{\Theta} = \mathbf{I}_M$), nous avons $e_{12} = e_{22}$ et $\nu(\alpha) = 0$ et donc la solution explicite

$$\bar{\alpha}^\star = \left(\frac{1+\tau^2\rho}{1-\tau^2}\right)\frac{1}{\beta\rho}. \tag{37}$$

Remarquez que $\bar{\alpha}^\star$ dans (37) est la solution *unique* positive de (34) et la démonstration se trouve en Appendice E.

En cas de CSIT imparfaite ($\tau^2 > 0$), le précodeur RZF-CDA et le précodeur MMSE avec paramètre de régularisation $\alpha_{\text{MMSE}} = \tau^2\beta^{-1} + 1/(\beta\rho)$ [64] ne sont plus identiques, même pour M, K asymptotiquement grands. Contrairement au cas de CSIT parfaite, $\bar{\alpha}^\star$ dépend maintenant de la matrice de corrélation $\mathbf{\Theta}$ par $e(\alpha)$ et $e_{ij}(\alpha)$.

L'impact du paramètre de régularisation sur la somme des débits ergodique est répresenté dans Figures 5 et 6.

Dans Figure 5, nous comparons la performance de la somme des débits ergodique pour différents paramètres de régularisation α avec une distorsion de CSIT $\tau_k^2 = \tau^2 = 0.1\ \forall k$. La borne supérieure $\alpha = \alpha^\star$ est obtenue en optimisant α pour chaque réalisation de canal, alors que $\alpha^\star_{\text{erg}}$ maximise la somme des débits ergodique. Nous observons que la performance de $\alpha^\star_{\text{erg}}$ et $\bar{\alpha}^\star$ est proche de l'optimum $\alpha^\star$. En plus, si la qualité de canal τ^2 est inconnue, et alors supposée égale à zéro, la performance se dégrade dès que τ^2 domine sur la variance de bruit σ^2 et s'approche de la somme des débits de précodage ZF pour fort SNR. Nous concluons (i) que l'adaptation du paramètre de régularisation donne une augmentation significative de la performance et (ii) que la performance du précodeur RZF-CDA proposé avec $\bar{\alpha}^\star$ est proche de l'optimum même pour des petites dimensions.

Dans Figure 6, nous évaluons l'impact de la corrélation en transmission dans le calcul de $\bar{\alpha}^\star$ sur la somme des débits. Pour cela, nous utilisons le modèle exponentiel, c'est-à-dire

$$[\mathbf{\Theta}]_{ij} = v^{|i-j|}.$$

Nous comparons deux précodeur différents : Un premier précodeur appelé « RZF common correlation aware » (RZF-CCA) qui prend en compte la corrélation de canal en calculant α selon (35). Le deuxième précodeur, appelé « RZF common correlation unaware » (RZF-CCU), ne prend pas en compte $\mathbf{\Theta}$ et calcule α selon (4.4). Nous observons que, pour une forte corrélation, c'est-à-dire $v = 0.9$, le précodeur RZF-CCA surpasse le précodeur RZF-CCU pour moyen et fort SNR alors que la performance des deux précodeurs est la même pour faibles SNRs. Alors nous concluons qu'il est favorable de prendre la corrélation en compte, notamment pour forte corrélation et forts SNRs.

4.2 Optimisation de Nombre d'Utilisateurs et Allocation de Puissance

Dans cette section nous traitons deux problèmes : (i) la détermination de nombre d'utilisateurs qui maximise la somme des débits par antenne d'émission pour un

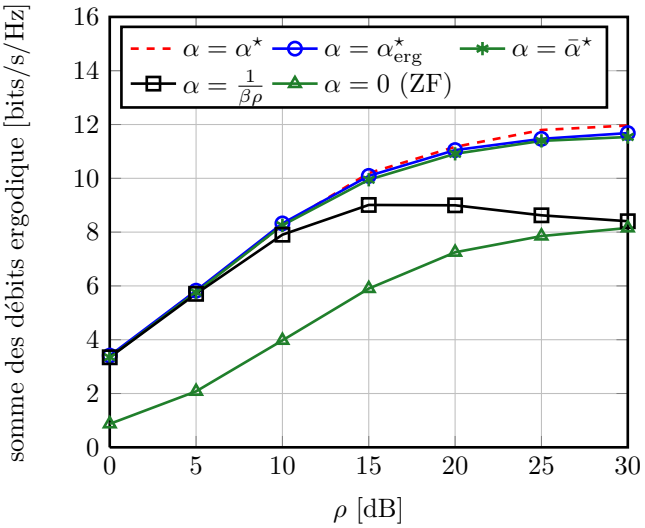

FIGURE 5: RZF, la somme des débits ergodique en fonction de SNR avec $M = K = 5$, $\mathbf{\Theta}_k = \mathbf{I}_M \ \forall k$, $\mathbf{P} = \frac{1}{K}\mathbf{I}_K$ et $\tau^2 = 0.1$.

M fixe et (ii) l'optimisation de la distribution de puissance parmi un ensemble d'utilisateurs *donné* avec qualités de CSIT différentes.

Considérons le problème (i). D'une façon intuitive, un nombre d'utilisateurs optimal $K^\star$ existe car servir plus d'utilisateurs crée plus d'interférence ce qui, de fait, réduit les débits d'utilisateurs. Au moment où la perte accumulée de débit, à cause de l'interférence rajoutée en servant un utilisateur de plus, va être plus grande que le gain en somme des débits et donc la somme des débits va se dégrader. En l'occurrence, nous considérons un scénario équitable où l'approximation du SINR est identique pour chaque utilisateur. Dans ce cas, la solution (approximée) s'écrit sur une forme fermée pour le précodeur ZF.

Dans le problème (ii), nous optimisons la matrice d'allocation de puissance $\mathbf{P}$ pour un K donné. Plus précisément, nous supposons une corrélation identique ($\mathbf{\Theta}_k = \mathbf{\Theta}\ \forall k$) avec qualités de CSIT τ_k^2 *différentes*, car dans ce cas la distribution de puissance optimale (approximée) $\mathbf{P}^\star$ est la solution d'un algorithme classique de *water-filling*.

Nombre optimal d'utilisateur

Considérons le problème consistant à trouver la charge optimale du système $\bar{\beta}^\star = \frac{M}{K^\star}$ qui maximise la somme des débits approximée par antenne d'émission pour un M fixe, c'est-à-dire

$$\bar{\beta}^\star = \arg\max_{\beta} \frac{1}{\beta}\frac{1}{K}\sum_{k=1}^{K} \log\left(1+\bar{\gamma}_k\right), \tag{38}$$

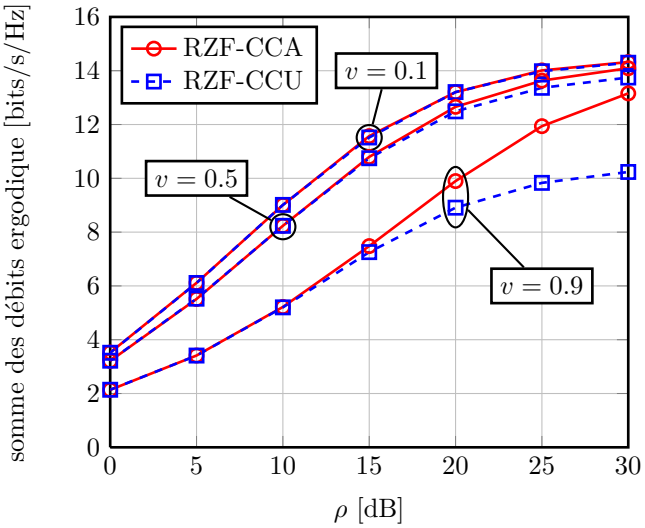

FIGURE 6: La somme des débits ergodique en fonction de SNR, l'impact de corrélation avec $M = K = 5$, $\mathbf{P} = \frac{1}{K}\mathbf{I}_K$ et $\tau_k^2 = 0.05$.

où $\bar{\gamma}_k$ désigne $\bar{\gamma}_{k,\text{zf}}$ avec $\beta > 1$ ou $\bar{\gamma}_{k,\text{mf}}$, $\bar{\gamma}_{k,\text{rzf}}$ avec $\beta \geq 1$. En général, la solution de (38) doit être calculée numériquement par une recherche exhaustive mono-dimensionnelle. Par contre, en cas de précodage ZF et antennes decorrélées, le problème (38) a une solution en forme fermée donnée dans la proposition suivante.

Proposition 3. *Soit $\mathbf{\Theta}_k = \mathbf{I}_M$, $\tau_k = \tau \ \forall k$ et $\mathbf{P} = \frac{P}{K}\mathbf{I}_K$, la charge du système $\bar{\beta}^\star$ qui maximise la somme des débits par antenne d'émission s'écrit*

$$\bar{\beta}^\star = \left(1 - \frac{1}{a}\right)\left(1 + \frac{1}{\mathcal{W}(x)}\right), \tag{39}$$

où $a = \frac{1-\tau^2}{\tau^2 + \frac{1}{\rho}}$, $x = \frac{a-1}{e}$ et $\mathcal{W}(x)$ est la fonction W de Lambert définie par $z = \mathcal{W}(z)e^{\mathcal{W}(z)}$, $z \in \mathbb{C}$.

Démonstration de la Proposition 3. La démonstration se trouve en Section 4.2.1. □

Pour $\tau \in [0, 1]$, $\beta > 1$ nous avons $w \geq -1$ et $x \geq -e^{-1}$. Dans ce cas, $\mathcal{W}(x)$ est une fonction bien définie. Si $\tau^2 = 0$, nous obtenons les résultats dans [22], bien que dans [22] ils ne sont pas donnés en forme fermée. Remarquez que pour $\tau^2 = 0$, nous avons $\lim_{\rho\to\infty} \bar{\beta}^\star = 1$, c'est-à-dire la charge optimale du système tend vers 1 pour fort SNR. En plus, remarquez qu'en pratique, seuls des nombres entiers de $M/\bar{\beta}^\star$ sont possible.

Figure 7 compare le nombre d'utilisateurs optimal $\bar{K}^\star = M/\bar{\beta}^\star$ dans (39) à $K^\star$ obtenu en choisissant le $K \in \{1, 2, \ldots, M\}$ tel que la somme des débits

ergodique est maximisée. En revanche, Figure 8 illustre l'impact d'un nombre d'utilisateurs sous-optimal sur la somme des débits ergodique du système.

De la Figure 7 nous observons que (i) les résultats approximés $\bar{K}^\star$ sont très proches des résultats de simulation même pour des petites dimensions, (ii) $(K^\star, \bar{K}^\star)$ augmente avec le SNR et (iii), pour $\tau^2 \neq 0$, $(K^\star, \bar{K}^\star)$ sature pour fort SNR vers une valeur inférieure à M. Alors, pour une CSIT imparfaite, il n'est plus optimal de servir le maximum d'utilisateur $K = M$ pour un SNR asymptotiquement fort. Au lieu de cela, en fonction de τ^2, un nombre d'utilisateurs $K < M$ devrait être servie même pour un fort SNR ce qui implique un gain de multiplexage du système réduit. L'impact de la charge du système sur la somme des débits est représenté dans Figure 8.

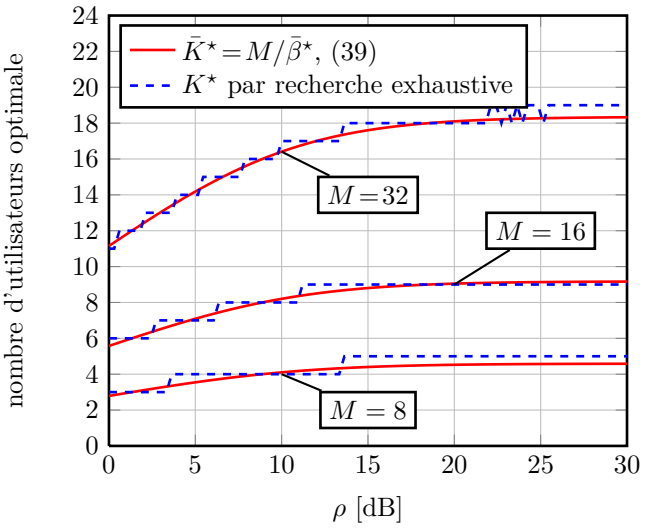

FIGURE 7: ZF, nombre d'utilisateurs maximisant la somme de débits en fonction de SNR avec $\mathbf{\Theta}_k = \mathbf{I}_M \ \forall k$, $\mathbf{P} = \frac{1}{K}\mathbf{I}_K$ et $\tau^2 = 0.1$.

De la Figure 8 nous observons que, (i) la solution approximée $\bar{K}^\star$ pour M grand atteint la plupart de la somme des débits et (ii) une adaptation du nombre d'utilisateurs est favorable comparé à un K fixe. Ensuite, de la Figure 7, nous identifions $K = 8$ comme la solution optimale pour moyens SNRs et, comme prévu, la performance est optimale pour moyens SNR et sous-optimale pour faible et fort SNR. De la Figure 7 il est évident que $K = 4$ est fortement sous-optimal pour moyens et forts SNRs et nous observons une perte significative. Par conséquence le nombre d'utilisateurs doit être adapté aux conditions de canal et la solution approximée $\bar{K}^\star$ est une bonne choix pour déterminer le nombre d'utilisateurs optimal dans le système.

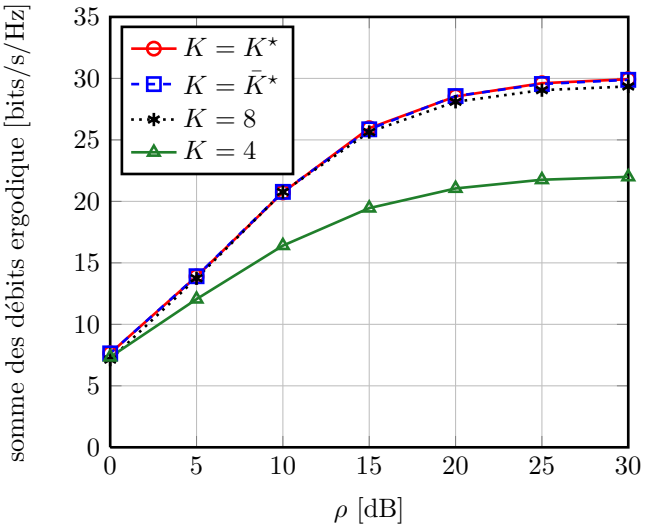

FIGURE 8: ZF, la somme des débits ergodique pour différents nombre d'utilisateurs avec $M = 16$, $\mathbf{\Theta}_k = \mathbf{I}_M \ \forall k$, $\mathbf{P} = \frac{1}{K}\mathbf{I}_K$ et $\tau^2 = 0.1$.

Optimisation de puissance avec corréllation identique

Sous l'hypothèse 2, nous avons $\lim_{M\to\infty} p_k/P = 0 \ \forall k$ et alors avec les corollaires 3.1, 3.7 et 3.9, la somme des débits approximée (32) pour précodage MF, RZF et ZF s'écrit

$$\hat{R}_{\text{sum}} = \sum_{k=1}^{K} \log\left[1 + p_k \bar{\nu}_k(\tau_k)\right], \tag{40}$$

avec $\bar{\nu}_k = \bar{\gamma}_k/p_k$, où $\bar{\gamma}_k$ est un équivalent déterministe du SINR avec précodage MF, RZF ou ZF et la seule dépendance sur l'utilisateur k est causée par τ_k. Les puissances $\bar{p}_k^\star$ qui maximisent (40), conformément à $\sum_{k=1}^{K} p_k \leq P$, $p_k \geq 0 \ \forall k$, sont données par la solution classique de *water-filling* [65]

$$\bar{p}_k^\star = \left[\mu - \frac{1}{\bar{\nu}_k}\right]^+, \tag{41}$$

où $[x]^+ \triangleq \max(0, x)$ et μ est le niveau choisi tel que $\sum_{k=1}^{K} p_k = P$. Pour $\tau_k^2 = \tau^2 \ \forall k$, les puissances d'utilisateurs optimales (41) sont toutes identiques, c'est-à-dire $\bar{p}_k^\star = \bar{p}^\star = P/K$ et $\bar{\mathbf{P}}^\star \triangleq \text{diag}(\bar{p}_1^\star, \ldots, \bar{p}_K^\star) = \frac{P}{K}\mathbf{I}_K$. Néanmoins, dans ce cas, une adaptation du nombre d'utilisateurs peut être avantageuse comme discuté en Section 4.2.

Dans les Figures 9 et 10 nous comparons la somme des débits ergodique avec précodage RZF-CDU pour trois allocations de puissance différentes : (i) allocation de puissance optimale $\mathbf{P} = \bar{\mathbf{P}}^\star$ dans (41), (ii) allocation de puissance uniforme $\mathbf{P} = \frac{P}{K}\mathbf{I}_K$ et (iii) toute la puissance disponible est distribuée

à l'utilisateur $k_{\min}$ avec distorsion de canal minimale, c'est-à-dire $p_{k_{\min}} = P$ avec $k_{\min} = \arg\min_{k=1,\ldots,K}\{\tau_k^2\}$. Du fait que la performance du système est limitée par l'interférence à fort SNR et pour tout M, K donné, l'allocation de puissance est optimale pour des SNRs asymptotiquement forts. Par contre, pour $M, K \to \infty$ la distribution de puissance (i) est optimale pour tout SNR sous l'Hypothèse 2. Mais remarquez que l'Hypothèse 2 exclue l'allocation de puissance (iii). Alors tant que l'Hypothèse 2 est vraie, l'allocation de puissance optimale est donnée par $\mathbf{P} = \bar{\mathbf{P}}^{\star}$ pour tout M large. Nous choisissons deux distributions de qualité de CSIT différentes : (i) la variation de la qualité parmi les utilisateurs est significative, c'est-à-dire les τ_k^2 sont uniformément distribués entre 0.05 et 0.8 ($\tau_k^2 = 0.05 + \frac{k-1}{K-1}(0.8 - 0.05)$) et (ii) les qualités de CSIT ne sont pas considérablement différentes, c'est-à-dire les τ_k^2 sont uniformément distribués entre 0.2 et 0.3 ($\tau_k^2 = 0.2 + \frac{k-1}{K-1}(0.3 - 0.2)$).

Dans la Figure 9, nous observons un gain significatif pour tout SNR avec allocation de puissance optimale comparé à l'allocation uniforme. Si la variation des qualités de CSIT est petite ($M = 3$), le gain est négligeable à fort SNR. En général, quand le SNR augmente, les SINRs se différencient de plus en plus en fonction de τ_k^2. Par conséquent, il peut être optimal de n'est pas servir les utilisateurs avec la qualité la plus mauvaise parmi tout les utilisateurs quand le SNR augmente. Cela explique pourquoi le gain en somme des débits est plus élévé à forts SNRs qu'à faibles SNRs. En plus, pour forts SNRs, l'allocation de puissance (iii) est plus performante que (i), qui donne une solution imprécise pour ces petites dimensions. Quand les dimensions augmentent, Figure 10, les résultats changent : maintenant l'allocation (i) est plus performante que (iii). Remarquez que la somme des débits se dégrade rapidement à forts SNRs à cause de précodeur RZF-CDU qui ne tient pas en compte la CSIT imparfaite. Par conséquent, si l'Hypothèse 2 est vraie, la performance de $\bar{\mathbf{P}}^{\star}$ va toujours être plus élévée que $p_{k_{\min}} = P$ pour M, K suffisamment grands.

Nous concluons que l'allocation de puissance optimale proposée dans (41) atteint un gain significatif comparé à une distribution de puissance uniforme, notamment pour forts SNRs et quand les qualités de CSIT varient considérablement parmi les utilisateurs.

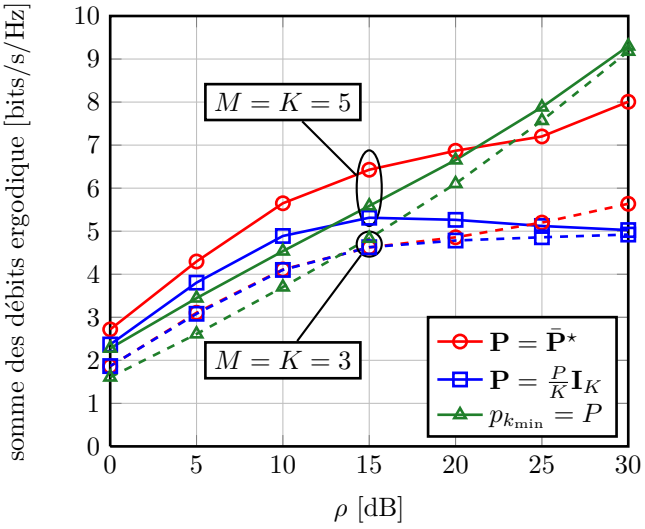

FIGURE 9: RZF-CDU, somme des débits ergodique en fonction de SNR pour différentes allocation de puissance avec $\alpha = 1/\rho$, $\mathbf{\Theta}_k = \mathbf{I}_M$, $P = 1$, $\tau_k^2 = 0.05 + \frac{k-1}{K-1}(0.8 - 0.05)$ pour $M = 5$ et $\tau_k^2 = 0.2 + \frac{k-1}{K-1}(0.3 - 0.2)$ pour $M = 3$

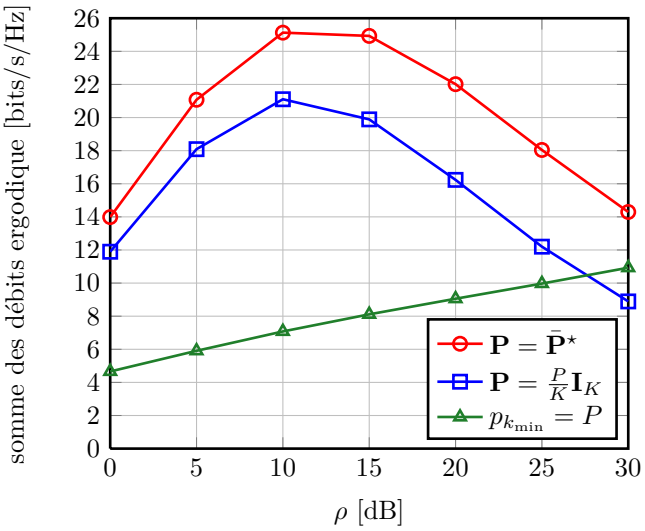

FIGURE 10: RZF-CDU, somme des débits ergodique en fonction de SNR pour différentes allocation de puissance avec $\alpha = 1/\rho$, $\mathbf{\Theta}_k = \mathbf{I}_M$ $\forall k$, $P = 1$, $M = K = 30$ et $\tau_k^2 = 0.05 + \frac{k-1}{K-1}(0.8 - 0.05)$.

5 Précodage Unitaire avec Module Constant

La technique de précodage unitaire avec module constant (CUBF) est motivée par des contraintes sur les récepteurs radio et par un ordonnancement d'utilisateur amélioré. Il est plus efficace d'avoir des puissances équilibrées sur les antennes d'émission, car tous les amplificateurs de puissance peuvent être dimensionés pour la même gamme dynamique. Des variations d'amplitude différentes du signal de transmission, à cause de l'opération de précodage, nécessitent une gamme linéaire d'amplificateur de puissance plus grande, ce qui les rend peu efficaces et plus chers. De plus, la propriété de la matrice de précodage d'être unitaire, permet aux utilisateurs de calculer la puissance d'interférence multi-utilisateur (MU) précisément. L'information sur la puissance d'interférence MU peut être utilisée dans les récepteurs pour améliorer leur capacité de décodage et donc ils peuvent supportés un débit plus élevé. En outre, un estimé du SINR plus précis à la réception améliore la performance de l'algorithme d'ordonnancement d'utilisateur. Par exemple, dans [74] les auteurs proposent d'exploiter l'interférence MU au récepteur pour augmenter la performance. Pour ces raisons, les normes LTE et LTE-A définissent des dictionnaires de matrices unitaires avec module constant dans leur mode MU-MIMO.

Le problème de dimensionner et paramétrer des dictionnaires unitaires optimaux pour MU-MISO a été traité dans [76]. Néanmoins, dans cette thèse, nous supposons que l'émetteur calcule le précodeur unitaire optimal basé sur la CSIT disponible. Une solution en forme fermée du précodeur *unitaire* maximisant la somme des débits pour $M = 2$ a été obtenue dans [77]. Pour M arbitraire, les auteurs dans [78] proposent un algorithme itératif basé sur des rotations de Givens successives pour calculer le précodeur unitaire optimal. Cet algorithme est plutôt complexe. Alors, nous proposons d'appliquer un algorithme efficace de la plus profonde descente dans l'espace riemannien de [79, 80] pour obtenir un précodeur linéaire qui maximise la somme des débits. Introduire la contrainte de module constant sur les entrées du précodeur unitaire réduit fortement les degrés de liberté pour l'optimisation du précodeur. Nous étudions le problème consistant à trouver la matrice CUBF qui maximise la somme des débits en utilisant une description de matrices de Hadamard complexe basée sur une relation d'équivalence [81].

5.1 Précodage Unitaire

Considérons $M = K$ et soit $\mathbf{H}$ la matrice de canal avec des entrées i.i.d. gaussiennes de moyenne nulle et de variance 1. La matrice de précodage *unitaire* est $\mathbf{G}_{\text{ubf}} = [\mathbf{g}_1, \ldots, \mathbf{g}_K] \in \mathbb{C}^{M \times K}$, $\mathbf{G}_{\text{ubf}}^{\mathsf{H}} \mathbf{G}_{\text{ubf}} = \mathbf{G}_{\text{ubf}} \mathbf{G}_{\text{ubf}}^{\mathsf{H}} = \mathbf{I}$. Sous ces hypothèses et avec allocation de puissance uniforme ($p_k = P/K \ \forall k$) le SINR $\gamma_{k,\text{ubf}}$ de l'utilisateur k s'écrit [82]

$$\gamma_{k,\text{ubf}} = \frac{\nu_k^2}{\xi_k + 1 - \nu_k^2}, \tag{42}$$

où $\xi_k = \frac{K\sigma^2}{P\|\mathbf{h}_k\|_2^2}$, $\nu_k = |\bar{\mathbf{h}}_k^{\mathsf{H}}\mathbf{g}_k| \in [0,1]$ est l'alignement entre la direction de canal $\bar{\mathbf{h}}_k = \frac{\mathbf{h}_k}{\|\mathbf{h}_k\|}$ et le vecteur de précodage $\mathbf{g}_k$ de l'utilisateur k. La matrice de précodage unitaire $\mathbf{G}_{\text{ubf}}^{\star}$ maximisant la somme des débits est la solution du problème d'optimisation suivant.

$$\mathbf{G}_{\text{ubf}}^{\star} = \arg\max_{\mathbf{G}_{\text{ubf}}} \{R_{\text{sum}}\} \tag{43}$$

$$\text{tel que} \quad \mathbf{G}_{\text{ubf}}^{\mathsf{H}}\mathbf{G}_{\text{ubf}} = \mathbf{I}_K, \tag{44}$$

où R_{sum} est définie dans (4). Ceci est un problème d'optimisation non-convexe avec des contraintes non-linéaires. Une solution en forme fermée, pour $M = 2$, a été proposée dans [77]. Dans [78] ce problème a été traité avec un algorithme itérative basé sur des rotations de Givens successives. Par contre, nous utilisons le « *self-tuning Riemannian steepest descent algorithm* » [79, Table II], détaillé dans Table 1, pour résoudre le problème d'optimisation dans (43). L'entrée (i,j) de la matrice jacobienne $\mathbf{\Gamma} = \nabla_{\mathbf{G}_{\text{ubf}}} R_{\text{sum}}$ s'écrit

$$[\mathbf{\Gamma}]_{ij} = \frac{\partial R_{\text{sum}}}{\partial [\mathbf{G}_{\text{ubf}}^{*}]_{ij}}. \tag{45}$$

La matrice jacobienne $\mathbf{\Gamma}$ de la fonction objectif dans (4) est donnée par

$$\mathbf{\Gamma} = [c_1\mathbf{h}_1\mathbf{h}_1^{\mathsf{H}}\mathbf{g}_1, \ldots, c_K\mathbf{h}_K\mathbf{h}_K^{\mathsf{H}}\mathbf{g}_K] \tag{46}$$

$$\text{avec} \quad c_k = \left(\xi_k + 1 - \nu_k^2\right)^{-1}. \tag{47}$$

La direction du gradient dans l'espace riemannien Φ est définie par [79]

$$\Phi = \mathbf{\Gamma}\mathbf{G}_{\text{ubf}}^{\mathsf{H}} - \mathbf{G}_{\text{ubf}}\mathbf{\Gamma}^{\mathsf{H}}. \tag{48}$$

Suivant le gradient Φ, l'algorithme dans Table 1 est garanti de converger vers un maximum local. Quand seulement une CSIT imparfaite $\hat{\mathbf{H}}$ est disponible à l'émetteur, alors l'algorithme d'optimisation prend $\hat{\mathbf{H}}$ en entrée au lieu de $\mathbf{H}$. Nous utilisons ce algorithme pour comparer la performance du précodeur unitaire au précodeur unitaire avec module constant.

5.2 Précodage Unitaire avec Module Constant

Cette section décrit les matrices CUBF en appliquant une description des matrices complexes de Hadamard.

Description des matrices complexes de Hadamard

Premièrement, nous introduisons plusieurs définitions qui nous servent plus tard pour paramétrer les matrices CUBF $\mathbf{G}_{\text{cubf}}$.

Définition 1. *Une matrice carrée* $\mathbf{A}$ *de taille* M *avec entrées de module constant* $|a_{ij}|^2 = \frac{1}{M}$; $i,j = 1,\ldots,M$, *est appelée matrice de Hadamard normalisée si*

$$\mathbf{A}\mathbf{A}^{\mathsf{H}} = \mathbf{I}_M. \tag{49}$$

ENTRÉE : $\mathbf{H}$, P, σ^2
SORTIE : $\mathbf{G}_{\text{ubf}}^{\star}$

Étape 1 : `# Initialisation`
$j = 0$, $\mathbf{G}_{\text{ubf}}^{(j)} = \mathbf{I}_M$ et $\mu = 1$
Étape 2 : `# Gradient de la somme des débits dans l'espace euclidien`
$\mathbf{\Gamma}^{(j)} = [c_1 \mathbf{h}_1 \mathbf{h}_1^{\mathsf{H}} \mathbf{g}_1^{(j)}, \ldots, c_K \mathbf{h}_K \mathbf{h}_K^{\mathsf{H}} \mathbf{g}_K^{(j)}]$ avec
$c_k^{(j)} = \left(\xi_k + 1 - (\nu_k^{(j)})^2 \right)^{-1}$
Étape 3 : `# Direction de gradient dans l'espace riemannien`
$\Phi^{(j)} = \mathbf{\Gamma}^{(j)} (\mathbf{G}_{\text{ubf}}^{(j)})^{\mathsf{H}} - \mathbf{G}_{\text{ubf}}^{(j)} (\mathbf{\Gamma}^{(j)})^{\mathsf{H}}$
Étape 4 :
Évaluer $\frac{1}{2} \Re(\text{tr} \Phi^{(j)} (\Phi^{(j)})^{\mathsf{H}})$, si suffisamment petit, STOP et $\mathbf{G}_{\text{ubf}}^{\star} = \mathbf{G}_{\text{ubf}}^{(j)}$
Étape 5 : `# Déterminer les matrices de rotations`
$\mathbf{R}^{(j)} = \exp(\mu \Phi^{(j)})$, $\mathbf{T}^{(j)} = \mathbf{R}^{(j)} \mathbf{R}^{(j)}$
Étape 6 :
while $|R_{\text{sum}}(\mathbf{G}_{\text{ubf}}^{(j)}) - R_{\text{sum}}(\mathbf{T}^{(j)} \mathbf{G}_{\text{ubf}}^{(j)})| \geq \frac{\mu}{2} \Re(\text{tr} \Phi^{(j)} (\Phi^{(j)})^{\mathsf{H}})$ **do**
  $\mathbf{R}^{(j)} = \mathbf{T}^{(j)}$, $\mathbf{T}^{(j)} = \mathbf{R}^{(j)} \mathbf{R}^{(j)}$, $\mu = 2\mu$
end while
Étape 7 :
while $|R_{\text{sum}}(\mathbf{G}_{\text{ubf}}^{(j)}) - R_{\text{sum}}(\mathbf{R}^{(j)} \mathbf{G}_{\text{ubf}}^{(j)})| < \frac{\mu}{4} \Re(\text{tr} \Phi^{(j)} (\Phi^{(j)})^{\mathsf{H}}))$ **do**
  $\mathbf{R}^{(j)} = \exp(\mu \Phi^{(j)})$, $\mu = \frac{\mu}{2}$
end while
Étape 8 : `# Mise à jour`
$\mathbf{G}_{\text{ubf}}^{(j+1)} = \mathbf{R}^{(j)} \mathbf{G}_{\text{ubf}}^{(j)}$, $j = j + 1$, aller à la **Étape 2**

TABLE 1: « Self-tuning Riemannian steepest descent algorithm » emprunté de [79, Table II] et appliqué pour calculer le précodeur unitaire $\mathbf{G}_{\text{ubf}}^{\star}$ maximisant la somme des débits.

L'ensemble des matrices complexes de Hadamard normalisées de taille M est $\mathcal{H}_M$. Dans le cas sans normalisation : $\mathbf{A}\mathbf{A}^{\mathsf{H}} = M \, \mathbf{I}_M$.

Définition 2. *[81, Définition 2.2] Les matrices complexes de Hadamard* $\{\mathbf{A}, \tilde{\mathbf{A}}\} \in \mathcal{H}_M$ *sont équivalentes, écrit* $\mathbf{A} \cong \tilde{\mathbf{A}}$*, si il existe des matrices unitaires diagonales* $\mathbf{D}_{\text{r}}, \mathbf{D}_{\text{c}}$ *et des matrices de permutation* $\mathbf{P}_{\text{r}}, \mathbf{P}_{\text{c}}$ *telles que*[1]

$$\mathbf{A} = \mathbf{D}_{\text{r}} \mathbf{P}_{\text{r}} \tilde{\mathbf{A}} \mathbf{P}_{\text{c}} \mathbf{D}_{\text{c}}. \tag{50}$$

[1]Dans cette définition les opérations transposées et complexe conjuguées sont exclues car ils sont inutiles dans l'application de précodage.

Il existe $M!$ matrices de permutation de lignes et colonnes $\mathbf{P}_{\mathrm{r}}$ et $\mathbf{P}_{\mathrm{c}}$, respectivement. La classe d'équivalence de $\mathbf{A} \in \mathcal{H}_M$ correspondante à la relation d'équivalence (50) *est*

$$\mathbf{Q}_M(\mathbf{A}) = \{\mathbf{B} \in \mathcal{H}_M | \mathbf{A} \cong \mathbf{B}\}. \tag{51}$$

Nous appelons $\mathcal{G}_M = \mathcal{H}_M/_{\cong}$, l'ensemble des classes de équivalence $\mathcal{G}_M$.

Dans la section suivante nous présentons l'ensemble $\mathcal{G}_M$ pour plusieurs dimensions M.

Classes de équivalence

Curieusement, l'ensemble complet des classes d'équivalence $\mathcal{G}_M$ est seulement connue pour $M < 6$. Le problème consistant à trouver *toutes* les classes d'équivalence pour des dimensions $M \geq 6$ reste ouvert et un catalogue des classes d'équivalence connues est disponible dans [81]. Dans ce qui suit nous présentons brièvement un aperçu sur les classes d'équivalence (sans normalisation) pour $M = 2, \ldots, 5$.

$M = 2$ Il existe seulement une classe d'équivalence $\mathcal{G}_2 = \{\mathbf{Q}_2(\mathbf{F}_2)\}$ avec

$$\mathbf{F}_2 = \begin{bmatrix} 1 & 1 \\ 1 & -1 \end{bmatrix}. \tag{52}$$

La matrice réelle de Hadamard correspond à la matrice de la transformée de Fourier discrète (TFD) $\mathbf{F}_2$, où $\mathbf{F}_M$ de taille M s'écrit

$$\mathbf{F}_M(m,n) = e^{-\mathbf{i}\frac{2\pi}{M}(m-1)(n-1)} \ ; \ m,n = 1,2,\ldots,M. \tag{53}$$

$M = 3$ Il existe seulement une classe d'équivalence $\mathcal{G}_3 = \{\mathbf{Q}_3(\mathbf{F}_3)\}$ égale à la matrice TFD $\mathbf{F}_3$ définie dans (53).

$M = 4$ Dans ce cas, il existe une famille *non dénombrable* de classes d'équivalence avec un paramètre libre $\mathcal{G}_4 = \{\mathbf{Q}_4(\mathbf{Q}_4^o(\theta)); \ \theta \in [\frac{\pi}{2}, \frac{3}{2}\pi)\}$, où $\mathbf{Q}_4^o(\theta)$ s'écrit

$$\mathbf{Q}_4^o(\theta) = \begin{bmatrix} 1 & 1 & 1 & 1 \\ 1 & -1 & e^{\mathbf{i}\theta} & -e^{\mathbf{i}\theta} \\ 1 & 1 & -1 & -1 \\ 1 & -1 & -e^{\mathbf{i}\theta} & e^{\mathbf{i}\theta} \end{bmatrix}. \tag{54}$$

Remarquez que la matrice réelle de Hadamard $\mathbf{Q}_4^o(\pi)$ et la matrice TFD $\mathbf{F}_4 \cong \mathbf{Q}_4^o(\frac{\pi}{2})$ sont des cas spéciaux de (54).

$M = 5$ Toutes les matrices complexes de Hadamard sont équivalentes à la matrice TFD, c'est-à-dire $\mathcal{G}_5 = \{\mathbf{Q}_5(\mathbf{F}_5)\}$.

Dans la section suivante, nous appliquons la description des matrices complexes de Hadamard correspondant à la relation d'équivalence (50) pour paramétrer les matrices CUBF qui représentent un cas spécial des matrices complexes de Hadamard.

Paramétrage des matrices CUBF dans le MISO BC

En général, l'ensemble des matrices CUBF est égal à l'ensemble des matrices complexes de Hadamard normalisées $\mathcal{H}_M$. La description de $\mathcal{H}_M$ est uniquement donnée par la relation d'équivalence (50) et les classes d'équivalence (51) et peut être utilisée pour paramétrer les matrices CUBF. Néanmoins, dépendant de la fonction objectif, quelques paramètres dans la description générale deviennent obsolètes. Si la matrice de précodage $\mathbf{G}_{\text{cubf}}$ est censée modifier le SINR de chaque utilisateur dans (42) (et donc la somme des débits), la matrice diagonale unitaire $\mathbf{D}_{\text{c}}$ dans (50) peut être négligée car elle n'altère pas le SINR (42). Par conséquent, la matrice diagonale unitaire $\mathbf{D}_{\text{r}}$ dans (50) s'écrit

$$\mathbf{D}_{\text{r}} = \text{diag}([1, e^{\mathbf{i}\varphi_1}, \ldots, e^{\mathbf{i}\varphi_{M-1}}]) \tag{55}$$

avec $\varphi_i \in [0, 2\pi),\ i = 1, 2, \ldots, M-1$.

Dans le cas $M = 4$, une autre description des matrices CUBF existe qui est basée sur la transformée d'Householder et est utilisée dans la norme 3GPP LTE [75]. L'ensemble $\mathcal{V}$ de toutes les matrices CUBF générées par la transformée d'Householder est

$$\mathcal{V} = \left\{ \mathbf{V} = \mathbf{I}_M - 2\frac{\mathbf{u}\mathbf{u}^{\mathsf{H}}}{\mathbf{u}^{\mathsf{H}}\mathbf{u}} \;\middle|\; \mathbf{u} \in \mathbf{C}^{M\times 1};\ |u_i| = 1;\ u_1 = 1 \right\}. \tag{56}$$

La construction de la matrice CUBF par la transformée d'Householder décrit seulement un sous-ensemble de toutes les matrices CUBF possibles. En effet, $\mathcal{V} \subset \mathbf{Q}_4^o(\pi) \subset \mathcal{H}_4$. Pour démontrer que $\mathcal{V} \subset \mathbf{Q}_4^o(\pi) \subset \mathcal{H}_4$, observons que $\mathbf{V} \cong \mathbf{Q}_4^o(\pi)$ car $\mathbf{Q}_4^o(\pi) = 2\mathbf{P}_{\text{r}}\mathbf{D}_1\mathbf{D}^{\mathsf{H}}\mathbf{V}\mathbf{D}\mathbf{D}_1\mathbf{P}_{\text{c}}$ avec $\mathbf{D} = \text{diag}(\mathbf{u})$, $\mathbf{D}_1 = \text{diag}([1, -1, -1, -1])$, $\mathbf{P}_{\text{c}} = [\mathbf{e}_1, \mathbf{e}_2, \mathbf{e}_4, \mathbf{e}_3]$ et $\mathbf{P}_{\text{r}} = [\mathbf{e}_1, \mathbf{e}_3, \mathbf{e}_2, \mathbf{e}_4]$, où $\mathbf{e}_i$ est la colonne i de $\mathbf{I}_M$. Alors, $\mathcal{V}$ est le sous-ensemble de $\mathcal{H}_4$ originaire de la classe d'équivalence réelle unique $\mathbf{Q}_4^o(\pi)$. Par conséquent, limiter $\mathbf{G}_{\text{cubf}} \in \mathcal{V}$ mène vers une perte de performance significative comme nous allons montrer par simulation en Section 5.3.

Optimisation des matrices CUBF

Sous l'hypothèse qu'il existe toujours $K = M$ utilisateurs et que la puissance d'émission est partagée uniformément parmi eux, nous pouvons formuler le problème d'optimisation de la façon suivante

$$\{\mathbf{D}_{\text{r}}^\star, \mathbf{Q}_M^\star, \mathbf{P}_c^\star, \mathbf{P}_r^\star\} = \underset{\mathbf{D}_{\text{r}}, \mathbf{Q}_M \in \mathcal{G}_M, \mathbf{P}_c, \mathbf{P}_r}{\arg\max} \left\{ \sum_{k=1}^{K} \log\left(1 + \gamma_k\right) \right\} \tag{57}$$

où γ_k est défini dans (42). La matrice diagonale unitaire contient $M-1$ angles. Les matrices de permutation optimales $\mathbf{P}_r^\star, \mathbf{P}_c^\star$ doivent être trouvées par une recherche exhaustive. D'une manière similaire, toutes les classes d'équivalence $\mathbf{Q}_M \in \mathcal{G}_M$ doivent être testées pour déterminer la classe optimale $\mathbf{Q}_M^\star$. Par conséquent, la matrice CUBF optimale s'écrit

$$\mathbf{G}_{\text{cubf}}^\star = \frac{1}{\sqrt{M}}\mathbf{D}_{\text{r}}^\star\mathbf{P}_r^\star\mathbf{Q}_M^\star\mathbf{P}_c^\star. \tag{58}$$

Soit $\mathcal{A} = \{\varphi_1, \ldots, \varphi_{M-1}, \theta\}$ l'ensemble des angles à optimiser. Remarquez que seulement pour $M = 4$, l'ensemble $\mathcal{A}$ contient un angle θ en plus. Après quelques manipulations algébriques, (57) prend la forme

$$\{\mathbf{D}_{\mathrm{r}}^{\star}, \mathbf{Q}_M^{\star}, \mathbf{P}_c^{\star}, \mathbf{P}_r^{\star}\} = \underset{\mathbf{D}_{\mathrm{r}}, \mathbf{Q}_M \in \mathcal{G}_M, \mathbf{P}_c, \mathbf{P}_r}{\arg\min} \left\{ \prod_{k=1}^{K} \left(1 + \xi_k - \nu_k^2\right) \right\}. \tag{59}$$

Ceci est toujours un problème d'optimisation non-convexe et un optimum global peut seulement être trouvé par une recherche exhaustive. Néanmoins, nous proposons un algorithme itératif pour calculer l'ensemble des angles optimaux $\mathcal{A}^{\star}$ en Section 5.4.1 mais une convergence globale n'est pas garantie.

5.3 Résultats Numériques

Dans cette section, nous comparons le précodeur CUBF aux dictionnaires qui contiennent des matrices CUBF (appelé CB-CUBF) tirées de la norme 3GPP LTE [75]. Dans le cas $M = 2$ le dictionnaire contient la matrice d'identité et deux rotations de la matrice TFD correspondantes à (5.9) avec $\varphi_1 = \{0, \frac{\pi}{2}\}$ et $\mathbf{P}_{\mathrm{r}} = \mathbf{P}_{\mathrm{c}} = \mathbf{I}_2$. Le dictionnaire pour 4 antennes d'émission est un sous-ensemble de $\mathcal{V}$ défini dans (5.15) généré par 16 vecteurs $\mathbf{u}$, où les entrées de $\mathbf{u}$ sont tirées de la constellation 8-PSK (« modulation par déplacement de phase ») et $u_1 = 1$. Le précodeur CB-CUBF optimal est calculé à l'émetteur par recherche exhaustive basée sur la CSIT disponible. La mesure de performance est la somme des débits ergodique $E[R_{\mathrm{sum}}]$. Pendant tout la section nous moyennons les résultats sur 10 000 réalisations du canal « Rayleigh block-fading ».

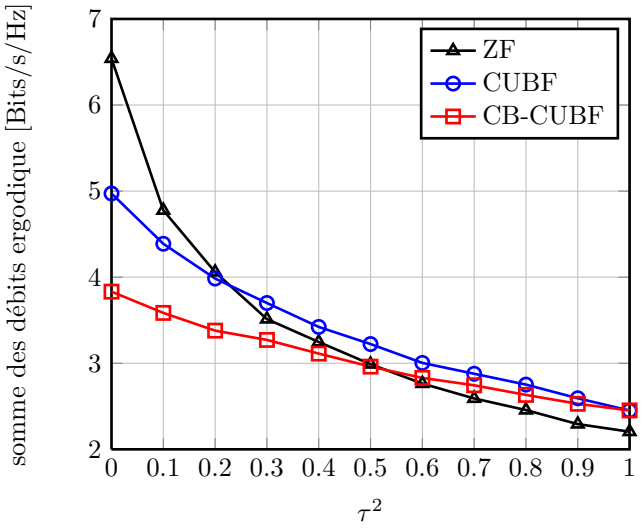

FIGURE 11: $M = K = 2$, l'impact de CSIT imparfaite sur la somme des débits ergodique avec SNR = 15 dB.

Figure 11 montre la robustesse des techniques de précodage CUBF, CB-CUBF et ZF aux erreurs dans la CSIT $\hat{\mathbf{h}}_k$. La CSIT imparfaite est modélisée comme dans (6) c'est-à-dire $\hat{\mathbf{h}}_k = \sqrt{1-\tau^2}\mathbf{z}_k + \tau\mathbf{e}_k$, où $\mathbf{z}_k$ et $\mathbf{e}_k$ ont des entrées i.i.d. gaussiennes de moyenne nulle est de variance 1. De la Figure 11 nous observons que les précodeurs CUBF et CB-CUBF ont une performance plus élevée que le précodeur ZF à partir de $\tau^2 \approx 0.22$ et de $\tau^2 \approx 0.5$, respectivement. Le précodage ZF qui atteint des performances très élevées pour CSIT parfaite, montre une forte dégradation en performance dès que la CSIT est moins précise. Dans des systèmes pratiques une telle technique est moins favorable car elle nécessite une CSIT très précise qui à son tour nécessite un haut débit sur la voie de retour.

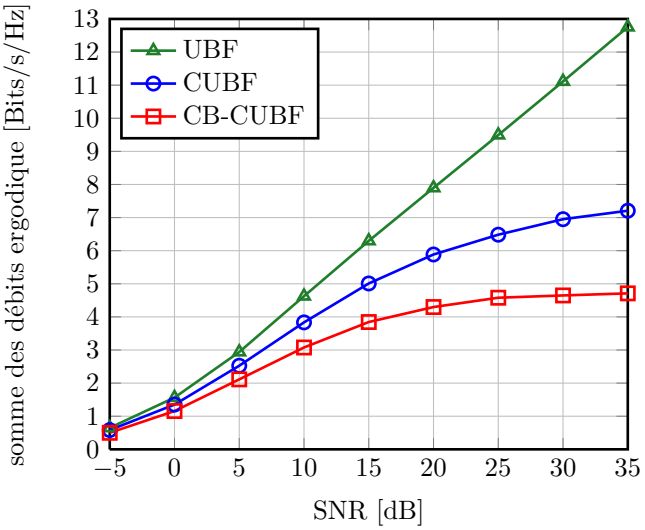

FIGURE 12: $M = K = 2$, la somme des débits ergodique en fonction de SNR.

Figures 12 et 13 présentent la somme des débits ergodique pour des systèmes de taille $M = K = 2$ et $M = K = 4$ respectivement. Nous observons que le précodeur CUBF atteint une performance plus élevée que le précodage CB-CUBF dans ces deux systèmes. Pour un SNR de 20 dB, le gain est environ 40 % et 30 %, respectivement. Ensuite, nous observons que le précodeur UBF est beaucoup plus performant que le précodage CUBF, ce qui suggère que la contrainte de module constant est une restriction très forte qui entraîne une perte de performance significative. En effet, avec précodage UBF la somme des débits ne sature pas, car les vecteurs de précodage $\mathbf{g}_k$ peuvent toujours être parfaitement alignés aux canaux $\mathbf{h}_k$, c'est-à-dire $\nu_k = 1$ et alors l'interférence de l'utilisateur k est nulle. De plus, pour le précodage CUBF, le niveau de saturation de la somme des débits est moins élevé pour $M = 4$ que pour $M = 2$. Ceci est causé par le fait que le nombre des degrés de liberté (le nombre d'angles à optimiser) de CUBF augmente beaucoup mois rapidement avec M que le nombre des

coefficients de canal. Alors, le précodeur CUBF est de plus en plus mal-adapté au canal et par conséquent le niveau d'interférence augmente résultant en un niveau de saturation de la somme de débits moins élevé. En plus, remarquez que la performance du précodeur CUBF peut être améliorée fortement si un ordonnancement d'utilisateur approprié ou des récepteurs avancés (conscient de l'interférence) sont appliqués. Néanmoins, pour limiter l'interférence MU, le récepteur nécessite une connaissance sur les vecteurs de précodage et la technique de modulation des utilisateurs interfèrents. Dans la norme actuelle LTE-A, ces informations ne sont pas signalées aux utilisateurs, ce qui les rendent difficiles à obtenir. Avec précodage unitaire, la puissance d'interférence MU peut être calculée sans connaissance sur les autres vecteurs de précodage mais la technique de modulation reste à estimer. En effet, les résultats dans [74] montrent que la performance du système augmente fortement si le récepteur prend en compte les interférences même sous des hypothèses de technique de modulation fausses.

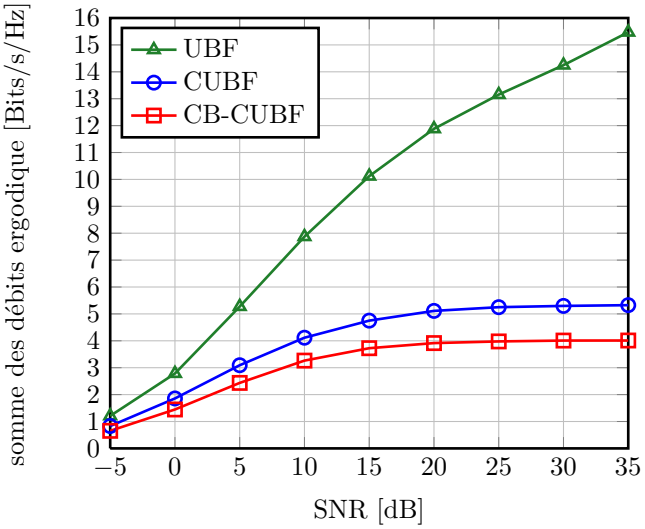

FIGURE 13: $M = K = 4$, la somme des débits ergodique en fonction de SNR.

6 Conclusion et Perspectives

Conclusion

Dans cette thèse, nous avons considéré la voie descendante du MU-MISO sous un précodage linéaire et CSIT imparfaite et nous avons analysé le comportement du système pour un grand nombre d'antennes d'émission et utilisateurs. Nous avons présenté un cadre cohérent pour l'étude de plusieurs techniques de précodage linéaire basés sur la théorie de matrices aléatoires à grandes dimensions. Les outils de la RMT nous ont permis d'envisager un modèle de canal très réaliste qui prend en compte une corrélation de canal par utilisateur ainsi que des gains de canaux individuels pour chaque lien. La performance du système dans ce type général de canal est extrêmement difficile à étudier pour des dimensions finies, mais devient possible en supposant des dimensions du système de grande taille. Grâce à la RMT à grandes dimensions, la performance du système (c'est-à-dire le SINR ou le débit) peut être approximée par un équivalent déterministe (indépendant des réalisations de canaux) qui est presque sûrement exacte étant donné que les dimensions du système sont asymptotiquement grandes avec un rapport borné. Les résultats des simulations ont montré que ces approximations sont très précises, même pour des dimensions petites du système et révèlent la dépendance déterministe de la performance du système sur plusieurs paramètres importants du système, tels que la corrélation d'émission, les puissances de signal et la qualité du SNR et de la CSIT. Appliquées à des problèmes d'optimisation pratiques, les approximations déterministes conduisent à des indications importantes sur le comportement du système, qui sont conformes avec les résultats précédents, mais vont aussi plus loin en les étendant à des modèles de canaux plus réalistes et d'autres techniques de précodage linéaire. En outre, les approximations de performances des canaux indépendants proposées peuvent être utilisées pour simuler le comportement du système sans avoir à effectuer un grand nombre de simulations Monte-Carlo. Bien que pas encore pratique, un grand nombre d'antennes d'émission devraient être largement déployées dans l'avenir, et les résultats de cette thèse pourront s'avérer d'autant plus pertinents. En outre, puisque les considérations pratiques limitent souvent les choix pour la technique de précodage, nous avons étudié le système de précodage adopté dans la norme 3GPP LTE et nous avons développé un algorithme pour évaluer la performance d'une telle technique de précodage.

Perspectives

D'un point de vue mathématique, l'équivalent déterministe de la transformée empirique de Stieltjes avec profil de variance généralisé est un résultat général et peut avoir des applications en dehors du domaine des communications mobiles.

Le cadre proposé a considéré une seule cellule isolée, mais est la base pour l'étude des multi-systèmes plus complexes. Par exemple, récemment, les résultats présentés dans cette thèse ont été appliqués pour étudier l'effet de la contamination pilote sur la performance du système dans les grands réseaux

multi-cellules. Mais d'autres scénarios peuvent être considérés aussi, par exemple l'impact de l'interférence intercellulaire peut être incluse dans le modèle du système. En outre, notre analyse peut être étendue aux systèmes multicellulaires à différents niveaux de coopération de la station de base (« coordinated beamforming »), avec une CSIT imparfaite aux stations de base en raison de la limitation de la capacité de *back haul*. De plus, il est possible d'élargir ce cadre à MU-MIMO avec un seul flux par utilisateur en considérant des filtres de réception linéaires. Au contraire, une extension à MU-MIMO avec de multiples flux par utilisateur est très compliquée et nécessite le développement d'outils de la théorie des matrices aléatoires plus avancés. Mais l'application des résultats présentés ne se limite pas aux canaux *broadcast*. Le cadre proposé peut être étendu aux canaux multi-utilisateurs de voie descendante linéairement précodés (MISO) *amplify-and forward*, où le signal est traité de façon linéaire au niveau des émetteur et relais avant d'être reçu par les utilisateurs. Enfin, la méthodologie proposée peut aussi être appliquée aux canaux d'interférence avec des filtres d'émission et de réception linéaires.

Chapter 1

Introduction

In this chapter, we introduce the communication scenario and motivate our work. We further explain in detail how this dissertation is organized and what contributions are made.

1.1 Multiuser MIMO Communications

The pioneering work in [1] and [2] revealed that the capacity of a point-to-point (single-user (SU)) multiple-input multiple-output (MIMO) channel can potentially increase linearly with the number of antennas. However, practical implementations quickly demonstrated that in most propagation environments the promised capacity gain of SU-MIMO is unachievable due to antenna correlation and line-of-sight components [3]. In a multi-user scenario, the inherent problems of SU-MIMO transmission can largely be overcome by exploiting multi-user (MU) diversity, i.e., sharing the spatial dimension not only between the antennas of a single receiver, but among multiple (non-cooperative) users. The underlying channel for MU-MIMO transmission is referred to as the MIMO broadcast channel (BC) or MU downlink channel. Although much more robust to channel correlation, the MIMO-BC suffers from inter-user interference at the receivers. This interference cannot be efficiently canceled since the receivers have no knowledge about the interfering channels nor the interfering symbol alphabet. Therefore, the advantage of transmitting to spatially separated receivers has the drawback of creating an increased interference level at the receivers. To overcome this disadvantage, the interference cancellation is shifted to the transmitter. Ideally, the transmitter can precode the signal such that the interference at the receivers is completely removed. However, to accomplish that, the transmitter requires perfect a priori knowledge of the downlink channel which,

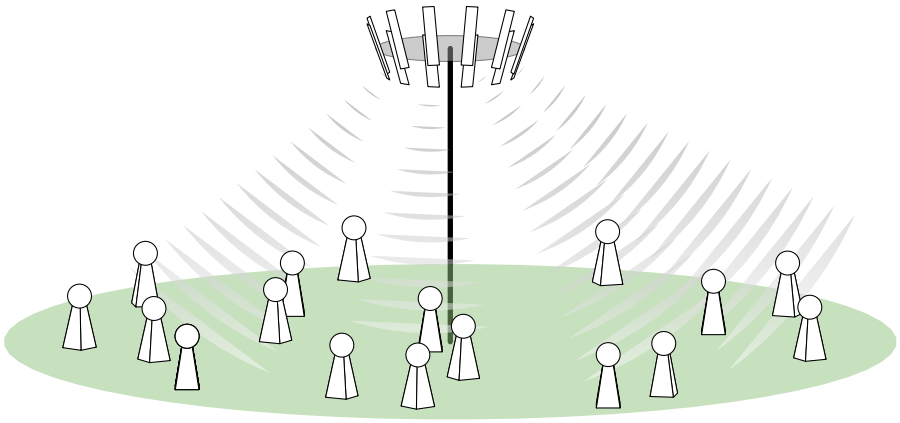

Figure 1.1: Heterogeneous MU-MIMO Single-cell Setup

in practice, is impossible to obtain. The problem of acquiring channel state information at the transmitter (CSIT) is discussed later.

Under perfect CSIT, it has been proved that dirty-paper coding (DPC) [4] is a capacity achieving precoding strategy for the Gaussian MIMO-BC [5–9]. However, the DPC precoder is non-linear and to this day too complex to be implemented efficiently in practical systems. It has been shown in [5, 10–12], that sub-optimal *linear* precoders can achieve a large portion of the BC rate region while featuring low computational complexity. Thus, a lot of research has recently focused on linear precoding strategies.

In general, the rate maximizing linear precoder has no explicit form. Several iterative algorithms have been proposed in [13–15], but no global convergence has been proved. These iterative algorithms have a high computational complexity which motivates the use of further sub-optimal linear transmit filters (i.e., precoders), by imposing more structure into the filter design. A straightforward technique is to precode by the inverse of the channel. This scheme is referred to as channel inversion or zero-forcing (ZF) [5, 10, 16].

Although it is legitimate that the works [10, 13, 14, 17] assume perfect CSIT to determine theoretically optimal performance, this assumption is untenable in practice. Also, it is a particularly strong assumption, since the performance of all precoding strategies is crucially depending on the CSIT. In practical systems, the transmitter has to acquire the channel state information (CSI) of the downlink channel by feedback signaling from the uplink. Since in practice the channel coherence time (i.e., the time the channel is approximately constant) is finite, the information of the instantaneous channel state is inherently incomplete. For this reason, a lot of research has been carried out to understand the impact of imperfect CSIT on the system behavior; see [18] for a recent survey.

In this dissertation, we consider a transmitter equipped with M antennas and K single-antenna receivers, i.e., a MU multiple-input single-output (MISO) system, under linear precoding and imperfect CSIT. In particular, we study

the optimal (weighted sum rate maximizing) linear precoder proposed in [13], matched-filter (MF) precoding, ZF precoding and regularized ZF (RZF) precoding. Our channel model accounts for per-user correlation, i.e., the vector channel $\mathbf{h}_k \in \mathbb{C}^M$ of user k ($k = 1, \ldots, K$) satisfies $E[\mathbf{h}_k \mathbf{h}_k^{\mathsf{H}}] = \mathbf{\Theta}_k$. Moreover, we assume imperfect CSIT which is modeled as a weighted sum of the true channel plus noise. To obtain insights into the system behavior, we approximate the signal-to-interference plus noise ratio (SINR) by a deterministic quantity.

The novelty of this thesis lies in the *large* system approach to approximate the system performance by a deterministic quantity. More precisely, we approximate the SINR γ_k of user k by a *deterministic equivalent* $\bar{\gamma}_k$ such that $\gamma_k - \bar{\gamma}_k \to 0$ almost surely, as the system dimensions M and K go jointly to infinity with bounded ratio $0 < \lim_{M\to\infty} \sup_M \frac{M}{K} = \beta < \infty$. Hence, $\bar{\gamma}_k$ becomes more accurate for increasing M, K. To derive $\bar{\gamma}_k$, we apply tools from the well-established field of large dimensional random matrix theory (RMT) [19, 20]. Large RMT studies the spectral behavior (mostly the eigenvalues) of matrices with large dimensions. For certain matrices, the empirical spectral distribution (e.s.d.) converges to a limiting spectral distribution (l.s.d.), almost surely, if the dimensions go jointly to infinity with bounded ratio. If no such convergence exists, one can still find deterministic equivalents of certain functionals of the e.s.d. , which are exact approximations for asymptotically large dimensions, almost surely. Previous work considered SINR approximations based on *bounds* on the average (with respect to the random channels $\mathbf{h}_k$) SINR. The deterministic equivalent $\bar{\gamma}_k$ is not a bound but a *tight* approximation, almost surely, for asymptotically large M, K. Furthermore, the RMT tools allow us to consider advanced channel models like the per-user correlation model, which are usually extremely difficult to study exactly for finite dimensions. Astonishingly, $\bar{\gamma}_k$ is very accurate even for small system dimension, e.g., $M = K = 16$. Currently, the 3GPP LTE-Advanced standard [21] already defines up to $M = 8$ transmit antennas further motivating the application of large system approximations to characterize the performance of wireless communication systems. In this thesis, we provide a consistent framework for the study of linear precoding techniques and derive deterministic equivalents $\bar{\gamma}_k$ for each of the considered linear precoding schemes.

Subsequently, we apply these SINR approximations to various practical optimization problems. In particular, we derive the optimal regularization term of the RZF precoder, which, depending on the correlation assumptions, is explicit or the solution of an implicit equation. Moreover, for uncorrelated channels, we find a closed-form solution for the optimal number of users per transmit antenna under ZF precoding and for MF, ZF, RZF precoding derive the optimal power allocation strategy for unequal CSIT qualities of the users. In this case, the optimal power allocation scheme is the solution of the classic water-filling algorithm. We further consider practical limited feedback systems, where the CSIT is obtained either through pilot signaling from the users or via feedback of the quantized channel. Pilot signaling is apt in time-division duplex (TDD) systems, where the uplink and downlink channels are be assumed reciprocal. In this TDD system, we derive the optimal amount of channel training if coherent

data transmission and channel training occur in the same channel coherence interval. Similarly, in systems employing channel quantization feedback, typically in frequency-division duplex (FDD) systems, we calculate the necessary feedback scaling to achieve full multiplexing gain under the assumption of random vector quantization (RVQ). Moreover, we compare the RVQ feedback to analog feedback, where the channel is directly fed back by modulating the carrier. In addition to optimal precoding, MF, ZF and RZF precoding, we consider a practical precoding scheme, coined constrained unitary beamforming (CUBF), where the precoding matrix is unitary with constant modulus elements. All current 3GPP standards define codebooks containing CUBF matrices for the MU-MIMO mode. Since the precoding vectors are orthogonal, each user can compute its SINR exactly without knowledge about the interfering precoding vectors. This accurate SINR determines the channel quality indicator (CQI) which in turn enables the base station to apply the correct scheduling as well as modulation and coding scheme. The property of constant modulus entries has the advantage to not increase the peak-to-average power ratio (PAPR) and therefore allows the radio-frequency (RF) power amplifiers to operate efficiently. However, it is too complicated to find a SINR approximation under CUBF using large system analysis. Therefore, we apply the theory of complex Hadamard matrices to parametrize and optimize the CUBF matrices. The resulting optimization algorithm provides an upper bound on the performance of the finite codebooks used in practical systems.

1.1.1 Related Literature

To the best of the author's knowledge, the authors in [22] were the first to carry out a large system analysis with $M, K \to \infty$ and finite ratio for linear precoding under the notion of "channel hardening". In particular they considered ZF precoding, called channel inversion (CI), for $M > K$ and showed that the SINR for independent and identical distributed (i.i.d.) Gaussian channels converges to $\rho(\beta - 1)$, where ρ is the SNR, independent of the applied power normalization strategy. They go on to derive the sum rate maximizing system loading $\bar{\beta}^\star$ for a given M. Their results are a special case of our analysis in Section 3.5 and Section 4.2.1. The authors in [22] conclude by showing that for $\beta > 1$, ZF achieves a large fraction of the linear (with respect to K) sum rate growth. The work in [10] extends the analysis in [22] to the case $M = K$ and shows that the sum rate of ZF is constant in M as $M \to \infty$, i.e., the linear sum rate growth is lost due to the large eigenvalue fluctuations of the channel matrix. The authors in [10] counter this problem by introducing a regularization term α in the inverse of the channel matrix. Under the assumption of large M, K and for any rotationally-invariant channel distribution, [10] derives the regularization term $\alpha = \bar{\alpha}^\star = 1/(\beta\rho)$ that maximizes the SINR. Note here that [10] does not apply the classic tools from large dimensional random matrix theory (RMT) to derive their results but rather find the solution by applying various expectations and approximations. In this dissertation, the RZF precoder of [10] is referred to as *channel distortion-unaware* RZF (RZF-CDU) precoder, since its design assumes

perfect CSIT, although the available CSIT is erroneous or distorted. It has been observed in [10] that the RZF-CDU precoder is very similar to the transmit filter derived under the minimum mean square error (MMSE) criterion [17] and both become identical in the large M, K limit. Likewise, we will observe some similarities between RZF and MMSE filters when considering imperfect CSIT. The RZF precoder in [10] has been extended in [23] to account for channel quantization feedback under random vector quantization (RVQ). The authors in [23] do not apply tools from large RMT but use the same techniques as in [10] and obtain different results for the optimal regularization parameter and SINR compared to our results in Section 4.4.

The first work applying tools from large RMT to derive the asymptotic SINR under ZF and RZF precoding for correlated channels was [24]. However, in [24] the regularization parameter of the considered RZF precoder was set to fulfill the total average power constraint. Similar work [25] was published later, where the authors considered the RZF precoder in [10] and derived the asymptotic SINR for *uncorrelated* Gaussian channels. Moreover, they derived the asymptotically optimal regularization parameter $\bar{\alpha}^\star = 1/(\beta\rho)$, already derived [10], which is a special case of the one derived in Section 4.1. Another work [26] reproducing our results, noticed that the optimal regularization parameter in [10, 25] is independent of transmit correlation when the correlation is identical for all users.

Regarding the MF precoder, the asymptotic SINR for channels with common transmit correlation under perfect CSIT have been derived in [27]. Recently, a deterministic equivalent of the SINR under MF precoding and pilot contamination in multi-cell systems has been derived in [28].

Concerning the optimal linear precoder, the following results are available. In the large system limit and for channels with i.i.d. entries, the cross correlations between the users' channels, and therefore the users' SINRs, are identical. It has been shown in [29] that for this symmetric case and equal noise variances, the SINR maximizing precoder is of closed form and coincides with the RZF precoder. Recently, the authors in [30] claimed that indeed the RZF precoder structure emerges as the optimal beamforming solution for $M, K \to \infty$. This asymptotic optimality motivates a detailed analysis of the RZF precoder for large system dimensions. An iterative algorithm to compute the linear precoder that maximizes the weighted sum rate (WSR) has been proposed in [13]. In Section 3.3, we will carry out a large system analysis of this algorithm under perfect CSIT. However, although the RZF structure emerges for sum rate maximization and common correlation under certain assumptions, we are not able to prove that the derived approximation for the SINR at iteration j is indeed a deterministic equivalent for the proposed precoder in [13]. Nevertheless, simulations show that the derived approximation is accurate.

1.2 Outline and Contributions

In this thesis, we provide a concise framework that directly extends and generalizes the results in [10,22,25–27] by accounting for per-user correlation and imperfect CSIT. Furthermore, we apply our SINR approximations to several limited-feedback scenarios that have been previously analyzed by applying bounds on the ergodic rate of finite dimensional systems. In addition, we study the CUBF for finite dimensions and propose an optimization algorithm to parametrize the CUBF.

This dissertation is organized as follows: Chapter 1 motivates the work, provides a detailed outline and introduces the system model. Chapter 2 gives a brief introduction to the field of large dimensional random matrices and provides the results required for the subsequent analysis. In Chapter 3, we derive deterministic equivalents of the SINR under various linear precoding schemes and correlation assumptions. In Chapter 4, we study several applications of the large system approximations. Chapter 5 analyzes a practical linear precoding scheme and presents an optimization algorithm to parametrize the precoder. Finally, in Chapter 6, we conclude the thesis and give an outlook.

The detailed contributions are summarized in the following sections.

1.2.1 Chapter 2: Mathematical Prerequisites: Large Dimensional Random Matrix Theory

In this chapter, we provide the mathematical basis for the subsequent large system analysis of the MISO-BC under linear precoding. In the course of the derivations of the SINR approximations, we have to deal with terms of the form $m(z) = \frac{1}{M}\mathrm{tr}(\frac{1}{M}\mathbf{H}^{\mathsf{H}}\mathbf{H} - z\mathbf{I}_M)^{-1}$, where $\mathbf{H} = [\mathbf{h}_1, \ldots, \mathbf{h}_K]^{\mathsf{H}} \in \mathbb{C}^{K\times M}$ is the compound channel and $z < 0$. The term $m(z)$ is the so called *Stieltjes transform* of the empirical spectral distribution (e.s.d). of matrix $\frac{1}{M}\mathbf{H}^{\mathsf{H}}\mathbf{H}$ at z. To compute a deterministic equivalent of the SINR, we first require a deterministic equivalent $\bar{m}(z)$ of $m(z)$, such that $m(z) - \bar{m}(z) \overset{M\to\infty}{\longrightarrow} 0$, almost surely. Depending on the assumptions for the entries of $\mathbf{H}$, many results exist. The most general result is provided in [31], where $\mathbf{H}$ has a certain variance profile, i.e., $\frac{1}{\sqrt{M}}[\mathbf{H}]_{ij} = \sigma_{ij}z_{ij}$ with z_{ij} i.i.d., zero mean and of variance $1/M$. However, the variance profile does not account for per-user correlation and is thus insufficient to study realistic MU-MISO channels. The channel model considered in this thesis goes further and assumes per-user correlation, i.e., $\frac{1}{M}\mathbf{H}^{\mathsf{H}}\mathbf{H} = \sum_{i=1}^{K}\boldsymbol{\Theta}_i^{1/2}\mathbf{z}_i\mathbf{z}_i^{\mathsf{H}}\boldsymbol{\Theta}_i^{1/2}$, where $\mathbf{z}_i = [z_{i,1}, \ldots, z_{i,M}]^{\mathsf{T}}$ which includes the variance profile as a special case, i.e., if $\boldsymbol{\Theta}_i = \mathrm{diag}(\sigma_{i1}^2, \ldots, \sigma_{iM}^2)$, we obtain the variance profile in [31]. Therefore, we need to extend the result in [31] to account for the channel model with per-user correlation also referred to as a channel with *generalized variance profile*. A deterministic equivalent of the empirical Stieltjes transform for channels with generalized variance profile is provided in Section 2.2. Furthermore, in Section 2.3, we derive the *Shannon transform* $\mathcal{V}(x) = \frac{1}{M}\log\det(\mathbf{I}_M + x\frac{1}{M}\mathbf{H}^{\mathsf{H}}\mathbf{H})$, $x > 0$, of the e.s.d. of $\frac{1}{M}\mathbf{H}^{\mathsf{H}}\mathbf{H}$ also extending the results in [31]. Note, that the proof for

the generalized variance profile of both Stieltjes and Shannon transform partly relies on adapting the techniques provided in [31]. These results are partly published in

- S. Wagner, R. Couillet, M. Debbah, D. T. M. Slock "Large System Analysis of Linear Precoding in Correlated MISO Broadcast Channels under Limited Feedback", *to appear in IEEE Trans. Inf. Theory*, arXiv Preprint 0906.3682.

1.2.2 Chapter 3: MISO BC under Linear Precoding: A Large System Analysis

Based on the deterministic equivalent of the Stieltjes transform with generalized variance profile provided in Chapter 2, we derive deterministic equivalents, i.e., approximations that are almost surely exact as $M, K \to \infty$, of the random SINR under MF (Section 3.2), optimal linear precoding (Section 3.3), RZF (Section 3.4) and ZF precoding (Section 3.5). In general, the deterministic SINR approximations are functions of fixed-point equations but are explicit for uncorrelated channels ($\mathbf{\Theta}_k = \mathbf{I}_M \ \forall k$). Unlike previous work, we derive deterministic equivalents and not asymptotic results, since for our channel model the e.s.d. of $\frac{1}{M}\mathbf{H}^{\mathsf{H}}\mathbf{H}$ does not converge to a limiting spectral distribution. In Section 3.6, we provide rate, sum rate and rate gap (between perfect and imperfect CSIT) approximations which are based on the SINR approximations. Simulation results show that the deterministic SINR approximations are very accurate even for small M, K. Hence, applied to practical optimization problems in Chapter 4, they yield close-to-optimal solutions, where the objective is typically to maximize the system sum rate. Those results have partially been published in

- R. Couillet, S. Wagner, M. Debbah, A. Silva, "The Space Frontier: Physical Limits of Multiple Antenna Information Transfer", *Proc. of the 3rd ACM International Conference on Performance Evaluation Methodologies and Tools (VALUETOOLS'08)*, Athens, Greece, 20-24 Oct. 2008, no. 84. **BEST STUDENT PAPER AWARD**,

  in which we apply tools from large RMT to derive the asymptotic SINR of ZF and RZF precoding, where the regularization term is set to fulfill the transmit power constraint, in MISO broadcast channels.

- R. Couillet, S. Wagner, M. Debbah, "Asymptotic Analysis of Correlated Multi-Antenna Broadcast Channels", *Proc. of the IEEE Wireless Communications & Networking Conference (WCNC'09)*, Budapest, Hungary, 5-8 Apr. 2009,

  where we consider ZF and RZF precoding and apply the results to systems with dense antenna packings at the transmitter.

- S. Wagner, R. Couillet, M. Debbah, D. T. M. Slock, "Deterministic Equivalent for the SINR of Regularized Zero-forcing Precoding in Correlated

MISO Broadcast Channels with Imperfect CSIT", *Proc. IEEE International Conference on Communications (ICC'11)*, Kyoto, Japan, 5-9 Jun. 2011,

where we derive the deterministic equivalent of the SINR under ZF and RZF precoding accounting for per-user correlation and imperfect CSIT and derive the SINR maximizing regularization term.

- S. Wagner and D. T. M. Slock "Weighted Sum Rate Maximization of Correlated MISO Broadcast Channels under Linear Precoding: A Large System Analysis", *Proc. IEEE 12th International Workshop on Signal Processing Advances in Wireless Communications (SPAWC'11)*, San Francisco, USA, 26-29 Jun. 2011,

  where we consider the weighted sum rate maximizing precoder in [13] and carry out a large system analysis and derive a deterministic equivalent of the SINR for MU-MISO with per-user correlation and perfect CSIT.

1.2.3 Chapter 4: Large MISO BC under Linear Precoding: Applications

In this chapter, we apply the deterministic SINR approximations derived in Chapter 3 to solve various optimization problems. More precisely, in Section 4.1, we compute the sum rate maximizing regularization term $\bar{\alpha}^\star$ for the RZF precoder under imperfect CSIT and common correlation ($\mathbf{\Theta}_k = \mathbf{\Theta}\ \forall k$), extending the results in [10, 25, 27]. In Section 4.2, we consider the problem of computing the sum rate maximizing number of users for a *fixed* number of transmit antennas. Under ZF precoding and uncorrelated channels ($\mathbf{\Theta}_k = \mathbf{I}_M\ \forall k$), we obtain a closed form solution which extends the result in [22] to imperfect CSIT. Furthermore, we solve the problem of optimal power allocation for channels with common correlation under MF, ZF and RZF precoding when the CSIT of the users is unequal. Under this assumption, the optimal power allocation strategy is the solution of a water-filling algorithm.

In Section 4.3, we study the optimal amount of channel training (pilot signaling) in a TDD system, where coherent transmission and channel training occur in the same channel coherence interval. This scheme has been studied in [32–34] for finite dimensional systems. We assume uncorrelated channels, MMSE estimation at the transmitter and we neglect the common training phase. The amount of training optimizing the net sum rate, i.e. the sum rate taking into account the reduced interval for coherent downlink data transmission, for MF, ZF and RZF precoding is the solution of a convex optimization problem. We derive approximated but closed form solutions for high downlink SNR. Our results are in line with [32–34] in terms of the scaling in the coherence interval (for a fixed SNR) and the SNR (for a fixed coherence interval) but extend them to RZF and MF precoding.

Section 4.4 considers a system where the CSIT is obtained by direct feedback of the quantized channel direction. In [35], an information-theoretic analysis of

the impact of quantized CSIT on the achievable rate of a ZF-precoded MU-MISO downlink channel with $M = K$ has been carried out. Hereby, the author derives an upper bound on the ergodic *per-user rate gap* between perfect CSIT and imperfect CSIT under RVQ with B feedback bits per user. Under finite-rate feedback, both [35] and [36] observe a sum rate ceiling for high SNR. In [35, Theorem 3] provides a formula for the minimum scaling of B to maintain an average per-user rate gap of $\log_2 b$ bits/s/Hz and hence to achieve the full multiplexing gain of K. Although derived for ZF, the author claims that for all SNR, [35, Theorem 3] is more accurate for the RZF-CDU precoder proposed in [10]. Similar to [35], we derive the necessary feedback scaling to maintain a target rate gap between perfect and imperfect CSIT. But unlike [35], the derived feedback scaling maintains the rate gap exactly as $M, K \to \infty$, almost surely. We find that our solutions, give more accurate results than [35] for large dimensions. Finally, as in [32], we compare quantized feedback to analog feedback in terms of rate gap between perfect and imperfect CSIT for MF, ZF and RZF precoding. The results have partially been published in

- S. Wagner, R. Couillet, D. T. M. Slock, M. Debbah "Large System Analysis of Zero-Forcing Precoding in MISO Broadcast Channels with Limited Feedback", *Proc. IEEE 11th International Workshop on Signal Processing Advances in Wireless Communications (SPAWC'10)*, Marrakech, Morocco, 20-23 Jun. 2010,

  where we derive a deterministic equivalent of the SINR under ZF precoding and apply this result to solve the problem of the sum rate maximizing number of users for a fixed number of transmit antennas.

- S. Wagner, R. Couillet, M. Debbah, D. T. M. Slock, "Optimal Training in Large TDD Multi-user Downlink Systems under Zero-forcing and Regularized Zero-forcing Precoding", *Proc. IEEE Global Communications Conference (GC'10)*, Miami, USA, 6-10 Dec. 2010,

  where we apply the deterministic equivalents of the SINR under ZF and RZF precoding to large TDD systems and derive the optimal amount of training for both schemes.

- S. Wagner, R. Couillet, M. Debbah, D. T. M. Slock "Large System Analysis of Linear Precoding in Correlated MISO Broadcast Channels under Limited Feedback", *to appear in IEEE Trans. Inf. Theory*, arXiv Preprint 0906.3682,

  where all applications are summarized and presented in detail.

The optimum linear precoder, MF, ZF and RZF precoders have several drawbacks that prevent their adoption into practical wireless communication standards like 3GPP LTE. First, they increase the PAPR and the power imbalance between the transmit antennas leading to a reduced efficiency of the RF power amplifiers. Secondly, they require significant amount of feedback overhead to provide accurate CSIT. Lastly, the receivers are unable to compute their exact

SINR since they have no knowledge about precoders of the interfering users. The inaccurate SINR results in an inaccurate CQI which translates into a system capacity loss since the CQI is used for scheduling and to adapt the modulation and coding scheme. Therefore, a different precoder is required to alleviate those drawbacks, which is discussed in the next chapter.

1.2.4 Chapter 5: Unitary Precoding with Constant Modulus Constraint

In this chapter, we consider a practical precoding scheme, where the precoding matrices are orthogonal and have entries of constant magnitude. Those precoders are attractive, since they do not increase the PAPR at the transmitter and allow for exact SINR computation at the receivers. All current 3GPP LTE standards adopted codebooks (to reduce the feedback overhead) of such matrices for the precoding in MU-MIMO mode. We apply the theory of complex Hadamard matrices to describe those constrained unitary beamformers (CUBF) and propose an algorithm for optimal parametrization of the CUBF matrices. Contrary to practical systems where the receivers feedback their preferred precoding matrix, the proposed algorithm assumes CSIT (in the form of a channel estimate) and therefore provides a benchmark for the evaluation of the codebooks used in practical systems. The results of this chapter have been published in

- S. Wagner, S. Sesia, D. T. M. Slock, "Unitary Beamforming under Constant Modulus Constraint in MIMO Broadcast Channels", *Proc. IEEE 10th Workshop on Signal Processing Advances in Wireless Communications (SPAWC'09)*, Perugia, Italy, 21-24 Jun. 2009,

  where we consider orthogonal precoding matrices with constant modulus entries and apply the description of complex Hadamard matrices to derive an algorithm that optimizes those precoders.

- S. Wagner, S. Sesia, D. T. M. Slock, "On Unitary Beamforming for MIMO Broadcast Channels", *Proc. IEEE International Conference on Communications (ICC'10)*, Cape Town, South Africa, 23-27 May 2010,

  where we compare the sum rate performance of unitary precoding to unitary precoding with constant modulus constraint for equal and optimal power allocation.

In the next section, we introduce the general system model of a MU-MIMO communications system.

1.3 General System Model

Consider a MU-MIMO (or point-to-multipoint) single-cell setup where a transmitter endowed with M antennas communicates with K non-cooperative receivers (or users) each equipped with N_k antennas, $k = 1, 2, \ldots, K$. We assume $M \geq K$, thus no user-scheduling is considered. Furthermore, we suppose narrow-band transmission, i.e., the channel remains constant over the entire transmission bandwidth (flat-fading). This assumption is appropriate when OFDM is applied and the frequency-selective wide-band channel is transformed into orthogonal frequency-flat sub-channels. Therefore, at every time instant (on any sub-channel) the received signal $\mathbf{y}_k \in \mathbb{C}^{N_k}$ of user k is given by

$$\mathbf{y}_k = \mathbf{H}_k \mathbf{x} + \mathbf{n}_k, \quad k = 1, 2, \ldots, K, \tag{1.1}$$

where $\mathbf{H}_k \in \mathbb{C}^{N_k \times M}$ is the random channel from the transmitter to user k, $\mathbf{x} \in \mathbb{C}^M$ is the transmit vector and $\mathbf{n}_k \sim \mathcal{CN}(\mathbf{0}, \sigma_k^2 \mathbf{I}_{N_k})$ is the noise. We assume that the channel $\mathbf{H}_k$ $\forall k$ evolves according to a block-fading model, i.e., the channel varies *independently* from block to block. The transmitter sends $S_k \leq \min(M, N_k)$ data symbols to the kth user. Define the total number of receive antennas as $N \triangleq \sum_{k=1}^{K} N_k$ and the total number of transmitted symbols as $S \triangleq \sum_{k=1}^{K} S_k$. The maximum number of symbols $S_{\max}$ supported by the system is then given by $S_{\max} = \min(M, N) \geq S$.

The transmit vector $\mathbf{x}$ is a linear combination of the user symbols $\mathbf{s}_k \in \mathbb{C}^{S_k}$ and can be written as

$$\mathbf{x} = \sum_{k=1}^{K} \mathbf{G}_k \mathbf{P}_k^{1/2} \mathbf{s}_k, \tag{1.2}$$

where $\mathbf{G}_k \in \mathbb{C}^{M \times S_k}$ and $\mathbf{P}_k = \operatorname{diag}(p_1, \ldots, p_{S_k})$, $p_i \geq 0$, $i = 1, 2, \ldots, S_k$ are the precoding (or beamforming) matrix and the power allocation matrix of user k, respectively. Subsequently, we assume that user k has perfect knowledge of $\mathbf{H}_k$ and the effective channel $\mathbf{H}_k \mathbf{G}_k$. An estimate of $\mathbf{H}_k \mathbf{G}_k$ can be obtained through dedicated training by precoding the pilots intended for user k by $\mathbf{G}_k$. A block diagram of this transmission scheme is depicted in Figure 1.2. The user symbols $\mathbf{s}_k$ are assumed to be independent, zero-mean and of unit variance, i.e., $E[\mathbf{s}_k \mathbf{s}_k^{\mathsf{H}}] = \mathbf{I}_{S_k}$ and $E[\mathbf{s}_k \mathbf{s}_j^{\mathsf{H}}] = \mathbf{0}$ for $k \neq j$, $k, j = 1, 2, \ldots, K$. We suppose that the transmitter has an average limited available power $P < \infty$ and thus the transmit signal is subject to an average total power constraint

$$E[\|\mathbf{x}\|_2^2] = \operatorname{tr} \sum_{k=1}^{K} \sum_{j=1}^{K} \mathbf{G}_k \mathbf{P}_k^{1/2} \, E[\mathbf{s}_k \mathbf{s}_j^{\mathsf{H}}] \mathbf{P}_j^{1/2} \mathbf{G}_j^{\mathsf{H}} = \sum_{k=1}^{K} \operatorname{tr}(\mathbf{P}_k \mathbf{G}_k^{\mathsf{H}} \mathbf{G}_k) \leq P. \tag{1.3}$$

Under the assumption that receiver k has no knowledge about the interference $\sum_{i=1, i \neq k}^{K} \mathbf{H}_k \mathbf{G}_i \mathbf{P}_i^{1/2} \mathbf{s}_i$, it is treated as noise and we define the effective noise $\tilde{\mathbf{n}}_k \triangleq \mathbf{n}_k + \sum_{i=1, i \neq k}^{K} \mathbf{H}_k \mathbf{G}_i \mathbf{P}_i^{1/2} \mathbf{s}_i$. The effective noise covariance matrix

$\mathbf{R}_{\tilde{\mathbf{n}}_k\tilde{\mathbf{n}}_k}$ at user k is then given by

$$\mathbf{R}_{\tilde{\mathbf{n}}_k\tilde{\mathbf{n}}_k} = E[\tilde{\mathbf{n}}_k\tilde{\mathbf{n}}_k^{\mathsf{H}}] = \sigma_k^2\mathbf{I}_{S_k} + \mathbf{H}_k\left(\sum_{i=1,i\neq k}^{K}\mathbf{G}_i\mathbf{P}_i\mathbf{G}_i^{\mathsf{H}}\right)\mathbf{H}_k^{\mathsf{H}}. \tag{1.4}$$

Furthermore, assuming Gaussian signaling, i.e., $\mathbf{s}_k \sim \mathcal{CN}(\mathbf{0}, \mathbf{I}_{S_k})\ \forall k$ and optimal decoding at the receiver, the achievable rate R_k of user k takes the form [37]

$$R_k = \log\det\left(\mathbf{I}_{S_k} + \mathbf{P}_k^{1/2}\mathbf{G}_k^{\mathsf{H}}\mathbf{H}_k^{\mathsf{H}}\mathbf{R}_{\tilde{\mathbf{n}}_k\tilde{\mathbf{n}}_k}^{-1}\mathbf{H}_k\mathbf{G}_k\mathbf{P}_k^{1/2}\right). \tag{1.5}$$

A meaningful performance measure in the cell is the weighted sum rate R_{wsum} (WSR) defined as

$$R_{\text{wsum}} = \sum_{k=1}^{K} u_k R_k, \tag{1.6}$$

where u_k is the rate weight of user k with $\text{tr}\mathbf{U} = K$ and $\mathbf{U} = \text{diag}(u_1, \ldots, u_K)$. The WSR measure can account for fairness among the users by adjusting the rate weights u_k. For instance, a user at the cell edge who experiences usually rather bad channel conditions can be assigned a large weight in order to increase his rate and guarantee a certain quality of service. If all the users are treated equally, i.e., $u_k = 1\ \forall k$, then we obtain the sum rate R_{sum} defined as

$$R_{\text{sum}} = \sum_{k=1}^{K} R_k. \tag{1.7}$$

Since the service operator is usually interested in optimizing the average system capacity, we will mainly deal with the average rates $E[R_k]$, $E[R_{\text{wsum}}]$ and $E[R_{\text{sum}}]$, where the expectation is taken over the random channels $\mathbf{H}_k$.

In the next section we introduce the channel model.

1.4 Channel Model

Each user channel $\mathbf{H}_k$ is modeled as

$$\mathbf{H}_k = \sqrt{M}\mathbf{\Phi}_k^{1/2}\mathbf{Z}_k\mathbf{\Theta}_k^{1/2}, \tag{1.8}$$

where $\mathbf{\Phi}_k \in \mathbb{C}^{N_k\times N_k}$ and $\mathbf{\Theta}_k \in \mathbb{C}^{M\times M}$ are the receive and transmit correlation matrices of user k and $\mathbf{Z}_k \in \mathbb{C}^{N_k\times M}$ has i.i.d. complex entries of zero mean and variance $1/M$. The model (1.8) assumes that the users are sufficiently spaced apart so that their respective channels are mutually uncorrelated. The receive and transmit correlation matrices are assumed to be slowly varying compared to the channel coherence time and thus are supposed to be perfectly known to the transmitter, whereas receiver k has only knowledge about $\mathbf{\Theta}_k$ and $\mathbf{\Phi}_k$.

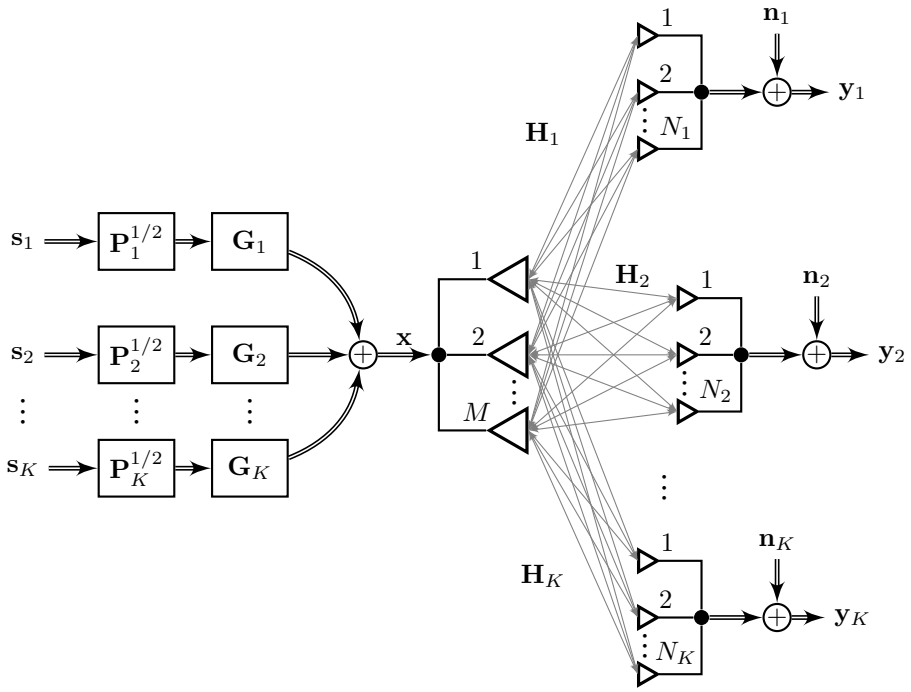

Figure 1.2: Block diagram of the MU-MIMO narrow-band transmission model.

Moreover, only an imperfect estimate $\hat{\mathbf{H}}_k$ of the true channel $\mathbf{H}_k$ is available at the transmitter which is modeled as [38–41]

$$\hat{\mathbf{H}}_k = \sqrt{M}\boldsymbol{\Phi}_k^{1/2}\left(\sqrt{1-\tau_k^2}\mathbf{Z}_k + \tau_k\mathbf{E}_k\right)\boldsymbol{\Theta}_k^{1/2} = \sqrt{M}\boldsymbol{\Phi}_k^{1/2}\hat{\mathbf{Z}}_k\boldsymbol{\Theta}_k^{1/2}, \qquad (1.9)$$

where $\hat{\mathbf{Z}}_k \triangleq \sqrt{1-\tau_k^2}\mathbf{Z}_k + \tau_k\mathbf{E}_k$ and $\mathbf{E}_k$ has i.i.d. entries of zero mean and variance $1/M$ independent of $\mathbf{Z}_k$ and $\mathbf{n}_k$. The parameter τ_k reflects the accuracy or quality of the channel estimate $\hat{\mathbf{H}}_k$, i.e., $\tau_k = 0$ corresponds to perfect CSIT, whereas for $\tau_k = 1$ the CSIT is completely uncorrelated to the true channel. The variation in the accuracy of the available CSIT $\hat{\mathbf{H}}_k$ between the different user channels $\mathbf{H}_k$ arises naturally. First, there might be low mobility users and high mobility users with large or small channel coherence intervals, respectively. Therefore, the CSIT of the high mobility users will be outdated quickly and hence be very inaccurate. On the other hand, the CSIT of the low mobility users remains accurate since their channel does not change significantly from the time of the channel estimation until the time of precoding and coherent data transmission. Secondly, different CSIT qualities arise when the feedback rate varies among the users. For instance, if the CSIT is obtained from uplink training, the training length of each user could be different, leading to different channel estimation errors at the transmitter. Similarly, if the users feed back

a quantized channel estimate, they could use channel quantization codebooks of different size depending on their channel quality and the available uplink resources. However, for simplicity, we assume identical CSIT qualities $\tau_k = \tau$ $\forall k$ for the optimization problems considered in Section 4.3 and Section 4.4.

Remark 1.1. *Note that in* (1.9) *the true channel* $\mathbf{H}_k = \sqrt{1-\tau_k^2}\sqrt{M}\mathbf{\Phi}_k^{1/2}\mathbf{Z}_k\mathbf{\Theta}_k^{1/2}$ *and the additive noise* $\tau_k\sqrt{M}\mathbf{\Phi}_k^{1/2}\mathbf{E}_k\mathbf{\Theta}_k^{1/2}$ *have identical correlation up to the scalars* $\sqrt{1-\tau_k^2}$ *and* τ_k*. This model is adequate for instance in a FDD system, where the columns or rows of the channel* $\mathbf{H}_k$ *are finely quantized using a random codebook of i.i.d. vectors. Since the correlation matrices* $\mathbf{\Theta}_k$ *and* $\mathbf{\Phi}_k$ *are known at both ends, user k solely quantizes the columns or rows of the fast fading channel component* $\mathbf{Z}_k$ *to the closest codebook vectors* $\hat{\mathbf{Z}}_k$*, which can be accurately approximated as* (1.9)*. Subsequently, the user sends the codebook indexes back to the transmitter, where the estimated downlink channel is reconstructed by multiplying with* $\sqrt{M}\mathbf{\Theta}_k^{1/2}$ *and* $\sqrt{M}\mathbf{\Phi}_k^{1/2}$*. For uncorrelated channels, this specific FDD system is studied in Section 4.4.*

1.5 Special Case: Single-Antenna Receivers

In practice it is often desirable that the user terminals are cost efficient. Roughly speaking, every additional receive antenna doubles the hardware and signal processing complexity since the whole RF chain has to be duplicated and the receiver has to estimate double the channel coefficients and perform interference cancellation or detection of additional symbols. Moreover, by adding more antennas on a small handheld device, correlation between the receive antennas is problematic and can result in significant performance loss. Therefore, we restrict our analysis to single-antenna receivers which lead to more compact expressions for the system model. When the users only have $N_k = 1$ $\forall k$ receive antenna and each scheduled user receives a single data stream $S_k = 1$ $\forall k$, the received signal y_k of user k takes the form

$$y_k = \sqrt{p_k}\mathbf{h}_k^{\mathsf{H}}\mathbf{g}_k s_k + \sum_{i=1, i\neq k}^{K} \sqrt{p_i}\mathbf{h}_k^{\mathsf{H}}\mathbf{g}_i s_i + n_k, \quad k = 1, 2, \ldots, K, \tag{1.10}$$

where the channel matrix $\mathbf{H}_k$ becomes the *row* vector $\mathbf{h}_k^{\mathsf{H}}$ and the precoding matrix $\mathbf{G}_k$ reduces to the precoding vector $\mathbf{g}_k$. The transmit power constraint (1.3) becomes

$$E[\|\mathbf{x}\|^2] = \mathrm{tr}(\mathbf{P}\mathbf{G}^{\mathsf{H}}\mathbf{G}) \leq P, \tag{1.11}$$

where we defined the overall precoding matrix $\mathbf{G} \triangleq [\mathbf{g}_1, \mathbf{g}_2, \ldots, \mathbf{g}_K] \in \mathbb{C}^{M\times K}$ and the power allocation matrix $\mathbf{P} = \mathrm{diag}(p_1, \ldots, p_K)$. A block-diagram of the MU-MISO system is depicted in Figure 1.3.

The SINR of the kth user is defined as

$$\gamma_k = \frac{p_k|\mathbf{h}_k^{\mathsf{H}}\mathbf{g}_k|^2}{\sum_{i=1, i\neq k}^{K} p_i|\mathbf{h}_k^{\mathsf{H}}\mathbf{g}_i|^2 + \sigma_k^2} \tag{1.12}$$

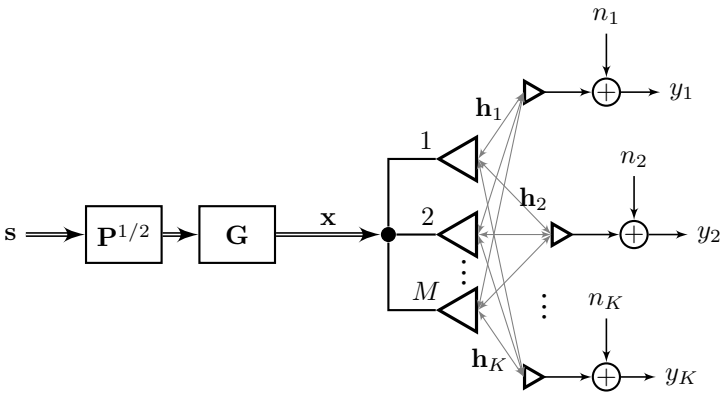

Figure 1.3: Block diagram of the MU-MISO narrow-band transmission model.

and the corresponding rate (1.5) reads

$$R_k = \log\left(1+\gamma_k\right). \tag{1.13}$$

The channel model for imperfect CSIT (1.9) rewrites

$$\hat{\mathbf{h}}_k^{\mathsf{H}} = \sqrt{M}\left(\sqrt{1-\tau_k^2}\mathbf{z}_k^{\mathsf{H}} + \tau_k \mathbf{e}_k^{\mathsf{H}}\right)\boldsymbol{\Theta}_k^{1/2} = \sqrt{M}\hat{\mathbf{z}}_k^{\mathsf{H}}\boldsymbol{\Theta}_k^{1/2}, \tag{1.14}$$

where $\hat{\mathbf{z}}_k \triangleq \sqrt{1-\tau_k^2}\mathbf{z}_k + \tau_k \mathbf{e}_k$. Define the compound true channel matrix $\mathbf{H} \triangleq [\mathbf{h}_1, \mathbf{h}_2, \ldots, \mathbf{h}_K]^{\mathsf{H}} \in \mathbb{C}^{K\times M}$ and the compound estimated channel matrix $\hat{\mathbf{H}} \triangleq [\hat{\mathbf{h}}_1, \hat{\mathbf{h}}_2, \ldots, \hat{\mathbf{h}}_K]^{\mathsf{H}} \in \mathbb{C}^{K\times M}$. Therefore, the matrix $\frac{1}{M}\hat{\mathbf{H}}^{\mathsf{H}}\hat{\mathbf{H}}$ can be written as

$$\frac{1}{M}\hat{\mathbf{H}}^{\mathsf{H}}\hat{\mathbf{H}} = \sum_{k=1}^{K} \boldsymbol{\Theta}_k^{1/2}\hat{\mathbf{z}}_k\hat{\mathbf{z}}_k^{\mathsf{H}}\boldsymbol{\Theta}_k^{1/2}. \tag{1.15}$$

The per-user channel correlation model is very general and encompasses various propagation environments. For instance, all channel coefficients $h_{k,i}$ of the vector channel $\mathbf{h}_k$ may have different variances $\sigma_{k,i}^2$ resulting from different attenuation of the signal while traveling to the receivers. This so called variance profile of the vector channel is obtained by setting $\boldsymbol{\Theta}_k = \mathrm{diag}(\sigma_{k,1}^2, \sigma_{k,2}^2, \ldots, \sigma_{k,M}^2)$, see [31, 42]. Another possible scenario consists of an environment where all user channels experience identical transmit correlation $\boldsymbol{\Theta}$, but where the users are heterogeneously scattered around the transmitter and hence experience different channel gains d_k. Such a setup can be modeled with $\boldsymbol{\Theta}_k = d_k\boldsymbol{\Theta}$. From a mathematical point of view, a homogeneous system with common user channel correlation $\boldsymbol{\Theta}_k = \boldsymbol{\Theta}\ \forall k$ is very attractive. In this case, the user channels are statistically equivalent and the deterministic SINR approximations can be computed by solving a single implicit equation instead of multiple systems of coupled implicit equations. A further simplification occurs when the channels

are uncorrelated $\mathbf{\Theta}_k = \mathbf{I}_M \ \forall k$, in which case the approximated SINRs are given explicitly.

The model in (1.15) has never been considered in large dimensional RMT and therefore no results are available. The most general model available, is the variance profile, first treated in [43] and extended in [31], which is a special case of the model in (1.15). Therefore, to be able to derive deterministic equivalents of the SINR, we need to extend the results in [31,43] to account for the per-user correlation model in (1.15), which is the subject of the next chapter.

Chapter 2

Mathematical Prerequisites: Large Dimensional Random Matrix Theory

This chapter provides the necessary tools to analyze the large MISO BC under linear precoding and per-user correlation. In this analysis, we encounter terms of the form $m(z) = \frac{1}{M}\mathrm{tr}(\frac{1}{M}\mathbf{H}^{\mathsf{H}}\mathbf{H} - z\mathbf{I}_M)^{-1}$ which is the Stieltjes transform of the e.s.d. of $\frac{1}{M}\mathbf{H}^{\mathsf{H}}\mathbf{H}$ in $z < 0$. From our channel model we have $\frac{1}{M}\hat{\mathbf{H}}^{\mathsf{H}}\hat{\mathbf{H}} = \sum_{k=1}^{K} \mathbf{\Theta}_k^{1/2}\hat{\mathbf{z}}_k\hat{\mathbf{z}}_k^{\mathsf{H}}\mathbf{\Theta}_k^{1/2}$, where $\hat{\mathbf{z}}_k$ has i.i.d. entries of zero mean and variance $1/M$. This model, referred to as *generalized variance profile*, has not yet been considered in the literature on large dimensional random matrices and therefore, we provide the required tools in this chapter as follows: In Section 2.1, we set the basis and introduce necessary definitions and methods. In Section 2.2, we consider the Hermitian $\mathbf{B}_N = \mathbf{X}_N^{\mathsf{H}}\mathbf{X}_N + \mathbf{S}_N \in \mathbb{C}^{N\times N}$, where $\mathbf{X}_N^{\mathsf{H}}\mathbf{X}_N$ is random with generalized variance profile and $\mathbf{S}_N$ is Hermitian nonnegative definite. We prove a theorem that provides a *deterministic equivalent* $\bar{m}_{\mathbf{B}_N,\mathbf{Q}_N}(z)$ of the empirical Stieltjes transform $m_{\mathbf{B}_N,\mathbf{Q}_N}(z) \triangleq \frac{1}{N}\mathrm{tr}\mathbf{Q}_N\left(\mathbf{B}_N - z\mathbf{I}_N\right)^{-1}$ such that $m_{\mathbf{B}_N,\mathbf{Q}_N}(z) - \bar{m}_{\mathbf{B}_N,\mathbf{Q}_N}(z) \overset{N\to\infty}{\longrightarrow} 0$, almost surely. Finally, in Section 2.3, we consider the Shannon transform $\mathcal{V}_{\mathbf{B}_N}(x) \triangleq \frac{1}{N}\log\det\left(\mathbf{I}_N + x\mathbf{B}_N\right)$ of the e.s.d. of $\mathbf{B}_N$ in $x > 0$ and derive a deterministic equivalent $\bar{\mathcal{V}}_{\mathbf{B}_N}(x)$ such that $E[\mathcal{V}_{\mathbf{B}_N}(x)] - \bar{\mathcal{V}}_{\mathbf{B}_N}(x) \overset{N\to\infty}{\longrightarrow} 0$. The result in Section 2.3 is not necessary for the derivations of the deterministic equivalents for the SINRs in Chapter 3, but are given here because they are novel and for the sake of completeness.

2.1 Introduction and Methods

The field of random matrix theory is commonly said to date back to the work of John Wishart in 1928 [44] who studied the behavior of sample covariance matrices $\mathbf{R}_n$ of i.i.d. observation vectors $\mathbf{x}_i \in \mathbb{C}^N$, $i = 1, 2, \ldots, n$, i.e.,

$$\mathbf{R}_n = \frac{1}{n} \sum_{i=1}^{n} \mathbf{x}_i \mathbf{x}_i^{\mathsf{H}}. \tag{2.1}$$

For $x_j \sim \mathcal{CN}(0, 1)$, $j = 1, 2, \ldots, N$, he derived the joint probability distribution of the entries of $\mathbf{R}_n$, where $\mathbf{R}_n$ is now referred to as a (central) *Wishart* matrix. Since then, many researcher studied such matrices, especially their eigenvalue distribution [45–48]. Marčenko and Pastur observed that for asymptotically large n, N with finite ratio N/n, the empirical spectral distribution (e.s.d.) $F^{\mathbf{R}_n}$ of matrix $\mathbf{R}_n$ converges to a *deterministic* limiting spectral distribution (l.s.d.) F_c known as the *Marčenko-Pastur law* [49]. The l.s.d. F_c is much more attractive to work with than the complicated joint probability density function (p.d.f.) of the eigenvalues of $\mathbf{R}_n$ derived in 1939 by [45–48].

In wireless communication systems, the channel $\mathbf{H}$ between transmitter and receiver is usually modeled as a random variable accounting for effects such as fading and shadowing in a scattering environment. For instance, $\mathbf{H} \in \mathbb{C}^{N \times n}$ with i.i.d. entries of zero mean and variance $1/n$ models the point-to-point MIMO flat-fading channel between an n-antenna base station and an N-antenna receiver. With the recent high capacity technologies like code-division multiple access (CDMA), or multi-antenna systems, the random channel matrix $\mathbf{H}$ is often of rather large dimensions. The current 3GPP LTE-Advanced standard [21] defines up to eight antennas at both transmitter and receiver. It turns out that already for these dimensions, the assumption of *large* n, N with subsequent analysis involving large dimensional random matrices $\mathbf{H}$, yields very accurate results even for a not so large 8×8 MIMO system. In the example of a point-to-point MIMO system, the ergodic channel capacity $\mathcal{I}(\rho)$ has been derived in [2] and reads

$$\mathcal{I}(\rho) = E\left[\log_2 \det\left(\mathbf{I}_N + \rho \mathbf{H}\mathbf{H}^{\mathsf{H}}\right)\right] \quad \text{bits/s/Hz}, \tag{2.2}$$

where ρ is the SNR at the receiver and the expectation is taken over the random channel realizations $\mathbf{H}$. From (2.2) it is clear that $\mathcal{I}(\rho)$ is a function of the eigenvalues of the Gram matrix of the random channel matrix $\mathbf{H}$, i.e., $\mathbf{H}\mathbf{H}^{\mathsf{H}}$. The exact analysis based on the joint p.d.f. of the eigenvalues of $\mathbf{H}\mathbf{H}^{\mathsf{H}}$ is somewhat complicated [2] and extremely complex if $\mathbf{H}$ does not contain i.i.d. entries. On the contrary, the assumption of large dimensional random matrices $\mathbf{H}$ yields more compact and insightful expressions for the channel capacity $\mathcal{I}(\rho)$, which are very accurate approximations even for small dimensions [19].

Another powerful tool is the *Stieltjes transform* $m_{F^{\mathbf{X}}}(z)$ of the e.s.d. $F^{\mathbf{X}}$ of the Hermitian $\mathbf{X} \in \mathbb{C}^{N \times N}$ given as $m_{F^{\mathbf{X}}}(z) \triangleq \frac{1}{N} \mathrm{tr}(\mathbf{X} - z\mathbf{I}_N)^{-1}$, $z \in \mathbb{C} \setminus \mathbb{R}^+$. It is particularly important in the large system analysis in Chapter 3, where we often encounter terms of the form $\frac{1}{M} \mathrm{tr} \mathbf{Q}(\mathbf{X} - z\mathbf{I}_M)^{-1}$ which is the Stieltjes transform of a nonnegative finite measure. The Stieltjes transform is defined as follows.

Definition 2.1 (Stieltjes transform)**.** *[19, Definition 3.1] Let F be a real-valued bounded measurable function over $\mathbb{R}$. Then the Stieltjes transform $m_F(z)$ of F, for z outside the support of F, is defined as*

$$m_F(z) \triangleq \int_{-\infty}^{\infty} \frac{1}{\lambda - z} dF(\lambda). \tag{2.3}$$

Note that F *uniquely* determines m_F and vice-versa [50].

The Stieltjes transform is an essential tool in the theory of large dimensional random matrices, since it is very difficult to show directly that the e.s.d. $F^{\mathbf{X}}$ converges to some l.s.d. F. Instead, it is very often much easier to derive the limit $m_F(z)$ of the Stieltjes transform $m_{F^{\mathbf{X}}}(z)$, where it is proved in [51, Theorem B.9] that F is the l.s.d. of $F^{\mathbf{X}}$. Therefore, showing the convergence of $m_{F^{\mathbf{X}}}$ to m_F is equivalent to showing the convergence of $F^{\mathbf{X}}$ to F. The Stieltjes transform is much more convenient to work with, because there exist mathematical tools such as the matrix inversion lemma (MIL), the resolvent identity (Lemma F.2) or the trace lemma (F.3) that make the proof of convergence much easier. The following proposition states the conditions under which m_F is a Stieltjes transform.

Proposition 2.1. *[31, Proposition 2.2] Let F be a nonnegative finite measure with density f. Then $m_F(z)$ is a Stieltjes transform of the form* (2.3) *if and only if the following conditions hold:*

1. $f(z) \in \mathbb{C}^+$ *if* $z \in \mathbb{C}^+$
2. $\lim_{y \to +\infty} -\mathbf{i}y f(\mathbf{i}y) < \infty$.

Moreover, if the condition

3. $zf(z) \in \mathbb{C}^+$ *for* $z \in \mathbb{C}^+$

is satisfied, then $F(\mathbb{R}^-) = 0$ has an analytic continuation on $\mathbb{C} \setminus \mathbb{R}^+$.

To directly evaluate the capacity of MIMO channels in (2.2), another transformation called the *Shannon* transform has been introduced in [20].

Definition 2.2 (Shannon transform)**.** *[20, Section 2.3.3] Let F be a probability distribution defined on $\mathbb{R}^+$. The Shannon transform $\mathcal{V}_F$ of F for $z \in \mathbb{R}^+$ is defined as*

$$\mathcal{V}_F(z) \triangleq \int_0^{\infty} \log(1 + z\lambda) dF(\lambda). \tag{2.4}$$

For $F = F^{\mathbf{H}\mathbf{H}^{\mathsf{H}}}$, the Shannon transform is the capacity of the point-to-point MIMO channel in (2.2) normalized by $1/N$. The Shannon transform is connected to the Stieltjes transform by the relation

$$\mathcal{V}_F(z) = \int_{\frac{1}{z}}^{\infty} \left[\frac{1}{t} - m_F(-t) \right] dt = \int_0^z \left[\frac{1}{t} - \frac{1}{t^2} m_F(-1/t) \right] dt. \tag{2.5}$$

Although the e.s.d. $F^{\mathbf{B}_N}$ converges to a limiting spectral distribution F if $\mathbf{B}_N$ is defined as in (2.1), convergence can often not be guaranteed for more involved matrices $\mathbf{B}_N$. Nevertheless, even if the Stieltjes transform of $F^{\mathbf{B}_N}$ does not converge to m_F, it might still be approximated by a deterministic quantity m_{F_N} such that $m_{F^{\mathbf{B}_N}} - m_{F_N} \overset{N\to\infty}{\longrightarrow} 0$, almost surely, where m_{F_N} $\forall N$ is the Stieltjes transform of a distribution function F_N such that $F^{\mathbf{B}_N} - F_N \Rightarrow 0$, almost surely. The quantity m_{F_N} is referred to as *deterministic equivalent* of $m_{F^{\mathbf{B}_N}}$. More formally, a deterministic equivalent is defined as follows.

Definition 2.3 (Deterministic equivalent)**.** *[52] Consider a general probability space $(\Omega, \mathcal{F}, P)$. Let $\{f_N\}_{N\geq 1}$ be the series of measurable complex-valued functions $f_N : \Omega \times \mathbb{C} \to \mathbb{C}$ and let $\{g_N\}_{N\geq 1}$ be a series of complex-valued functions with $g_N : \mathbb{C} \to \mathbb{C}$. Then $\{g_N\}_{N\geq 1}$ is a deterministic equivalent of $\{f_N\}_{N\geq 1}$ on $D \subset \mathbb{C}$, if there exists a set $A \subset \Omega$ with $P(A) = 1$ such that*

$$f_N(w, z) - g_N(z) \to 0 \tag{2.6}$$

for all $\omega \in A$ and for all $z \in D$.

That is, $g_N(z)$ is an approximation of $f_N(w, z)$ for any pair (ω, z) with increasing accuracy as N grows large and the *series* $\{g_N\}_{N\geq 1}$ approximating $\{f_N\}_{N\geq 1}$ is called *deterministic equivalent*.

In case of large dimensional random matrices, denote $\{\mathbf{B}_N(\omega)\}_{N\geq 1}$ a series of matrices $\mathbf{B}_N(\omega) \in \mathbb{C}^{N\times N}$ of increasing size N, defined on a probability space $(\Omega, \mathcal{F}, P)$.[1] Then $\{f_N(\mathbf{B}_N, z)\}_{N\geq 1}$ defines a series of certain functionals $f_N(\omega, z)$, e.g., the Stieltjes transform $f_N(\omega, z) = m_{F^{\mathbf{B}_N}}(z) = \frac{1}{N}\mathrm{tr}(\mathbf{B}_N(\omega) - z\mathbf{I}_N)^{-1}$ or the Shannon transform $f_N(\omega, x) = \mathcal{V}_F(x) = \frac{1}{N}\log\det(\mathbf{I}_N + x\mathbf{B}_N(\omega))$, $x \in \mathbb{R}^+$.

In the following section, we prove the main theorem which provides deterministic equivalent m_{F_N} of the empirical Stieltjes transform $m_{F^{\mathbf{B}_N}}$ where $\mathbf{B}_N$ is random with generalized variance profile. The theorem extends the results in [31,53] but the proof strongly relies on the techniques applied in [31,53]. Note also that, for the here considered model of $\mathbf{B}_N$, a deterministic equivalent $\bar{\mu}_p$ of the pth order moment $\mu_p = \frac{1}{N}\mathrm{tr}\mathbf{B}_N^p$ such that $\mu_p - \bar{\mu}_p \overset{N\to\infty}{\longrightarrow} 0$, almost surely, has been derived in [54].

Subsequently, we simplify the notation and write $m_{\mathbf{X}} \triangleq m_{F^{\mathbf{X}}}$ and $\bar{m}_{\mathbf{X}} = m_{F_N}$.

2.2 A Deterministic Equivalent of the Empirical Stieltjes Transform of Matrices with Generalized Variance Profile

The following theorem extends the results in [31, 53] matrices with generalized variance profile. The results in this theorem are very general and its applications

[1] Note that, for $\omega \in \mathbb{C}$ the model $\{\mathbf{B}_N(\omega)\}_{N\geq 1}$ generates a whole series of matrices $\mathbf{B}_N(\omega)$ of increasing size.

are not restricted to mobile communications. However, in this dissertation the results in the theorem are applied to derive SINR approximations in large MU-MISO systems under various linear precoding techniques for the per-user channel correlation model in (1.15).

Theorem 2.1 (Main Theorem)**.** *Let* $\mathbf{B}_N = \mathbf{X}_N^{\mathsf{H}}\mathbf{X}_N + \mathbf{S}_N$ *with* $\mathbf{S}_N \in \mathbb{C}^{N\times N}$ *Hermitian nonnegative definite and* $\mathbf{X}_N \in \mathbb{C}^{n\times N}$ *random. The* i*th column* $\mathbf{x}_i$ *of* $\mathbf{X}_N^{\mathsf{H}}$ *is* $\mathbf{x}_i = \mathbf{\Psi}_i\mathbf{y}_i$*, where the entries of* $\mathbf{y}_i \in \mathbb{C}^{r_i}$ *are i.i.d. of zero mean, variance* $1/N$ *and have eighth order moment of order* $O\left(\frac{1}{N^4}\right)$*. The matrices* $\mathbf{\Psi}_i \in \mathbb{C}^{N\times r_i}$ *are deterministic. Furthermore, let* $\mathbf{\Theta}_i = \mathbf{\Psi}_i\mathbf{\Psi}_i^{\mathsf{H}} \in \mathbb{C}^{N\times N}$ *and define* $\mathbf{Q}_N \in \mathbb{C}^{N\times N}$ *deterministic. Assume* $\limsup_{N\to\infty} \sup_{1\le i\le n} \|\mathbf{\Theta}_i\| < \infty$ *and let* $\mathbf{Q}_N$ *be of uniformly bounded spectral norm (with respect to* N*). Define*

$$m_{\mathbf{B}_N,\mathbf{Q}_N}(z) \triangleq \frac{1}{N}\mathrm{tr}\mathbf{Q}_N\left(\mathbf{B}_N - z\mathbf{I}_N\right)^{-1}. \tag{2.7}$$

Then, for $z \in \mathbb{C}\setminus\mathbb{R}^+$*, as* n, N *grow large with ratios* $\beta_{N,i} \triangleq N/r_i$ *and* $\beta_N \triangleq N/n$ *such that* $0 < \liminf_N \beta_N \le \limsup_N \beta_N < \infty$ *and* $0 < \liminf_N \beta_{N,i} \le \limsup_N \beta_{N,i} < \infty$*, we have that*

$$m_{\mathbf{B}_N,\mathbf{Q}_N}(z) - \bar{m}_{\mathbf{B}_N,\mathbf{Q}_N}(z) \overset{N\to\infty}{\longrightarrow} 0, \tag{2.8}$$

almost surely, with $\bar{m}_{\mathbf{B}_N,\mathbf{Q}_N}(z)$ *given by*

$$\bar{m}_{\mathbf{B}_N,\mathbf{Q}_N}(z) = \frac{1}{N}\mathrm{tr}\mathbf{Q}_N\left(\frac{1}{N}\sum_{j=1}^{n}\frac{\mathbf{\Theta}_j}{1+e_{N,j}(z)} + \mathbf{S}_N - z\mathbf{I}_N\right)^{-1} \tag{2.9}$$

where $e_{N,1}(z), \ldots, e_{N,n}(z)$ *form the unique positive solution of*

$$e_{N,i}(z) = \frac{1}{N}\mathrm{tr}\mathbf{\Theta}_i\left(\frac{1}{N}\sum_{j=1}^{n}\frac{\mathbf{\Theta}_j}{1+e_{N,j}(z)} + \mathbf{S}_N - z\mathbf{I}_N\right)^{-1} \tag{2.10}$$

which is the Stieltjes transform of a nonnegative finite measure on $\mathbb{R}^+$*. Moreover, for* $z < 0$*, the* $e_{N,1}(z), \ldots, e_{N,n}(z)$ *are the unique nonnegative solutions to* (2.10)*.*

Once the $e_{N,i}(z)$ have been computed from (2.10), a deterministic equivalent $\bar{m}_{\mathbf{B}_N,\mathbf{Q}_N}(z)$ in (2.9) is given explicitly. The following proposition proves that, properly initialized, the fixed-point equations defined by (2.10) converge.

Proposition 2.2 (Convergence of the Fixed Point Algorithm)**.** *Let* $z \in \mathbb{C}\setminus\mathbb{R}^+$ *and* $\{e_{N,i}^{(k)}(z)\}$ *(*$k \ge 0$*) be the sequence defined by* $e_{N,i}^{(0)}(z) = -\frac{1}{z}$ *and*

$$e_{N,i}^{(k)}(z) = \frac{1}{N}\mathrm{tr}\mathbf{\Theta}_i\left(\frac{1}{N}\sum_{j=1}^{n}\frac{\mathbf{\Theta}_j}{1+e_{N,j}^{(k-1)}(z)} + \mathbf{S}_N - z\mathbf{I}_N\right)^{-1} \tag{2.11}$$

for $k > 0$*. Then,* $\lim_{k\to\infty} e_{N,i}^{(k)}(z) = e_{N,i}(z)$ *defined in* (2.10) *for* $i \in \{1, 2, \ldots, n\}$*.*

Theorem 2.1 provides a *deterministic* approximation $\bar{m}_{\mathbf{B}_N,\mathbf{Q}_N}(z)$ of the random variable $m_{\mathbf{B}_N,\mathbf{Q}_N}(z)$ which becomes more accurate for increasing N and is a function of n couples fixed-point equations 2.10.

The remainder of this section is dedicated to the proof of Theorem 2.1, which is structured as follows: In Section 2.2.1, we prove that $m_{\mathbf{B}_N,\mathbf{Q}_N}(z) - \frac{1}{N}\mathrm{tr}\mathbf{D}^{-1} \overset{N\to\infty}{\longrightarrow} 0$ almost surely, where $\mathbf{D}$ is an auxiliary random variable involving the terms $m_{\mathbf{B}_N,\mathbf{\Theta}_i}(z)$. Section 2.2.2 shows that the sequence $\{e_{N,i}^{(k)}(z)\}$ defined by (2.11) converges to $e_{N,i}$ (2.10) as $k \to \infty$ if properly initialized. Finally, in Section 2.2.3 we demonstrate that $e_{N,i}$ satisfies $|m_{\mathbf{B}_N,\mathbf{\Theta}_i} - e_{N,i}| \overset{N\to\infty}{\longrightarrow} 0$, almost surely.

2.2.1 Convergence to an Auxiliary Variable

The objective is to approximate the random variable $m_{\mathbf{B}_N,\mathbf{Q}_N}(z)$ by an appropriate functional $\frac{1}{N}\mathrm{tr}\mathbf{D}^{-1}$ such that

$$\frac{1}{N}\mathrm{tr}\mathbf{Q}_N\left(\mathbf{B}_N - z\mathbf{I}_N\right)^{-1} - \frac{1}{N}\mathrm{tr}\mathbf{D}^{-1} \overset{N\to\infty}{\longrightarrow} 0, \tag{2.12}$$

almost surely. From (2.12) we proceed by applying Lemma F.2 and obtain

$$\begin{aligned}&\mathbf{Q}_N\left(\mathbf{B}_N - z\mathbf{I}_N\right)^{-1} - \mathbf{D}^{-1}\\ &= \mathbf{D}^{-1}\left[\mathbf{D} - (\mathbf{X}_N^{\mathsf{H}}\mathbf{X}_N + \mathbf{S}_N - z\mathbf{I}_N)\mathbf{Q}_N^{-1}\right]\mathbf{Q}_N\left(\mathbf{B}_N - z\mathbf{I}_N\right)^{-1}.\end{aligned} \tag{2.13}$$

We choose $\mathbf{D}$ as

$$\mathbf{D} = \left(\mathbf{R} + \mathbf{S}_N - z\mathbf{I}_N\right)\mathbf{Q}_N^{-1}, \tag{2.14}$$

where $\mathbf{R}$ is to be determined later, and obtain

$$\begin{aligned}&\mathbf{Q}_N\left(\mathbf{B}_N - z\mathbf{I}_N\right)^{-1} - \mathbf{D}^{-1}\\ &= \mathbf{D}^{-1}\mathbf{R}\left(\mathbf{B}_N - z\mathbf{I}_N\right)^{-1} - \mathbf{D}^{-1}\mathbf{X}_N^{\mathsf{H}}\mathbf{X}_N\left(\mathbf{B}_N - z\mathbf{I}_N\right)^{-1}.\end{aligned}$$

Consider the term $\mathbf{D}^{-1}\mathbf{X}_N^{\mathsf{H}}\mathbf{X}_N\left(\mathbf{B}_N - z\mathbf{I}_N\right)^{-1}$. Taking the trace, together with the definition $\mathbf{X}_N^{\mathsf{H}}\mathbf{X}_N = \sum_{i=1}^n \mathbf{\Psi}_i\mathbf{y}_i\mathbf{y}_i^{\mathsf{H}}\mathbf{\Psi}_i^{\mathsf{H}}$, we have

$$\begin{aligned}\frac{1}{N}\mathrm{tr}\mathbf{D}^{-1}\mathbf{X}_N^{\mathsf{H}}\mathbf{X}_N\left(\mathbf{B}_N - z\mathbf{I}_N\right)^{-1} &= \frac{1}{N}\mathrm{tr}\mathbf{D}^{-1}\sum_{i=1}^n \mathbf{\Psi}_i\mathbf{y}_i\mathbf{y}_i^{\mathsf{H}}\mathbf{\Psi}_i^{\mathsf{H}}\left(\mathbf{B}_N - z\mathbf{I}_N\right)^{-1}\\ &= \frac{1}{N}\sum_{i=1}^n \mathbf{y}_i^{\mathsf{H}}\mathbf{\Psi}_i^{\mathsf{H}}\left(\mathbf{B}_N - z\mathbf{I}_N\right)^{-1}\mathbf{D}^{-1}\mathbf{\Psi}_i\mathbf{y}_i.\end{aligned}$$

Denoting $\mathbf{B}_{[i]} = \mathbf{B}_N - \mathbf{\Psi}_i\mathbf{y}_i\mathbf{y}_i^{\mathsf{H}}\mathbf{\Psi}_i^{\mathsf{H}}$ and applying Lemma F.1, we obtain

$$\frac{1}{N}\mathrm{tr}\mathbf{D}^{-1}\mathbf{X}_N^{\mathsf{H}}\mathbf{X}_N\left(\mathbf{B}_N - z\mathbf{I}_N\right)^{-1} = \frac{1}{N}\sum_{i=1}^n \frac{\mathbf{y}_i^{\mathsf{H}}\mathbf{\Psi}_i^{\mathsf{H}}\left(\mathbf{B}_{[i]} - z\mathbf{I}_N\right)^{-1}\mathbf{D}^{-1}\mathbf{\Psi}_i\mathbf{y}_i}{1 + \mathbf{y}_i^{\mathsf{H}}\mathbf{\Psi}_i^{\mathsf{H}}\left(\mathbf{B}_{[i]} - z\mathbf{I}_N\right)^{-1}\mathbf{\Psi}_i\mathbf{y}_i}.$$

Therefore, the left-hand side of (2.12) takes the form

$$\frac{1}{N}\mathrm{tr}\mathbf{Q}_N\left(\mathbf{B}_N - z\mathbf{I}_N\right)^{-1} - \frac{1}{N}\mathrm{tr}\mathbf{D}^{-1}$$
$$= \frac{1}{N}\mathrm{tr}\mathbf{D}^{-1}\mathbf{R}\left(\mathbf{B}_N - z\mathbf{I}_N\right)^{-1} - \frac{1}{N}\sum_{i=1}^{n}\frac{\mathbf{y}_i^{\mathsf{H}}\boldsymbol{\Psi}_i^{\mathsf{H}}\left(\mathbf{B}_{[i]} - z\mathbf{I}_N\right)^{-1}\mathbf{D}^{-1}\boldsymbol{\Psi}_i\mathbf{y}_i}{1+\mathbf{y}_i^{\mathsf{H}}\boldsymbol{\Psi}_i^{\mathsf{H}}\left(\mathbf{B}_{[i]} - z\mathbf{I}_N\right)^{-1}\boldsymbol{\Psi}_i\mathbf{y}_i}. \quad (2.15)$$

The choice of an appropriate value for $\mathbf{R}$, such that (2.12) is satisfied, requires some intuition. From Lemma F.4 we know that $\mathbf{y}_i^{\mathsf{H}}\boldsymbol{\Psi}_i^{\mathsf{H}}\left(\mathbf{B}_{[i]} - z\mathbf{I}_N\right)^{-1}\boldsymbol{\Psi}_i\mathbf{y}_i - \frac{1}{N}\mathrm{tr}\boldsymbol{\Theta}_i\left(\mathbf{B}_{[i]} - z\mathbf{I}_N\right)^{-1} \overset{N\to\infty}{\longrightarrow} 0$, almost surely. Then, from Lemma F.8, we surely have

$$\frac{1}{N}\mathrm{tr}\boldsymbol{\Theta}_i\left(\mathbf{B}_{[i]} - z\mathbf{I}_N\right)^{-1} - \frac{1}{N}\mathrm{tr}\boldsymbol{\Theta}_i\left(\mathbf{B}_N - z\mathbf{I}_N\right)^{-1} \overset{N\to\infty}{\longrightarrow} 0.$$

From the previous arguments, $\mathbf{R}$ will be chosen as

$$\mathbf{R} = \frac{1}{N}\sum_{i=1}^{n}\frac{\boldsymbol{\Theta}_i}{1+\frac{1}{N}\mathrm{tr}\boldsymbol{\Theta}_i\left(\mathbf{B}_N - z\mathbf{I}_N\right)^{-1}}. \quad (2.16)$$

Note that $\mathbf{R}$ is random since it depends on $\mathbf{B}_N$. The remainder of this section proves (2.12) for the specific choice of $\mathbf{R}$ in (2.16). Substituting (2.16) into (2.15) we obtain

$$w_N \triangleq w_{\mathbf{Q}_N} \triangleq \frac{1}{N}\mathrm{tr}\mathbf{Q}_N\left(\mathbf{B}_N - z\mathbf{I}_N\right)^{-1} - \frac{1}{N}\mathrm{tr}\mathbf{D}^{-1} \quad (2.17)$$
$$= \frac{1}{N}\sum_{i=1}^{n}\frac{\frac{1}{N}\mathrm{tr}\boldsymbol{\Theta}_i\left(\mathbf{B}_N - z\mathbf{I}_N\right)^{-1}\mathbf{D}^{-1}}{1+\frac{1}{N}\mathrm{tr}\boldsymbol{\Theta}_i\left(\mathbf{B}_N - z\mathbf{I}_N\right)^{-1}} - \frac{1}{N}\sum_{i=1}^{n}\frac{\mathbf{y}_i^{\mathsf{H}}\boldsymbol{\Psi}_i^{\mathsf{H}}\left(\mathbf{B}_{[i]} - z\mathbf{I}_N\right)^{-1}\mathbf{D}^{-1}\boldsymbol{\Psi}_i\mathbf{y}_i}{1+\mathbf{y}_i^{\mathsf{H}}\boldsymbol{\Psi}_i^{\mathsf{H}}\left(\mathbf{B}_{[i]} - z\mathbf{I}_N\right)^{-1}\boldsymbol{\Psi}_i\mathbf{y}_i}. \quad (2.18)$$

In order to prove that $w_N \overset{N\to\infty}{\longrightarrow} 0$, almost surely, we divide the left-hand side of (2.18) into $4n$ terms, i.e.,

$$w_N = \frac{1}{N}\sum_{i=1}^{n}\left[d_i^{(1)} + d_i^{(2)} + d_i^{(3)} + d_i^{(4)}\right]. \quad (2.19)$$

It is then easier to show that each $d_i^{(l)}$, $(l = 1, 2, 3, 4)$, converges to zero, sufficiently fast, as $N \to \infty$, which will imply $w_N \overset{N\to\infty}{\longrightarrow} 0$, almost surely. The $d_i^{(l)}$ are

chosen as

$$d_i^{(1)} = \frac{\mathbf{y}_i^{\mathsf{H}}\boldsymbol{\Psi}_i^{\mathsf{H}}\left(\mathbf{B}_{[i]} - z\mathbf{I}_N\right)^{-1}\mathbf{D}_{[i]}^{-1}\boldsymbol{\Psi}_i\mathbf{y}_i}{1+\mathbf{y}_i^{\mathsf{H}}\boldsymbol{\Psi}_i^{\mathsf{H}}\left(\mathbf{B}_{[i]} - z\mathbf{I}_N\right)^{-1}\boldsymbol{\Psi}_i\mathbf{y}_i} - \frac{\mathbf{y}_i^{\mathsf{H}}\boldsymbol{\Psi}_i^{\mathsf{H}}\left(\mathbf{B}_{[i]} - z\mathbf{I}_N\right)^{-1}\mathbf{D}^{-1}\boldsymbol{\Psi}_i\mathbf{y}_i}{1+\mathbf{y}_i^{\mathsf{H}}\boldsymbol{\Psi}_i^{\mathsf{H}}\left(\mathbf{B}_{[i]} - z\mathbf{I}_N\right)^{-1}\boldsymbol{\Psi}_i\mathbf{y}_i}$$

$$d_i^{(2)} = \frac{\frac{1}{N}\mathrm{tr}\boldsymbol{\Theta}_i\left(\mathbf{B}_{[i]} - z\mathbf{I}_N\right)^{-1}\mathbf{D}_{[i]}^{-1}}{1+\mathbf{y}_i^{\mathsf{H}}\boldsymbol{\Psi}_i^{\mathsf{H}}\left(\mathbf{B}_{[i]} - z\mathbf{I}_N\right)^{-1}\boldsymbol{\Psi}_i\mathbf{y}_i} - \frac{\mathbf{y}_i^{\mathsf{H}}\boldsymbol{\Psi}_i^{\mathsf{H}}\left(\mathbf{B}_{[i]} - z\mathbf{I}_N\right)^{-1}\mathbf{D}_{[i]}^{-1}\boldsymbol{\Psi}_i\mathbf{y}_i}{1+\mathbf{y}_i^{\mathsf{H}}\boldsymbol{\Psi}_i^{\mathsf{H}}\left(\mathbf{B}_{[i]} - z\mathbf{I}_N\right)^{-1}\boldsymbol{\Psi}_i\mathbf{y}_i}$$

$$d_i^{(3)} = \frac{\frac{1}{N}\mathrm{tr}\boldsymbol{\Theta}_i\left(\mathbf{B}_N - z\mathbf{I}_N\right)^{-1}\mathbf{D}^{-1}}{1+\mathbf{y}_i^{\mathsf{H}}\boldsymbol{\Psi}_i^{\mathsf{H}}\left(\mathbf{B}_{[i]} - z\mathbf{I}_N\right)^{-1}\boldsymbol{\Psi}_i\mathbf{y}_i} - \frac{\frac{1}{N}\mathrm{tr}\boldsymbol{\Theta}_i\left(\mathbf{B}_{[i]} - z\mathbf{I}_N\right)^{-1}\mathbf{D}_{[i]}^{-1}}{1+\mathbf{y}_i^{\mathsf{H}}\boldsymbol{\Psi}_i^{\mathsf{H}}\left(\mathbf{B}_{[i]} - z\mathbf{I}_N\right)^{-1}\boldsymbol{\Psi}_i\mathbf{y}_i}$$

$$d_i^{(4)} = \frac{\frac{1}{N}\mathrm{tr}\boldsymbol{\Theta}_i\left(\mathbf{B}_N - z\mathbf{I}_N\right)^{-1}\mathbf{D}^{-1}}{1+\frac{1}{N}\mathrm{tr}\boldsymbol{\Theta}_i\left(\mathbf{B}_N - z\mathbf{I}_N\right)^{-1}} - \frac{\frac{1}{N}\mathrm{tr}\boldsymbol{\Theta}_i\left(\mathbf{B}_N - z\mathbf{I}_N\right)^{-1}\mathbf{D}^{-1}}{1+\mathbf{y}_i^{\mathsf{H}}\boldsymbol{\Psi}_i^{\mathsf{H}}\left(\mathbf{B}_{[i]} - z\mathbf{I}_N\right)^{-1}\boldsymbol{\Psi}_i\mathbf{y}_i},$$

where we defined

$$\mathbf{D}_{[i]}^{-1} = \mathbf{Q}_N\left(\frac{1}{N}\sum_{i=1}^{n}\frac{\boldsymbol{\Theta}_i}{1+m_{\mathbf{B}_{[i]},\boldsymbol{\Theta}_i}(z)} - z\mathbf{I}_N + \mathbf{S}_N\right)^{-1},$$

where $m_{\mathbf{B}_{[i]},\boldsymbol{\Theta}_i}(z) = \frac{1}{N}\mathrm{tr}\boldsymbol{\Theta}_i\left(\mathbf{B}_{[i]} - z\mathbf{I}_N\right)^{-1}$.

In the course of development of the proof, we require the existence of moments of order p of w_N in (2.19), i.e., $E\left[|w_N|^p\right] \neq 0$, for some integer p. First we bound (2.19) as $E[|w_N|^p] \leq E[(\sum_{i=1}^{4n}\tilde{d}_i)^p]$. The application of Hölder's inequality yields

$$E\left[|w_N|^p\right] \leq \left(\frac{4}{\beta}\right)^{p-1}\frac{1}{N}\sum_{i=1}^{n}\sum_{l=1}^{4}E\left[|d_i^{(l)}|^p\right].$$

Furthermore, for some $T, Q < \infty$, we can uniformly bound $\boldsymbol{\Theta}_i$ and $\mathbf{Q}_N$ as

$$\limsup_{N\to\infty}\sup_{1\leq i\leq n}\|\boldsymbol{\Theta}_i\| \leq T \tag{2.20}$$

$$\limsup_{N\to\infty}\|\mathbf{Q}_N\| \leq Q. \tag{2.21}$$

Proposition 2.3. *Let the following upper bounds be well defined and let the entries of* $\mathbf{y}_i$ *have eighth order moment of order* $O\left(\frac{1}{N^4}\right)$*. Then the pth order*

moments $E\left[|d_i^{(l)}|^p\right]$, *(*$l = 1, 2, 3, 4$*) can be bounded as*

$$
\begin{aligned}
E\left[|d_i^{(1)}|^p\right] &\leq 2^{p-1}\left(\frac{\beta T^3 Q|z|^3}{(\Im z)^7}\right)^p \frac{1}{N^p}\left(\frac{C_p^{(1)}}{N^{p/2}}+1\right) \\
E\left[|d_i^{(2)}|^p\right] &\leq \frac{|z|^4}{(\Im z)^4}\frac{C_p^{(2)}}{N^{p/2}}, \\
E\left[|d_i^{(3)}|^p\right] &\leq \left(\frac{|z|TQ}{N(\Im z)^3}\right)^p\left[1+\frac{\beta T^2|z|^2}{(\Im z)^4}\right]^p, \\
E\left[|d_i^{(4)}|^p\right] &\leq 2^{p-1}\left(\frac{TQ|z|^2}{(\Im z)^4}\right)^p\left[\frac{C_p^{(4)}}{N^{p/2}}+\frac{T^p}{N^p(\Im z)^p}\right],
\end{aligned}
\tag{2.22}
$$

where the $C_p^{(i)}$, $i \in \{1, 2, 4\}$ *are constants depending only on* p.

Proof. The proof of Proposition 2.3 is provided in Appendix A. □

From Proposition 2.3, we conclude that all $E[|d_i^{(l)}|^p]$ are summable if $p = 2 + \varepsilon$, $\varepsilon > 0$. Therefore, $E\left[|w_N|^p\right]$ is summable for $p = 2 + \varepsilon$ and hence the Borel-Cantelli Lemma [50] implies that $w_N \overset{N\to\infty}{\longrightarrow} 0$, almost surely. Note that with the same approach, the convergence region can be extended to $z \in \mathbb{C} \setminus \mathbb{R}^+$.

We now prove the existence and uniqueness of a solution to (2.10).

2.2.2 Proof of Convergence of the Fixed Point Equation

In this section we consider the fixed point equation (2.10). We first prove that, properly initialized, the sequence $\{e_{N,i}^{(k)}\}$, $(k = 1, 2, \dots)$, converges to a limit $e_{N,i}$ as $k \to \infty$. Subsequently, we show that this limit $e_{N,i}$ satisfies $|m_{\mathbf{B}_N,\mathbf{\Theta}_i} - e_{N,i}| \overset{N\to\infty}{\longrightarrow} 0$, almost surely.

Proposition 2.4. *Let* $z \in \mathbb{C}^+$ *and* $\{e_{N,i}^{(k)}(z)\}$ *(*$k \geq 0$*) be the sequence defined by* (2.11)*. If* $\{e_{N,i}^{(0)}(z)\}$ *is a Stieltjes transform, then all* $\{e_{N,i}^{(k)}(z)\}$ *(*$k > 0$*) are Stieltjes transforms as well.*

Proof. Suppose (2.11) is initialized by $e_{N,i}^{(0)}(z) = -1/z$, which is the Stieltjes transform of a function with a single mass in zero. We demonstrate that at all subsequent iterations $k > 0$ the corresponding $e_{N,i}^{(k)}(z)$ are Stieltjes transforms for all N. For ease of notation we omit the dependence on z, the $e_{N,i}^{(k+1)}$ are given by

$$
e_{N,i}^{(k+1)} = \frac{1}{N}\mathrm{tr}\mathbf{\Theta}_i\left(\frac{1}{N}\sum_{j=1}^{n} c_{N,j}^{(k)}\mathbf{\Theta}_j + \mathbf{S}_N - z\mathbf{I}_N\right)^{-1} = \frac{1}{N}\mathrm{tr}\mathbf{\Theta}_i\mathbf{A}_k, \tag{2.23}
$$

where $c_{N,j}^{(k)} = 1/(1+e_{N,j}^{(k)})$ and we defined

$$\mathbf{A}_k \triangleq \left(\frac{1}{N} \sum_{j=1}^{n} c_{N,j}^{(k)} \mathbf{\Theta}_j + \mathbf{S}_N - z\mathbf{I}_N \right)^{-1}. \tag{2.24}$$

Multiplying $\mathbf{A}_k$ in (2.23) from the right by $(\mathbf{A}_k^{\mathsf{H}})^{-1}\mathbf{A}_k^{\mathsf{H}}$, we obtain

$$e_{N,i}^{(k+1)} = \frac{1}{N}\mathrm{tr}\mathbf{A}_k^{\mathsf{H}}\mathbf{\Theta}_i\mathbf{A}_k \left[\frac{1}{N} \sum_{j=1}^{n} c_{N,j}^{*,(k)} \mathbf{\Theta}_j \right] + v_i^{(k)}, \tag{2.25}$$

where $v_i^{(k)} = \frac{1}{N}\mathrm{tr}\mathbf{A}_k^{\mathsf{H}}\mathbf{\Theta}_i\mathbf{A}_k \left[\mathbf{S}_N - z^*\mathbf{I}_N\right]$. Denoting

$$\mathbf{r}_i^{(k)} \triangleq \frac{1}{N} \left[\frac{1}{N}\mathrm{tr}\mathbf{A}_k^{\mathsf{H}}\mathbf{\Theta}_i\mathbf{A}_k\mathbf{\Theta}_1, \ldots, \frac{1}{N}\mathrm{tr}\mathbf{A}_k^{\mathsf{H}}\mathbf{\Theta}_i\mathbf{A}_k\mathbf{\Theta}_n \right]^{\mathsf{T}}$$

and $\mathbf{c}_N^{(k)} \triangleq [c_{N,1}^{(k)}, \ldots, c_{N,n}^{(k)}]^{\mathsf{T}}$, (2.25) takes the form

$$e_{N,i}^{(k+1)} = \mathbf{r}_i^{\mathsf{T},(k)}\mathbf{c}_N^{\mathsf{H},(k)} + v_i^{(k)}. \tag{2.26}$$

Since the $\mathbf{\Theta}_i$ are uniformly bounded with respect to N, we have $\mathbf{r}_i^{(k)}, v_i^{(k)} > 0$. To show that $e_{N,i}^{(k+1)}$ are Stieltjes transforms of a nonnegative finite measure, the three conditions in Proposition 2.1 must hold true. From (2.26) it is easy to verify that all three conditions are met, which completes the proof.

□

We are now in a position to show that any sequence $\{e_{N,i}^{(k)}(z)\}$, $(k > 0)$ converges to a limit $e_{N,i}(z)$ as $k \to \infty$.

Proposition 2.5. *Any sequence* $\{e_{N,i}^{(k)}(z)\}$, $(k>0)$ *defined by* (2.11) *converges to* $e_{N,i}(z)$ *as* $k\to\infty$ *if* $e_{N,i}^{(0)}(z)$ *is a Stieltjes transform.*

Proof. Let $e_{N,i}^{(k)}(z) = \frac{1}{N}\mathrm{tr}\mathbf{\Theta}_i\mathbf{A}^{(k-1)}$ and $e_{N,i}^{(k+1)}(z) = \frac{1}{N}\mathrm{tr}\mathbf{\Theta}_i\mathbf{A}^{(k)}$, where

$$\mathbf{A}^{(k-1)} = \left(\frac{1}{N} \sum_{j=1}^{n} \frac{\mathbf{\Theta}_j}{1+e_{N,j}^{(k-1)}(z)} + \mathbf{S}_N - z\mathbf{I}_N \right)^{-1}$$

$$\mathbf{A}^{(k)} = \left(\frac{1}{N} \sum_{j=1}^{n} \frac{\mathbf{\Theta}_j}{1+e_{N,j}^{(k)}(z)} + \mathbf{S}_N - z\mathbf{I}_N \right)^{-1}.$$

Applying Lemma F.2, the difference $|e_{N,i}^{(k)}(z) - e_{N,i}^{(k+1)}(z)|$ reads

$$|e_{N,i}^{(k)} - e_{N,i}^{(k+1)}| = \left| \frac{1}{N}\mathrm{tr}\mathbf{A}^{(k+1)}\mathbf{\Theta}_i\mathbf{A}^{(k)} \left[\frac{1}{N} \sum_{j=1}^{n} \mathbf{\Theta}_j \frac{e_{N,j}^{(k)} - e_{N,j}^{(k-1)}}{\left[1+e_{N,j}^{(k)}\right]\left[1+e_{N,j}^{(k-1)}\right]} \right] \right|. \tag{2.27}$$

With Lemmas F.9, F.11 and F.12, (2.27) can be bounded as

$$|e_{N,i}^{(k)} - e_{N,i}^{(k+1)}| \leq C \sup_{1\leq i\leq n} |e_{N,i}^{(k)} - e_{N,i}^{(k-1)}|, \tag{2.28}$$

where $C = \frac{\beta T^2 |z|^2}{(\Im z)^4}$. Clearly, the sequence $\{e_{N,i}^{(k)}\}$ converges to a limit $e_{N,i}$ for z restricted to the set $\{z \in \mathbb{C}^+ : C < 1\}$. Proposition 2.4 shows that all $\{e_{N,i}^{(k)}\}$ are uniformly bounded Stieltjes transforms and therefore analytic. Since $\{e_{N,i}^{(k)}(z)\}$ for $\{z \in \mathbb{C}^+ : C < 1\}$ is at least countable, it has a cluster point. Thus, Vitali's convergence theorem [19, Theorem 3.11] ensures that the sequence $\{e_{N,i}^{(k)}\}$ must converge for all $z \in \mathbb{C} \setminus \mathbb{R}^+$. □

Remark 2.1. *For $z < 0$, the existence of a unique solution to* (2.10) *as well as the convergence of* (2.11) *from any real initial point can be proved within the framework of standard interference functions [55]. The strategy is as follows. Let $\bar{\mathbf{e}}_N \triangleq \bar{\mathbf{e}}_N(z) = [\bar{e}_{N,1}(z), \bar{e}_{N,2}(z), \ldots, \bar{e}_{N,n}(z)]^\mathsf{T} \in \mathbb{R}^n$ and define $\mathbf{f}(\bar{\mathbf{e}}_N) = [f_1(\bar{\mathbf{e}}_N), f_2(\bar{\mathbf{e}}_N), \ldots, f_n(\bar{\mathbf{e}}_N)]^\mathsf{T} \in \mathbb{R}^n$, where*

$$f_i(\bar{\mathbf{e}}_N) = \frac{1}{N}\mathrm{tr}\boldsymbol{\Theta}_i \left(\frac{1}{N} \sum_{j=1}^{n} \frac{\boldsymbol{\Theta}_j}{1 + \bar{e}_{N,j}(z)} + \mathbf{S}_N - z\mathbf{I}_N \right)^{-1}.$$

Theorems 1 and 2 in [55] prove that, if $\mathbf{f}(\bar{\mathbf{e}}_N)$ is a feasible standard interference function, then (2.11) *converges to a unique solution $\mathbf{e}_N$ with all nonnegative entries for any initial point $e_{N,i}^{(0)}, \ldots, e_{N,n}^{(0)}$. The proof that $\mathbf{f}(\bar{\mathbf{e}}_N)$ is feasible as well as a standard interference function is straightforward and details are omitted here.*

o The uniqueness of $\mathbf{e}_N$, whose entries are Stieltjes transforms of nonnegative finite measures, ensures the functional uniqueness of $e_{N,i}(z), \ldots, e_{N,n}(z)$ as a Stieltjes transform solution to (2.10) for $z \in \mathbb{C} \setminus \mathbb{R}^+$. This completes the proof of uniqueness.

Denote $m_{\mathbf{B}_N,\boldsymbol{\Theta}_i}(z) \triangleq \frac{1}{N}\mathrm{tr}\boldsymbol{\Theta}_i (\mathbf{B}_N - z\mathbf{I}_N)^{-1}$. In the following section, we prove that $e_{N,i}(z) = \lim_{k\to\infty} e_{N,i}^{(k)}(z)$ satisfies $|m_{\mathbf{B}_N,\boldsymbol{\Theta}_i}(z) - e_{N,i}(z)| \overset{N\to\infty}{\longrightarrow} 0$ almost surely.

2.2.3 Proof of Convergence of the Deterministic Equivalent

In Section 2.2.1, we showed that

$$w_N = \frac{1}{N}\mathrm{tr}\mathbf{Q}_N (\mathbf{B}_N - z\mathbf{I}_N)^{-1} - \frac{1}{N}\mathrm{tr}\mathbf{Q}_N (\mathbf{R} + \mathbf{S}_N - z\mathbf{I}_N) \overset{N\to\infty}{\longrightarrow} 0,$$

almost surely. Furthermore in Section 2.2.2 we proved that the sequence defined by (2.10) converges to a limit $e_{N,i}$. It remains to prove that

$$\begin{aligned} m_{\mathbf{B}_N,\mathbf{\Theta}_i} - e_{N,i} =& \frac{1}{N}\mathrm{tr}\mathbf{\Theta}_i \left(\mathbf{B}_N - z\mathbf{I}_N\right)^{-1} \\ & - \frac{1}{N}\mathrm{tr}\mathbf{\Theta}_i \left(\frac{1}{N}\sum_{j=1}^{n}\frac{\mathbf{\Theta}_j}{1+e_{N,j}(z)} + \mathbf{S}_N - z\mathbf{I}_N\right)^{-1} \overset{N\to\infty}{\longrightarrow} 0, \end{aligned} \tag{2.29}$$

almost surely. Denote $w_{N,i} \triangleq w_{\mathbf{\Theta}_i}$ with $w_{\mathbf{\Theta}_i}$ defined in (2.17). Applying Lemma F.2, (2.29) can be written as

$$\begin{aligned} m_{\mathbf{B}_N,\mathbf{\Theta}_i} - e_{N,i} &= w_{N,i} + \frac{1}{N}\mathrm{tr}\mathbf{\Theta}_i \left(\mathbf{A} + \mathbf{S}_N - z\mathbf{I}_N\right)^{-1} - e_{N,i}(z) \\ &= w_{N,i} - \frac{1}{N}\mathrm{tr}\mathbf{\Theta}_i \left(\mathbf{A} + \mathbf{S}_N - z\mathbf{I}_N\right)^{-1}\left[\mathbf{A}-\mathbf{B}\right]\left(\mathbf{B} + \mathbf{S}_N - z\mathbf{I}_N\right)^{-1}, \end{aligned}$$

where $\mathbf{A} \triangleq \frac{1}{N}\sum_{l=1}^{n}\frac{\mathbf{\Theta}_l}{1+\frac{1}{N}\mathrm{tr}\mathbf{\Theta}_l(\mathbf{B}_N - z\mathbf{I}_N)^{-1}}$ and $\mathbf{B} \triangleq \frac{1}{N}\sum_{j=1}^{n}\frac{\mathbf{\Theta}_j}{1+e_{N,j}}$. Applying Lemmas F.9 and F.11, $|m_{\mathbf{B}_N,\mathbf{\Theta}_i} - e_{N,i}|$ can be bounded as

$$\begin{aligned} |m_{\mathbf{B}_N,\mathbf{\Theta}_i} - e_{N,i}| \leq & |w_{N,i}| + \|\mathbf{\Theta}_i\|\|(\mathbf{A} + \mathbf{S}_N - z\mathbf{I}_N)^{-1}\| \\ & \times \|(\mathbf{B} + \mathbf{S}_N - z\mathbf{I}_N)^{-1}\| \left\| \frac{1}{N}\sum_{j=1}^{n}\mathbf{\Theta}_j \frac{|m_{\mathbf{B}_N,\mathbf{\Theta}_j} - e_{N,j}|}{(1+m_{\mathbf{B}_N,\mathbf{\Theta}_j})(1+e_{N,j})} \right\|. \end{aligned} \tag{2.30}$$

Similar to (2.28), with Lemma F.12, (2.30) can be further bounded as

$$|m_{\mathbf{B}_N,\mathbf{\Theta}_i} - e_{N,i}| \leq |w_{N,i}| + C \sup_{1\leq i\leq n} |m_{\mathbf{B}_N,\mathbf{\Theta}_i} - e_{N,i}|,$$

where $C = \frac{\beta T^2 |z|^2}{(\Im z)^4}$. Taking the supremum over all $i = 1, \ldots, n$, we obtain

$$\sup_{1\leq i\leq n} |m_{\mathbf{B}_N,\mathbf{\Theta}_i} - e_{N,i}|\,[1-C] \leq \sup_{1\leq i\leq n} |w_{N,i}|. \tag{2.31}$$

From (2.31), on the set $\{z \in \mathbb{C}^+ : 0 < C < 1\} \neq \emptyset$, it suffices to show that $\sup_{1\leq i\leq n} |w_{N,i}|$ goes to zero sufficiently fast. For any $\varepsilon > 0$ we have

$$\begin{aligned} P\left(\sup_{1\leq i\leq n} |w_{N,i}| > \varepsilon\right) &\leq P\left(\sum_{i=1}^{n} |w_{N,i}| > \varepsilon\right) \\ &\leq \sum_{i=1}^{n} P\left(|w_{N,i}| > \varepsilon\right) = \sum_{i=1}^{n} P\left(|w_{N,i}|^p > \varepsilon^p\right). \end{aligned} \tag{2.32}$$

Applying Markov's inequality, (2.32) can be further bounded as

$$P\left(\sup_{1\leq i\leq n} |w_{N,i}| \geq \varepsilon\right) \leq \frac{1}{\varepsilon^p}\sum_{i=1}^{n} E\left[|w_{N,i}|^p\right].$$

For all n and $p = 4 + \varepsilon$ with $\varepsilon > 0$, the term $\sum_{i=1}^{n} E\left[|w_{N,i}|^p\right]$ is summable and we can apply the Borel-Cantelli Lemma which implies $\sup_{1\leq i\leq n} w_{N,i} \overset{N\to\infty}{\longrightarrow} 0$, almost surely.

On $\{z\in\mathbb{C}^+ : 0 < C < 1\}$, the $e_{N,i}(z)$ are summable and have a cluster point. Furthermore, Proposition 2.4 assures that the $e_{N,i}(z)$ are Stieltjes transforms and hence uniformly bounded on every closed set in $\mathbb{C}\setminus\mathbb{R}^+$. Therefore, Vitali's convergence theorem applies, and extends the convergence region of (2.29) to $z\in\mathbb{C}\setminus\mathbb{R}^+$.

Since (2.29) holds true, the following convergence holds almost surely

$$\frac{1}{N}\mathrm{tr}\mathbf{D}^{-1} - \frac{1}{N}\mathrm{tr}\mathbf{Q}_N\left(\frac{1}{N}\sum_{i=1}^{n}\frac{\mathbf{\Theta}_i}{1+e_{N,i}} + \mathbf{S}_N - z\mathbf{I}_N\right)^{-1} \overset{N\to\infty}{\longrightarrow} 0. \tag{2.33}$$

The convergence in (2.33) implies the convergence in (2.8), which completes the proof.

2.3 Shannon Transform of Matrices with Generalized Variance Profile

Although we will not apply the result in this thesis, a recent application to random beamforming can be found in [56]. The following theorem is novel and extends the results in [31, 53].

Theorem 2.2 (Shannon transform of $\mathbf{B}_N$)**.** *Let $x > 0$ and $\mathbf{S}_N$ be uniformly bounded spectral norm with respect to N, given the assumptions of Theorem 2.1, denote the Shannon transform of $\mathbf{B}_N$ by $\mathcal{V}_{\mathbf{B}_N}(x) \triangleq \frac{1}{N}\log\det\left(\mathbf{I}_N + x\mathbf{B}_N\right)$. Then,*

$$E[\mathcal{V}_{\mathbf{B}_N}(x)] - \bar{\mathcal{V}}_{\mathbf{B}_N}(x) \overset{N\to\infty}{\longrightarrow} 0, \tag{2.34}$$

with $\bar{\mathcal{V}}_{\mathbf{B}_N}(x)$ given by

$$\begin{aligned}\bar{\mathcal{V}}_{\mathbf{B}_N}(x) = \frac{1}{N}\log\det&\left(\mathbf{I}_N + x\left[\mathbf{S}_N + \frac{1}{N}\sum_{j=1}^{n}\frac{\mathbf{\Theta}_i}{1+e_{N,j}(-1/x)}\right]\right)\\ &+ \frac{1}{N}\sum_{j=1}^{n}\log\left[1+e_{N,j}(-1/x)\right] - \frac{1}{N}\sum_{j=1}^{n}\frac{e_{N,j}(-1/x)}{1+e_{N,j}(-1/x)},\end{aligned} \tag{2.35}$$

where the $e_{N,1}(-1/x),\ldots,e_{N,n}(-1/x)$ form the unique solution of (2.10) *with $z = -1/x$.*

Proof of Theorem 2.2. The proof of (2.35) exploits the fact that the Shannon transform can be expressed as a function of the Stieltjes transform as (2.5)

$$\mathcal{V}_{\mathbf{B}_N}(x) = \int_{1/x}^{\infty}\left(\frac{1}{\omega} - m_{\mathbf{B}_N}(-\omega)\right)d\omega. \tag{2.36}$$

First notice that

$$\frac{1}{z} - \bar{m}_{\mathbf{B}_N}(-z) = \frac{1}{N}\mathrm{tr}\left[(z\mathbf{I}_N)^{-1} - \left(z\left[\mathbf{I}_N + \frac{1}{z}\mathbf{S}_N + \sum_{j=1}^{n}\bar{e}_{N,j}(-z)\mathbf{\Theta}_j\right]\right)^{-1}\right]$$
$$= \sum_{j=1}^{n} e_{N,j}(-z)\bar{e}_{N,j}(-z) + \frac{1}{z}\bar{m}_{\mathbf{B}_N,\mathbf{S}_N}(-z), \tag{2.37}$$

where $\bar{e}_{N,j}(z) = -\left[Nz(1+e_{N,j}(z))\right]^{-1}$ and $e_{N,j}(z)$ is given by (2.10). To apply (2.36), we require an expression that, when integrated with respect to z, yields (2.37). Observe that

$$\frac{\partial}{\partial z}\frac{1}{N}\log\det\left(\sum_{j=1}^{n}\bar{e}_{N,j}(-z)\mathbf{\Theta}_j + \mathbf{I}_N + \frac{1}{z}\mathbf{S}_N\right)$$
$$= -z\sum_{j=1}^{n} e_{N,j}(-z)\bar{e}'_{N,j}(-z) - \frac{1}{z}\bar{m}_{\mathbf{B}_N,\mathbf{S}_N}(-z) \tag{2.38}$$

$$\frac{\partial}{\partial z}\sum_{j=1}^{n}\frac{1}{N}\log\det\left[1+e_{N,j}(-z)\right] = -z\sum_{j=1}^{n}\bar{e}_{N,j}(-z)e'_{N,j}(-z) \tag{2.39}$$

$$\frac{\partial}{\partial z}\left[z\sum_{j=1}^{n} e_{N,j}(-z)\bar{e}_{N,j}(-z)\right] = \sum_{j=1}^{n} e_{N,j}(-z)\bar{e}_{N,j}(-z)$$
$$- z\left[\sum_{j=1}^{n} e_{N,j}(-z)\bar{e}'_{N,j}(-z) + \sum_{j=1}^{n}\bar{e}_{N,j}(-z)e'_{N,j}(-z)\right]. \tag{2.40}$$

Subtracting (2.38) and (2.39) from (2.40) yields (2.37). Applying (2.36) along with $\lim_{N\to 0}\mathcal{V}_{\mathbf{B}_N}(x) = 0$ leads to (2.35).

It remains to prove $E[\mathcal{V}_{\mathbf{B}_N}(x)] - \bar{\mathcal{V}}_{\mathbf{B}_N}(x) \overset{N\to\infty}{\longrightarrow} 0$, where $E[\mathcal{V}_{\mathbf{B}_N}(x)]$ is given by

$$E[\mathcal{V}_{\mathbf{B}_N}(x)] = \int_{1/x}^{\infty}\left(\frac{1}{\omega} - \frac{1}{N}E[m_{\mathbf{B}_N}(-\omega)]\right)d\omega. \tag{2.41}$$

The proof is similar to the one provided in [31, Section C.1]. The dominated convergence Theorem [50, Theorem 16.4] together with (2.8) ensures that for all $\omega > 0$,

$$\frac{1}{\omega} - \frac{1}{N}\mathrm{tr}\left(\frac{1}{N}\sum_{j=1}^{n}\frac{\mathbf{\Theta}_j}{1+e_{N,j}(-\omega)} + \omega\mathbf{I}_N + \mathbf{S}_N\right)^{-1}$$
$$- \left[\frac{1}{\omega} - \frac{1}{N}E[\mathrm{tr}\left(\mathbf{B}_N + \omega\mathbf{I}_N\right)^{-1}]\right] \overset{N\to\infty}{\longrightarrow} 0.$$

Now, observe that

$$\left|\frac{1}{\omega} - \bar{m}_{\mathbf{B}_N}(-\omega) - \left[\frac{1}{\omega} - E[m_{\mathbf{B}_N}(-\omega)]\right]\right| \tag{2.42}$$

$$\leq \left|\frac{1}{\omega} - \bar{m}_{\mathbf{B}_N}(-\omega)\right| + \left|\frac{1}{\omega} - E[m_{\mathbf{B}_N}(-\omega)]\right| \tag{2.43}$$

$$= \left|\int_0^\infty \left(\frac{1}{\omega} - \frac{1}{\lambda+\omega}\right) d\bar{F}_{\mathbf{B}_N}(\lambda)\right| + \left|E\left[\int_0^\infty \left(\frac{1}{\omega} - \frac{1}{\lambda+\omega}\right) dF_{\mathbf{B}_N}(\lambda)\right]\right| \tag{2.44}$$

$$\leq \left|\frac{1}{\omega^2}\int_0^\infty \lambda d\bar{F}_{\mathbf{B}_N}(\lambda)\right| + \left|\frac{1}{\omega^2}\, E\left[\int_0^\infty \lambda dF_{\mathbf{B}_N}(\lambda)\right]\right| \tag{2.45}$$

$$\leq 2\frac{\beta T}{\omega^2}, \tag{2.46}$$

where $F_{\mathbf{B}_N}$ and $\bar{F}_{\mathbf{B}_N}$ are the distribution functions with respective Stieltjes transforms $m_{\mathbf{B}_N}$ and $\bar{m}_{\mathbf{B}_N}$. The upper bound (2.46) is integrable in ω over $(1/x, \infty)$. Therefore, the dominated convergence theorem ensures $E[\mathcal{V}_{\mathbf{B}_N}(x)] - \bar{\mathcal{V}}_{\mathbf{B}_N}(x) \overset{N\to\infty}{\longrightarrow} 0$, which completes the proof. □

Chapter 3

MISO BC under Linear Precoding: A Large System Analysis

In this chapter, we consider the MISO broadcast channel under the following linear precoding techniques: Matched filter (MF), WSR maximizing (WSRM) linear precoding, regularized zero-forcing (RZF) and zero-forcing (ZF) precoding. We suppose that the system is *large* in the sense that the number of users K and the number of transmit antennas M grow large with finite ratio $M/K \to \beta < \infty$. Under this assumption, we will derive deterministic equivalents $\bar{\gamma}_k$ of the random SINR γ_k of user k for each of the precoding schemes. The chapter is structured as follows: In Section 3.1, we introduce the problem. In Sections 3.2, 3.3, 3.4 and 3.5, we derive a deterministic equivalent of the SINR under MF, WSRM linear precoding, RZF and ZF precoding, respectively. Section 3.6 discusses approximations of the rate based on the deterministic equivalent of the SINR. Finally, Section 3.7 presents simulation results to evaluate the accuracy of the proposed approximations.

3.1 Introduction

To gain valuable insights into the system behavior, it is necessary to determine the fundamental dependence of the system performance measure (e.g. the SINR γ_k or the rate $R_k = \log(1+\gamma_k)$ of user k) on the relevant system parameters (e.g. SNR, imperfect CSIT, correlation,...) through the *random* channel. That is, to predict how the change of a certain parameter will most likely change the

system performance. To accomplish this, one can consider the average system performance and approximate or bound it by a *deterministic* quantity, which then predicts how a particular system parameter affects the average system performance. The derivation of accurate bounds becomes extremely difficult for advanced channel models such as the per-user channel correlation model. However, another possibility to approximate the system performance is to assume that the system dimensions, i.e., the number of users K and the number of transmit antennas M, grow large with finite ratio $M/K \to \beta < \infty$. Under this assumption one can resort to the advanced tools of large RMT to derive a *deterministic equivalent* $\bar{\gamma}_k$ such that $\gamma_k - \bar{\gamma}_k \overset{M\to\infty}{\longrightarrow} 0$ almost surely. Under the per-user channel correlation model (or generalized variance profile) some important tools have been provided in the previous Chapter. In this chapter, we apply those tools to derive $\bar{\gamma}_k$ for each of the considered linear precoding schemes in MISO broadcast channels. As a result, we obtain asymptotically exact (almost surely) approximations of the SINR or per-user rate with *deterministic* dependencies on the important system parameters. The results in this chapter provide powerful tools that can be applied to solve various optimization problems, which is the subject of Chapter 4.

In order to also demonstrate the current limitations of large system analysis, consider the MU-MIMO setting with $S_k = N_k$ streams per user. In general, the objective of the large system analysis is to find a deterministic approximation of the communication rate R_k of user k. For MU-MIMO channels, the rate of user k is given in (1.5), which is the scaled Shannon transform of the e.s.d. of the matrix $\mathbf{B}_{N_k} \triangleq \mathbf{P}_k^{1/2}\mathbf{G}_k^{\mathsf{H}}\mathbf{H}_k^{\mathsf{H}}\mathbf{R}_{\tilde{\mathbf{n}}_k\tilde{\mathbf{n}}_k}^{-1}\mathbf{H}_k\mathbf{G}_k\mathbf{P}_k^{1/2}$. It is quite clear that for a channel-dependent precoding matrix $\mathbf{G}_k$, like MF, ZF or RZF precoding, the matrix model for $\mathbf{B}_{N_k}$ may be very complicated since it may depend in a non-trivial way on the random channels $\mathbf{H}_k$ as opposed to point-to-point MIMO channels [42, 57, 58]. It is complicated to derive a deterministic equivalent of the Shannon transform or equivalently (by exploiting the relation in (2.5)) the Stieltjes transform of the e.s.d. of $\mathbf{B}_{N_k}$, assuming that the number of receive antennas N_k of user k and the number of transmit antennas M grow large with $\frac{M}{N_k}$ bounded for a *finite* number of users K. For instance, under the simple MF precoder and perfect CSIT with $\mathbf{G}_k = \xi\mathbf{H}_k^{\mathsf{H}}$ (where ξ is such that (1.3) is satisfied) and $\mathbf{P}_k = \mathbf{I}_{N_k}$, the matrix $\mathbf{B}_{N_k}$ takes the form

$$\mathbf{B}_{N_k} = \xi^2\mathbf{H}_k\mathbf{H}_k^{\mathsf{H}}\left[\sigma_k^2\mathbf{I}_{N_k} + \mathbf{H}_k\left(\xi^2\sum_{i=1,i\neq k}^{K}\mathbf{H}_i^{\mathsf{H}}\mathbf{H}_i\right)\mathbf{H}_k^{\mathsf{H}}\right]^{-1}\mathbf{H}_k\mathbf{H}_k^{\mathsf{H}}. \tag{3.1}$$

Even for this simple case, a deterministic equivalent of the Stieltjes transform of the e.s.d. of $\mathbf{B}_{N_k}$ is unknown. In our subsequent analysis we assume $N_k = 1$, since single-antenna receivers are practical, and let M, K grow jointly to infinity with bounded ratio. In this case $R_k = \log(1+\gamma_k)$, where γ_k is given in (1.12) and it suffices to find a deterministic equivalent $\bar{\gamma}_k$ for the SINR γ_k, which immediately yields the deterministic equivalent $\bar{R}_k$ of the rate of user k.

The deterministic equivalents obtained in this chapter are useful approxi-

mations, since applied to practical optimization problems, cf. Chapter 4, they yield very accurate approximate solutions even for small realistic values of M, e.g. $M = 5$ or $M = 10$.

In the following, the notation $M \to \infty$ implies that both M and K grow asymptotically large while $1 \leq \lim_{M\to\infty} \frac{M}{K} = \beta < \infty$. Subsequently, to evaluate the large system results for finite dimensions, we replace β by its finite value $\frac{M}{K}$.

3.1.1 Technical Assumptions

Let us first clarify several technical assumptions that are required for the large system analysis.

Assumption 3.1. *All correlation matrices $\mathbf{\Theta}_k$ have uniformly bounded spectral norm on M, i.e.,*

$$\limsup_{M\to\infty} \sup_{1\leq k\leq K} \|\mathbf{\Theta}_k\| < \infty. \tag{3.2}$$

We further require the subsequent assumption on the power allocation matrix $\mathbf{P}$.

Assumption 3.2. *The power $p_{\max} = \max(p_1, \ldots, p_K)$ is of order $O(1/K)$, i.e.,*

$$\|\mathbf{P}\| = O(1/K). \tag{3.3}$$

Furthermore, we have to restrict the matrix containing the rate weights $\mathbf{U} = \mathrm{diag}(u_1, \ldots, u_K)$.

Assumption 3.3. *The rate weight matrix $\mathbf{U}$ has uniformly bounded spectral norm on M, i.e.,*

$$\limsup_{M\to\infty} \|\mathbf{U}\| < \infty. \tag{3.4}$$

Moreover, we require the following assumption

Assumption 3.4. *The matrix $\frac{1}{M}\hat{\mathbf{H}}^{\mathsf{H}}\hat{\mathbf{H}}$ has uniformly bounded spectral norm on M with probability one, i.e.,*

$$\limsup_{M\to\infty} \left\| \frac{1}{M}\hat{\mathbf{H}}^{\mathsf{H}}\hat{\mathbf{H}} \right\| < \infty, \tag{3.5}$$

with probability one.

Remark 3.1. *Assumption 3.4 holds true if $\sup_K |\{\mathbf{\Theta}_k : k = 1, 2, \ldots, K\}| < \infty$, where $|\mathcal{A}|$ denotes the cardinality of the set $\mathcal{A}$. That is, $\{\mathbf{\Theta}_k\}$ belongs to a finite family [57]. In practice, we typically deal with finite many distinct $\mathbf{\Theta}_k$. For instance consider the channel model for MIMO systems in 3GPP LTE [59], where the transmit correlation $\mathbf{\Theta}_k$ only comprises three different matrices corresponding to low, medium and high correlation. In particular, if $\mathbf{\Theta}_k = \mathbf{\Theta}$ $\forall k$, then Assumption 3.4 is satisfied, since $\frac{1}{M}\|\hat{\mathbf{H}}^{\mathsf{H}}\hat{\mathbf{H}}\| \leq \|\mathbf{\Theta}\|\|\hat{\mathbf{Z}}^{\mathsf{H}}\hat{\mathbf{Z}}\|$, where $\hat{\mathbf{Z}} = [\hat{\mathbf{z}}_1, \ldots, \hat{\mathbf{z}}_K]^{\mathsf{H}}$ and both $\|\mathbf{\Theta}\|$ and $\|\hat{\mathbf{Z}}^{\mathsf{H}}\hat{\mathbf{Z}}\|$ are uniformly bounded for all large M with probability one [60].*

In the following, we derive deterministic equivalents of the SINR for all considered precoding schemes. Hereby, apart from the results in Chapter 2, we will apply various results summarized in Appendix B.1 and Appendix F.

3.2 Matched Filter Precoding

The simplest transmit precoder is the matched filter (MF) defined as

$$\mathbf{G}_{\mathrm{mf}} = \frac{\xi_{\mathrm{mf}}}{M}\hat{\mathbf{H}}^{\mathsf{H}}, \tag{3.6}$$

where ξ_{mf} is such that the transmit power constraint $\mathrm{tr}(\mathbf{P}\mathbf{G}_{\mathrm{mf}}^{\mathsf{H}}\mathbf{G}_{\mathrm{mf}}) \leq P$ is satisfied with equality. The MF maximizes the signal power of user k but completely ignores the inter-user interference, which in turn leads to a rate saturation at high SNR due to the residual interference, even under perfect CSIT. The SINR $\gamma_{k,\mathrm{mf}}$ of user k under MF precoding is given by

$$\gamma_{k,\mathrm{mf}} = \frac{p_k \frac{\xi_{\mathrm{mf}}^2}{M^2}|\mathbf{h}_k^{\mathsf{H}}\hat{\mathbf{h}}_k|^2}{\xi_{\mathrm{mf}}^2 \sum\limits_{i=1,i\neq k}^{K} \frac{p_i}{M^2}|\mathbf{h}_k^{\mathsf{H}}\hat{\mathbf{h}}_i|^2 + \sigma_k^2} = \frac{\frac{p_k}{M^2}|\mathbf{h}_k^{\mathsf{H}}\hat{\mathbf{h}}_k|^2}{\frac{1}{M^2}\mathbf{h}_k^{\mathsf{H}}\hat{\mathbf{H}}_{[k]}^{\mathsf{H}}\mathbf{P}_{[k]}\hat{\mathbf{H}}_{[k]}\mathbf{h}_k + \frac{\sigma_k^2}{\xi_{\mathrm{mf}}^2}}, \tag{3.7}$$

where we defined

$$\hat{\mathbf{H}}_{[k]} \triangleq [\hat{\mathbf{h}}_1, \ldots, \hat{\mathbf{h}}_{k-1}, \hat{\mathbf{h}}_{k+1}, \ldots, \hat{\mathbf{h}}_K]^{\mathsf{H}} \in \mathbb{C}^{K-1\times M} \tag{3.8}$$

$$\mathbf{P}_{[k]} \triangleq \mathrm{diag}(p_1, \ldots, p_{k-1}, p_{k+1}, \ldots, p_K). \tag{3.9}$$

The following theorem gives a deterministic equivalent $\bar{\gamma}_{k,\mathrm{mf}}$ of the SINR $\gamma_{k,\mathrm{mf}}$ under MF precoding.

Theorem 3.1. *Let Assumption 3.1, 3.2 and 3.4 hold true and let $\gamma_{k,\mathrm{mf}}$ be the SINR of user k under MF precoding defined in* (3.7)*. Then*

$$\gamma_{k,\mathrm{mf}} - \bar{\gamma}_{k,\mathrm{mf}} \overset{M\to\infty}{\longrightarrow} 0, \tag{3.10}$$

almost surely, where $\bar{\gamma}_{k,\mathrm{mf}}$ is given by

$$\bar{\gamma}_{k,\mathrm{mf}} = \frac{p_k(1-\tau_k^2)\left[\frac{1}{M}\mathrm{tr}\boldsymbol{\Theta}_k\right]^2}{\frac{1}{M^2}\sum\limits_{i=1,i\neq k}^{K} p_i \mathrm{tr}\boldsymbol{\Theta}_k\boldsymbol{\Theta}_i + \frac{1}{\rho_k}\frac{1}{M}\sum\limits_{j=1}^{K} p_j \frac{1}{M}\mathrm{tr}\boldsymbol{\Theta}_j}, \tag{3.11}$$

where $\rho_k \triangleq P/\sigma_k^2$ is the SNR at user k.

Proof of Theorem 3.1. In the following, we will consider the terms ξ_{mf}^2, $\frac{1}{M}\mathbf{h}_k^{\mathsf{H}}\hat{\mathbf{h}}_k$ and $\frac{1}{M^2}\mathbf{h}_k^{\mathsf{H}}\hat{\mathbf{H}}_{[k]}^{\mathsf{H}}\mathbf{P}_{[k]}\hat{\mathbf{H}}_{[k]}\mathbf{h}_k$ separately and compute a deterministic equivalent

for each of them, which then (under Assumption 3.2) constitute a deterministic equivalent for the SINR. Note that, unlike the other considered precoding schemes, we do not require the Stieltjes transform (and thus the results in the previous Chapter) in this proof. Consider the term $\frac{1}{M}\mathbf{h}_k^{\mathsf{H}}\hat{\mathbf{h}}_k$, which rewrites using (1.14) as

$$\frac{1}{M}\mathbf{h}_k^{\mathsf{H}}\hat{\mathbf{h}}_k = \sqrt{1-\tau_k^2}\mathbf{z}_k^{\mathsf{H}}\boldsymbol{\Theta}_k\mathbf{z}_k + \tau_k\mathbf{z}_k^{\mathsf{H}}\boldsymbol{\Theta}_k\mathbf{e}_k. \tag{3.12}$$

Applying Lemma F.4 and Lemma F.5, we obtain

$$\mathbf{z}_k^{\mathsf{H}}\boldsymbol{\Theta}_k\mathbf{z}_k - \frac{1}{M}\mathrm{tr}\boldsymbol{\Theta}_k \overset{M\to\infty}{\longrightarrow} 0, \tag{3.13}$$

$$\mathbf{z}_k^{\mathsf{H}}\boldsymbol{\Theta}_k\mathbf{e}_k \overset{M\to\infty}{\longrightarrow} 0, \tag{3.14}$$

almost surely, and therefore

$$\frac{1}{M}\mathbf{h}_k^{\mathsf{H}}\hat{\mathbf{h}}_k - \sqrt{1-\tau_k^2}\frac{1}{M}\mathrm{tr}\boldsymbol{\Theta}_k \overset{M\to\infty}{\longrightarrow} 0, \tag{3.15}$$

almost surely. The transmit power constraint $\mathrm{tr}(\mathbf{P}\mathbf{G}_{\mathrm{mf}}^{\mathsf{H}}\mathbf{G}_{\mathrm{mf}}) = P$ yields

$$\xi_{\mathrm{mf}}^2 = \frac{P}{\frac{1}{M^2}\mathrm{tr}\mathbf{P}\hat{\mathbf{H}}\hat{\mathbf{H}}^{\mathsf{H}}}, \tag{3.16}$$

where the term $\frac{1}{M^2}\mathrm{tr}\mathbf{P}\hat{\mathbf{H}}\hat{\mathbf{H}}^{\mathsf{H}}$ takes the form

$$\frac{1}{M^2}\mathrm{tr}\mathbf{P}\hat{\mathbf{H}}\hat{\mathbf{H}}^{\mathsf{H}} = \frac{1}{M^2}\sum_{j=1}^{K} p_j\hat{\mathbf{h}}_j^{\mathsf{H}}\hat{\mathbf{h}}_j = \frac{1}{M}\sum_{j=1}^{K} p_j\hat{\mathbf{z}}_j^{\mathsf{H}}\boldsymbol{\Theta}_j\hat{\mathbf{z}}_j. \tag{3.17}$$

Applying Lemma F.4, we obtain $\bar{\xi}_{\mathrm{mf}}^2$ such that $\xi_{\mathrm{mf}}^2 - \bar{\xi}_{\mathrm{mf}}^2 \overset{M\to\infty}{\longrightarrow} 0$ almost surely, as

$$\bar{\xi}_{\mathrm{mf}}^2 = \frac{P}{\frac{1}{M}\sum_{j=1}^{K} p_j\frac{1}{M}\mathrm{tr}\boldsymbol{\Theta}_j}. \tag{3.18}$$

Finally, the interference power $\frac{1}{M^2}\mathbf{h}_k^{\mathsf{H}}\hat{\mathbf{H}}_{[k]}^{\mathsf{H}}\mathbf{P}_{[k]}\hat{\mathbf{H}}_{[k]}\mathbf{h}_k$ rewrites as

$$\frac{1}{M^2}\mathbf{h}_k^{\mathsf{H}}\hat{\mathbf{H}}_{[k]}^{\mathsf{H}}\mathbf{P}_{[k]}\hat{\mathbf{H}}_{[k]}\mathbf{h}_k = \frac{1}{M}\mathbf{z}_k^{\mathsf{H}}\boldsymbol{\Theta}_k^{1/2}\hat{\mathbf{H}}_{[k]}^{\mathsf{H}}\mathbf{P}_{[k]}\hat{\mathbf{H}}_{[k]}\boldsymbol{\Theta}_k^{1/2}\mathbf{z}_k. \tag{3.19}$$

In order to apply Lemma F.4, we need to ensure that the spectral norm of $\frac{1}{M}\boldsymbol{\Theta}_k^{1/2}\hat{\mathbf{H}}_{[k]}^{\mathsf{H}}\mathbf{P}_{[k]}\hat{\mathbf{H}}_{[k]}\boldsymbol{\Theta}_k^{1/2}$ is uniformly bounded on M. Applying Lemma F.8 and Lemma F.12, for all large M, we have that $\frac{1}{M}\|\boldsymbol{\Theta}_k^{1/2}\hat{\mathbf{H}}_{[k]}^{\mathsf{H}}\mathbf{P}_{[k]}\hat{\mathbf{H}}_{[k]}\boldsymbol{\Theta}_k^{1/2}\| \leq \frac{1}{M}\|\boldsymbol{\Theta}_k\|\cdot\|\hat{\mathbf{H}}^{\mathsf{H}}\mathbf{P}\hat{\mathbf{H}}\| \leq \frac{1}{M}\|\boldsymbol{\Theta}_k\|\cdot\|\mathbf{P}\|\cdot\|\hat{\mathbf{H}}^{\mathsf{H}}\hat{\mathbf{H}}\|$. Under the channel model (1.14), it has not been proved that $\frac{1}{M}\|\hat{\mathbf{H}}^{\mathsf{H}}\hat{\mathbf{H}}\| < \infty$ uniformly on M. However, taking Assumption 3.4 for granted and applying Lemma F.4, we obtain

$$\frac{1}{M}\mathbf{z}_k^{\mathsf{H}}\boldsymbol{\Theta}_k^{1/2}\hat{\mathbf{H}}_{[k]}^{\mathsf{H}}\mathbf{P}_{[k]}\hat{\mathbf{H}}_{[k]}\boldsymbol{\Theta}_k^{1/2}\mathbf{z}_k - \frac{1}{M^2}\mathrm{tr}\boldsymbol{\Theta}_k\hat{\mathbf{H}}_{[k]}^{\mathsf{H}}\mathbf{P}_{[k]}\hat{\mathbf{H}}_{[k]} \overset{M\to\infty}{\longrightarrow} 0, \tag{3.20}$$

almost surely. Rewriting

$$\frac{1}{M^2}\mathrm{tr}\boldsymbol{\Theta}_k\hat{\mathbf{H}}_{[k]}^{\mathsf{H}}\mathbf{P}_{[k]}\hat{\mathbf{H}}_{[k]} = \frac{1}{M}\sum_{i=1,i\neq k}^{K} p_i\hat{\mathbf{z}}_i^{\mathsf{H}}\boldsymbol{\Theta}_i^{1/2}\boldsymbol{\Theta}_k\boldsymbol{\Theta}_i^{1/2}\hat{\mathbf{z}}_i$$

and again applying Lemma F.4, yields

$$\frac{1}{M^2}\mathbf{h}_k^{\mathsf{H}}\hat{\mathbf{H}}_{[k]}^{\mathsf{H}}\mathbf{P}_{[k]}\hat{\mathbf{H}}_{[k]}\mathbf{h}_k - \frac{1}{M^2}\sum_{i=1,i\neq k}^{K} p_i\mathrm{tr}\boldsymbol{\Theta}_k\boldsymbol{\Theta}_i \overset{M\to\infty}{\longrightarrow} 0, \tag{3.21}$$

almost surely. For a finite total transmit power $P < \infty$, the deterministic equivalents of the terms $\frac{1}{M}\mathbf{h}_k^{\mathsf{H}}\hat{\mathbf{h}}_k$ and $\frac{1}{M^2}\mathbf{h}_k^{\mathsf{H}}\hat{\mathbf{H}}_{[k]}^{\mathsf{H}}\mathbf{P}_{[k]}\hat{\mathbf{H}}_{[k]}\mathbf{h}_k$ are finite and strictly positive. However, if $p_k = P$ the interference power is zero and we have $\bar{\xi}_{\mathrm{mf}}^2 \leq \frac{M}{\|\boldsymbol{\Theta}_k\|}$. Thus, the SINR approximation (3.11) increases unbounded in M and the convergence in (3.10) does not hold. Therefore, we require Assumption 3.2 for the convergence to hold true and thus the SINR is well-defined for all large M and given by (3.11), which completes the proof. □

Under common correlation, the approximated SINR is summarized in the following corollary.

Corollary 3.1. *Let Assumptions 3.1 and 3.2 hold true and let $\boldsymbol{\Theta}_k = \boldsymbol{\Theta}$ $\forall k$, then $\bar{\gamma}_{k,\mathrm{mf}}$ takes the form*

$$\bar{\gamma}_{k,\mathrm{mf}} = \frac{p_k}{P/K}\frac{(1-\tau_k^2)\beta\left[\frac{1}{M}\mathrm{tr}\boldsymbol{\Theta}\right]^2}{\frac{1}{M}\mathrm{tr}\boldsymbol{\Theta}^2(1-\frac{p_k}{P})+\frac{1}{\rho_k}\frac{1}{M}\mathrm{tr}\boldsymbol{\Theta}}. \tag{3.22}$$

Remark 3.2. *Note that from Assumption 3.2 it follows that $\frac{p_k}{P} \overset{M\to\infty}{\longrightarrow} 0$ $\forall k$ and thus by setting $\frac{p_k}{P} = 0$, we still have $\gamma_{k,\mathrm{mf}} - \bar{\gamma}_{k,\mathrm{mf}} \overset{M\to\infty}{\longrightarrow} 0$, almost surely. However, for small system dimensions and especially for unequal power allocation, the expression in* (3.22) *is more accurate. Thus, we decide to keep the term $\frac{p_k}{P}$ also it is not strictly necessary for the convergence in* (3.10) *to hold. This remark applies for all subsequently discussed linear precoding schemes.*

For uncorrelated channels, the approximated SINR in Theorem 3.1 reduces to a simple expression given in the following corollary.

Corollary 3.2. *Let Assumption 3.2 hold true and let $\boldsymbol{\Theta}_k = \mathbf{I}_M$ $\forall k$, then $\bar{\gamma}_{k,\mathrm{mf}}$ takes the form*

$$\bar{\gamma}_{k,\mathrm{mf}} = \frac{p_k}{P/K}\frac{(1-\tau_k^2)\beta}{1-\frac{p_k}{P}+\frac{1}{\rho_k}}. \tag{3.23}$$

Moreover, under equal power allocation, with $\lim_{M\to\infty}\frac{1}{K} = 0$, we have

Corollary 3.3. *Let $\boldsymbol{\Theta}_k = \mathbf{I}_M$ and $p_k = P/K$ $\forall k$, then $\bar{\gamma}_{k,\mathrm{mf}}$ takes the form*

$$\bar{\gamma}_{k,\mathrm{mf}} = \frac{(1-\tau_k^2)\beta}{1+\frac{1}{\rho_k}}. \tag{3.24}$$

From the SINR approximation (3.11), it is clear that the quality of the CSIT (represented by τ_k^2) simply results in a scaling of the signal power by $1-\tau_k^2$, whereas the interference power is independent of τ_k^2. That implies that the SINR of user k saturates at high SNR ρ_k even under perfect CSIT and the multiplexing gain is zero, since $\lim_{\rho_k\to\infty}\frac{\log(1+\bar{\gamma}_{k,\mathrm{mf}})}{\log\rho_k}=0$. Hence, the MF precoding scheme is interference-limited rather than feedback-limited. Moreover, from Corollary 3.1, observe that the SINR $\bar{\gamma}_{k,\mathrm{mf}}$ is proportional to β and thus to M. Therefore, to increase the system sum rate, it would make sense to drastically increase the number of transmit antennas for a given number of users, an idea originally proposed by Marzetta [61, 62]. However, a practical solution to employ hundreds of antennas at a base station without running into significant correlation issues has yet to be found. Furthermore, even linear precoding schemes in such a scenario would result in matrix operations involving huge matrices which becomes prohibitive. The only feasible precoding scheme may be MF precoding, not to speak of the complexity and feasibility of CSIT acquisition. Simulations suggest (cf. Section 3.7) that MF precoding is very sensitive to transmit correlation and relatively robust to CSIT imperfections, which further discourages the use of massive antenna arrays. On the bright side, recent work [28] on MF precoding in large TDD multi-cell systems under pilot contamination suggests that MF precoding achieves close-to-optimal performance as the system dimensions grow asymptotically large. Furthermore, the performance of simple precoding schemes such as MF precoding could significantly increase if the receivers have interference cancellation capabilities allowing to mitigate inter-user interference.

3.3 WSR Maximizing Linear Precoder with Perfect CSIT

Consider the *iterative* weighted sum rate (WSR) maximizing precoder proposed in [13] under *perfect* CSIT ($\tau_k=0\ \forall k$), equal power allocation ($p_k=1\ \forall k$) and identical noise variances ($\sigma_k^2=\sigma^2\ \forall k$). We strive to find a deterministic approximation of the SINR (and thus the rate) of user k at every iteration of the precoding algorithm in [13] given in Table 3.1.

3.3.1 Optimization Problem and Solution

Consider the WSR maximizing precoder $\mathbf{G}_{\mathrm{wsrm}}$ which is the solution of the following optimization problem

$$\mathbf{G}_{\mathrm{wsrm}}=\arg\max_{\mathbf{G}}\sum_{k=1}^{K}u_kR_k\quad\text{s.t.}\quad\mathrm{tr}\mathbf{G}\mathbf{G}^{\mathsf{H}}\leq P. \tag{3.25}$$

The optimization problem in (3.25) is hard to solve directly, since it is highly nonconvex in the precoding matrix $\mathbf{G}$. However, to solve the problem (3.25), consider the virtual linear receive filters $a_k\in\mathbb{C}\ \forall k$, which in case of MISO

channels are scalars. The error variance (mean square error) e_k after the linear receive filtering reads

$$e_k = E\left[|a_k y_k - s_k|^2\right]. \tag{3.26}$$

By introducing additional weighting scalars $w_k \geq 0$, the cost function (3.25) can be modified and an equivalent optimization problem can be formulated as [13]

$$\{\mathbf{G}_{\text{wsrm}}, a_k^\star, w_k^\star\} = \underset{\mathbf{G},a_k,w_k}{\arg\min} \left\{ w_k e_k - u_k \left[\log(u_k^{-1} w_k) - 1\right]\right\} \quad \text{s.t.} \quad \text{tr}\mathbf{G}\mathbf{G}^{\mathsf{H}} \leq P. \tag{3.27}$$

From (3.27), the optimal filters can be derived easily and read

$$a_k^\star = \mathbf{g}_{k,\text{wsrm}}^{\mathsf{H}} \mathbf{h}_k \left(\sigma^2 + \mathbf{h}_k^{\mathsf{H}} \mathbf{G}_{\text{wsrm}} \mathbf{G}_{\text{wsrm}}^{\mathsf{H}} \mathbf{h}_k\right)^{-1} \tag{3.28}$$

$$e_k^\star = (1 + \gamma_{k,\text{wsrm}})^{-1} \quad \text{with} \quad \gamma_{k,\text{wsrm}} = \frac{|\mathbf{h}_k^{\mathsf{H}} \mathbf{g}_{k,\text{wsrm}}|^2}{\sum_{i=1, i\neq k}^{K} |\mathbf{h}_k^{\mathsf{H}} \mathbf{g}_{i,\text{wsrm}}|^2 + \sigma^2} \tag{3.29}$$

$$w_k^\star = u_k (e_k^\star)^{-1} \tag{3.30}$$

$$\mathbf{G}_{\text{wsrm}} = \xi_{\text{wsrm}} \left(\mathbf{H}^{\mathsf{H}} \mathbf{D} \mathbf{H} + \frac{\text{tr}\mathbf{D}}{\rho} \mathbf{I}_M\right)^{-1} \mathbf{H}^{\mathsf{H}} \mathbf{A}^{\mathsf{H}} \mathbf{W}, \tag{3.31}$$

where ξ_{wsrm} is such that $\text{tr}\mathbf{G}_{\text{wsrm}}\mathbf{G}_{\text{wsrm}}^{\mathsf{H}} = P$ and we defined the SNR $\rho = P/\sigma^2$, the diagonal matrices $\mathbf{W} \triangleq \text{diag}(w_1^\star, \ldots, w_K^\star)$, $\mathbf{A} \triangleq \text{diag}(a_1^\star, \ldots, a_K^\star)$ and $\mathbf{D} \triangleq \text{diag}(d_1^\star, \ldots, d_K^\star)$ with $d_k^\star = w_k^\star (a_k^\star)^2 \ \forall k$. From the solutions in (3.28) and (3.31), it can be observed that transmit and receive filters depend on each other which leads to the iterative algorithm given in Table 3.1 to compute $\mathbf{G}_{\text{wsrm}}$. For notational convenience, we drop the superscript $\star$ in the sequel. The number of iterations N_{iter} is chosen large enough for the algorithm to converge. The convergence of the algorithm in Table 3.1 to a local optimum $\mathbf{G}_{\text{wsrm}}$ is proved in [13]. Moreover, the algorithm has to be initialized by precoding matrix $\mathbf{G}_{\text{init}}$, e.g., the MF precoder in (3.6).

The primary objective is to find a deterministic approximation $\bar{\gamma}_{k,\text{wsrm}}^{(j)}$ of the SINR $\gamma_{k,\text{wsrm}}^{(j)}$ at iteration j defined as

$$\gamma_{k,\text{wsrm}}^{(j)} = \frac{|\mathbf{h}_k^{\mathsf{H}} \mathbf{g}_{k,\text{wsrm}}^{(j)}|^2}{\sum_{i=1, i\neq k}^{K} |\mathbf{h}_k^{\mathsf{H}} \mathbf{g}_{i,\text{wsrm}}^{(j)}|^2 + \sigma^2}, \tag{3.32}$$

which will be derived in the next section.

3.3.2 Large System Analysis

In this section, we wish to derive a deterministic equivalent $\bar{\gamma}_{k,\text{wsrm}}^{(j)}$ of the SINR $\gamma_{k,\text{wsrm}}^{(j)}$ in (3.32) such that $\gamma_{k,\text{wsrm}}^{(j)} - \bar{\gamma}_{k,\text{wsrm}}^{(j)} \overset{M\to\infty}{\longrightarrow} 0$, almost surely at every iteration j for the precoder (3.31). However, the precoder (3.31) at iteration j depends in a non-trivial way on the channel $\mathbf{H}$ through the terms $a_k^{(j)}$ and $w_k^{(j)}$

INPUT: $\mathbf{H}$, σ^2, $\mathbf{G}_{\text{init}}$, N_{iter}
OUTPUT: $\mathbf{G}_{\text{wsrm}}$

`# Initialization`
$j = 0$
$\mathbf{G}_{\text{wsrm}}^{(0)} = \mathbf{G}_{\text{init}}$
$\gamma_{k,\text{wsrm}}^{(0)} = \frac{|\mathbf{h}_k^{\mathsf{H}}\mathbf{g}_{k,\text{wsrm}}^{(0)}|^2}{\sum_{i=1,i\neq k}^{K}|\mathbf{h}_k^{\mathsf{H}}\mathbf{g}_{i,\text{wsrm}}^{(0)}|^2+\sigma^2}$, $\forall k$
`# Main loop`
while $j < N_{\text{iter}}$ **do**
$j = j + 1$
$a_k^{(j)} = (\mathbf{g}_{k,\text{wsrm}}^{(j-1)})^{\mathsf{H}}\mathbf{h}_k \left(\sigma^2 + \mathbf{h}_k^{\mathsf{H}}\mathbf{G}_{\text{wsrm}}^{(j-1)}(\mathbf{G}_{\text{wsrm}}^{(j-1)})^{\mathsf{H}}\mathbf{h}_k\right)^{-1}$, $\forall k$
$e_k^{(j)} = \left(1 + \gamma_{k,\text{wsrm}}^{(j-1)}\right)^{-1}$, $\forall k$
$w_k^{(j)} = u_k(e_k^{(j)})^{-1}$, $\forall k$
$\mathbf{W}^{(j)} \triangleq \text{diag}(w_1^{(j)}, \ldots, w_K^{(j)})$
$\mathbf{A}^{(j)} \triangleq \text{diag}(a_1^{(j)}, \ldots, a_K^{(j)})$
$\mathbf{D}^{(j)} \triangleq \text{diag}(d_1^{(j)}, \ldots, d_K^{(j)})$ with $d_k^{(j)} = w_k^{(j)}(a_k^{(j)})^2$ $\forall k$
$\mathbf{G}_{\text{wsrm}}^{(j)} = \xi_{\text{wsrm}}^{(j)} \left(\mathbf{H}^{\mathsf{H}}\mathbf{D}^{(j)}\mathbf{H} + \frac{\text{tr}\mathbf{D}^{(j)}}{\rho}\mathbf{I}_M\right)^{-1} \mathbf{H}^{\mathsf{H}}(\mathbf{A}^{(j)})^{\mathsf{H}}\mathbf{W}^{(j)}$
$\gamma_{k,\text{wsrm}}^{(j)} = \frac{|\mathbf{h}_k^{\mathsf{H}}\mathbf{g}_{k,\text{wsrm}}^{(j)}|^2}{\sum_{i=1,i\neq k}^{K}|\mathbf{h}_k^{\mathsf{H}}\mathbf{g}_{i,\text{wsrm}}^{(j)}|^2+\sigma^2}$, $\forall k$
end while
$\mathbf{G}_{\text{wsrm}} = \mathbf{G}_{\text{wsrm}}^{(j)}$

Table 3.1: Iterative algorithm to compute $\mathbf{G}_{\text{wsrm}}$.

which renders the derivation of $\bar{\gamma}_{k,\text{wsrm}}^{(j)}$ difficult if not impossible. Therefore, we consider a different precoder. where we substitute the random variables $a_k^{(j)}$ and $w_k^{(j)}$ by finite deterministic values $\bar{a}_k^{(j)}$ and $\bar{w}_k^{(j)}$, respectively. More precisely, $\bar{a}_k^{(j)}$ and $\bar{w}_k^{(j)}$ are such that $a_k^{(j)} - \bar{a}_k^{(j)} \overset{M\to\infty}{\longrightarrow} 0$ and $w_k^{(j)} - \bar{w}_k^{(j)} \overset{M\to\infty}{\longrightarrow} 0$ $\forall k$, almost surely, where both $\bar{a}_k^{(j)}$ and $\bar{w}_k^{(j)}$ exist. It follows that $d_k^{(j)} - \bar{d}_k^{(j)} \overset{M\to\infty}{\longrightarrow} 0$ $\forall k$, almost surely, where $\bar{d}_k^{(j)} = \bar{w}_k^{(j)}(\bar{a}_k^{(j)})^2$. Thus, the modified precoder $\tilde{\mathbf{G}}_{\text{wsrm}}^{(j)}$ takes the form

$$\tilde{\mathbf{G}}_{\text{wsrm}}^{(j)} = \tilde{\xi}_{\text{wsrm}}^{(j)} \left(\mathbf{H}^{\mathsf{H}}\bar{\mathbf{D}}^{(j)}\mathbf{H} + \frac{\text{tr}\bar{\mathbf{D}}^{(j)}}{\rho}\mathbf{I}_M\right)^{-1} \mathbf{H}^{\mathsf{H}}(\bar{\mathbf{A}}^{(j)})^{\mathsf{H}}\bar{\mathbf{W}}^{(j)}, \tag{3.33}$$

where $\tilde{\xi}_{\text{wsrm}}^{(j)}$ is such that $\text{tr}\tilde{\mathbf{G}}_{\text{wsrm}}^{(j)}(\tilde{\mathbf{G}}_{\text{wsrm}}^{(j)})^{\mathsf{H}} = P$ and $\bar{\mathbf{W}}^{(j)} \triangleq \text{diag}(\bar{w}_1^{(j)}, \ldots, \bar{w}_K^{(j)})$, $\bar{\mathbf{A}}^{(j)} \triangleq \text{diag}(\bar{a}_1^{(j)}, \ldots, \bar{a}_K^{(j)})$ and $\bar{\mathbf{D}}^{(j)} \triangleq \text{diag}(\bar{d}_1^{(j)}, \ldots, \bar{d}_K^{(j)})$. Define $\tilde{\gamma}_{k,\text{wsrm}}^{(j)}$ the

SINR of user k for the proposed precoder in (3.33) at iteration j as

$$\tilde{\gamma}_{k,\text{wsrm}}^{(j)} = \frac{|\mathbf{h}_k^{\mathsf{H}} \tilde{\mathbf{g}}_{k,\text{wsrm}}^{(j)}|^2}{\sum_{i=1,i\neq k}^{K} |\mathbf{h}_k^{\mathsf{H}} \tilde{\mathbf{g}}_{i,\text{wsrm}}^{(j)}|^2 + \sigma^2}. \tag{3.34}$$

It is important to note that we are not able to prove that the derived deterministic equivalent $\bar{\tilde{\gamma}}_{k,\text{wsrm}}^{(j)}$ of the SINR (3.34) under the proposed precoder (3.33) is a deterministic equivalent for the WSRM precoder in (3.31). However, simulations suggest that $\tilde{\gamma}_{k,\text{wsrm}}^{(j)}$ is an accurate approximation of $\gamma_{k,\text{wsrm}}^{(j)}$ in (3.32).

Under the precoder (3.33), a deterministic equivalent $\bar{\tilde{\gamma}}_{k,\text{wsrm}}^{(j)}$ of the SINR is provided in the following theorem.

Theorem 3.2. *Let Assumptions 3.1, 3.3 and 3.4 hold and let $\tilde{\gamma}_{k,\text{wsrm}}^{(j)}$ be the SINR of user k for the precoder* (3.33) *defined in* (3.34)*. Then, a deterministic equivalent $\bar{\tilde{\gamma}}_{k,\text{wsrm}}^{(j)}$ at iteration $j > 0$ such that*

$$\tilde{\gamma}_{k,\text{wsrm}}^{(j)} - \bar{\tilde{\gamma}}_{k,\text{wsrm}}^{(j)} \overset{M\to\infty}{\longrightarrow} 0, \tag{3.35}$$

almost surely, is given by

$$\bar{\tilde{\gamma}}_{k,\text{wsrm}}^{(j)} = \frac{\bar{w}_k^{(j)} (e_k^{(j)})^2}{\bar{\Upsilon}_{k,\text{wsrm}}^{(j)} + \bar{d}_k^{(j)} \frac{\bar{\Psi}_{\text{wsrm}}^{(j)}}{\rho} (1 + e_k^{(j)})^2}, \tag{3.36}$$

where the $e_1^{(j)}, \ldots, e_K^{(j)}$ form the unique positive solutions of

$$e_i^{(j)} = \frac{1}{M} \text{tr} \bar{\mathbf{\Theta}}_i^{(j)} \mathbf{T}^{(j)} \tag{3.37}$$

$$\mathbf{T}^{(j)} = \left(\frac{1}{M} \sum_{i=1}^{K} \frac{\bar{\mathbf{\Theta}}_i^{(j)}}{1 + e_i^{(j)}} + \bar{\alpha}^{(j)} \mathbf{I}_M \right)^{-1}, \tag{3.38}$$

and $\bar{\Psi}_{\text{wsrm}}^{(j)}$ and $\bar{\Upsilon}_{k,\text{wsrm}}^{(j)}$ read

$$\bar{\Psi}_{\text{wsrm}}^{(j)} = \frac{1}{M} \sum_{i=1}^{K} \frac{\bar{w}_i^{(j)} e_i'^{,(j)}}{(1 + e_i^{(j)})^2}, \tag{3.39}$$

$$\bar{\Upsilon}_{k,\text{wsrm}}^{(j)} = \frac{1}{M} \sum_{i=1,i\neq k}^{K} \frac{\bar{w}_i^{(j)} e_{i,k}'^{,(j)}}{(1 + e_i^{(j)})^2}, \tag{3.40}$$

with $\bar{\mathbf{\Theta}}_k^{(j)} = \bar{d}_k^{(j)}\mathbf{\Theta}_k$, $\bar{\alpha}^{(j)} \triangleq \frac{\mathrm{tr}\bar{\mathbf{D}}^{(j)}}{M\rho}$ *and* $\bar{a}_k^{(j)}$, $\bar{w}_k^{(j)}$ *and* $\bar{d}_k^{(j)}$ *are given by*

$$\bar{a}_k^{(j)} = \frac{1}{\sqrt{\bar{P}_{S,k}^{(j-1)}}} \frac{\bar{\bar{\gamma}}_{k,\mathrm{wsrm}}^{(j-1)}}{1+\bar{\bar{\gamma}}_{k,\mathrm{wsrm}}^{(j-1)}} \tag{3.41}$$

$$\sqrt{\bar{P}_{S,k}^{(j-1)}} = \frac{1}{\bar{a}_k^{(j-1)}} \sqrt{\frac{P}{\bar{\Psi}_{\mathrm{wsrm}}^{(j-1)}}} \frac{e_k^{(j-1)}}{1+e_k^{(j-1)}} \tag{3.42}$$

$$\bar{w}_k^{(j)} = u_k \left(1+\bar{\bar{\gamma}}_{k,\mathrm{wsrm}}^{(j-1)}\right) \tag{3.43}$$

$$\bar{d}_k^{(j)} = \bar{w}_k^{(j)} (\bar{a}_k^{(j)})^2. \tag{3.44}$$

Define $\mathbf{e}'^{,(j)} = [e_1'^{,(j)}, \ldots, e_K'^{,(j)}]^{\mathsf{T}}$ *and* $\mathbf{e}_k'^{,(j)} = [e_{1,k}'^{,(j)}, \ldots, e_{K,k}'^{,(j)}]^{\mathsf{T}}$, *which are given as*

$$\mathbf{e}'^{,(j)} = (\mathbf{I}_K - \mathbf{J})^{-1}\mathbf{v}, \tag{3.45}$$

$$\mathbf{e}_k'^{,(j)} = (\mathbf{I}_K - \mathbf{J})^{-1}\mathbf{v}_k, \tag{3.46}$$

where $\mathbf{J}$, $\mathbf{v}$ *and* $\mathbf{v}_k$ *take the form*

$$[\mathbf{J}]_{ij} = \frac{\frac{1}{M}\mathrm{tr}\bar{\mathbf{\Theta}}_i\mathbf{T}^{(j)}\bar{\mathbf{\Theta}}_j\mathbf{T}^{(j)}}{M(1+e_j^{(j)})^2},$$

$$\mathbf{v} = \left[\frac{1}{M}\mathrm{tr}\bar{\mathbf{\Theta}}_1(\mathbf{T}^{(j)})^2, \ldots, \frac{1}{M}\mathrm{tr}\bar{\mathbf{\Theta}}_K(\mathbf{T}^{(j)})^2\right]^{\mathsf{T}},$$

$$\mathbf{v}_k = \left[\frac{1}{M}\mathrm{tr}\bar{\mathbf{\Theta}}_1\mathbf{T}^{(j)}\bar{\mathbf{\Theta}}_k\mathbf{T}^{(j)}, \ldots, \frac{1}{M}\mathrm{tr}\bar{\mathbf{\Theta}}_K\mathbf{T}^{(j)}\bar{\mathbf{\Theta}}_k\mathbf{T}^{(j)}\right]^{\mathsf{T}}.$$

If the algorithm in Table 3.1 is initialized with the matched filter, i.e., $\mathbf{G}_{\mathrm{init}} = \mathbf{G}_{\mathrm{mf}} = \frac{\xi_{\mathrm{mf}}}{M}\mathbf{H}^{\mathsf{H}}$, we have $\bar{\bar{\gamma}}_{k,\mathrm{wsrm}}^{(0)} = \bar{\gamma}_{k,\mathrm{mf}}$, given in Theorem 3.1, and $\bar{P}_{S,k}^{(0)} = \frac{(\frac{1}{M}\mathrm{tr}\mathbf{\Theta}_k)^2}{\frac{1}{MK}\sum_{j=1}^{K}\frac{1}{M}\mathrm{tr}\mathbf{\Theta}_j}$, cf. (3.15) and (3.18).

Proof of Theorem 3.2. Similar to the proof of Theorem 3.1, we derive deterministic equivalents for the power normalization $\tilde{\xi}_{\mathrm{wsrm}}^{(j)}$, the signal power $|\mathbf{h}_k^{\mathsf{H}}\tilde{\mathbf{g}}_k^{(j)}|^2$ and the interference power $\sum_{i=1,i\neq k}^{K}|\mathbf{h}_k^{\mathsf{H}}\tilde{\mathbf{g}}_i^{(j)}|^2$ which together constitute $\bar{\bar{\gamma}}_{k,\mathrm{wsrm}}^{(j)}$.

First, the power normalization scalar $\tilde{\xi}_{\mathrm{wsrm}}^{(j)}$ takes the form

$$\tilde{\xi}_{\mathrm{wsrm}}^{(j)} = \sqrt{\frac{P}{\mathrm{tr}\tilde{\mathbf{G}}^{(j)}(\tilde{\mathbf{G}}^{(j)})^{\mathsf{H}}}} = \sqrt{\frac{P}{\Psi_{\mathrm{wsrm}}^{(j)}}}, \tag{3.47}$$

where $\Psi_{\mathrm{wsrm}}^{(j)} \triangleq \mathrm{tr}\tilde{\mathbf{G}}^{(j)}(\tilde{\mathbf{G}}^{(j)})^{\mathsf{H}}$ which rewrites as

$$\Psi_{\mathrm{wsrm}}^{(j)} = \mathrm{tr}\left(\mathbf{H}^{\mathsf{H}}\bar{\mathbf{D}}^{(j)}\mathbf{H} + \frac{\mathrm{tr}\bar{\mathbf{D}}^{(j)}}{\rho}\mathbf{I}_M\right)^{-2}\mathbf{H}^{\mathsf{H}}(\bar{\mathbf{A}}^{(j)})^{\mathsf{H}}(\bar{\mathbf{W}}^{(j)})^2\bar{\mathbf{A}}^{(j)}\mathbf{H} \tag{3.48}$$

$$= \mathrm{tr}\left(\mathbf{H}^{\mathsf{H}}\bar{\mathbf{D}}^{(j)}\mathbf{H} + M\bar{\alpha}^{(j)}\mathbf{I}_M\right)^{-2}\mathbf{H}^{\mathsf{H}}(\bar{\mathbf{D}}^{(j)})^{1/2}\bar{\mathbf{W}}^{(j)}(\bar{\mathbf{D}}^{(j)})^{1/2}\mathbf{H}. \tag{3.49}$$

The term $(\bar{\mathbf{D}}^{(j)})^{1/2}\mathbf{H}$ multiplies every row of $\mathbf{H}$, i.e., every channel $\mathbf{h}_k^{\mathsf{H}}$, by the corresponding $\sqrt{\bar{d}_k^{(j)}}$. Hence, we can include the $\bar{d}_k^{(j)}$ in the correlation matrices $\mathbf{\Theta}_k$ and define $\bar{\mathbf{\Theta}}_k^{(j)} \triangleq \bar{d}_k^{(j)}\mathbf{\Theta}_k$ as well as $\bar{\mathbf{H}}^{(j)} \triangleq (\bar{\mathbf{D}}^{(j)})^{1/2}\mathbf{H}$. Thus, (3.49) becomes

$$\Psi_{\text{wsrm}}^{(j)} = \text{tr}\left((\bar{\mathbf{H}}^{(j)})^{\mathsf{H}}\bar{\mathbf{H}}^{(j)} + M\bar{\alpha}^{(j)}\mathbf{I}_M\right)^{-2}(\bar{\mathbf{H}}^{(j)})^{\mathsf{H}}\bar{\mathbf{W}}^{(j)}\bar{\mathbf{H}}^{(j)}. \tag{3.50}$$

From Assumption 3.3, it follows that $\|\bar{\mathbf{W}}^{(j)}\| < \infty$ and $\|\bar{\mathbf{D}}^{(j)}\| < \infty$ uniformly on M. Thus $\|\bar{\mathbf{\Theta}}_k^{(j)}\| < \infty$ uniformly on M. Furthermore, for all finite ρ we have $\bar{\alpha}^{(j)} > 0$. Applying Lemma B.1, we obtain $\bar{\Psi}_{\text{wsrm}}^{(j)}$, such that $\Psi_{\text{wsrm}}^{(j)} - \bar{\Psi}_{\text{wsrm}}^{(j)} \overset{M\to\infty}{\longrightarrow} 0$ almost surely, as

$$\bar{\Psi}_{\text{wsrm}}^{(j)} = \frac{1}{M}\sum_{k=1}^{K}\frac{\bar{w}_k^{(j)}e_k'^{,(j)}}{(1+e_k^{(j)})^2}, \tag{3.51}$$

where $e_k^{(j)}$ and $e_k'^{,(j)}$ are defined in (3.37) and (3.45), respectively.

The signal power $P_{S,k}^{(j)} \triangleq |\mathbf{h}_k^{\mathsf{H}}\tilde{\mathbf{g}}_k^{(j)}|^2$ takes the form

$$P_{S,k}^{(j)} = (\tilde{\xi}_{\text{wsrm}}^{(j)}\Phi_k^{(j)})^2, \tag{3.52}$$

where $\Phi_k^{(j)} = (\bar{a}_k^{(j)})^{-1}(\bar{\mathbf{h}}_k^{(j)})^{\mathsf{H}}\left((\bar{\mathbf{H}}^{(j)})^{\mathsf{H}}\bar{\mathbf{H}}^{(j)} + M\bar{\alpha}^{(j)}\mathbf{I}_M\right)^{-1}\bar{\mathbf{h}}_k^{(j)}$ and $\bar{\mathbf{h}}_k^{(j)}$ is the kth column of $(\bar{\mathbf{H}}^{(j)})^{\mathsf{H}}$. We can directly apply Lemma B.2 to $\Phi_k^{(j)}$ and obtain $\bar{P}_{S,k}^{(j)}$ such that $P_{S,k}^{(j)} - \bar{P}_{S,k}^{(j)} \overset{M\to\infty}{\longrightarrow} 0$, almost surely, as

$$\bar{P}_{S,k}^{(j)} = \left[\frac{\bar{\tilde{\xi}}^{(j)}}{\bar{a}_k^{(j)}}\frac{e_k^{(j)}}{1+e_k^{(j)}}\right]^2, \tag{3.53}$$

where $\bar{\tilde{\xi}}^{(j)} = \sqrt{P/\bar{\Psi}_{\text{wsrm}}^{(j)}}$. Moreover, from (3.28) and the algorithm in Table 3.1, the term $a_k^{(j)}$ can be rewritten as

$$a_k^{(j)} = \frac{1}{\sqrt{P_{S,k}^{(j-1)}}}\frac{\tilde{\gamma}_{k,\text{wsrm}}^{(j-1)}}{1+\tilde{\gamma}_{k,\text{wsrm}}^{(j-1)}}. \tag{3.54}$$

A deterministic equivalent $\bar{a}_k^{(j)}$ such that $a_k^{(j)} - \bar{a}_k^{(j)} \overset{M\to\infty}{\longrightarrow} 0$ almost surely is easily obtained by replacing the signal power $P_{S,k}^{(j-1)}$ and the SINR $\tilde{\gamma}_{k,\text{wsrm}}^{(j-1)}$ by their respective deterministic equivalents which yields $\bar{a}_k^{(j)}$ given in (3.41). Similarly, we have the deterministic equivalent $\bar{w}_k^{(j)} = u_k(1+\bar{\tilde{\gamma}}_{k,\text{wsrm}}^{(j-1)})$ which together with $\bar{a}_k^{(j)}$ constitutes $\bar{d}_k^{(j)} = \bar{w}_k^{(j)}(\bar{a}_k^{(j)})^2$.

Denoting $\mathbf{C}^{(j)} = [(\bar{\mathbf{H}}^{(j)})^{\mathsf{H}}\bar{\mathbf{H}}^{(j)} + M\bar{\alpha}^{(j)}\mathbf{I}_M]^{-1}$, the interference power $P_{I,k} = \sum_{i=1,i\neq k}^{K} |\mathbf{h}_k^{\mathsf{H}}\tilde{\mathbf{g}}_i^{(j)}|^2$ can be written as

$$P_{I,k} = (\tilde{\xi}_{\text{wsrm}}^{(j)})^2 \mathbf{h}_k^{\mathsf{H}}\mathbf{C}^{(j)} \left[\sum_{i=1,i\neq k}^{K} (\bar{a}_i^{(j)})^2 (\bar{w}_i^{(j)})^2 \mathbf{h}_i\mathbf{h}_i^{\mathsf{H}}\right] \mathbf{C}^{(j)}\mathbf{h}_k \tag{3.55}$$

$$= \frac{(\tilde{\xi}_{\text{wsrm}}^{(j)})^2}{\bar{d}_k^{(j)}} (\bar{\mathbf{h}}_k^{(j)})^{\mathsf{H}}\mathbf{C}^{(j)} (\bar{\mathbf{H}}_{[k]}^{(j)})^{\mathsf{H}} \bar{\mathbf{W}}_{[k]}^{(j)} \bar{\mathbf{H}}_{[k]}^{(j)} \mathbf{C}^{(j)} \bar{\mathbf{h}}_k^{(j)}, \tag{3.56}$$

where $\bar{\mathbf{H}}_{[k]}^{(j)} = [\bar{d}_1^{(j)}\mathbf{h}_1 \ldots, \bar{d}_{k-1}^{(j)}\mathbf{h}_{k-1}, \bar{d}_{k+1}^{(j)}\mathbf{h}_{k+1}, \ldots, \bar{d}_K^{(j)}\mathbf{h}_K]^{\mathsf{H}}$ and the diagonal matrix $\bar{\mathbf{W}}_{[k]}^{(j)}$ is defined as $\bar{\mathbf{W}}_{[k]}^{(j)} = \text{diag}(\bar{w}_1^{(j)}, \ldots, \bar{w}_{k-1}^{(j)}, \bar{w}_{k+1}^{(j)}, \ldots, \bar{w}_K^{(j)})$. Applying Lemma B.3 with $\tau_k = 0\ \forall k$ and $\mathbf{P}_{[k]} = \bar{\mathbf{W}}_{[k]}^{(j)}$ yields $\bar{P}_{I,k}$ such that $P_{I,k} - \bar{P}_{I,k} \overset{M\to\infty}{\longrightarrow} 0$ almost surely as

$$\bar{P}_{I,k} = \frac{\bar{\tilde{\xi}}^{2,(j)} \bar{\Upsilon}_{k,\text{wsrm}}^{(j)}}{\bar{d}_k^{(j)}(1+e_k^{(j)})^2}, \tag{3.57}$$

where $\bar{\Upsilon}_{k,\text{wsrm}}^{(j)}$ is given by (3.40). The terms $\bar{\Psi}_{\text{wsrm}}^{(j)}$, $\bar{P}_{S,k}^{(j)}$ and $\bar{P}_{I,k}$ are all positive and finite. Therefore, the convergence in (3.35) holds, which completes the proof. □

The SINR expression (3.36) simplifies significantly if the transmit correlation is identical for all users, i.e., $\mathbf{\Theta}_k = \mathbf{\Theta}\ \forall k$. The result is summarized in the following corollary.

Corollary 3.4. *Let Assumptions 3.1 and 3.3 hold true and let $\mathbf{\Theta}_k = \mathbf{\Theta}\ \forall k$, then $\bar{\tilde{\gamma}}_{k,\text{wsrm}}^{(j)}$ takes the form*

$$\bar{\tilde{\gamma}}_{k,\text{wsrm}}^{(j)} = e^{(j)}\bar{w}_k^{(j)}(\eta_1^{(j)})^2 \frac{\bar{d}_k^{(j)} e^{(j)}[1 - c^{(j)}e_2^{(j)}]}{e_2^{(j)}\nu_k^{(j)} + \frac{e_1^{(j)}}{\rho}\nu^{(j)}(1+\bar{d}_k^{(j)}e^{(j)})^2}, \tag{3.58}$$

where $e^{(j)}$ is the unique positive solution of

$$e^{(j)} = \frac{1}{M}\text{tr}\mathbf{\Theta}\mathbf{T} \tag{3.59}$$

$$\mathbf{T} = \left(\eta_1^{(j)}\mathbf{\Theta} + \bar{\alpha}^{(j)}\mathbf{I}_M\right)^{-1}, \tag{3.60}$$

where $\bar{\alpha}^{(j)} = \frac{\text{tr}\bar{\mathbf{D}}^{(j)}}{M\rho}$, $\eta_1^{(j)} \triangleq \frac{1}{M}\sum_{i=1}^{K}(\frac{1}{\bar{d}_i^{(j)}} + e^{(j)})^{-1}$. Further denoting $\nu^{(j)} \triangleq \frac{1}{M}\sum_{i=1}^{K}\frac{\bar{w}_i^{(j)}}{\bar{d}_i^{(j)}}(\frac{1}{\bar{d}_i^{(j)}} + e^{(j)})^{-2}$, $\nu_k^{(j)} \triangleq \frac{1}{M}\sum_{i=1,i\neq k}^{K}\frac{\bar{w}_i^{(j)}}{\bar{d}_i^{(j)}}(\frac{1}{\bar{d}_i^{(j)}} + e^{(j)})^{-2}$ and $\eta_2^{(j)} \triangleq \frac{1}{M}\sum_{i=1}^{K}(\frac{1}{\bar{d}_i^{(j)}} + e^{(j)})^{-2}$ with $c^{(j)} \triangleq \eta_2^{(j)}/[\eta_1^{(j)}]^2$, the terms $e_1^{(j)}$ and $e_2^{(j)}$ are given

by

$$e_1^{(j)} = (\eta_1^{(j)})^2 \frac{1}{M} \mathrm{tr}\boldsymbol{\Theta}\mathbf{T}^2 \tag{3.61}$$

$$e_2^{(j)} = (\eta_1^{(j)})^2 \frac{1}{M} \mathrm{tr}\boldsymbol{\Theta}^2\mathbf{T}^2. \tag{3.62}$$

Proof of Corollary 3.4. Substituting $\boldsymbol{\Theta}_k = \boldsymbol{\Theta}\ \forall k$, we obtain $e^{(j)} = e_i^{(j)}/\bar{d}_i^{(j)}$ given in (3.59). With (3.61) and (3.62), we further have

$$e'^{,(j)} = \frac{e_i'^{,(j)}}{\bar{d}_i^{(j)}} = \frac{1}{[\eta_1^{(j)}]^2} \frac{e_1^{(j)}}{1 - c^{(j)} e_2^{(j)}} \tag{3.63}$$

$$e_k'^{,(j)} = \frac{e_{i,k}'^{,(j)}}{\bar{d}_i^{(j)}} = \frac{\bar{d}_k^{(j)}}{[\eta_1^{(j)}]^2} \frac{e_2^{(j)}}{1 - c^{(j)} e_2^{(j)}}. \tag{3.64}$$

Substituting (3.63) and (3.64) into (3.39) and (3.40), respectively, we obtain $\bar{\Psi}_{\mathrm{wsrm}}^{(j)} = e'^{,(j)}\nu^{(j)}$ and $\bar{\Upsilon}_{k,\mathrm{wsrm}}^{(j)} = e_k'^{,(j)}\nu_k^{(j)}$, respectively. Subsequently, (3.36) can be written as (3.58), which completes the proof. □

To compute (3.58) only a *single* fixed point equation (3.59) has to be solved as opposed to K fixed-point equations in Theorem 3.2. Still, the SINR in Corollary 3.4 has to be calculated iteratively since the rate weights u_k may be unequal among the users. By assigning equal rate weights to all users ($u_k = 1\ \forall k$), the SINR approximation is independent of iteration j and of user k and is given in the subsequent corollary.

Corollary 3.5. *Let Assumption 3.1 hold true and let* $\boldsymbol{\Theta}_k = \boldsymbol{\Theta}$ *and* $u_k = 1\ \forall k$, *then* $\bar{\tilde{\gamma}}_{k,\mathrm{wsrm}}^{(j)}$ *takes the form*

$$\bar{\tilde{\gamma}}_{k,\mathrm{wsrm}}^{(j)} = \tilde{m}, \tag{3.65}$$

where $\tilde{m}$ *is the unique positive solution of*

$$\tilde{m} = \frac{1}{M} \mathrm{tr}\boldsymbol{\Theta} \left(\frac{\boldsymbol{\Theta}/\beta}{1+\tilde{m}} + \frac{1}{\beta\rho}\mathbf{I}_M \right)^{-1}. \tag{3.66}$$

Proof of Corollary 3.5. For $u_k = 1$ and $\boldsymbol{\Theta}_k = \boldsymbol{\Theta}\ \forall k$, we have $\bar{w}_k^{(j)} = \bar{w}$, $\bar{d}_k^{(j)} = \bar{d}$ and $c^{(j)} = \beta$. Moreover, $\nu^{(j)} = \nu$ and $\nu_k^{(j)} = \frac{K-1}{K}\nu$, which, for large K, converges to $\lim_{K\to\infty} \nu_k^{(j)} = \nu$. Substitution into (3.58) with $\tilde{m} \triangleq e^{(j)}\bar{d}$, $e_1^{(j)} = e_1$ and $e_2^{(j)} = e_2$ yields

$$\bar{\tilde{\gamma}}_{k,\mathrm{wsrm}}^{(j)} = \bar{\tilde{\gamma}}_{\mathrm{wsrm}} = \frac{\tilde{m}}{\beta} \frac{\tilde{m}(1-\beta e_2)}{e_2 + \frac{e_1}{\rho}(1+\tilde{m})^2}. \tag{3.67}$$

With $\bar{\alpha}^{(j)} = \frac{\bar{d}}{\beta\rho}$, $\tilde{m}$ takes the form given in (3.66). Rewriting $\tilde{m}$ as

$$\begin{aligned}\tilde{m} &= \frac{1}{M} \mathrm{tr}\boldsymbol{\Theta} \left(\frac{\boldsymbol{\Theta}/\beta}{1+\tilde{m}} + \frac{1}{\beta\rho}\mathbf{I}_M \right)^{-1} \left[\frac{\boldsymbol{\Theta}/\beta}{1+\tilde{m}} + \frac{1}{\beta\rho}\mathbf{I}_M \right] \left(\frac{\boldsymbol{\Theta}/\beta}{1+\tilde{m}} + \frac{1}{\beta\rho}\mathbf{I}_M \right)^{-1} \\ &= \beta(1+\tilde{m})e_2 + \frac{\beta}{\rho}(1+\tilde{m})^2 e_1,\end{aligned}$$

we have $\tilde{m}(1-\beta e_2) = \beta[e_2 + \frac{1}{\rho}(1+\tilde{m})^2 e_1]$ which substituted into (3.67) yields (3.65), which completes the proof. □

Therefore, if the correlation of all user channels is identical and sum rate is considered, the SINR in (3.58) is the solution of an implicit equation and independent of iteration j and user k. Moreover, the deterministic equivalent of the SINR in Corollary 3.5 can be obtained by a closed-form precoder given in the subsequent proposition.

Proposition 3.1. *Let Assumption 3.1 hold true and let* $\mathbf{\Theta}_k = \mathbf{\Theta}$ *and* $u_k = 1$ $\forall k$*, then the precoder in* (3.33) *takes the form*

$$\tilde{\mathbf{G}}_{\text{wsrm}} = \tilde{\xi}_{\text{wsrm}} \left(\mathbf{H}^{\mathsf{H}}\mathbf{H} + \frac{K}{\rho}\mathbf{I}_M \right)^{-1} \mathbf{H}^{\mathsf{H}}, \tag{3.68}$$

where $\tilde{\xi}_{\text{wsrm}} = \sqrt{P/\text{tr}\tilde{\mathbf{G}}_{\text{wsrm}}\tilde{\mathbf{G}}_{\text{wsrm}}^{\mathsf{H}}}$.

Proof of Proposition 3.1. From Theorem 3.2, observe that both $\bar{a}^{(j)} \triangleq \bar{a}_k^{(j)}$ and $\bar{w}^{(j)} \triangleq \bar{w}_k^{(j)}$ are identical for all users and thus $\bar{\mathbf{D}}^{(j)} = (\bar{a}^{(j)})^2 \bar{w}^{(j)} \mathbf{I}_K$. Therefore, (3.33) takes the form

$$\hat{\tilde{\mathbf{G}}}_{\text{wsrm}}^{(j)} = \frac{\tilde{\xi}_{\text{wsrm}}^{(j)}}{\bar{a}^{(j)}} \left(\mathbf{H}^{\mathsf{H}}\mathbf{H} + \frac{K}{\rho}\mathbf{I}_M \right)^{-1} \mathbf{H}^{\mathsf{H}} \tag{3.69}$$

$$(\tilde{\xi}_{\text{wsrm}}^{(j)})^2 = \frac{(\bar{a}^{(j)})^2 P}{\text{tr}\left(\mathbf{H}^{\mathsf{H}}\mathbf{H} + \frac{K}{\rho}\mathbf{I}_M \right)^{-2} \mathbf{H}^{\mathsf{H}}\mathbf{H}} \tag{3.70}$$

and can be written as (3.68), which completes the proof. □

By further assuming uncorrelated channels, the SINR approximation in Theorem 3.2 is given explicitly.

Corollary 3.6. *Let* $\mathbf{\Theta} = \mathbf{I}_M$ *and* $u_k = 1$ $\forall k$*, then* $\bar{\tilde{\gamma}}_{k,\text{wsrm}}^{(j)} \triangleq \bar{\tilde{\gamma}}_{\text{wsrm}}$ *is given explicitly and reads*

$$\bar{\tilde{\gamma}}_{\text{wsrm}} = \frac{1}{2}\left[\rho(\beta-1) + \chi - 1\right], \tag{3.71}$$

where χ *is given by*

$$\chi = \sqrt{(\beta-1)^2\rho^2 + 2(1+\beta)\rho + 1}. \tag{3.72}$$

Proof of Corollary 3.6. Substituting $\mathbf{\Theta} = \mathbf{I}_M$ into Corollary 3.5, we obtain a quadratic equation in $\tilde{m}$ for which the only positive solution is given by (3.71), which completes the proof. □

Proposition 3.1 states that the *proposed* linear precoder in (3.33), is of closed form and has the well-known RZF structure for common transmit correlation and sum rate maximization.

To compute the optimal linear precoder in Table 3.1 is computational complex. Therefore, we consider the sub-optimal RZF precoder in the next section, since it offers a good performance/complexity trade-off.

3.4 Regularized Zero-forcing Precoding with Imperfect CSIT

Consider the RZF precoding matrix

$$\mathbf{G}_{\text{rzf}} = \xi_{\text{rzf}} \left(\hat{\mathbf{H}}^{\mathsf{H}} \hat{\mathbf{H}} + M\alpha \mathbf{I}_M \right)^{-1} \hat{\mathbf{H}}^{\mathsf{H}}, \tag{3.73}$$

where $\hat{\mathbf{H}} \triangleq [\hat{\mathbf{h}}_1, \hat{\mathbf{h}}_2, \ldots, \hat{\mathbf{h}}_K]^{\mathsf{H}} \in \mathbb{C}^{K \times M}$ is the channel estimate available at the transmitter, ξ_{rzf} is a normalization scalar to fulfill the power constraint (1.11) and $\alpha > 0$ is the regularization term. Here, α is scaled by M to ensure that α itself converges to a constant, as $M, K \to \infty$.

From the total power constraint (1.11), we obtain ξ_{rzf}^2 as

$$\xi_{\text{rzf}}^2 = \frac{P}{\text{tr}\mathbf{P}\hat{\mathbf{H}}(\hat{\mathbf{H}}^{\mathsf{H}}\hat{\mathbf{H}} + M\alpha\mathbf{I}_M)^{-2}\hat{\mathbf{H}}^{\mathsf{H}}} = \frac{P}{\Psi_{\text{rzf}}},$$

where we defined $\Psi_{\text{rzf}} \triangleq \text{tr}\mathbf{P}\hat{\mathbf{H}}(\hat{\mathbf{H}}^{\mathsf{H}}\hat{\mathbf{H}} + M\alpha\mathbf{I}_M)^{-2}\hat{\mathbf{H}}^{\mathsf{H}}$. Denote $\hat{\mathbf{W}} \triangleq (\hat{\mathbf{H}}^{\mathsf{H}}\hat{\mathbf{H}} + M\alpha\mathbf{I}_M)^{-1}$, the SINR (1.12) of user k under RZF precoding takes the form

$$\gamma_{k,\text{rzf}} = \frac{p_k |\mathbf{h}_k^{\mathsf{H}} \hat{\mathbf{W}} \hat{\mathbf{h}}_k|^2}{\mathbf{h}_k^{\mathsf{H}} \hat{\mathbf{W}} \hat{\mathbf{H}}_{[k]}^{\mathsf{H}} \mathbf{P}_{[k]} \hat{\mathbf{H}}_{[k]} \hat{\mathbf{W}} \mathbf{h}_k + \frac{\Psi_{\text{rzf}}}{\rho}}, \tag{3.74}$$

where $\hat{\mathbf{H}}_{[k]}$ and $\mathbf{P}_{[k]}$ are defined in (3.8) and (3.9), respectively.

The following theorem provides a deterministic approximation $\bar{\gamma}_{k,\text{rzf}}$ of $\gamma_{k,\text{rzf}}$ defined in (3.74), which is almost surely exact as $M, K \to \infty$.

Theorem 3.3. *Let Assumptions 3.1, 3.2 and 3.4 hold true and let $\alpha > 0$ and $\gamma_{k,\text{rzf}}$ be the SINR of user k defined in* (3.74)*. Then*

$$\gamma_{k,\text{rzf}} - \bar{\gamma}_{k,\text{rzf}} \overset{M \to \infty}{\longrightarrow} 0,$$

almost surely, where $\bar{\gamma}_{k,\text{rzf}}$ is given by

$$\bar{\gamma}_{k,\text{rzf}} = \frac{p_k (1 - \tau_k^2) e_k^2}{\bar{\Upsilon}_{k,\text{rzf}} (1 - \tau_k^2 [1 - (1 + e_k)^2]) + \frac{\bar{\Psi}_{\text{rzf}}}{\rho} (1 + e_k)^2}, \tag{3.75}$$

where the $e_1, \ldots, e_K$ form the unique positive solutions of

$$e_i = \frac{1}{M} \text{tr} \mathbf{\Theta}_i \mathbf{T} \tag{3.76}$$

$$\mathbf{T} = \left(\frac{1}{M} \sum_{j=1}^{K} \frac{\mathbf{\Theta}_j}{1 + e_j} + \alpha \mathbf{I}_M \right)^{-1} \tag{3.77}$$

and $\bar{\Psi}_{\mathrm{rzf}}$ *and* $\bar{\Upsilon}_{k,\mathrm{rzf}}$ *read*

$$\bar{\Psi}_{\mathrm{rzf}} = \frac{1}{M}\sum_{j=1}^{K}\frac{p_j e'_j}{(1+e_j)^2},$$
$$\bar{\Upsilon}_{k,\mathrm{rzf}} = \frac{1}{M}\sum_{j=1,j\neq k}^{K}\frac{p_j e'_{j,k}}{(1+e_j)^2}.$$

Define $\mathbf{e}' = [e'_1,\ldots,e'_K]^{\mathsf{T}}$ *and* $\mathbf{e}'_k = [e'_{1,k},\ldots,e'_{K,k}]^{\mathsf{T}}$*, which are given as*

$$\mathbf{e}' = (\mathbf{I}_K - \mathbf{J})^{-1}\mathbf{v},$$
$$\mathbf{e}'_k = (\mathbf{I}_K - \mathbf{J})^{-1}\mathbf{v}_k,$$

where $\mathbf{J}$*,* $\mathbf{v}$ *and* $\mathbf{v}_k$ *take the form*

$$[\mathbf{J}]_{ij} = \frac{\frac{1}{M}\mathrm{tr}\boldsymbol{\Theta}_i\mathbf{T}\boldsymbol{\Theta}_j\mathbf{T}}{M(1+e_j)^2},$$
$$\mathbf{v} = \left[\frac{1}{M}\mathrm{tr}\boldsymbol{\Theta}_1\mathbf{T}^2,\ldots,\frac{1}{M}\mathrm{tr}\boldsymbol{\Theta}_K\mathbf{T}^2\right]^{\mathsf{T}},$$
$$\mathbf{v}_k = \left[\frac{1}{M}\mathrm{tr}\boldsymbol{\Theta}_1\mathbf{T}\boldsymbol{\Theta}_k\mathbf{T},\ldots,\frac{1}{M}\mathrm{tr}\boldsymbol{\Theta}_K\mathbf{T}\boldsymbol{\Theta}_k\mathbf{T}\right]^{\mathsf{T}}.$$

Proof of Theorem 3.3. The strategy is similar to the proof of Theorem 3.2: The SINR $\gamma_{k,\mathrm{rzf}}$ in (3.74) consists of three terms, (i) the scaled signal power $|\mathbf{h}_k^{\mathsf{H}}\hat{\mathbf{W}}\hat{\mathbf{h}}_k|^2$, (ii) the scaled power of the interference $\mathbf{h}_k^{\mathsf{H}}\hat{\mathbf{W}}\hat{\mathbf{H}}_{[k]}^{\mathsf{H}}\mathbf{P}_{[k]}\hat{\mathbf{H}}_{[k]}\hat{\mathbf{W}}\mathbf{h}_k$ (both scaled by ξ_{rzf}^{-2}) and (iii) the term Ψ_{rzf} of the power normalization. To find a deterministic equivalent of Ψ_{rzf}, we can directly apply Lemma B.1. Similarly, applying Lemma B.2 to $\mathbf{h}_k^{\mathsf{H}}\hat{\mathbf{W}}\hat{\mathbf{h}}_k$ and Lemma B.3 to $\mathbf{h}_k^{\mathsf{H}}\hat{\mathbf{W}}\hat{\mathbf{H}}_{[k]}^{\mathsf{H}}\mathbf{P}_{[k]}\hat{\mathbf{H}}_{[k]}\hat{\mathbf{W}}\mathbf{h}_k$ yields a deterministic equivalent for the scaled signal power and the scaled interference power, respectively. Together, the deterministic equivalents of these three terms constitute the final expression for $\bar{\gamma}_{k,\mathrm{rzf}}$. If all available transmit power is allocated to a single user (i.e., $p_k = P$), both $\bar{\Psi}_{\mathrm{rzf}}$ and $\bar{\Upsilon}_{k,\mathrm{rzf}}$ are of order $O(1/M)$ and hence $\bar{\gamma}_{k,\mathrm{rzf}}$ increases unbounded with M. Therefore, we require Assumption 3.2 to ensure that the convergence in (3.3) holds true, which completes the proof. □

Corollary 3.7. *Let Assumptions 3.1 and 3.2 hold true and let* $\alpha > 0$ *and* $\boldsymbol{\Theta}_k = \boldsymbol{\Theta}$ $\forall k$*, then* $\bar{\gamma}_{k,\mathrm{rzf}}$ *takes the form*

$$\bar{\gamma}_{k,\mathrm{rzf}} = \frac{p_k}{P/K}\frac{e\ (1-\tau_k^2)\left[e_{22}+\alpha\beta(1+e)^2e_{12}\right]}{e_{22}(1-p_k/P)\left[1-\tau_k^2(1-(1+e)^2)\right]+\frac{1}{\rho}(1+e)^2e_{12}}, \tag{3.78}$$

where e is the unique positive solution of

$$e = \frac{1}{M}\mathrm{tr}\boldsymbol{\Theta}\mathbf{T} \tag{3.79}$$

$$\mathbf{T} = \left(\frac{\boldsymbol{\Theta}/\beta}{1+e} + \alpha\mathbf{I}_M\right)^{-1} \tag{3.80}$$

and e_{ij} is given by

$$e_{ij} = \frac{1}{(1+e)^j}\frac{1}{M}\mathrm{tr}\boldsymbol{\Theta}^i\mathbf{T}^j. \tag{3.81}$$

Proof of Corollary 3.7. Substituting $\boldsymbol{\Theta}_k = \boldsymbol{\Theta}\ \forall k$ into Theorem 3.3, we have $e_i = e_k = e$ given in (3.79), $e_i' = e' = \beta(1+e)^2 e_{11}(\beta - e_{22})^{-1}$ and $e_{i,k}' = \tilde{e}' = \beta(1+e)^2 e_{22}(\beta - e_{22})^{-1}$. Therefore, the terms $\bar{\Psi}_{\mathrm{rzf}}$ and $\bar{\Upsilon}_{k,\mathrm{rzf}}$ become $(P/K)e_{11}(\beta - e_{22})^{-1}$ and $(P/K)[1-p_k/P]e_{22}(\beta - e_{22})^{-1}$, respectively. Furthermore, e can be written as

$$\begin{aligned} e &= \frac{1}{M}\mathrm{tr}\boldsymbol{\Theta}\mathbf{T}\left(\frac{\boldsymbol{\Theta}/\beta}{1+e} + \alpha\mathbf{I}_M\right)\mathbf{T} \\ &= \alpha(1+e)^2 e_{11} + \frac{1}{\beta}(1+e)e_{22}. \end{aligned} \tag{3.82}$$

Substituting these terms into (3.75) yields (3.78), which completes the proof. □

Corollary 3.8. *Let Assumption 3.2 hold true and let $\alpha > 0$ and $\boldsymbol{\Theta}_k = \mathbf{I}_M\ \forall k$, then $\bar{\gamma}_{k,\mathrm{rzf}}$ takes the form*

$$\bar{\gamma}_{k,\mathrm{rzf}} = \frac{p_k}{P/K}\frac{e(1-\tau_k^2)\left[1+\alpha\beta(1+e)^2\right]}{(1-p_k/P)\left[1-\tau_k^2(1-(1+e)^2)\right] + \frac{1}{\rho}(1+e)^2}, \tag{3.83}$$

where e is the given as

$$e = \frac{\beta - 1 - \beta\alpha + \sqrt{(\beta-1)^2 + 2(1+\beta)\alpha\beta + \alpha^2\beta^2}}{2\alpha\beta}. \tag{3.84}$$

Proof of Corollary 3.8. Substituting $\boldsymbol{\Theta} = \mathbf{I}_M$ into Corollary 3.7, we have $e_{11} = e_{22}$ which yields (3.83). Moreover, (3.79) becomes a quadratic equation in e with unique positive solution (3.84), which completes the proof. □

In this thesis, we will consider two different RZF precoders. The first one corresponds to the precoder in [10], where $\alpha = \frac{1}{\beta\rho}$ and is optimal (maximizing the sum rate) under common correlation and *perfect* CSIT for large M, K [10, 25, 26]. This precoder is referred to as RZF *channel distortion unaware* (RZF-CDU) precoder. Under imperfect CSIT the RZF-CDU precoder is mismatched to the true channel. The second RZF precoder maximizes the sum rate under common correlation and *imperfect* CSIT and will be derived in Section 4.1. This precoder is will be called RZF *channel distortion aware* (RZF-CDA) precoder.

Moreover, there are two limiting cases of the RZF precoder corresponding to $\alpha \to \infty$ and $\alpha \to 0$. For $\alpha \to \infty$ the RZF precoder converges to the matched filter (MF) precoder $\mathbf{G}_{\mathrm{mf}} = \frac{\xi_{\mathrm{mf}}}{M}\hat{\mathbf{H}}^{\mathsf{H}}$ in (3.6). A deterministic equivalent $\bar{\gamma}_{k,\mathrm{mf}}$ for the MF precoder is provided in Theorem 3.1. However, note that $\bar{\gamma}_{k,\mathrm{mf}}$ can also be derived by taking the limit $\bar{\gamma}_{k,\mathrm{mf}} = \lim_{\alpha\to\infty} \bar{\gamma}_{k,\mathrm{rzf}}$. This approach is straightforward, since $\bar{\gamma}_{k,\mathrm{rzf}}$ is well-behaved as $\alpha \to \infty$, but will not be detailed in this thesis.

In the case of $\alpha \to 0$, the RZF precoder converges to the ZF precoder, which is the subject of the next section.

3.5 Zero-forcing Precoding

For $\alpha = 0$, the RZF precoding matrix in (3.73) reduces to the ZF precoding matrix $\mathbf{G}_{\mathrm{zf}}$ which reads

$$\mathbf{G}_{\mathrm{zf}} = \xi_{\mathrm{zf}}\hat{\mathbf{H}}^{\mathsf{H}}\left(\hat{\mathbf{H}}\hat{\mathbf{H}}^{\mathsf{H}}\right)^{-1},$$

where ξ_{zf} is a scaling factor to fulfill the power constraint (1.11) and is given by

$$\xi_{\mathrm{zf}}^2 = \frac{P}{\mathrm{tr}\mathbf{P}(\hat{\mathbf{H}}\hat{\mathbf{H}}^{\mathsf{H}})^{-1}} = \frac{P}{\Psi_{\mathrm{zf}}},$$

where $\Psi_{\mathrm{zf}} \triangleq \mathrm{tr}\mathbf{P}(\hat{\mathbf{H}}\hat{\mathbf{H}}^{\mathsf{H}})^{-1}$. Defining $\hat{\bar{\mathbf{W}}} \triangleq \hat{\mathbf{H}}^{\mathsf{H}}(\hat{\mathbf{H}}\hat{\mathbf{H}}^{\mathsf{H}})^{-2}\hat{\mathbf{H}}$, the SINR (1.12) of user k under ZF precoding reads

$$\gamma_{k,\mathrm{zf}} = \frac{p_k|\mathbf{h}_k^{\mathsf{H}}\hat{\bar{\mathbf{W}}}\hat{\mathbf{h}}_k|^2}{\mathbf{h}_k^{\mathsf{H}}\hat{\bar{\mathbf{W}}}\hat{\mathbf{H}}_{[k]}^{\mathsf{H}}\mathbf{P}_{[k]}\hat{\mathbf{H}}_{[k]}\hat{\bar{\mathbf{W}}}\mathbf{h}_k + \frac{\Psi_{\mathrm{zf}}}{\rho}}. \tag{3.85}$$

To obtain a deterministic equivalent of the SINR (3.85), we need to ensure that the minimum eigenvalue of $\hat{\mathbf{H}}\hat{\mathbf{H}}^{\mathsf{H}}$ is bounded away from zero for all large M, almost surely. As discussed in [10], for $M = K$, the smallest eigenvalue of the l.s.d. of $\hat{\mathbf{H}}\hat{\mathbf{H}}^{\mathsf{H}}$ includes zero. Therefore, $\|(\hat{\mathbf{H}}\hat{\mathbf{H}}^{\mathsf{H}})^{-1}\|$ is unbounded in M and a deterministic equivalent of the $\gamma_{k,\mathrm{zf}}$ does not exist. Therefore, we require the following assumption.

Assumption 3.5. *There exists $\varepsilon > 0$ such that, for all large M, we have $\lambda_{\min}(\frac{1}{M}\hat{\mathbf{H}}\hat{\mathbf{H}}^{\mathsf{H}}) > \varepsilon$ with probability one.*

Remark 3.3. *If $\mathbf{\Theta}_k = \mathbf{\Theta}$ $\forall k$ and $\lambda_{\min}(\mathbf{\Theta}) > \varepsilon > 0$ (i.e., in contrast to Theorem 3.3, $\mathbf{\Theta}$ must be invertible), for all M, then Assumption 3.5 holds true if $\beta > 1$. Indeed, for $\beta > 1$, from [60], there exists $\zeta > 0$ such that, for all large M, $\lambda_{\min}(\hat{\mathbf{Z}}\hat{\mathbf{Z}}^{\mathsf{H}}) > \zeta$, where $\hat{\mathbf{Z}} = [\hat{\mathbf{z}}_1, \ldots, \hat{\mathbf{z}}_K]^{\mathsf{H}}$, with probability one. Therefore, for all large M, $\lambda_{\min}(\frac{1}{M}\hat{\mathbf{H}}\hat{\mathbf{H}}^{\mathsf{H}}) \geq \lambda_{\min}(\hat{\mathbf{Z}}\hat{\mathbf{Z}}^{\mathsf{H}})\lambda_{\min}(\mathbf{\Theta}) > \zeta\varepsilon > 0$ almost surely.*

Furthermore, we require the following assumption for the channel model with per-user correlation.

Assumption 3.6. *Assume that* $\underline{e}_i = \lim_{\alpha\to 0} \alpha e_i(\alpha)$ *exists for all* i *and* $\underline{e}_i > \varepsilon$ $\forall i$ *for some* $\varepsilon > 0$*, for all* M*.*

Remark 3.4. *Under these conditions, the* $\underline{e}_1, \ldots, \underline{e}_K$ *are the unique positive solutions of* (3.89)*. In particular, Assumption 3.6 holds true if* $\boldsymbol{\Theta}_k = \boldsymbol{\Theta}$ $\forall k$*,* $\beta > 1$ *and* $\lambda_{\min}(\boldsymbol{\Theta}) > \varepsilon > 0$*. This is detailed in the proof of Corollary 3.9.*

A deterministic equivalent $\bar{\gamma}_{k,\mathrm{zf}}$ of $\gamma_{k,\mathrm{zf}}$ is given in the following theorem.

Theorem 3.4. *Let Assumptions 3.1, 3.2, 3.4, 3.5 and 3.6 hold true and let* $\gamma_{k,\mathrm{zf}}$ *be the SINR of user* k *under ZF precoding defined in* (3.85)*. Then*

$$\gamma_{k,\mathrm{zf}} - \bar{\gamma}_{k,\mathrm{zf}} \overset{M\to\infty}{\longrightarrow} 0, \tag{3.86}$$

almost surely, where $\bar{\gamma}_{k,\mathrm{zf}}$ *is given by*

$$\bar{\gamma}_{k,\mathrm{zf}} = p_k \frac{1-\tau_k^2}{\tau_k^2 \bar{\Upsilon}_{k,\mathrm{zf}} + \frac{\bar{\Psi}_{\mathrm{zf}}}{\rho}}, \tag{3.87}$$

where $\bar{\Psi}_{\mathrm{zf}}$ *and* $\bar{\Upsilon}_{k,\mathrm{zf}}$ *read*

$$\begin{aligned} \bar{\Psi}_{\mathrm{zf}} &= \frac{1}{M}\sum_{j=1}^{K} \frac{p_j}{\underline{e}_j}, \\ \bar{\Upsilon}_{k,\mathrm{zf}} &= \frac{1}{M}\sum_{j=1,j\neq k}^{K} p_j \frac{\underline{e}'_{j,k}}{\underline{e}_j^2}. \end{aligned} \tag{3.88}$$

The functions $\underline{e}_1, \ldots, \underline{e}_K$ *form the unique positive solution of*

$$\underline{e}_i = \frac{1}{M}\mathrm{tr}\boldsymbol{\Theta}_i \underline{\mathbf{T}} \tag{3.89}$$

$$\underline{\mathbf{T}} = \left(\frac{1}{M}\sum_{j=1}^{K} \frac{\boldsymbol{\Theta}_j}{\underline{e}_j} + \mathbf{I}_M \right)^{-1}. \tag{3.90}$$

Further, define $\underline{\mathbf{e}}'_k = [\underline{e}'_{1,k}, \ldots, \underline{e}'_{K,k}]^{\mathsf{T}}$*, which is given as*

$$\underline{\mathbf{e}}'_k = (\mathbf{I}_K - \underline{\mathbf{J}})^{-1} \underline{\mathbf{v}}_k, \tag{3.91}$$

where $\underline{\mathbf{J}}$ *and* $\underline{\mathbf{v}}_k$ *take the form*

$$\begin{aligned} [\underline{\mathbf{J}}]_{ij} &= \frac{\frac{1}{M}\mathrm{tr}\boldsymbol{\Theta}_i \underline{\mathbf{T}} \boldsymbol{\Theta}_j \underline{\mathbf{T}}}{M\,\underline{e}_j^2}, \\ \underline{\mathbf{v}}_k &= \left[\frac{1}{M}\mathrm{tr}\boldsymbol{\Theta}_1 \underline{\mathbf{T}} \boldsymbol{\Theta}_k \underline{\mathbf{T}}, \ldots, \frac{1}{M}\mathrm{tr}\boldsymbol{\Theta}_K \underline{\mathbf{T}} \boldsymbol{\Theta}_k \underline{\mathbf{T}} \right]^{\mathsf{T}}. \end{aligned}$$

Proof. The proof of Theorem 3.4 is given in Appendix C. □

Corollary 3.9. *Let Assumptions 3.1 and 3.2 hold true. Further, let $\beta > 1$, $\mathbf{\Theta}_k = \mathbf{\Theta}$ $\forall k$ with $\lambda_{\min}(\mathbf{\Theta}) > \varepsilon$, $\varepsilon > 0$, for all M, then Theorem 3.4 holds true and $\bar{\gamma}_{k,\mathrm{zf}}$ takes the form*

$$\bar{\gamma}_{k,\mathrm{zf}} = \frac{p_k}{P/K} \frac{1-\tau_k^2}{\tau_k^2 \bar{\Upsilon}_{\mathrm{zf}} \left[1 - \frac{p_k}{P}\right] + \frac{\bar{\Psi}_{\mathrm{zf}}}{\rho}}$$

with

$$\bar{\Psi}_{\mathrm{zf}} = \frac{1}{\beta \underline{e}}, \tag{3.92}$$

$$\bar{\Upsilon}_{\mathrm{zf}} = \frac{\underline{e}_2/\underline{e}^2}{\beta - \underline{e}_2/\underline{e}^2}, \tag{3.93}$$

$$\underline{e}_2 = \frac{1}{M} \mathrm{tr} \mathbf{\Theta}^2 \underline{\mathbf{T}}^2$$

where $\underline{e}$ is the unique positive solution of

$$\underline{e} = \frac{1}{M} \mathrm{tr} \mathbf{\Theta} \underline{\mathbf{T}}, \tag{3.94}$$

$$\underline{\mathbf{T}} = \left(\mathbf{I}_M + \frac{1}{\underline{e}\beta} \mathbf{\Theta} \right)^{-1}. \tag{3.95}$$

Proof of Corollary 3.9. For $\mathbf{\Theta}_k = \mathbf{\Theta}$ $\forall k$, we obtain from (3.76)

$$\begin{aligned} \underline{e}_i &= \lim_{\alpha \to 0} \alpha e_i(\alpha) = \underline{e} \\ &= \lim_{\alpha \to 0} \left\{ \frac{1}{M} \mathrm{tr} \mathbf{\Theta} \left(\frac{1}{\beta} \frac{\mathbf{\Theta}}{\alpha + \alpha e(\alpha)} + \mathbf{I}_M \right)^{-1} \right\} \\ &= \frac{1}{M} \mathrm{tr} \mathbf{\Theta} \left(\frac{\mathbf{\Theta}}{\beta \underline{e}} + \mathbf{I}_M \right)^{-1}. \end{aligned} \tag{3.96}$$

A lower bounded of (3.96) is given as $\underline{e} \geq \lambda_{\min}(\mathbf{\Theta})(1 - 1/\beta)$ which is uniformly bounded away from zero if $\mathbf{\Theta}$ is invertible and $\beta > 1$. Thus, under these conditions, Assumption 3.6 is satisfied. Moreover, the $\underline{e}'_{j,k}$ in (3.91) rewrite

$$\underline{e}'_{j,k} = \underline{e}' = \frac{\beta \underline{e}_2}{\beta - \frac{\underline{e}_2}{\underline{e}^2}}$$

and therefore,

$$\bar{\Upsilon}_{k,\mathrm{zf}} = \frac{\underline{e}_2/\underline{e}^2}{\beta - \frac{\underline{e}_2}{\underline{e}^2}} \frac{P}{K} \left[1 - \frac{p_k}{P}\right].$$

Dividing $\bar{\Upsilon}_{k,\mathrm{zf}}$ by $\frac{P}{K}\left[1 - \frac{p_k}{P}\right]$ and $\bar{\Psi}_{\mathrm{zf}} = \frac{P}{\underline{e} M}$ by P/K, we obtain $\bar{\Upsilon}_{\mathrm{zf}}$ given in (3.93) and $\bar{\Psi}_{\mathrm{zf}}$ given in (3.92), respectively, which completes the proof. □

Thus, the $\bar{\gamma}_{k,\mathrm{zf}}$ requires the solution of only a single fixed point equation (3.94).

Corollary 3.10. *Let Assumption 3.2 hold true and let $\beta > 1$ and $\mathbf{\Theta}_k = \mathbf{I}_M \ \forall k$, then $\bar{\gamma}_{k,\mathrm{zf}}$ takes the explicit form*

$$\bar{\gamma}_{k,\mathrm{zf}} = \frac{p_k}{P/K} \frac{1-\tau_k^2}{\tau_k^2[1-\frac{p_k}{P}]+\frac{1}{\rho}}(\beta-1). \tag{3.97}$$

Proof of Corollary 3.10. By substituting $\mathbf{\Theta} = \mathbf{I}_M$ into (3.94), $\underline{e}$ is explicitly given by $\underline{e} = (\beta-1)/\beta$. We further have $\frac{e_2}{\underline{e}^2} = 1$ and $\bar{\Psi}_{\mathrm{zf}} = \bar{\Upsilon}_{\mathrm{zf}} = (\beta-1)^{-1}$. □

Corollary 3.11. *Let $\beta > 1$ and $\mathbf{\Theta}_k = \mathbf{I}_M$, $p_k = P/K$, $\tau_k = \tau \ \forall k$, then for K large $\bar{\gamma}_{k,\mathrm{zf}}$ takes the form*

$$\bar{\gamma}_{k,\mathrm{zf}} = \bar{\gamma}_{\mathrm{zf}} = \frac{1-\tau^2}{\tau^2+\frac{1}{\rho}}(\beta-1). \tag{3.98}$$

Proof of Corollary 3.11. From Remark 3.2, the convergence in (3.86) holds true if $\bar{\gamma}_{k,\mathrm{zf}}$ is given by (3.98). □

3.6 Rate Approximations

Previously we derived deterministic large system approximations $\bar{\gamma}_k$ of the SINR γ_k such that $\gamma_k - \bar{\gamma}_k \overset{M\to\infty}{\longrightarrow} 0$ almost surely for various linear precoders. Roughly speaking, the true random SINR γ_k can be accurately approximated by a deterministic quantity $\bar{\gamma}_k$ due to the fact that, as the system dimensions increase, the empirical eigenvalue distribution of the random matrix $\mathbf{HH}^{\mathsf{H}}$ converges weakly to a deterministic measure. Since the logarithm is a continuous function, by applying the continuous mapping theorem [50], it follows from $\gamma_k - \bar{\gamma}_k \overset{M\to\infty}{\longrightarrow} 0$, almost surely that

$$R_k - \bar{R}_k \overset{M\to\infty}{\longrightarrow} 0, \tag{3.99}$$

almost surely, where $\bar{R}_k = \log(1+\bar{\gamma}_k)$.

As we are interested in the average system behavior, we define an approximation $\hat{R}_{\mathrm{sum}}$ of the ergodic sum rate $E[R_{\mathrm{sum}}]$, where the instantaneous (i.e., without averaging over the channel distribution) SINR γ_k is replaced by its the large system approximation $\bar{\gamma}_k$, i.e.,

$$\hat{R}_{\mathrm{sum}} = \sum_{k=1}^{K} \log\left(1+\bar{\gamma}_k\right). \tag{3.100}$$

It follows that

$$\frac{1}{K}\left(R_{\mathrm{sum}} - \hat{R}_{\mathrm{sum}}\right) \overset{M\to\infty}{\longrightarrow} 0, \tag{3.101}$$

holds true almost surely. Corroborated by simulation results in the next section, it turns out that $\hat{R}_{\mathrm{sum}}$ approximates the ergodic sum rate very accurately even for small system dimensions.

Another quantity of interest is the rate gap between the achievable rate under perfect and imperfect CSIT. We define the rate gap ΔR_k of user k as

$$\Delta R_k \triangleq R_k^{\circ} - R_k, \tag{3.102}$$

where R_k° the rate of user k under perfect CSIT, i.e., for $\tau_k^2 = 0\ \forall k$. Then, from (3.99) it follows that a deterministic equivalent $\Delta\bar{R}_k$ of the rate gap of user k such that

$$\Delta R_k - \Delta\bar{R}_k \overset{M\to\infty}{\longrightarrow} 0,$$

almost surely, is given by

$$\Delta\bar{R}_k = \bar{R}_k^{\circ} - \bar{R}_k, \tag{3.103}$$

where $\bar{R}_k^{\circ}$ is a deterministic equivalent of the rate of user k under perfect CSIT.

Since we require the per-user rate gaps for uncorrelated channels ($\mathbf{\Theta}_k = \mathbf{I}_M\ \forall k$) in the limited feedback analysis in Chapter 4, Sections 4.3 and 4.4, we will state at this point $\Delta\bar{R}_k$ for each of the precoding schemes.

Corollary 3.12 (MF precoding)**.** *Let $\mathbf{\Theta}_k = \mathbf{I}_M\ \forall k$, $p_k = P/K\ \forall k$ and define $\Delta R_{k,\mathrm{mf}}$ as the rate gap of user k under MF precoding. Then a deterministic equivalent $\Delta\bar{R}_{k,\mathrm{mf}}$ such that*

$$\Delta R_{k,\mathrm{mf}} - \Delta\bar{R}_{k,\mathrm{mf}} \overset{M\to\infty}{\longrightarrow} 0$$

almost surely, is given by

$$\Delta\bar{R}_{k,\mathrm{mf}} = \log\left(\frac{1+\frac{1}{\rho}+\beta}{1+\frac{1}{\rho}+\beta(1-\tau_k^2)}\right).$$

Proof of Corollary 3.12. Substitute the SINR from Corollary 3.3 into (3.103). □

Corollary 3.13 (RZF-CDU precoding)**.** *Let $\mathbf{\Theta}_k = \mathbf{I}_M\ \forall k$, $p_k = P/K\ \forall k$, $\alpha = 1/(\beta\rho)$ and define $\Delta R_{k,\mathrm{rzf-cdu}}$ as the rate gap of user k under RZF-CDU precoding. Then a deterministic equivalent $\Delta\bar{R}_{k,\mathrm{rzf-cdu}}$ such that*

$$\Delta R_{k,\mathrm{rzf-cdu}} - \Delta\bar{R}_{k,\mathrm{rzf-cdu}} \overset{M\to\infty}{\longrightarrow} 0$$

almost surely, is given by

$$\Delta\bar{R}_{k,\mathrm{rzf-cdu}} = \log\left(\frac{1+e}{1+\frac{e(1-\tau_k^2)\left[1+\frac{1}{\rho}(1+e)^2\right]}{1-\tau_k^2+(1+e)^2\left[\tau_k^2+\frac{1}{\rho}\right]}}\right),$$

where e is given in (3.84).

Proof of Corollary 3.13. With Corollary 3.8, compute $\Delta\bar{R}_{k,\mathrm{rzf-cdu}}$ as defined in (3.103), where $\bar{R}_{k,\mathrm{rzf-cdu}}^{\circ} = \log(1+e)$. □

Corollary 3.14 (ZF precoding)**.** *Let $\mathbf{\Theta}_k = \mathbf{I}_M \ \forall k$, $p_k = P/K \ \forall k$ and define $\Delta R_{k,\mathrm{zf}}$ to be the rate gap of user k under ZF precoding. Then*

$$\Delta R_{k,\mathrm{zf}} - \Delta \bar{R}_{k,\mathrm{zf}} \overset{M\to\infty}{\longrightarrow} 0$$

almost surely, with $\Delta \bar{R}_{k,\mathrm{zf}}$ given by

$$\Delta \bar{R}_{k,\mathrm{zf}} = \log\left(\frac{1+\rho(\beta-1)}{1+\rho\omega_k(\beta-1)}\right)$$

where ω_k is defined given by

$$\omega_k = \frac{1-\tau_k^2}{1+\tau_k^2\rho}. \tag{3.104}$$

Proof of Corollary 3.14. Substitute the SINR from Corollary 3.10 into (3.103). □

Remark 3.5. *In practice, one is often interested in the average system performance, e.g., the ergodic SINR $E[\gamma_k]$ or ergodic rate $E[R_k]$. Since the SINR γ_k is uniformly bounded on M for the considered precoding schemes, we can apply the dominated convergence theorem [50, Theorem 16.4] and obtain*

$$E[\gamma_k] - \bar{\gamma}_k \overset{M\to\infty}{\longrightarrow} 0,$$

where the expectation is taken over the probability space generating the sequence $\{\mathbf{H}(\omega),\ M \geq 1\}$ with $\mathbf{H} = [\mathbf{h}_1, \ldots, \mathbf{h}_K]^{\mathsf{H}} \in \mathbb{C}^{K\times M}$. The same holds true for the per-user rate R_k, i.e., $E[R_k] - \bar{R}_k \overset{M\to\infty}{\longrightarrow} 0$.

3.7 Numerical Results

In this section, we will validate the large system approximations in Theorems 3.1, 3.2, 3.3 and 3.4 by performing numerical simulations for finite system dimensions. Particularly, we compare the ergodic weighted sum rate $E[R_{\mathrm{wsum}}]$ and ergodic sum rate $E[R_{\mathrm{sum}}]$, averaged over at least 1 000 i.i.d. Rayleigh block-fading channel realizations, to their large system approximation $\hat{R}_{\mathrm{wsum}}$ and $\hat{R}_{\mathrm{sum}}$, respectively. One set of simulations investigates the accuracy of the large system approximations as a function of increasing system dimensions. Another set of simulations compares the ergodic (weighted) sum rate with error bars indicating the standard deviation to the deterministic approximations. All simulations are carried out under equal power allocation, i.e., $\mathbf{P} = \frac{1}{K}\mathbf{I}_K$.

The correlation $\mathbf{\Theta}_k$ of the kth user channel is modeled as in [63] by assuming a diffuse two-dimensional field of isotropic scatterers around the receivers. The waves impinge the receiver k uniformly at an azimuth angle θ ranging from $\theta_{k,\min}$ to $\theta_{k,\max}$. Denoting d_{ij} the distance between transmit antenna i and j, the correlation is modeled as

$$[\mathbf{\Theta}_k]_{ij} = \frac{1}{\theta_{k,\max} - \theta_{k,\min}} \int_{\theta_{k,\min}}^{\theta_{k,\max}} e^{\,\mathbf{i}\frac{2\pi}{\lambda} d_{ij}\cos(\theta)} d\theta, \tag{3.105}$$

where λ denotes the signal wavelength. The users are assumed to be distributed uniformly around the transmitter at an angle $\varphi_k = 2\pi k/K$ and as a simple example we choose $\theta_{k,\min} = -\pi$ and $\theta_{k,\max} = \varphi_k - \pi$. Note that for small $\theta_{k,\max} - \theta_{k,\min}$ (in our example for small values of k), the corresponding signal of user k is highly correlated since the signal is arriving from a very narrow angle. Thus, the correlation model (3.105) yields rank-deficient correlating matrices for some users and hence constitutes a limiting case for our large system approximations. That is, the fixed-point equations take longer to converge (if they converge at all) and the deterministic equivalent of the SINR are less accurate than for users with better-conditioned correlation matrices. To construct a less severe case of correlation we use the standard exponential correlation model, i.e.,

$$[\mathbf{\Theta}_k]_{ij} = v_k^{|i-j|}, \tag{3.106}$$

where $i, j = 1, 2, \ldots, M$. In particular, we let the correlation coefficient v_k of user k vary between zero and 0.5, more precisely we set $v_k = 0.5(k-1)/(K-1)$. In both correlation models, the transmitter is equipped with a uniform linear array (ULA). To ensure that $\|\mathbf{\Theta}_k\|$ is bounded as M grows large, we assume that the distance between adjacent antennas is independent of M, i.e., the length of the ULA increases with M. In the following, the notation "$\mathbf{\Theta}_k \neq \mathbf{I}_M$" indicates that $\mathbf{\Theta}_k$ is modeled according to (3.105) with $d_{ij}/\lambda = 0.5$. The exponential correlation model (3.106) is denoted "$\mathbf{\Theta}_k \sim \exp$".

3.7.1 MF Precoding

In Figure 3.1, we compare the accuracy of the approximation in Theorem 3.1 for the MF precoder to the ergodic sum rate $E[R_{\text{sum}}]$ as a function of the system dimension M and in Figure 3.2 as a function of the SNR ρ [dB].

From Figure 3.1, we observe that the approximation becomes more accurate for increasing dimensions, although for $\mathbf{\Theta}_k \neq \mathbf{I}_M$ the convergence appears to be rather slow. Figure 3.2 shows that the approximation lies approximately within one standard deviation of the simulation results over the whole SNR range.

3.7.2 Optimal Linear Precoding

We perform simulations of both weighted sum rate and sum rate performance. For simplicity, we model the rate weights u_k as $u_k = k\frac{2}{K+1}$ so that $\sum_{k=1}^{K} u_k = K$, which is indicated by the notation "$u_k \neq 1$". Moreover, we use the algorithm called WSRBF-WMMSE2 in [13] with $N_{\text{iter}} = 10$ iterations and MF initialization.

From Figure 3.3, we observe that the accuracy of the large system approximation $\hat{R}_{\text{wsum}}$ increases with increasing M. Moreover, Figure 3.4 suggests that the approximation $\hat{R}_{\text{wsum}}$ lies within one standard deviation of the simulation results.

Figure 3.5 compares the ergodic weighted sum rate to the large system approximation at each iteration j for an SNR of 30 dB. It can be observed that the

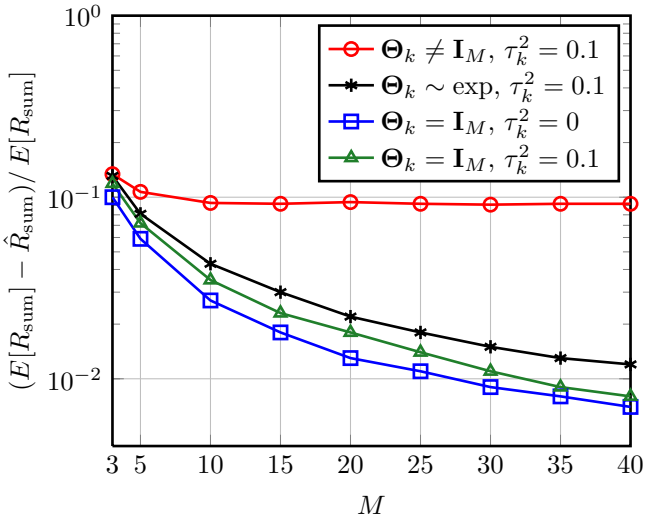

Figure 3.1: MF, Accuracy vs. M for a fixed SNR of $\rho = 10$ dB and $M = K$.

WSR increases significantly for consecutive iterations. Furthermore, the large system approximation $\hat{R}_{\text{wsum}}$ lies approximately within the standard deviation of the WSR R_{wsum} and we conclude that Theorem 3.2 is accurate for large M at every iteration.

In Figure 3.6 we plot the *sum rate* as a function of the SNR and compare $E[R_{\text{wsum}}]$ to $\hat{R}_{\text{wsum}}$. We first observe that for $\boldsymbol{\Theta}_k = \mathbf{I}_M$ and $\beta = 1$, the large system approximation is very inaccurate especially at high SNR. One possible reason is the following: From Corollary 3.6, the SINR approximation $\bar{\bar{\gamma}}_{\text{wsrm}}$ is the Stieltjes transform $\bar{m}_{\mathbf{X}^{\mathsf{H}}\mathbf{X}}(z)$ in $z = \frac{1}{\beta\rho}$ of the l.s.d. of $\mathbf{X}^{\mathsf{H}}\mathbf{X}$, where $\mathbf{X} \in \mathbb{C}^{M\times K}$ has i.i.d. entries of zero mean and variance $1/M$. Thus, for high SNR, z goes to zero, but $\bar{m}_{\mathbf{X}^{\mathsf{H}}\mathbf{X}}(0)$ is not defined for $\beta = 1$, since the support of the l.s.d. of $\mathbf{X}^{\mathsf{H}}\mathbf{X}$ (i.e. the Marčenko-Pastur law) includes zero. The bounds in Proposition 2.3 are therefore proportional to the SNR, because $\frac{1}{\Im(z)} = \frac{1}{|z|} = \frac{1}{\alpha} = \beta\rho$. Hence, to increase the accuracy of the approximated SINR, larger dimensions are required in the high SNR regime. Furthermore, comparing the accuracy at high SNR to the WSR performance in Figure 3.4, we observe that the WSR approximation is significantly more accurate than the sum rate approximation for $\beta = 1$ and $\boldsymbol{\Theta}_k = \mathbf{I}_M$. From Corollary 3.4, for $\boldsymbol{\Theta} = \mathbf{I}_M$, the approximated SINR $\bar{\bar{\gamma}}_{k,\text{wsrm}}^{(j)}$ is a function of $\bar{m}_i^{(j)} = \bar{d}_i^{(j)}\bar{m}^{(j)}$ which is the Stieltjes transform $\bar{m}_{\mathbf{X}^{\mathsf{H}}\bar{\mathbf{D}}^{(j)}\mathbf{X},\bar{d}_i^{(j)}\mathbf{I}_M}(z)$ in $z = \bar{\alpha}^{(j)} = -\frac{\text{tr}\bar{\mathbf{D}}^{(j)}}{M\rho}$. The support of the l.s.d. of $\mathbf{X}^{\mathsf{H}}\bar{\mathbf{D}}^{(j)}\mathbf{X}$ still includes eigenvalues arbitrarily close to zero but $\bar{\alpha}^{(j)}$ does not converge to zero, since the $\bar{d}_k^{(j)}$ grow with the SINR $\bar{\bar{\gamma}}_{k,\text{wsrm}}^{(j)}$ and hence with the SNR.

Figure 3.6 further suggests that the large system approximation is significantly more accurate at high SNR when the channel is correlated or if $M > K$.

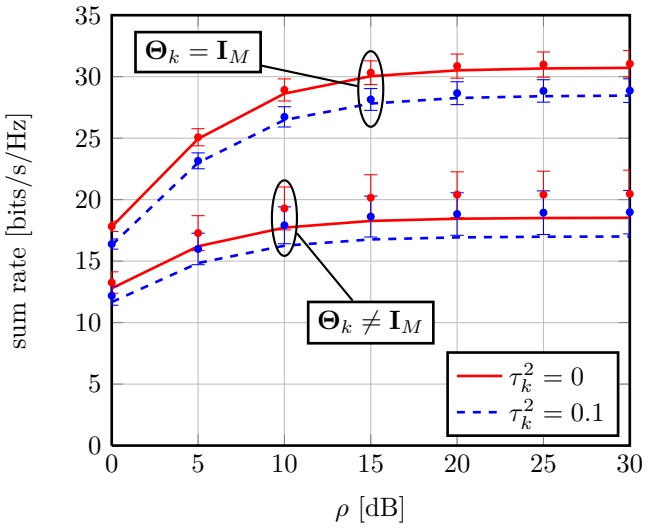

Figure 3.2: MF, Sum rate vs. SNR with $M = K = 30$, simulation results are indicated by circle marks with error bars indicating the standard deviation

The reason is again, that the channel matrix is better conditioned and that minimum eigenvalue of $\mathbf{H}^{\mathsf{H}}\mathbf{H}$ is bounded away from zero.

3.7.3 ZF and RZF Precoding

The simulation results presented in Figures 3.7 and 3.9 depict the absolute error of the sum rate approximation $\hat{R}_{\text{sum}}$ under RZF-CDU and ZF precoding compared to the ergodic sum rate $E[R_{\text{sum}}]$, respectively, averaged over 10 000 independent channel realizations. From Figures 3.7 and 3.9, we observe that the approximated sum rate $\hat{R}_{\text{sum}}$ becomes more accurate with increasing M, although under ZF precoding in Figure 3.9 the convergence significantly depends on $\mathbf{\Theta}_k$ and τ_k^2.

Figures 3.8 and 3.10 compare the ergodic sum rate to the deterministic approximation (3.100) under RZF and ZF precoding, respectively. The error bars indicate the standard deviation of the simulation results. It can be observed that the approximation lies roughly within one standard deviation of the Monte-Carlo simulations. From Figure 3.8, under imperfect CSIT ($\tau_k^2 = 0.1$), the sum rate is decreasing for high SNR, because the regularization parameter α does not account for τ_k^2 and thus the matrix $\hat{\mathbf{H}}^{\mathsf{H}}\hat{\mathbf{H}} + M\alpha\mathbf{I}_M$ in the RZF precoder becomes ill-conditioned. Figure 3.10 shows that, for $M > K$, the sum rate is not decreasing at high SNR, because the CSIT $\hat{\mathbf{H}}$ is much better conditioned. The optimal regularization is discussed in Section 4.2. Further observe that in Figure 3.8 the deterministic approximation becomes less accurate for high SNR. The reason has been discussed in Section 3.7.2.

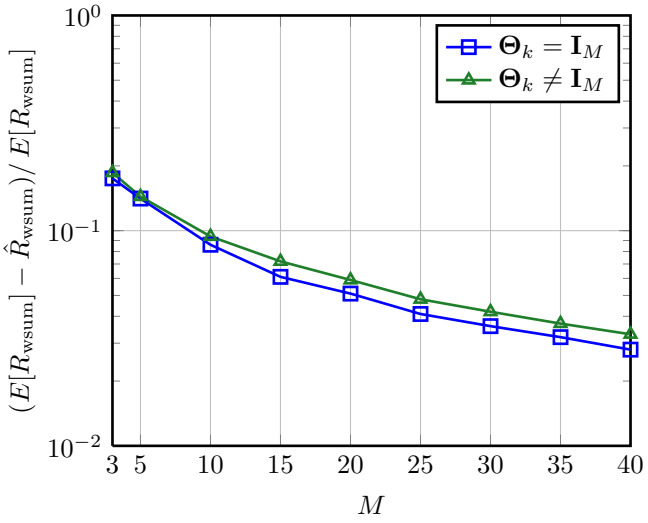

Figure 3.3: Optimal linear precoding, accuracy vs. M for a fixed SNR of $\rho = 10$ dB, $M = K$, $u_k \neq 1$ and $N_{\text{iter}} = 10$

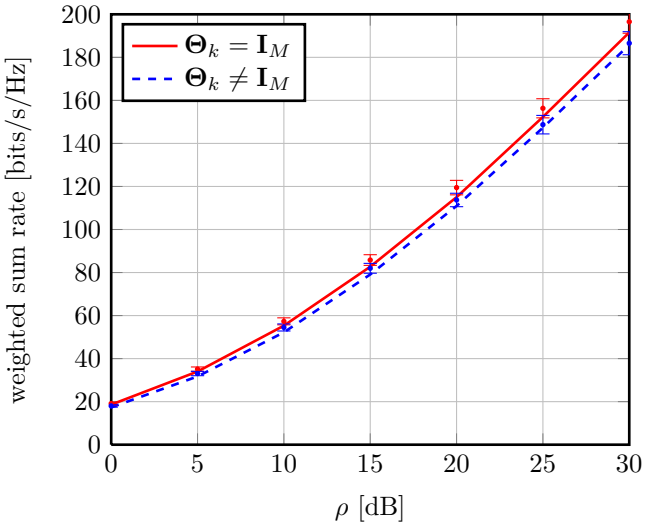

Figure 3.4: Optimal linear precoding, sum rate vs. SNR with $M = K = 30$, $u_k \neq 1$ and $N_{\text{iter}} = 10$, simulation results are indicated by circle marks with error bars indicating the standard deviation.

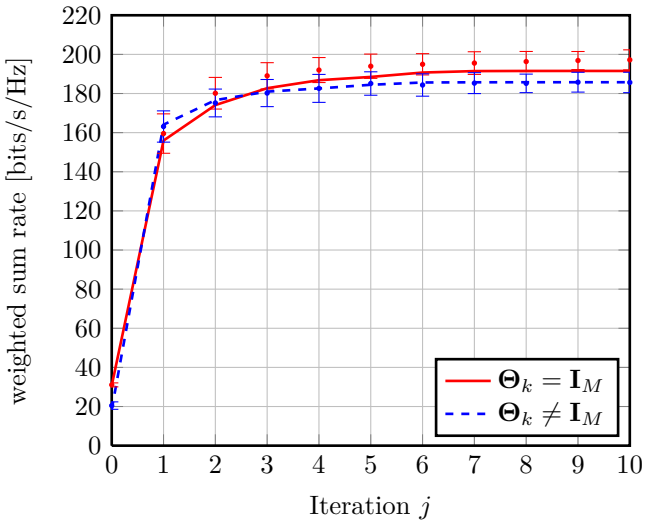

Figure 3.5: Optimal linear precoding, WSR vs. iteration j with $\rho = 30$ dB, $M = K = 30$ and $u_k \neq 1$.

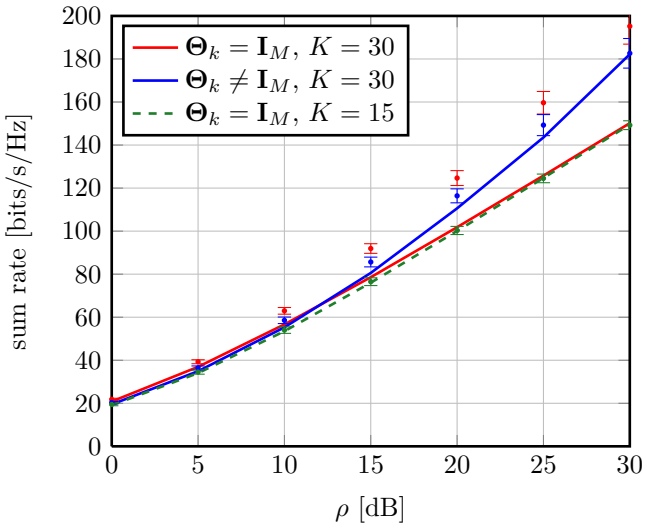

Figure 3.6: Optimal linear precoding, $M = 30$, $u_k = 1\ \forall k$ and simulation results are indicated by circle marks with error bars indicating the standard deviation.

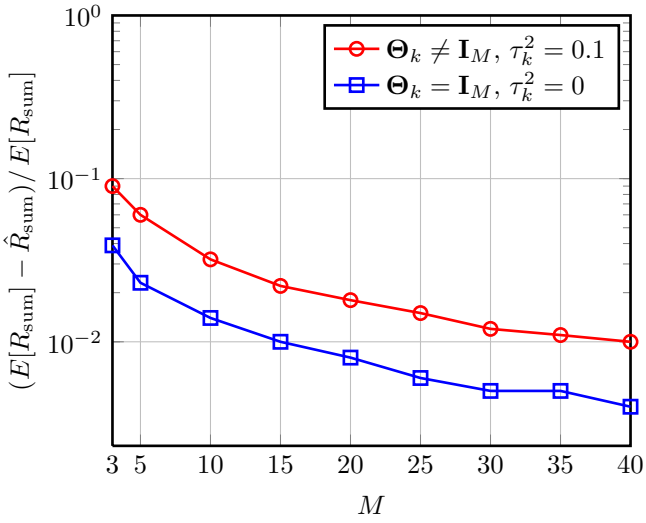

Figure 3.7: RZF-CDU, accuracy vs. M for a fixed SNR of $\rho = 10$ dB with $M = K$ and $\alpha = 1/\rho$.

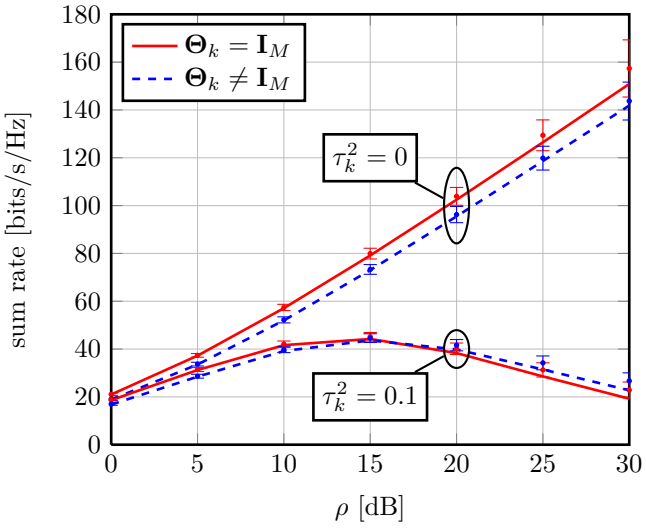

Figure 3.8: RZF-CDU, sum rate vs. SNR with $M = K = 30$ and $\alpha = 1/\rho$, simulation results are indicated by circle marks with error bars indicating the standard deviation.

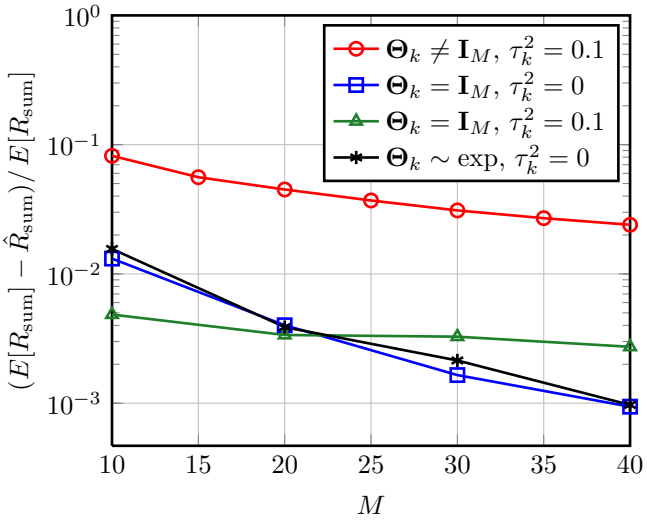

Figure 3.9: ZF, accuracy vs. M for a fixed SNR of $\rho = 10$ dB.

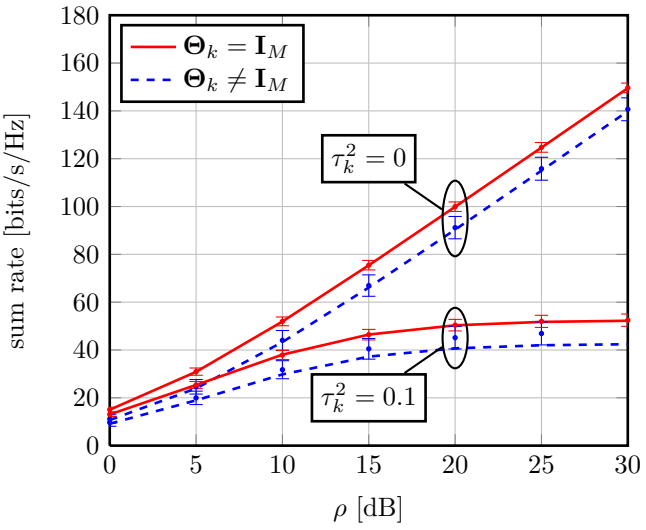

Figure 3.10: ZF, sum rate vs. SNR with $M = 30$, $K = 15$, simulation results are indicated by circle marks with error bars indicating the standard deviation.

Chapter 4

Large MISO BC under Linear Precoding: Applications

This chapter presents several applications of the SINR approximations under various linear precoding schemes derived in the previous chapter. These applications demonstrate that the large system approximations lead to insightful results which turn out to be close-to-optimal even for small system dimensions. The chapter is organized as follows: In Section 4.1, we derive the sum rate maximizing regularization term for RZF precoding. Section 4.2 studies the sum rate maximizing number of users per transmit antenna as well as the optimal power allocation strategy for unequal CSIT quality across the users. Section 4.3 considers a TDD system where we study the impact of MMSE channel estimation at the transmitter and derive the sum rate maximizing amount of channel training. Finally, in Section 4.4, we analyze the effect of channel quantization on the sum rate in large multi-user FDD systems, where we assume random vector quantization and derive the necessary feedback scaling to achieve full multiplexing gain. Moreover, we compare the digital feedback scheme to analog feedback.

4.1 Sum Rate Maximizing Regularization

From the structure of the optimal linear precoder under perfect CSIT (3.31), it is clear that the RZF precoder defined in (3.73) is sub-optimal since it assumes $\mathbf{A} = \mathbf{W} = \mathbf{I}_K$. However, for the proposed linear precoder (3.33) under sum rate

maximization ($u_k = 1\ \forall k$) and common transmit correlation ($\mathbf{\Theta}_k = \mathbf{\Theta}\ \forall k$), the virtual receive filters $\mathbf{A}$ and the MSE weights $\mathbf{W}$ are equal as $M, K \to \infty$, cf. Proposition 3.1. In this case and under perfect CSIT, the optimal regularization term $\bar{\alpha}^\star$ is of the form $\bar{\alpha}^\star = \frac{K}{M\rho}$, cf. (3.68). In the following, for RZF precoding, we will derive the regularization term $\bar{\alpha}^\star$ maximizing (3.100) under imperfect CSIT. For the general correlation model $\mathbf{\Theta}_k \neq \mathbf{\Theta}_i$ $(i \neq k)$, where the RZF precoder is sub-optimal, the optimal regularization parameter $\bar{\alpha}^\star$ is defined as

$$\bar{\alpha}^\star = \arg\max_{\alpha>0} \sum_{k=1}^{K} \log\left(1 + \bar{\gamma}_{k,\mathrm{rzf}}\right). \tag{4.1}$$

In general, the optimization problem (4.1) is not convex in α and the solution has to be computed via a one-dimensional line search. Subsequently, the RZF precoder with sum rate maximizing regularization (4.1) is referred to as RZF channel distortion aware (RZF-CDA) precoder. In the following, we confine ourselves to the case of common correlation $\mathbf{\Theta}_k = \mathbf{\Theta}\ \forall k$, since the proposed precoder in (3.33) is of closed form for all large M, as discussed above. Moreover, given that under common transmit correlation the users' channels are statistically equivalent, we subsequently assume that the distortions τ_k^2 of the CSIT $\hat{\mathbf{h}}_k$ are identical for all users, i.e., $\tau_k^2 = \tau^2\ \forall k$. In these conditions, equal power allocation $\mathbf{P} = \frac{1}{K}\mathbf{I}_K$ maximizes (3.100)[1] and the optimization problem (4.1) has the following solution.

Proposition 4.1. *Let $\mathbf{\Theta}_k = \mathbf{\Theta}$, $0 \leq \tau_k = \tau < 1\ \forall k$ and $p_k = P/K\ \forall k$. The approximated SINR $\bar{\gamma}_{k,\mathrm{rzf}}$ of user k under RZF precoding (equivalently, the approximated per-user rate and the sum rate) is maximized for a regularization term $\alpha \triangleq \bar{\alpha}^\star$, given as a positive solution to the fixed point equation*

$$\bar{\alpha}^\star = \frac{\left[1 + \nu(\bar{\alpha}^\star) + \tau^2\rho\frac{e_{22}(\bar{\alpha}^\star)}{e_{12}(\bar{\alpha}^\star)}\right]\frac{1}{\beta\rho}}{(1-\tau^2)[1+\nu(\bar{\alpha}^\star)] + \tau^2\nu(\bar{\alpha}^\star)[1+e(\bar{\alpha}^\star)]^2} \tag{4.2}$$

where $e(\alpha)$ is defined in (3.79) *and $\nu(\alpha)$ is given by*

$$\nu(\alpha) = \frac{1}{(1+e)e_{22}}\frac{e_{13}}{e_{12}}\left[\frac{e_{22}}{e_{12}} - \frac{e_{23}}{e_{13}}\right] \tag{4.3}$$

with e_{ij} defined in (3.81).

Proof. The proof of Proposition 4.1 is provided in Appendix D. □

Note that the solution in Proposition 4.1 assumes a *fixed* distortion τ^2. Later in Section 4.4 the distortion becomes a function of the quantization codebook size and in Section 4.3 it depends on the uplink SNR as well as the amount of channel training.

Under perfect CSIT ($\tau^2 = 0$), Proposition 4.1 simplifies to the well-known solution $\bar{\alpha}^\star = 1/(\beta\rho)$, which has previously been derived in [10,25,27] and is also

[1] This is clear from Corollary 3.7, but will be discussed in more detail in Section 4.2.2.

an immediate result from Proposition 3.1. As mentioned in [10], for *large* M the RZF precoder is identical to the MMSE precoder in [17, 64]. Furthermore, the authors in [27] showed that, under *perfect* CSIT, $\bar{\alpha}^\star$ is independent of the correlation $\mathbf{\Theta}$. This conclusion is also clear from Proposition 3.1. However, for imperfect CSIT ($\tau^2 > 0$), the optimal regularization parameter (4.2) depends on the transmit correlation through $e(\alpha)$ and $e_{ij}(\alpha)$. For uncorrelated channels ($\mathbf{\Theta} = \mathbf{I}_M$), we have $e_{12} = e_{22}$ and $\nu(\alpha) = 0$ and therefore the explicit solution

$$\bar{\alpha}^\star = \left(\frac{1+\tau^2\rho}{1-\tau^2}\right)\frac{1}{\beta\rho}. \tag{4.4}$$

The solution $\bar{\alpha}^\star$ in (4.4) is the *unique* positive solution to (4.1). The proof of (4.4) can be found in Appendix E.

For imperfect CSIT ($\tau^2 > 0$), the RZF-CDA precoder and the MMSE precoder with regularization term $\alpha_{\text{MMSE}} = \tau^2/\beta + 1/(\beta\rho)$ [64] are not identical anymore, even in the large M limit. Unlike the case of perfect CSIT, $\bar{\alpha}^\star$ now depends on the correlation matrix $\mathbf{\Theta}$ through $e(\alpha)$ and $e_{ij}(\alpha)$. The impact of e and e_{ij} on the sum rate of RZF-CDA precoding is evaluated through numerical simulations in Figure 4.2. Further note that since $e(\alpha)$ and $e_{ij}(\alpha)$ are bounded from above under the conditions explained in Remark 4.1 below, at asymptotically high SNR, the regularization term $\bar{\alpha}^\star$ in (4.2) converges to $\bar{\alpha}^\star_\infty \triangleq \lim_{\rho\to\infty}\bar{\alpha}^\star$, where $\bar{\alpha}^\star_\infty$ is a positive solution of

$$\bar{\alpha}^\star_\infty = \frac{\frac{\tau^2}{\beta}\frac{e_{22}(\bar{\alpha}^\star_\infty)}{e_{12}(\bar{\alpha}^\star_\infty)}}{(1-\tau^2)[1+\nu(\bar{\alpha}^\star_\infty)] + \tau^2\nu(\bar{\alpha}^\star_\infty)[1+e(\bar{\alpha}^\star_\infty)]^2}. \tag{4.5}$$

For uncorrelated channels, the limit in (4.5) takes the form

$$\bar{\alpha}^\star_\infty = \frac{\tau^2}{(1-\tau^2)\beta}.$$

Thus, for asymptotically high SNR, RZF-CDA is *not* ZF precoding, since the regularization parameter $\bar{\alpha}^\star$ is non-zero due to the residual interference caused by the imperfect CSIT. Similar observations have been made in [64] for the MMSE precoder.

Remark 4.1. *Note that in* (4.5) *we apply the limit* $\rho \to \infty$ *on a result obtained from an SINR approximation which is almost surely exact as* $M \to \infty$. *This is correct if* $\Psi_{\text{rzf}} = \text{tr}\mathbf{P}\hat{\mathbf{H}}(\hat{\mathbf{H}}^{\mathsf{H}}\hat{\mathbf{H}} + M\alpha\mathbf{I}_M)^{-2}\hat{\mathbf{H}}^{\mathsf{H}}$ *in* (3.74) *is bounded for asymptotically high SNR as* $M \to \infty$. *For* $\tau^2 > 0$ *it is clear that* $\bar{\Psi}_{\text{rzf}}$ *is bounded since* $\bar{\alpha}^\star > 0$ *for all SNR. In the case where* $\tau^2 = 0$, *we have* $\lim_{\rho\to\infty}\bar{\alpha}^\star = 0$ *and thus for* $\beta = 1$ *the support of the limiting eigenvalue distribution of* $\frac{1}{M}\hat{\mathbf{H}}\hat{\mathbf{H}}^{\mathsf{H}}$ *includes zero resulting in an unbounded* $\bar{\Psi}_{\text{rzf}}$. *From Remark 3.3, for* $\beta > 1$, $\mathbf{\Theta}_k = \mathbf{\Theta}$ *and* $\lambda_{\min}(\mathbf{\Theta}) > \varepsilon > 0$ *there exists* $\xi > 0$ *such that* $\lambda_{\min}(\frac{1}{M}\hat{\mathbf{H}}\hat{\mathbf{H}}^{\mathsf{H}}) > \xi$ *for all large* M. *Thus,* $\bar{\Psi}_{\text{rzf}}$ *is bounded. On the contrary, for* $\mathbf{\Theta}_k \neq \mathbf{\Theta}_j$ $(k \neq j)$, $\beta > 1$ *and* $\lambda_{\min}(\mathbf{\Theta}_k) > \varepsilon > 0\ \forall k$, *it has not been proved that* $\lambda_{\min}(\frac{1}{M}\hat{\mathbf{H}}\hat{\mathbf{H}}^{\mathsf{H}}) > \xi$ *and we have to evoke Assumption 3.5 to ensure that* $\bar{\Psi}_{\text{rzf}}$ *is bounded. Thus, for* $\tau^2 = 0$,

the limit (4.5) *is only well defined for* $\beta > 1$. *Further note that if* $\bar{\Psi}_{\mathrm{rzf}}$ *is bounded as* $M \to \infty$ *the limits* $M \to \infty$ *and* $\rho \to \infty$ *can be inverted without affecting the result.*

For various special cases, substituting (4.2) into the deterministic equivalent of the SINR $\bar{\gamma}_{k,\mathrm{rzf}}$ in (E.2) yields the following simplified expressions.

Corollary 4.1. *Let Assumptions 3.1 and 3.2 hold true and let* $\mathbf{\Theta}_k = \mathbf{\Theta}$, $\tau_k^2 = 0$, $p_k = P/K \ \forall k$, $\bar{\alpha}^\star = \frac{1}{\beta\rho}$ *and* $\gamma_{k,\mathrm{rzf-cda}}$ *be the sum rate maximizing SINR of user* k *under RZF precoding. Then* $\gamma_{k,\mathrm{rzf-cda}} - \bar{\gamma}_{k,\mathrm{rzf-cda}} \overset{M\to\infty}{\longrightarrow} 0$, *almost surely, where* $\bar{\gamma}_{k,\mathrm{rzf-cda}}$ *is given by*

$$\bar{\gamma}_{k,\mathrm{rzf-cda}} \triangleq \bar{\gamma}_{\mathrm{rzf-cda}} = e(-\bar{\alpha}^\star), \tag{4.6}$$

where $e(-\bar{\alpha}^\star)$ *is the unique positive solution to*

$$e(-\bar{\alpha}^\star) = \frac{1}{M}\mathrm{tr}\mathbf{\Theta}\left(\frac{\mathbf{\Theta}/\beta}{1+e(-\bar{\alpha}^\star)} + \bar{\alpha}^\star\mathbf{I}_M\right)^{-1}.$$

Proof of Corollary 4.1. Substituting $\bar{\alpha}^\star = \frac{1}{\beta\rho}$ into Corollary 3.7 together with $\tau^2 = 0$, we obtain (4.6), which completes the proof. □

For uncorrelated channels $\mathbf{\Theta}_k = \mathbf{I}_M \ \forall k$, the solution to (3.58) is explicit and summarized in the following corollary.

Corollary 4.2. *Let* $\mathbf{\Theta}_k = \mathbf{I}_M$, $\tau_k^2 = \tau^2$, $p_k = P/K \ \forall k$ *and* $\gamma_{k,\mathrm{rzf-cda}}$ *be the sum rate maximizing SINR of user* k *under RZF precoding. Then* $\gamma_{k,\mathrm{rzf-cda}} - \bar{\gamma}_{k,\mathrm{rzf-cda}} \overset{M\to\infty}{\longrightarrow} 0$, *almost surely, where* $\bar{\gamma}_{k,\mathrm{rzf-cda}}$ *is given by*

$$\bar{\gamma}_{k,\mathrm{rzf-cda}} \triangleq \bar{\gamma}_{\mathrm{rzf-cda}} = e(-\bar{\alpha}^\star) = \frac{\omega}{2}\rho(\beta-1) + \frac{\chi(\omega)}{2} - \frac{1}{2}, \tag{4.7}$$

where $\omega \in [0,1]$ *and* χ *are given by*

$$\omega = \frac{1-\tau^2}{1+\tau^2\rho}, \tag{4.8}$$

$$\chi(\omega) = \sqrt{(\beta-1)^2\omega^2\rho^2 + 2(\beta+1)\omega\rho + 1}. \tag{4.9}$$

Proof. Substituting $\mathbf{\Theta} = \mathbf{I}_M$ into Corollary 4.1 leads to a quadratic equation in $e(-\bar{\alpha}^\star)$ for which the only positive solution is given by (4.7), which completes the proof. □

Note that under perfect CSIT $\tau^2 = 0$, Corollaries 4.1 and 4.2 are identical to Corollaries 3.5 and 3.6 under the proposed linear precoder (3.33) for WSR maximization, respectively.

Define $\kappa \triangleq \omega\rho$. For asymptotically high SNR, we have

$$\kappa_\infty = \lim_{\rho\to\infty} \kappa = \frac{1-\tau^2}{\tau^2} \tag{4.10}$$

and further

$$\chi_\infty = \lim_{\rho\to\infty} \chi = \sqrt{(\beta-1)^2\kappa_\infty^2 + 2(\beta+1)\kappa_\infty + 1}. \tag{4.11}$$

Hence the SINR (4.7) saturates at

$$\lim_{\rho\to\infty} \bar{\gamma}_{\mathrm{rzf-cda}} = \frac{\kappa_\infty}{2}(\beta-1) + \frac{\chi_\infty}{2} - \frac{1}{2}. \tag{4.12}$$

Moreover, for $\beta > 1$ as the SNR grows large, the SINR gap between RZF-CDA and ZF precoding converges to the limits

$$\lim_{\rho\to\infty} (\bar{\gamma}_{\mathrm{rzf-cda}} - \bar{\gamma}_{\mathrm{zf}}) = \begin{cases} \frac{1}{\beta-1} & \text{if } \tau^2 = 0 \\ \frac{\chi_\infty}{2} - \frac{\kappa_\infty}{2}\rho(\beta-1) - \frac{1}{2} & \text{if } \tau^2 > 0. \end{cases} \tag{4.13}$$

That is, the asymptotic SINR gap is constant under perfect CSIT. In fact, for $\tau^2 = 0$ the asymptotic SINR gap approaches zero as β grows large, but recall that the large system approximations of the SINR are derived under the assumption $\beta < \infty$ and are invalid for $\beta \to \infty$. Therefore, even under perfect CSIT there is an offset between the SINRs of RZF-CDA and ZF precoding for large M, K. However, the *rate* difference still converges to zero at high SNR, i.e., $\lim_{\rho\to\infty} \log(\frac{1+\bar{\gamma}_{\mathrm{rzf-cda}}}{1+\bar{\gamma}_{\mathrm{zf}}}) = 0$, hence both schemes achieve the same rate for asymptotically high SNR.

A deterministic equivalent $\Delta\bar{R}_{k,\mathrm{rzf-cda}}$ of the rate gap $\Delta R_{k,\mathrm{rzf-cda}}$ of user k under RZF-CDA precoding is given in the following corollary.

Corollary 4.3. *Let $\mathbf{\Theta}_k = \mathbf{I}_M$ $\forall k$, $p_k = P/K$ $\forall k$, $\tau_k^2 = \tau^2$ $\forall k$ and define $\Delta R_{k,\mathrm{rzf-cda}}$ as the rate gap of user k under RZF-CDA precoding. Then*

$$\Delta R_{k,\mathrm{rzf-cda}} - \Delta\bar{R}_{k,\mathrm{rzf-cda}} \overset{M\to\infty}{\longrightarrow} 0$$

almost surely, with

$$\Delta\bar{R}_{k,\mathrm{rzf-cda}} = \log\left(\frac{1+\rho(\beta-1)+\chi(1)}{1+\omega\rho(\beta-1)+\chi(\omega)}\right),$$

where ω and χ are defined in (4.8) *and* (4.9)*, respectively.*

Proof of Corollary 4.3. With Corollary 4.2, compute $\Delta\bar{R}_{\mathrm{rzf-cda}}$ as defined in (3.103). □

The impact of the regularization term on the ergodic sum rate is depicted in Figures 4.1 and 4.2. We assume a rather small system with $M = K = 5$.

In Figure 4.1, we compare the ergodic sum rate performance for different regularization parameters α with fixed CSIT distortion $\tau^2 = 0.1$. The upper bound $\alpha = \alpha^\star$ is obtained by optimizing α for every channel realization, whereas $\alpha_{\mathrm{erg}}^\star$ maximizes the ergodic sum rate. It can be observed that both $\alpha_{\mathrm{erg}}^\star$ and $\bar{\alpha}^\star$ are close to the optimal $\alpha^\star$. Furthermore, if the channel uncertainty τ^2 is unknown at the transmitter (and hence assumed zero), the performance decreases

as soon as τ^2 dominates the noise power σ^2 (i.e. the inter-user interference limits the performance) and approaches the sum rate of ZF precoding for high SNR. We conclude (i) that adapting the regularization term yields a significant performance increase and (ii) that the proposed RZF-CDA precoder with $\bar{\alpha}^\star$ performs close-to-optimal even for small system dimensions.

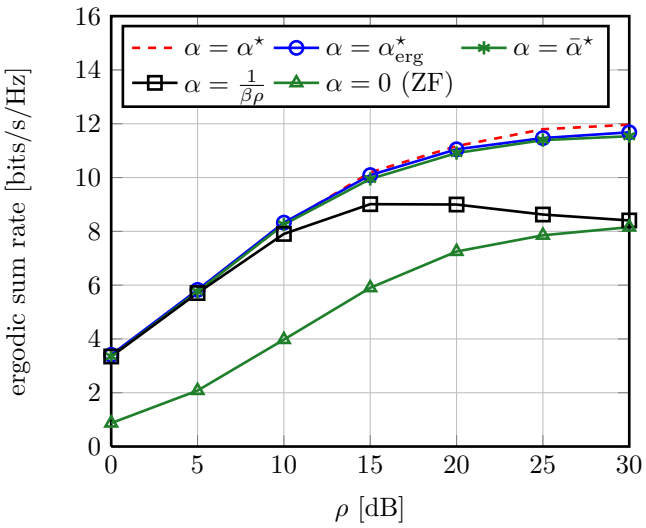

Figure 4.1: Ergodic sum rate vs. SNR for different regularization parameters with $\boldsymbol{\Theta}_k = \mathbf{I}_M$ and $\tau_k^2 = 0.1$.

In Figure 4.2, we simulate the impact of transmit correlation in the computation of $\bar{\alpha}^\star$ on the sum rate. For this purpose, we use the standard exponential correlation model in (3.106). We compare two different RZF precoders. A precoder coined RZF common correlation aware (RZF-CCA) that takes the channel correlation into account and computes α according to (4.2). The second precoder, called RZF common correlation unaware (RZF-CCU), does not take $\boldsymbol{\Theta}$ into account and computes α as in (4.4). We observe that for high correlation, i.e., $v = 0.9$, the RZF-CCA precoder significantly outperforms the RZF-CCU precoder at medium to high SNR, whereas both precoder perform equally at low SNR. Therefore, we conclude that it is beneficial to account for transmit correlation, especially in highly correlated channels. Further simulations suggest that the sum rate gain of RZF-CCA over RZF-CCU precoding is less pronounced for lower CSIT qualities (i.e., increasing τ^2), because in this case the impact of the CSIT quality τ^2 is more significant than the impact of $\boldsymbol{\Theta}$ on the sum rate.

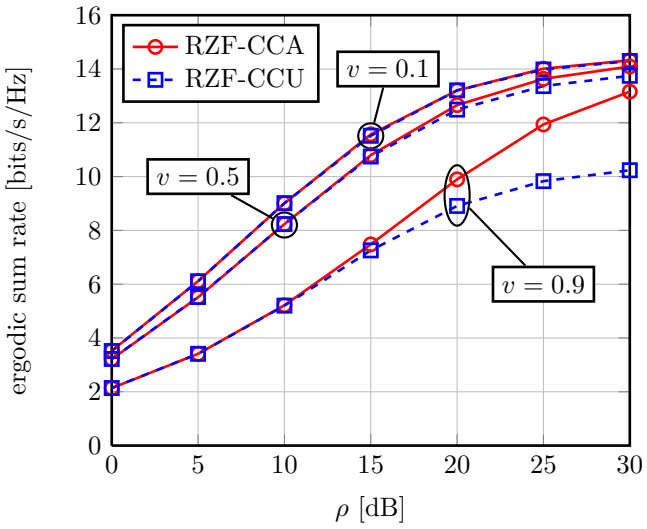

Figure 4.2: Ergodic sum rate vs. SNR, impact of correlation with $M = K = 5$, $\mathbf{P} = \frac{1}{K}\mathbf{I}_K$ and $\tau_k^2 = 0.05$.

4.2 Optimal Number of Users and Power Allocation

In this section, we address two problems: (i) the determination of the sum rate maximizing number of users per transmit antenna for a fixed M and (ii) the optimization of the power distribution among a *given* set of users with unequal CSIT qualities.

Consider problem (i). Intuitively, an optimal number of users $K^\star$ exists because serving more users creates more interference which in turn reduces the user rates. At some point the accumulated rate loss, due to the additional interference caused by scheduling another user, will outweigh the sum rate gain and hence the system sum rate will decrease. In particular, we consider a fair scenario, where the SINR approximations of all users are equal. Here, the optimal solution can be expressed in a closed form under ZF precoding.

In problem (ii), we optimize the power allocation matrix $\mathbf{P}$ for a given K. More precisely, we focus on common correlation $\mathbf{\Theta}_k = \mathbf{\Theta}$ $\forall k$ with *different* CSIT qualities τ_k^2. In this case, the (approximated) optimal power distribution $\bar{\mathbf{P}}^\star$ can be expressed in closed form and is the solution of a classical water-filling algorithm.

4.2.1 Sum Rate Maximizing Number of Users

Consider the problem of finding the optimal system loading $\bar{\beta}^\star = \frac{M}{K^\star}$ maximizing the approximated sum rate per transmit antenna for a *fixed* M, i.e.,

$$\bar{\beta}^\star = \arg\max_{\beta} \frac{1}{\beta} \frac{1}{K} \sum_{k=1}^{K} \log\left(1+\bar{\gamma}_k\right), \tag{4.14}$$

where $\bar{\gamma}_k$ denotes either $\bar{\gamma}_{k,\mathrm{zf}}$ with $\beta > 1$ or $\bar{\gamma}_{k,\mathrm{mf}}$, $\bar{\gamma}_{k,\mathrm{rzf}}$ with $\beta \geq 1$. In general (4.14) has to be solved by a one-dimensional line search. However, in the case of ZF precoding and uncorrelated antennas the optimization problem (4.14) has a closed-form solution given in the following proposition.

Proposition 4.2. *Let* $\mathbf{\Theta}_k = \mathbf{I}_M$, $\tau_k = \tau \ \forall k$ *and* $\mathbf{P} = \frac{P}{K}\mathbf{I}_K$, *the sum rate maximizing system loading per transmit antenna* $\bar{\beta}^\star$ *is given by*

$$\bar{\beta}^\star = \left(1 - \frac{1}{a}\right)\left(1 + \frac{1}{\mathcal{W}(x)}\right), \tag{4.15}$$

where $a = \frac{1-\tau^2}{\tau^2 + \frac{1}{\rho}}$, $x = \frac{a-1}{e}$ *and* $\mathcal{W}(x)$ *is the Lambert W-function defined as* $z = \mathcal{W}(z)e^{\mathcal{W}(z)}$, $z \in \mathbb{C}$.

Proof of Proposition 4.2. Substituting the SINR in Corollary 3.10 into (4.14) and differentiating along β yields

$$\frac{a\beta}{1+a(\beta-1)} = \log\left(1+a(\beta-1)\right) \tag{4.16}$$

Denoting $w(\beta) = \frac{a-1}{a(\beta-1)+1}$, we can rewrite (4.16) as

$$w(\beta)e^{w(\beta)} = x.$$

Noticing that $w(\beta) = \mathcal{W}(x)$ and solving for β yields (4.15), which completes the proof. □

For $\tau \in [0,1]$, $\beta > 1$ we have $w \geq -1$ and $x \geq -e^{-1}$. In this case $\mathcal{W}(x)$ is a well-defined function. If $\tau^2 = 0$, we obtain the results in [22], although in [22] they are not given in closed form. Note that for $\tau^2 = 0$, we have $\lim_{\rho\to\infty} \bar{\beta}^\star = 1$, i.e., the optimal system loading tends to one at high SNR. Further note that only integer values of $M/\bar{\beta}^\star$ are meaningful in practice.

4.2.2 Power Optimization under Common Correlation

Under Assumption 3.2, we have $\lim_{M\to\infty} p_k/P = 0 \ \forall k$ (cf. Remark 3.2) and thus, from Corollaries 3.1, 3.7 and 3.9, the approximated sum rate (3.100) for MF, RZF and ZF precoding takes the form

$$\hat{R}_{\mathrm{sum}} = \sum_{k=1}^{K} \log\left[1 + p_k \bar{\nu}_k(\tau_k)\right], \tag{4.17}$$

with $\bar{\nu}_k = \bar{\gamma}_k/p_k$, where $\bar{\gamma}_k$ is a deterministic equivalent of the SINR of either MF, RZF or ZF precoding and the only dependence on user k stems from τ_k. The user powers $\bar{p}_k^\star$ that maximize (4.17), subject to $\sum_{k=1}^K p_k \leq P$, $p_k \geq 0$ $\forall k$, are thus given by the classical water-filling solution [65]

$$\bar{p}_k^\star = \left[\mu - \frac{1}{\bar{\nu}_k}\right]^+, \tag{4.18}$$

where $[x]^+ \triangleq \max(0, x)$ and μ is the water level chosen to satisfy $\sum_{k=1}^K p_k = P$. For $\tau_k^2 = \tau^2$ $\forall k$, the optimal user powers (4.18) are all equal, i.e., $\bar{p}_k^\star = \bar{p}^\star = P/K$ and $\bar{\mathbf{P}}^\star \triangleq \operatorname{diag}(\bar{p}_1^\star, \ldots, \bar{p}_K^\star) = \frac{P}{K}\mathbf{I}_K$. In this case though, it could still be beneficial to adapt the number of users as discussed previously in Section 4.2.1.

4.2.3 Numerical Results

Figure 4.3 compares the optimal number of users $\bar{K}^\star = M/\bar{\beta}^\star$ in (4.15) to $K^\star$ obtained by choosing the $K \in \{1, 2, \ldots, M\}$ such that the ergodic sum rate is maximized, whereas Figure 4.4 depicts the impact of a sub-optimal number of users on the ergodic sum rate of the system.

From Figure 4.3 it can be observed, that (i) the approximated results $\bar{K}^\star$ do fit well with the simulation results even for small dimensions, (ii) $(K^\star, \bar{K}^\star)$ increase with the SNR and (iii), for $\tau^2 \neq 0$, $(K^\star, \bar{K}^\star)$ saturate for high SNR at a value lower than M. Therefore, under imperfect CSIT, it is not optimal anymore to serve the maximum number of users $K = M$ for asymptotically high SNR. Instead, depending on τ^2, a lower number of users $K < M$ should be served even at high SNR which implies a reduced multiplexing gain of the system. The impact of the system loading on the sum rate is depicted in Figure 4.4.

From Figure 4.4 we observe that, (i) the approximate large M solution $\bar{K}^\star$ achieves most of the sum rate and (ii) adapting the number of users is beneficial compared to a fixed K. Moreover, from Figure 4.3, we identify $K = 8$ as a optimal choice (for $M = 16$) for medium SNR and, as expected, the performance is optimal in the medium SNR regime and sub-optimal at low and high SNR. From Figure 4.3 it is clear that $K = 4$ is highly sub-optimal in the medium and high SNR range and we observe a significant loss in sum rate. Consequently, the number of users must be adapted to the channel conditions and the approximate result $\bar{K}^\star$ is a good choice to determine the number of users in the system.

In Figures 4.5 and 4.6 for RZF-CDU precoding and in Figure 4.7 for MF precoding, we compare the ergodic sum rate performance under RZF-CDU precoding and MF precoding, respectively, for three different power allocation strategies: (i) optimal power allocation $\mathbf{P} = \bar{\mathbf{P}}^\star$ in (4.18), (ii) equal power allocation $\mathbf{P} = \frac{P}{K}\mathbf{I}_K$ and (iii) all available transmit power is allocated to the user $k_{\min}$ with minimum channel distortion, i.e., $p_{k_{\min}} = P$ with $k_{\min} = \arg\min_{k=1,\ldots,K}\{\tau_k^2\}$. Since the system becomes interference-limited for high SNR and for all given M, K, the power allocation strategy (iii) is optimal for asymptotically high SNR. However, for $M, K \to \infty$ power allocation scheme (i) is optimal for any SNR

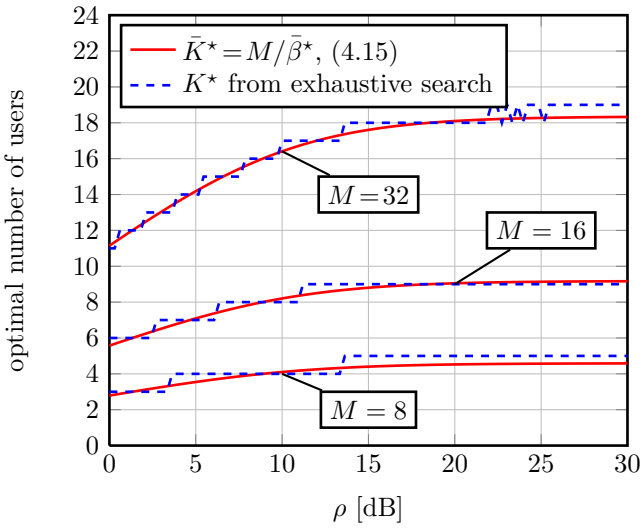

Figure 4.3: ZF, Sum rate maximizing number of users vs. SNR with $\mathbf{\Theta}_k = \mathbf{I}_M \; \forall k$, $\mathbf{P} = \frac{1}{K}\mathbf{I}_K$ and $\tau^2 = 0.1$.

under Assumption 3.2. But note that Assumption 3.2 excludes power allocation strategy (iii). Therefore, as long as the optimal power allocation satisfies Assumption 3.2 it is given by $\mathbf{P} = \bar{\mathbf{P}}^\star$ for all large M. We choose RZF-CDU precoding and not RZF-CDA precoding for simplicity, since under RZF-CDA precoding the optimal regularization term for different τ_k is not of closed form and has to be computed via a one-dimensional line search. We choose two different CSIT quality distributions: (i) the quality of the CSIT varies significantly among the users, i.e., the τ_k^2 are linearly spaced between 0.05 and 0.8 ($\tau_k^2 = 0.05 + \frac{k-1}{K-1}(0.8 - 0.05)$) and (ii) the quality of the CSIT does not differ considerably, i.e., the τ_k^2 are uniformly distributed between 0.2 and 0.3 ($\tau_k^2 = 0.2 + \frac{k-1}{K-1}(0.3 - 0.2)$).

In Figure 4.5, for RZF-CDU precoding, we observe a significantly gain over the whole SNR range when optimal power allocation is applied compared to equal power allocation. If the CSIT qualities differ only slightly ($M = 3$), there is only a small gain at high SNR. In general, for increasing SNR, the SINRs become increasingly distinct depending on the τ_k^2. Therefore, it might be optimal to turn off the users with lowest CSIT accuracy as the SNR increases, which explains why the sum rate gain is larger at high SNR than for low SNR. Moreover, at high SNR, concentrating all power on the best user significantly outperforms power allocation strategy (i), which yields an inaccurate solution for these small system dimensions. If we increase the system dimensions, cf. Figure 4.6, the picture changes, now the water-filling power allocation algorithm outperforms the other strategies over the simulated SNR range. Note that the sum rate decreases rapidly for high SNR due to the RZF-CDU precoder which

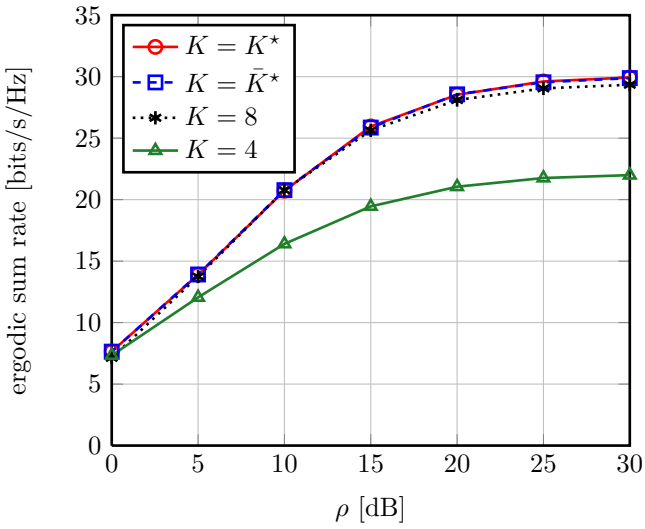

Figure 4.4: ZF, Ergodic sum rate for different numbers of users with $M = 16$, $\boldsymbol{\Theta}_k = \mathbf{I}_M \ \forall k$, $\mathbf{P} = \frac{1}{K}\mathbf{I}_K$ and $\tau^2 = 0.1$.

does not account for imperfect CSIT. Thus, if Assumption 3.2 holds true, $\bar{\mathbf{P}}^\star$ will always outperform $p_{k_{\min}} = P$ for large enough M, K. The same is true for MF precoding in Figure 4.7.

We conclude that the optimal power allocation proposed in (4.18) achieves significant performance gains over equal power allocation, especially at high SNR, when the quality of the available CSIT varies considerably among the users' channels. Furthermore, (4.18) is the optimal power allocation scheme for large dimension under Assumption 3.2.

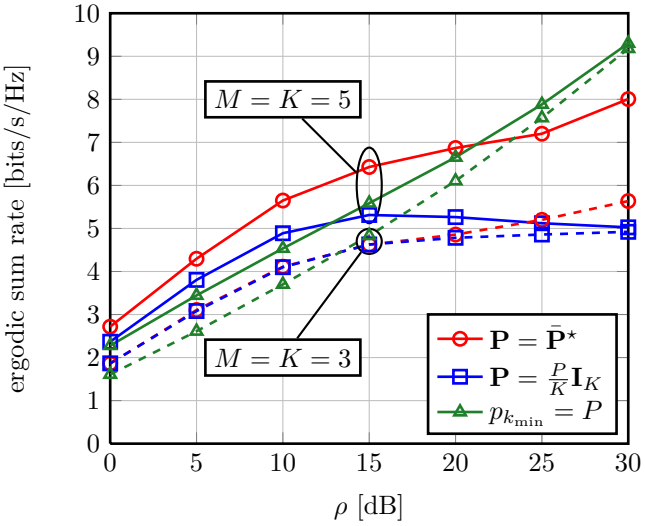

Figure 4.5: RZF-CDU, ergodic sum rate vs. SNR for different power allocation strategies with $\alpha = 1/\rho$, $\mathbf{\Theta}_k = \mathbf{I}_M$, $P = 1$, $\tau_k^2 = 0.05 + \frac{k-1}{K-1}(0.8 - 0.05)$ for $M = 5$ and $\tau_k^2 = 0.2 + \frac{k-1}{K-1}(0.3 - 0.2)$ for $M = 3$

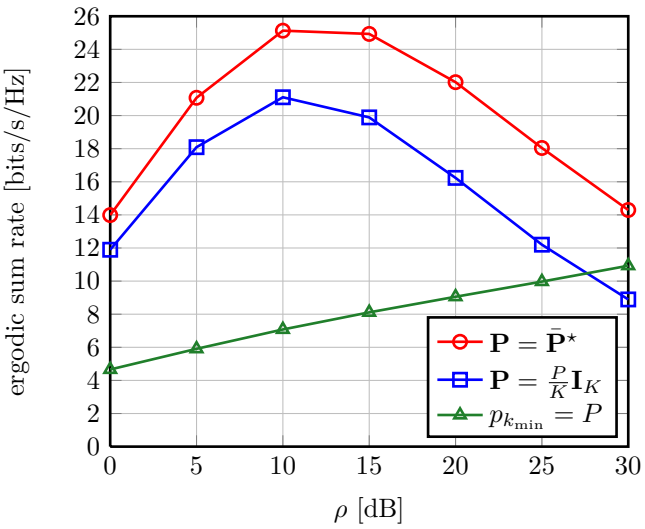

Figure 4.6: RZF-CDU, ergodic sum rate vs. SNR for different power allocation strategies with $\alpha = 1/\rho$, $\mathbf{\Theta}_k = \mathbf{I}_M$, $P = 1$, $M = K = 30$ and $\tau_k^2 = 0.05 + \frac{k-1}{K-1}(0.8 - 0.05)$.

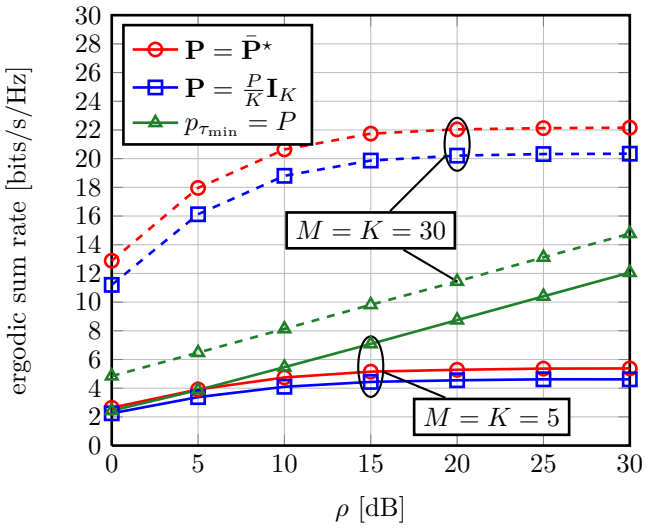

Figure 4.7: MF Precoding, ergodic sum rate vs. SNR for different power allocation strategies with $\mathbf{\Theta}_k = \mathbf{I}_M$, $\tau_k^2 = 0.05 + \frac{k-1}{K-1}(0.8 - 0.05)$ and $P = 1$.

4.3 Optimal Training in Large TDD Multi-user Systems

Consider a time-division duplex (TDD) system where uplink (UL) and downlink (DL) share the *same* channel at different times. Therefore, the transmitter estimates the channel from known pilot signaling of the receivers. We investigate a single isolated cell and thus neglect the possible effects of pilot contamination resulting from the reuse of pilot symbols in the neighboring cells. The channel coherence interval T, i.e., the amount of channel uses for which the channel is approximately constant, is divided into T_t channel uses for UL training and $T - T_t$ channel uses for coherent transmission in the DL. Note that in order to coherently decode the information symbols, the users need to know their effective (precoded) channels. This is usually accomplished by a dedicated training phase (using precoded pilots) in the DL prior to the data transmission. As shown in [66], a minimal amount of training (at most one pilot symbol) is sufficient when data and pilots are processed jointly. Therefore, we assume that the users have *perfect* knowledge of their effective channels and we neglect the overhead associated with the DL training.

In the considered TDD system, the imperfections in the CSIT are caused by (i) channel estimation errors in the UL, (ii) imperfect channel reciprocity due to different hardware in the transmitter and receiver and (iii) the channel coherence interval T. In what follows, we assume that the channel is perfectly reciprocal and we study the joint impact of (i) and (iii) for uncorrelated channels ($\boldsymbol{\Theta}_k = \mathbf{I}_M \ \forall k$).

4.3.1 Uplink Training Phase

In our setup, the distortion τ^2 of the CSIT is solely caused by an imperfect channel estimation at the transmitter and is identical for all entries of $\mathbf{H}$. To acquire CSIT, each user transmits the same amount of $T_t \geq K$ *orthogonal* pilot symbols over the UL channel to the transmitter. Subsequently, the transmitter estimates all K channels simultaneously. At the transmitter, the signal $\mathbf{r}_k$ received from user k is given by

$$\mathbf{r}_k = \sqrt{T_t P_{ul}}\mathbf{h}_k + \mathbf{n}_k,$$

where we assumed perfect reciprocity of UL and DL channels and P_{ul} is the average available transmit power at the receivers. That is, the UL and DL channel coefficients are equal and the UL noise $\mathbf{n}_k = [n_1, n_2, \ldots, n_M]^{\mathsf{T}}$ is assumed identical for all users and statistically equivalent to its DL analog. Subsequently, the transmitter performs an MMSE estimation of each channel coefficient $h_{ij} \sim \mathcal{CN}(0,1)$ ($i = 1, \ldots, K$, $j = 1, \ldots, M$). Due to the orthogonality property of the MMSE estimation [67], the estimates $\hat{h}_{ij}$ of h_{ij} and the corresponding estimation errors $\tilde{h}_{ij} = h_{ij} - \hat{h}_{ij}$ are uncorrelated and i.i.d. complex Gaussian distributed. Hence, we can write

$$\hat{h}_{ij} = h_{ij} + \tilde{h}_{ij},$$

where h_{ij} and $\tilde{h}_{ij}$ are independent with zero mean and variance $1-\tau^2$ and τ^2, respectively. The variance τ^2 of the estimation error $\tilde{h}_{ij}$ is given by [32]

$$\tau^2 = \frac{1}{1+T_t\rho_{ul}}, \tag{4.19}$$

where we define the uplink SNR ρ_{ul} as $\rho_{ul} \triangleq P_{ul}/\sigma^2$.

4.3.2 Optimization of Channel Training

We focus on equal power allocation among the users, i.e., $p_k = P/K\ \forall k$, because it is optimal for large M and $\tau_k^2 = \tau^2\ \forall k$, cf. Section 4.2.2. Since T_t channel uses have already been consumed to train the transmitter about the user channels, there remains an interval of length $T-T_t$ for DL data transmission and thus we have the pre-log factor $1-T_t/T$. The net sum rate approximation reads

$$\hat{R}_{\text{sum}} = K\left(1-\frac{T_t}{T}\right)\log\left(1+\bar{\gamma}_k\right). \tag{4.20}$$

To compute the training length T_t that maximizes the net sum rate approximation (4.20), we substitute $\bar{\gamma}_{k,\text{mf}}$ from Corollary 3.3 into (4.20), the net approximated sum rate $\hat{R}_{\text{sum}}^{\text{mf}}$ under MF precoding takes the form

$$\hat{R}_{\text{sum}}^{\text{mf}} = K\left(1-\frac{T_{t,\text{mf}}}{T}\right)\log\left(1+\frac{\beta(1-\tau^2)}{1+\frac{1}{\rho_{dl}}}\right), \tag{4.21}$$

where $\rho_{dl} \triangleq P/\sigma^2$ is the downlink SNR. Likewise, substituting $\bar{\gamma}_{k,\text{zf}}$ from Corollary 3.11 into (3.100), the approximated net sum rate $\hat{R}_{\text{sum}}^{\text{zf}}$ under ZF precoding takes the form

$$\hat{R}_{\text{sum}}^{\text{zf}} = K\left(1-\frac{T_{t,\text{zf}}}{T}\right)\log\left(1+\frac{1-\tau^2}{\tau^2+\frac{1}{\rho_{dl}}}(\beta-1)\right), \tag{4.22}$$

Similarly, for RZF precoding the approximated net sum rate $\hat{R}_{\text{sum}}^{\text{rzf}}$ reads

$$\hat{R}_{\text{sum}}^{\text{rzf}} = K\left(1-\frac{T_{t,\text{rzf}}}{T}\right)\log\left(1+\bar{\gamma}_{\text{rzf}}\right), \tag{4.23}$$

where $\bar{\gamma}_{\text{rzf}}$ is given in Corollary 3.8 and Corollary 4.2 for RZF-CDU and RZF-CDA precoding, respectively. Subsequently, the notation "RZF" refers to both, RZF-CDU and RZF-CDA precoding.

Substituting (4.19) into (4.21), (4.22) and (4.23), we obtain

$$\hat{R}_{\text{sum}}^{\text{mf}} = K\left(1-\frac{T_{t,\text{mf}}}{T}\right)\log\left(1+\frac{\beta T_{t,\text{mf}}\rho_{ul}}{1+T_{t,\text{mf}}\rho_{ul}+T_{t,\text{mf}}\frac{\rho_{ul}}{\rho_{dl}}+\frac{1}{\rho_{dl}}}\right), \quad (4.24)$$

$$\hat{R}_{\text{sum}}^{\text{zf}} = K\left(1-\frac{T_{t,\text{zf}}}{T}\right)\log\left(1+\frac{T_{t,\text{zf}}\rho_{ul}(\beta-1)}{1+T_{t,\text{zf}}\frac{\rho_{ul}}{\rho_{dl}}+\frac{1}{\rho_{dl}}}\right), \quad (4.25)$$

$$\hat{R}_{\text{sum}}^{\text{rzf}-\text{cda}} = K\left(1-\frac{T_{t,\text{rzf}-\text{cda}}}{T}\right)\log\left(\frac{1}{2}+\frac{1}{2}\omega\rho_{dl}(\beta-1)+\frac{\chi(\omega)}{2}\right), \quad (4.26)$$

$$(4.27)$$

where $\chi(\omega)$ and ω take the form

$$\chi(\omega) = \sqrt{(\beta-1)^2\omega^2\rho_{dl}^2+2\omega\rho_{dl}(1+\beta)+1}, \quad (4.28)$$

$$\omega = \frac{T_{t,\text{rzf}-\text{cda}}\rho_{ul}}{1+T_{t,\text{rzf}-\text{cda}}\rho_{ul}+\rho_{dl}}$$

and with $e=\frac{1}{2}[1+\rho_{dl}(\beta-1)+\chi(1)]$, $\delta_1 \triangleq e[1+\frac{1}{\rho_{dl}}(1+e)^2]$ and $\delta_2 \triangleq (1+e)^2[1+\frac{1}{\rho_{dl}}+T_{t,\text{rzf}-\text{cdu}}\frac{\rho_{ul}}{\rho_{dl}}]$ we have

$$\hat{R}_{\text{sum}}^{\text{rzf}-\text{cdu}} = K\left(1-\frac{T_{t,\text{rzf}-\text{cdu}}}{T}\right)\log\left(1+\frac{T_{t,\text{rzf}-\text{cdu}}\rho_{ul}\delta_1}{T_{t,\text{rzf}-\text{cdu}}\rho_{ul}+\delta_2}\right). \quad (4.29)$$

For $\beta > 1$ under ZF precoding and $\beta \geq 1$ for MF and RZF precoding, it is easy to verify that the functions $\hat{R}_{\text{sum}}$ are strictly concave in T_t in the interval $[K, T]$, where K is the minimum amount of training required, due to the orthogonality constraint of the pilot sequences. Therefore, we can apply standard convex optimization algorithms [68] to evaluate

$$\bar{T}_t^{\star} = \underset{K\leq T_t\leq T}{\arg\max}\left\{\hat{R}_{\text{sum}}\right\}, \quad (4.30)$$

for all considered precoders. In the following, for high SNR, we derive the scaling of $\bar{T}_t^{\star}$ with the downlink SNR ρ_{dl} for a fixed coherence interval T and the scaling of $\bar{T}_t^{\star}$ with T for a fixed ρ_{dl}. To accomplish this, we derive a high-SNR approximation of $\hat{R}_{\text{sum}}$. We distinguish two cases, (i) the UL and DL SNR vary with finite ratio $c \triangleq \rho_{dl}/\rho_{ul}$ and (ii) ρ_{dl} varies while ρ_{ul} remains finite. In contrast to case (i), the system in case (ii) is interference-limited for high ρ_{dl} due to the finite transmit power of the users.

Case 1: Finite ratio ρ_{dl}/ρ_{ul}

In the first case, we consider that the ρ_{ul} is of the same order as ρ_{dl}. We approximate $\hat{R}_{\text{sum}}$ for high SNR and derive solutions for the optimal training intervals $\bar{T}_{t,\text{mf}}^{\star}$, $\bar{T}_{t,\text{zf}}^{\star}$, $\bar{T}_{t,\text{rzf}-\text{cda}}^{\star}$ and $\bar{T}_{t,\text{rzf}-\text{cdu}}^{\star}$ in the high SNR regime and derive their limiting values for asymptotically low SNR.

High SNR Regime The following proposition provides approximate solutions of the optimal amount of training $\bar{T}_t$ for MF, ZF, RZF-CDA and RZF-CDU precoding derived under the assumption of high SNR.

Proposition 4.3. *Let ρ_{dl}, ρ_{ul} be large with $c \triangleq \rho_{dl}/\rho_{ul}$ constant. Then, an approximation of the sum rate maximizing amount of channel training $\bar{T}^{\star}_{t,\mathrm{mf}}$, $\bar{T}^{\star}_{t,\mathrm{zf}}$, $\bar{T}^{\star}_{t,\mathrm{rzf-cda}}$ and $\bar{T}^{\star}_{t,\mathrm{rzf-cdu}}$ under MF, ZF, RZF-CDA and RZF-CDU precoding, respectively, is given by*

$$\bar{T}^{\star}_{t,\mathrm{mf}} \approx \max\left[\frac{\sqrt{c\beta T(1+\beta)}}{\sqrt{\rho_{dl}\bar{R}^{\circ}_{\mathrm{mf}}\left(1+\beta+\frac{1}{\rho_{dl}}\right)}}, K\right], \tag{4.31}$$

$$\bar{T}^{\star}_{t,\mathrm{zf}} \approx \max\left[\frac{c}{2}\sqrt{1+2\frac{2T+c}{c\bar{R}^{\circ}_{\mathrm{zf}}}} - \frac{c}{2}, K\right], \tag{4.32}$$

$$\bar{T}^{\star}_{t,\mathrm{rzf-cda}} \approx \begin{cases} \max\left[\frac{c}{2}\sqrt{1+\frac{2T+c}{c\bar{R}^{\circ}_{\mathrm{rzf}}}} - \frac{c}{2}, K\right] & \text{if } \beta = 1, \\ \max\left[\frac{c}{2}\sqrt{1+2\frac{2T+c}{c\bar{R}^{\circ}_{\mathrm{rzf}}}} - \frac{c}{2}, K\right] & \text{if } \beta > 1, \end{cases} \tag{4.33}$$

$$\bar{T}^{\star}_{t,\mathrm{rzf-cdu}} \approx \begin{cases} \max\left[\frac{c}{4}\sqrt{1+2\frac{4T+c}{c\bar{R}^{\circ}_{\mathrm{rzf}}}} - \frac{c}{4}, K\right] & \text{if } \beta = 1, \\ \max\left[\frac{c}{2}\sqrt{1+2\frac{2T+c}{c\bar{R}^{\circ}_{\mathrm{rzf}}}} - \frac{c}{2}, K\right] & \text{if } \beta > 1, \end{cases} \tag{4.34}$$

where $\bar{R}^{\circ}_{\mathrm{mf}} = \log(1+\frac{\beta}{1+1/\rho_{dl}})$, $\bar{R}^{\circ}_{\mathrm{zf}} = \log(1+\rho_{dl}(\beta-1))$ and $\bar{R}^{\circ}_{\mathrm{rzf}} = \log(\frac{1}{2}+\frac{1}{2}\rho_{dl}(\beta-1)+\frac{\chi(1)}{2})$.

Proof of Proposition 4.3. The sum rate $\hat{R}_{\mathrm{sum}}$ can be written as a function of the per-user rate under perfect CSIT $\bar{R}^{\circ}$ and the per-user rate gap $\Delta\bar{R}$ as

$$\hat{R}_{\mathrm{sum}} = K\left(1-\frac{T_t}{T}\right)\left[\bar{R}^{\circ} - \Delta\bar{R}\right].$$

The per-user rate under perfect CSIT $\bar{R}^{\circ}$ under MF, ZF and RZF precoding are given by $\bar{R}^{\circ}_{\mathrm{mf}} = \log(1+\frac{\beta}{1+1/\rho_{dl}})$, $\bar{R}^{\circ}_{\mathrm{zf}} = \log(1+\rho_{dl}(\beta-1))$ and $\bar{R}^{\circ}_{\mathrm{rzf}} = \log(\frac{1}{2}+\frac{1}{2}\rho_{dl}(\beta-1)+\frac{\chi(1)}{2})$, respectively. Note that the rates of RZF-CDA and RZF-CDU precoding are identical under perfect CSIT. The corresponding

per-user rate gaps read

$$\Delta\bar{R}_{\mathrm{mf}} = \log\left(\frac{1+\frac{1}{\rho_{dl}}+\beta}{1+\frac{1}{\rho_{dl}}+\frac{\beta T_{t,\mathrm{mf}}\rho_{ul}}{1+T_{t,\mathrm{mf}}\rho_{ul}}}\right)$$

$$\Delta\bar{R}_{\mathrm{zf}} = \log\left(\frac{(\beta-1)(\rho_{dl}+1)}{1+\frac{1}{\rho_{dl}}+T_{t,\mathrm{zf}}[\frac{1}{c}+\rho_{ul}(\beta-1)]}\right)$$

$$\Delta\bar{R}_{\mathrm{rzf-cda}} = \log\left(\frac{1+\rho_{dl}(\beta-1)+\chi(1)}{1+\omega\rho_{dl}(\beta-1)+\chi(\omega)}\right)$$

$$\Delta\bar{R}_{\mathrm{rzf-cdu}} = \log\left(\frac{(1+e)[T_{t,\mathrm{rzf-cdu}}\rho_{ul}+\delta_2]}{T_{t,\mathrm{rzf-cdu}}\rho_{ul}(1+\delta_1)+\delta_2}\right),$$

where $\chi(\omega)$ is defined in (4.28). Denoting $\phi \triangleq 1+T_{t,\mathrm{mf}}\rho_{ul}(1+\frac{1}{\rho_{dl}})+\frac{1}{\rho_{dl}}$ and $\psi \triangleq 1+\frac{1}{\rho_{dl}}+T_{t,\mathrm{zf}}[\frac{1}{c}+\rho_{ul}(\beta-1)]$, the derivatives take the form

$$\frac{d\hat{R}^{\mathrm{mf}}_{\mathrm{sum}}}{dT_{t,\mathrm{mf}}} = -\frac{K}{T}(\bar{R}^{\circ}_{\mathrm{mf}}-\Delta\bar{R}_{\mathrm{mf}}) + K\left(1-\frac{T_{t,\mathrm{mf}}}{T}\right)\frac{\beta\rho_{ul}(1+1/\rho_{dl})}{(\phi+\beta T_{t,\mathrm{mf}}\rho_{ul})\phi} \tag{4.35}$$

$$\begin{aligned}\frac{d\hat{R}^{\mathrm{zf}}_{\mathrm{sum}}}{dT_{t,\mathrm{zf}}} &= -\frac{K}{T}(\bar{R}^{\circ}_{\mathrm{zf}}-\Delta\bar{R}_{\mathrm{zf}}) \\ &\quad + K\left(1-\frac{T_{t,\mathrm{zf}}}{T}\right)\frac{(\beta-1)(\rho_{dl}+1)[\frac{1}{c}+\rho_{ul}(\beta-1)]}{\psi^2+(\beta-1)(\rho_{dl}+1)\psi},\end{aligned} \tag{4.36}$$

$$\begin{aligned}\frac{d\hat{R}^{\mathrm{rzf-cda}}_{\mathrm{sum}}}{dT_{t,\mathrm{rzf-cda}}} &= -\frac{K}{T}(\bar{R}^{\circ}_{\mathrm{rzf}}-\Delta\bar{R}_{\mathrm{rzf-cda}}) \\ &\quad + K\left(1-\frac{T_{t,\mathrm{rzf-cda}}}{T}\right)\frac{\omega'\rho_{dl}(\beta-1)+\chi'}{1+\omega\rho_{dl}(\beta-1)+\chi},\end{aligned} \tag{4.37}$$

$$\begin{aligned}\frac{d\hat{R}^{\mathrm{rzf-cdu}}_{\mathrm{sum}}}{dT_{t,\mathrm{rzf-cdu}}} &= -\frac{K}{T}(\bar{R}^{\circ}_{\mathrm{rzf}}-\Delta\bar{R}_{\mathrm{rzf-cdu}}) + K\left(1-\frac{T_{t,\mathrm{rzf-cdu}}}{T}\right) \\ &\quad \times \frac{\rho_{ul}(1+e)^2\delta_1(1+\frac{1}{\rho_{dl}})}{[T_{t,\mathrm{rzf-cdu}}\rho_{ul}(1+\delta_1)+\delta_2][T_{t,\mathrm{rzf-cdu}}\rho_{ul}+\delta_1]},\end{aligned} \tag{4.38}$$

where $\omega' = d\omega/dT_{t,\mathrm{rzf-cda}} = (1/\rho_{ul}+c)/(T_{t,\mathrm{rzf-cda}}+1/\rho_{ul}+c)^2$ and $\chi' = d\chi/dT_{t,\mathrm{rzf-cda}} = [(\beta-1)^2\omega\omega'\rho_{dl}^2+\omega'\rho_{dl}(1+\beta)+1]/\chi$. In (4.35)–(4.38) the per-user rate gaps $\Delta\bar{R}$ can be neglected for high SNR since $\Delta\bar{R} \ll \bar{R}^{\circ}$. Treating the $\bar{R}^{\circ}$ as constant, for $\rho_{dl},\rho_{ul}\to\infty$ and $c=\rho_{dl}/\rho_{ul}$ finite, equating (4.35)–(4.38) to zero and solving for $T_{t,\mathrm{mf}}$, $T_{t,\mathrm{zf}}$, $T_{t,\mathrm{rzf-cda}}$ and $T_{t,\mathrm{rzf-cdu}}$, respectively, yields (4.31)–(4.34), respectively. Since we assumed $T_t \geq K$, the solutions to (4.35)–(4.38) are lower bounded by K, which completes the proof. □

Thus, for a fixed DL SNR ρ_{dl}, the optimal training intervals scale as $\bar{T}_t^{\star} \sim \sqrt{T}$ for all precoders. Likewise, for a constant T, the optimal training intervals scale as $\bar{T}^{\star}_{t,\mathrm{zf}}, \bar{T}^{\star}_{t,\mathrm{rzf-cda}}, \bar{T}^{\star}_{t,\mathrm{rzf-cdu}} \sim 1/\sqrt{\log(\rho_{dl})}$, whereas for MF precoding $\bar{T}^{\star}_{t,\mathrm{mf}} \sim 1/\sqrt{\rho_{dl}}$ since $\lim_{\rho_{dl}\to\infty}\bar{R}^{\circ}_{\mathrm{mf}} = \log(1+\beta)$. Under ZF precoding, the

same scaling has been reported in [33, 69, 70]. From this scaling it is clear that, as $\rho_{dl} \to \infty$, $\bar{T}_t^\star$ tends to K, the minimum amount of training.

Moreover, for $\beta > 1$, $\bar{R}^\circ_{\mathrm{rzf-cda}} \geq \bar{R}^\circ_{\mathrm{zf}}$ with equality if $\rho_{dl} \to \infty$. Therefore, RZF-CDA requires less training than ZF, but the training interval of both schemes is equal for asymptotically high SNR. In case of full system loading ($\beta = 1$), RZF-CDA precoding requires less training compared to the scenario where $\beta > 1$.

For $\beta = 1$, we have $\bar{T}^\star_{t,\mathrm{rzf-cda}} \geq \bar{T}^\star_{t,\mathrm{rzf-cdu}}$. Furthermore, for asymptotically high SNR $\bar{T}^\star_{t,\mathrm{zf}} = \bar{T}^\star_{t,\mathrm{rzf-cdu}}$, since both precoding schemes are identical for $\rho_{dl} \to \infty$.

Low SNR Regime For asymptotically low SNR $\rho_{dl}, \rho_{ul} \to 0$ with constant ratio $c = \rho_{dl}/\rho_{ul}$ the optimal amount of training is given in the subsequent proposition.

Proposition 4.4. *Let $\rho_{dl}, \rho_{ul} \to 0$ with constant ratio $c \triangleq \rho_{dl}/\rho_{ul}$ and $T \geq 2K$. Then, the sum rate maximizing amount of channel training $\bar{T}^\star_{t,\mathrm{mf}}$, $\bar{T}^\star_{t,\mathrm{zf}}$ and $\bar{T}^\star_{t,\mathrm{rzf}}$ under MF, ZF and RZF-CDA precoding converges to*

$$\lim_{\rho_{dl}\to 0} \bar{T}^\star_{t,\mathrm{mf}} = \lim_{\rho_{dl}\to 0} \bar{T}^\star_{t,\mathrm{zf}} = \lim_{\rho_{dl}\to 0} \bar{T}^\star_{t,\mathrm{rzf}} = \frac{T}{2}. \tag{4.39}$$

Proof of Proposition 4.4. Applying $\log(1+x) = x + O(x^2)$ and $\rho_{ul} = \rho_{dl}/c$, equations (4.25) and (4.26) take the form

$$\hat{R}^{\mathrm{mf}}_{\mathrm{sum}} = K\left(1 - \frac{T_{t,\mathrm{mf}}}{T}\right)\frac{T_{t,\mathrm{mf}}\beta}{c}\rho_{dl}^2 + O(\rho_{dl}^4), \tag{4.40}$$

$$\hat{R}^{\mathrm{zf}}_{\mathrm{sum}} = K\left(1 - \frac{T_{t,\mathrm{zf}}}{T}\right)\frac{T_{t,\mathrm{zf}}(\beta-1)}{c}\rho_{dl}^2 + O(\rho_{dl}^4), \tag{4.41}$$

$$\hat{R}^{\mathrm{rzf}}_{\mathrm{sum}} = K\left(1 - \frac{T_{t,\mathrm{rzf}}}{T}\right)\frac{T_{t,\mathrm{rzf}}\beta}{c}\rho_{dl}^2 + O(\rho_{dl}^4). \tag{4.42}$$

Maximizing equations (4.40), (4.41) and (4.42) with respect to $T_{t,\mathrm{mf}}$, $T_{t,\mathrm{zf}}$ and $T_{t,\mathrm{rzf}}$, respectively, yields (4.39). Since, by definition, we assume orthogonal pilot sequences, hence $T_t \geq K$, the result (4.39) implies that $T \geq 2K$. □

For ZF precoding, the limit (4.39) has also been reported in [34]. Note that MF and RZF precoding are equivalent at asymptotically low SNR since the regularization term tends to infinity. Therefore, (4.40) and (4.42) have identical first order approximation in ρ_{dl} for small ρ_{dl}.

Case 2: $\rho_{dl} \gg \rho_{ul}$ with finite ρ_{ul}

This scenario models a high capacity DL channel where the primary sum rate loss stems from the inaccurate CSIT estimate due to limited rate UL signaling caused, e.g., by a finite transmit power of the users. Thus, the system becomes interference-limited and the optimal amount of channel training under ZF precoding is given in the following proposition.

Proposition 4.5. *Let $\rho_{dl} \to \infty$ and ρ_{ul} finite. Then the sum rate maximizing amount of channel training under ZF precoding $\bar{T}^{\star}_{t,\mathrm{zf}}$ is given by*

$$\bar{T}^{\star}_{t,\mathrm{zf}} = \frac{1}{\rho_{ul}(\beta-1)} \left(\frac{a}{\mathcal{W}(ae)} - 1 \right), \tag{4.43}$$

where $\mathcal{W}(z)$ is the Lambert W-function, defined as the unique solution to $z = \mathcal{W}(z)e^{\mathcal{W}(z)}$, $z \in \mathbb{C}$.

Proof of Proposition 4.5. For ZF precoding and $\rho_{dl} \to \infty$, the sum rate (4.25) can be approximated as

$$\hat{R}^{\mathrm{zf}}_{\mathrm{sum}} \approx K \left(1 - \frac{T_{t,\mathrm{zf}}}{T} \right) \log\left(1 + T_{t,\mathrm{zf}}\rho_{ul}(\beta-1)\right). \tag{4.44}$$

Setting the derivative of (4.44) with respect to $T_{t,\mathrm{zf}}$ to zero, yields

$$\log(a/\omega(T_{t,\mathrm{zf}})) = \omega(T_{t,\mathrm{zf}}) - 1, \tag{4.45}$$

where $a \triangleq \rho_{ul}T(\beta-1)+1$ and $\omega(T_{t,\mathrm{zf}}) \triangleq (Ta)/[T + T_{t,\mathrm{zf}}(a-1)]$. Equation (4.45) can be written as

$$\omega(T_{t,\mathrm{zf}})e^{\omega(T_{t,\mathrm{zf}})} = ae.$$

Notice that $\omega(T_{t,\mathrm{zf}}) = \mathcal{W}(ae)$. Thus, solving $\omega(T_{t,\mathrm{zf}}) = \mathcal{W}(ae)$ for $T_{t,\mathrm{zf}}$ yields (4.43). □

For asymptotically low ρ_{ul}, we obtain $\lim_{\rho_{ul}\to 0} \bar{T}^{\star}_{t,\mathrm{zf}} = T/2$ implying that $T \geq 2K$.

Under MF and RZF precoding, no accurate closed-form solution to (4.30) has yet been found.

4.3.3 Numerical Results

Figures 4.8 and 4.9 depict the relative amount of training T_t/T as a function of the downlink SNR under MF, ZF and RZF precoding.

In Figure 4.8, we plot $\bar{T}^{\star}_t/T$ obtained from the convex optimization in (4.30) for MF (triangle markers), ZF (no markers) and RZF-CDA (circle markers) precoding, respectively. We observe that $\bar{T}^{\star}_t/T$ decreases with increasing SNR. That is, for increasing SNR the estimation becomes more accurate and resources for channel training are reallocated to data transmission. Furthermore, $\bar{T}^{\star}_t/T$ saturates at K/T due to the orthogonality constraint on the pilot sequences. Moreover, as expected from (4.32) and (4.33), we observe that the optimal amount of training is lower for RZF-CDA than for ZF precoding which in turn are both greater than $\bar{T}^{\star}_{t,\mathrm{mf}}/T$ under MF precoding. That is expected, since at high SNR, $\bar{T}^{\star}_{t,\mathrm{mf}}$ decreases as $1/\sqrt{\rho_{dl}}$ which is faster than $1/\sqrt{\log(\rho_{dl})}$ for ZF and RZF-CDA precoding. Furthermore, the relative amount of training $\bar{T}^{\star}_t/T$ for MF, ZF and RZF-CDA precoding converges at low SNR to 1/2, as predicted by the theoretical analysis.

Figure 4.9 compares the optimal solution $T_t^\star/T$, obtained from exhaustive search and averaged over 1 000 channel realizations, to the approximate solution $\bar{T}_t^\star/T$ from either convex optimization or the high SNR closed-form approximations in Proposition 4.3. The simulations are carried out for MF (triangle markers) and ZF (no markers) precoding. We do not plot the results for RZF-CDA precoding since they are similar to those of ZF precoding and to improve the readability of the figure. We choose a large coherence interval $T = 100\,000$ to ensure that $T_t^\star/T$ is not saturating at K/T for most of the simulated SNR range (saturation occurs for MF precoding at a SNR of 40 dB). We observe that the approximate solutions $\bar{T}_t^\star/T$ are very accurate for $M = 32$ and $K = 16$. Moreover, the high-SNR approximations become already very accurate for a SNR of about 0 dB.

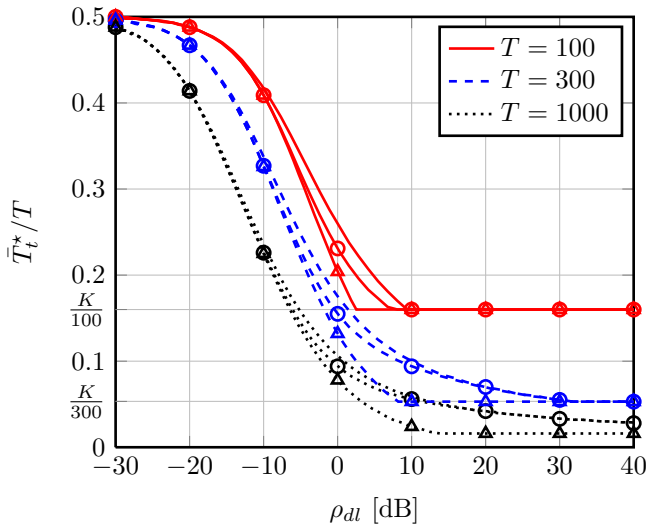

Figure 4.8: Comparison of $\bar{T}_t^\star/T$ obtained by convex optimization for different T with $M = 32$, $K = 16$, $\rho_{dl}/\rho_{ul} = 10$, $\mathbf{\Theta}_k = \mathbf{I}_M$, $\mathbf{P} = \frac{1}{K}\mathbf{I}_K$, RZF and MF are indicated by circle and triangle marks, respectively.

In Figures 4.10 and 4.11, we plot the approximated optimal training interval $\bar{T}_t^\star$ as a function of the coherence interval T for a fixed SNR and compare to the optimal $T_t^\star$ computed via exhaustive search and averaged over 1 000 independent channel realizations. In Figure 4.10, we compare the approximated optimal training intervals $\bar{T}_{t,\mathrm{zf}}^\star$ and $\bar{T}_{t,\mathrm{rzf}}^\star$ to $T_{t,\mathrm{zf}}^\star$ and $T_{t,\mathrm{rzf}}^\star$, respectively. During the exhaustive search under RZF-CDA precoding, the regularization term α is computed using the large system approximation $\bar{\alpha}^\star$ in (4.4). Figure 4.10 shows that the approximate solutions $\bar{T}_{t,\mathrm{zf}}^\star, \bar{T}_{t,\mathrm{rzf}}^\star$ become very accurate for $K = 16$. Further notice that for $M/K = 2$, ZF and RZF need approximately the same amount of training, as predicted by equations (4.32) and (4.33). Figure 4.11 depicts the results under MF precoding for a fixed downlink SNR of 5 dB.

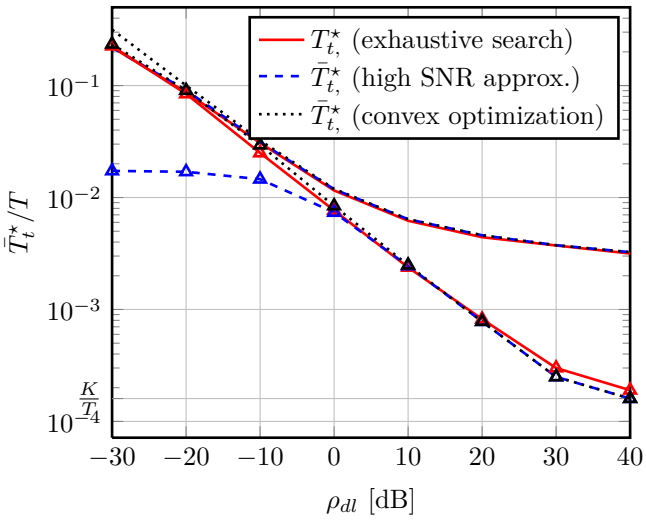

Figure 4.9: Accuracy of high SNR approximations with $T = 100\,000$, $M = 32$, $K = 16$, $\rho_{dl}/\rho_{ul} = 10$, $\mathbf{\Theta}_k = \mathbf{I}_M$, $\mathbf{P} = \frac{1}{K}\mathbf{I}_K$, RZF and MF are indicated by circle and triangle marks, respectively.

We observe that the approximated optimal amount of training $\bar{T}^\star_{t,\mathrm{mf}}$ becomes accurate for $K = 16$. Moreover, it can be observed that the high SNR approximation in (4.31) matches very well with the solution of the convex optimization in (4.30).

Figure 4.12 shows the ergodic sum rate under ZF precoding with fixed UL SNR $\rho_{ul} = 5$ dB for various training intervals. We observe (i) no significant difference in the performance of the schemes employing either optimal training $T^\star_{t,\mathrm{zf}}$, computed via exhaustive search, or $\bar{T}^\star_{t,\mathrm{zf}}$ obtained from a convex optimization of the large system approximation (4.25), (ii) a small performance loss at low and medium SNR of the (high-SNR) approximation of $\bar{T}^\star_{t,\mathrm{zf}}$ in (4.43) and (iii) a significant performance loss if the minimum training interval $T_{t,\mathrm{zf}} = K$ is used for all SNR. We conclude that our approximation in (4.43) achieves very good performance and can therefore be utilized to compute $T_{t,\mathrm{zf}}$ very efficiently.

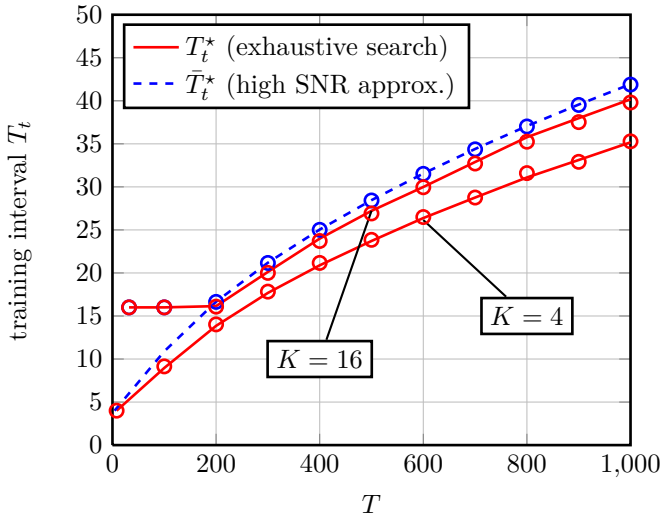

Figure 4.10: RZF-CDU precoding, optimal amount of training vs. T with $\rho_{dl} = 20$ dB, $\rho_{ul} = 10$ dB, $\mathbf{\Theta}_k = \mathbf{I}_M$, $\mathbf{P} = \frac{1}{K}\mathbf{I}_K$ and $M/K = 2$, RZF is indicated by circle marks.

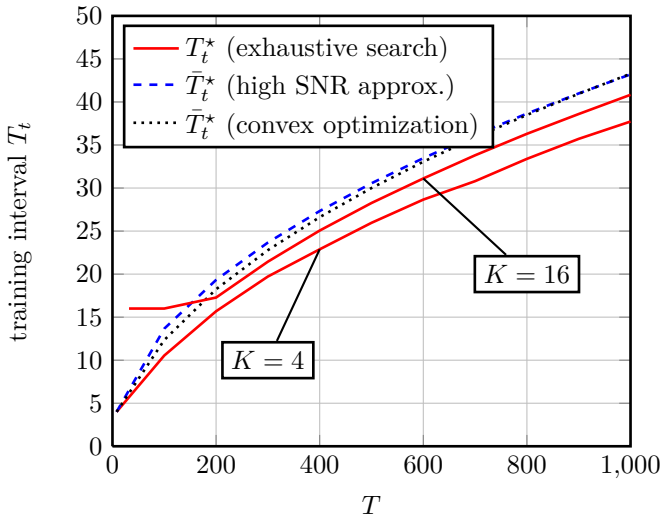

Figure 4.11: MF Precoding, optimal amount of training vs. T with $\rho_{dl} = 5$ dB, $\rho_{ul} = -5$ dB $\mathbf{\Theta}_k = \mathbf{I}_M$, $\mathbf{P} = \frac{1}{K}\mathbf{I}_K$ and $M/K = 2$.

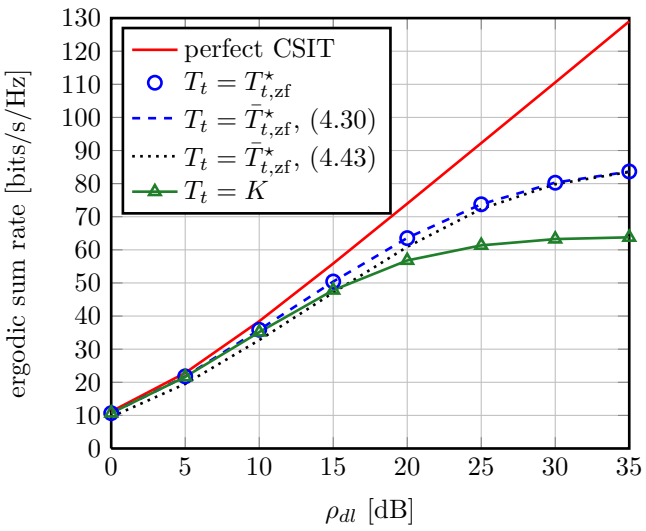

Figure 4.12: ZF, ergodic sum rate vs. downlink SNR with $M = 32$, $K = 16$, $\rho_{ul} = 5$ dB, $\mathbf{\Theta}_k = \mathbf{I}_M$, $\mathbf{P} = \frac{1}{K}\mathbf{I}_K$ and $T = 1000$.

4.4 Optimal Feedback in Large FDD Multi-user Systems

Consider a frequency-division duplex (FDD) system, where the users quantize their perfectly estimated channel vectors and send the codebook quantization index back to the transmitter over an independent feedback channel of limited rate. The feedback channels are assumed to be error-free and of zero delay. The quantization codebooks are generated prior to transmission and are known to both transmitter and respective receiver. Due to the finite rate feedback link, imposing a finite codebook size, the transmitter has only access to an imperfect estimate of the true downlink channel. To obtain tractable expressions, we restrict the subsequent analysis to i.i.d. Gaussian channels $\mathbf{h}_k \sim \mathcal{CN}(\mathbf{0}, \mathbf{I}_M)\ \forall k$.

In the sequel, we follow the limited feedback analysis in [35], where each user's *channel direction* $\tilde{\mathbf{h}}_k \triangleq \frac{\mathbf{h}_k}{\|\mathbf{h}_k\|_2}$ is quantized using B bits which are subsequently fed back to the transmitter. Under Rayleigh fading, the channel $\mathbf{h}_k$ can be decomposed as $\mathbf{h}_k = \|\mathbf{h}_k\|_2 \cdot \tilde{\mathbf{h}}_k$, where we suppose that the channel magnitude $\|\mathbf{h}_k\|_2$ is perfectly known to the transmitter since it can be efficiently quantized with only a few bits [35]. Without loss of generality[2], we assume random vector quantization (RVQ), where each user *independently* generates a random codebook $\mathcal{C}_k \triangleq \{\mathbf{w}_{ki}, \ldots, \mathbf{w}_{k2^B}\}$ containing 2^B vectors $\mathbf{w}_{ki} \in \mathbb{C}^M$ that are isotropically distributed on the M-dimensional unit sphere. Subsequently, user k quantizes its channel direction $\tilde{\mathbf{h}}_k$ to the closest $\mathbf{w}_{ki}$ according to

$$\hat{\tilde{\mathbf{h}}}_k = \arg \max_{\mathbf{w}_{ki} \in \mathcal{C}_k} \|\tilde{\mathbf{h}}_k^{\mathsf{H}} \mathbf{w}_{ki}\|.$$

Under RVQ, the quantized channel direction $\hat{\tilde{\mathbf{h}}}_k \in \mathcal{C}_k$ is isotropically distributed on the M-dimensional unit sphere due to the statistical properties of both, the random codebook $\mathcal{C}_k$ and the channels $\mathbf{h}_k$. Thus, for *fine quantization* with small errors, the entries of both $\tilde{\mathbf{h}}_k$ and $\hat{\mathbf{h}}_k = \|\mathbf{h}_k\|_2 \cdot \hat{\tilde{\mathbf{h}}}_k$ can be modeled with good approximation as i.i.d. Gaussian of zero mean and unit variance. The quantization error vector $\mathbf{e}_k$ can be approximated as $\mathbf{e}_k \sim \mathcal{CN}(\mathbf{0}, \mathbf{I}_M)$ [71] and we can write

$$\hat{\mathbf{h}}_k = \sqrt{1 - \tau_k^2}\mathbf{h}_k + \tau_k \mathbf{e}_k, \tag{4.46}$$

where τ_k^2 is the quantization error variance. The scaling in (4.46) is required to ensure that the elements of $\hat{\mathbf{h}}_k$ have unit variance. Therefore, the effect of imperfect CSIT under RVQ (4.46) is captured by the channel model (1.9). For RVQ, the quantization error $\tau_k^2 \triangleq \|\tilde{\mathbf{h}}_k^{\mathsf{H}} \hat{\tilde{\mathbf{h}}}_k\|$ can be upper bounded as [35, Lemma 1]

$$\tau_k^2 < 2^{-\frac{B}{M-1}}. \tag{4.47}$$

The bound in (4.47) is tight for large B [35]. Moreover, since the quantization codebooks of the users are supposed to be of equal size, the resulting CSIT

[2]The derived scaling results hold for *any* quantization codebook [35].

distortions are assumed identical, i.e., $\tau_k^2 = \tau^2 \ \forall k$. Under this assumption and equal power allocation, for large M, the SINR $\bar{\gamma}$ is identical for all users and, hence, optimizing $\bar{\gamma}$ is equivalent to optimizing the per-user rate $\bar{R} = \log_2(1+\bar{\gamma})$ bits/s/Hz and the sum rate $\hat{R}_{\text{sum}} = K\bar{R}$.

In the following, in particular under RVQ, we will derive the necessary scaling of the distortion τ^2 to ensure that

$$\Delta R_k - \log_2 b \overset{M\to\infty}{\longrightarrow} 0,$$

almost surely, where ΔR_k is defined in (3.102) and $b \geq 1$. That is, a constant rate gap of $\log_2 b$ is maintained *exactly* as $M, K \to \infty$. A constant rate gap ensures that the full multiplexing gain of K is achieved. Thus, the proposed scaling also guarantees a larger but constant rate gap to the optimal DPC solution with perfect CSIT. The choice of a rate offset $\log_2 b$ is motivated by mere mathematical convenience to avoid terms of the form 2^b and to be compliant with [35].

With this strategy we closely follow [35]. In [35, Theorem 1], the author derived an upper bound of the *ergodic* per-user gap $\Delta\tilde{R}_{\text{zf}}$ for ZF precoding with $M = K$ and *unit norm* precoding vectors under RVQ, which is given by

$$\Delta\tilde{R}_{\text{zf}} < \log_2\left(1 + \rho \cdot 2^{-\frac{B}{M-1}}\right). \tag{4.48}$$

We cannot directly compare the deterministic equivalents to the upper bound in (4.48) for two reasons, (i) under ZF precoding and $M = K$, a deterministic equivalent for the per-user rate gap does not exist and (ii) [35] considers unit norm precoding vectors, whereas in this thesis we only impose a total power constraint (1.11). Concerning (i), at high SNR, we can use the deterministic equivalent for RZF-CDU precoding given in Corollary 3.13 as a good approximation for ZF precoding, since for high SNR the rates of RZF-CDU and ZF precoding converge. Regarding (ii), deriving a deterministic equivalent of the SINR under linear precoding with a unit norm power constraint on the precoding vectors is difficult, since it introduces an additional non-trivial dependence on the channel. However, it is useful to compare the accuracy of the upper bound in (4.48) and the deterministic equivalent $\Delta\bar{R}_{k,\text{rzf}-\text{cdu}}$ in Corollary 3.13 at high SNR.

Figure 4.13, depicts the per-user rate gap as a function of the feedback bits B per user under ZF precoding at a SNR of 25 dB. We simulated the ergodic per-user rate gap $\Delta\tilde{R}_{\text{zf}}$ and $E[\Delta R_{k,\text{zf}}]$ of ZF precoding with unit norm precoding vectors and total power constraint, respectively. We compare the numerical results to the upper bound (4.48) and to the deterministic equivalent $\Delta\bar{R}_{k,\text{rzf}-\text{cdu}}$ for $M = K = 5$ and $M = K = 10$. For both system dimensions $\Delta\tilde{R}_{\text{zf}}$ and $E[\Delta R_{k,\text{zf}}]$ are close, suggesting that our results derived under the total power constraint may be a good approximation for the case of unit norm precoding vectors as well. As mentioned in [35], the accuracy of the upper bound increases with increasing B but the deterministic equivalent $\Delta\bar{R}_{k,\text{rzf}-\text{cdu}}$ appears to be more accurate for both $M = K = 5$ and $M = K = 10$. In fact,

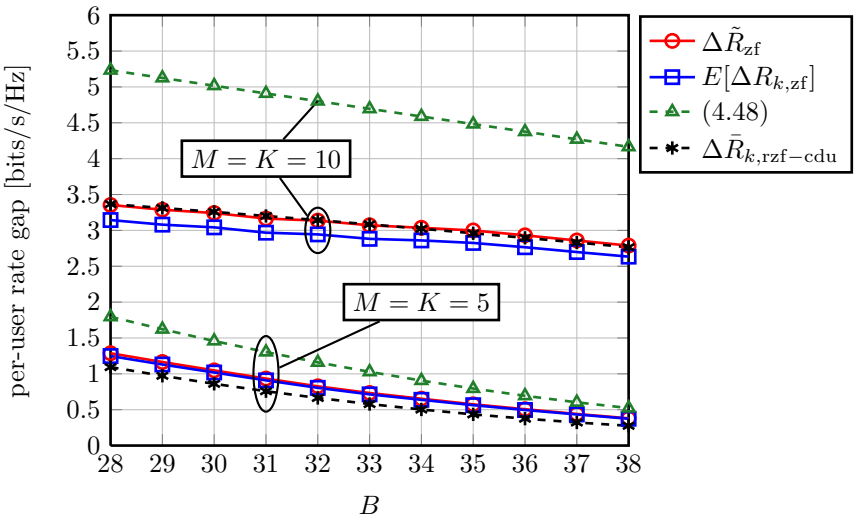

Figure 4.13: ZF, per-user rate gap vs. number of bits per user with $\rho = 25$ dB, $\mathbf{\Theta}_k = \mathbf{I}_M$.

for $M = K = 10$, $\Delta\bar{R}_{k,\mathrm{rzf-cdu}}$ approximates the per-user rate gap significantly more accurately than the upper bound (4.48) for the given SNR. We conclude, that the proposed deterministic equivalent $\Delta\bar{R}_{k,\mathrm{rzf-cdu}}$ is sufficiently accurate and can be used to derive scaling laws for the optimal feedback rate.

In the following, we compare the scaling of τ^2 under RZF-CDA, RZF-CDU and ZF ($M > K$) precoding to the upper bound given for ZF ($M = K$) precoding in [35, Theorem 3]. For the sake of comparison we restate [35, Theorem 3].

Theorem 4.1. *[35, Theorem 3]. In order to maintain a rate offset no larger than* $\log_2 b$ *(per user) between zero-forcing with perfect CSIT and with finite-rate feedback (i.e.,* $\Delta R(\rho) \leq \log_2 b \; \forall \rho$*), it is sufficient to scale the number of feedback bits per mobile according to*

$$\begin{aligned} B_{\mathrm{zf}} &= (M-1)\log_2 \rho - (M-1)\log_2(b-1) \\ &\approx \frac{M-1}{3}\rho_{\mathrm{dB}} - (M-1)\log_2(b-1), \end{aligned}$$

where $\rho_{\mathrm{dB}} = 10\log_{10}\rho$. It is also mentioned that the result in [35, Theorem 3] holds true for RZF-CDU precoding for high SNR, since ZF and RZF-CDU precoding converge for asymptotically high SNR. Furthermore, it is claimed, corroborated by simulation results, that [35, Theorem 3] is true under RZF-CDU precoding for *all* SNR.

In order to correctly interpret the subsequent results, it is important to understand the differences between our approach and the approach in [35]. The scaling given in [35, Theorem 3] is a strict upper bound on the *ergodic* per-user

rate gap $E_{\mathbf{H}}[\Delta R_k]$ for all SNR and all $M = K$ under a unit norm constraint on the precoding vectors. In contrast, our approach yields a necessary scaling of τ^2 that maintains a given *instantaneous* target rate gap $\log_2 b$ *exactly* as $M, K \to \infty$ under a total power constraint. Therefore, our results are *not* upper bounds for small M, i.e., we cannot guarantee that $\Delta R_k < \log_2 b$ for small dimensions. But since for asymptotically large M, the rate gap is maintained exactly and we apply an upper bound on the CSIT distortion under RVQ (4.47), it follows that our results become indeed upper bounds for large M. Simulations reveal that under the derived scaling of τ^2, the per-user rate gap is very close to $\log_2 b$ even for small dimension, e.g., $M = 10$. Concerning the ergodic and instantaneous per-user rate gap, the reader is reminded that our results hold also for ergodic per-user rates as a consequence of the dominated convergence theorem, cf. Remark 3.5.

Consequently, a comparison of the results in [35] to our solutions is meaningful especially for larger values of M, where our results become upper bounds.

In the following section, we apply the deterministic equivalents of the per-user rate gap under RZF-CDA, RZF-CDU and ZF precoding provided in Corollaries 4.3, 3.13 and 3.14, respectively, to derive scaling laws for the amount of feedback necessary to achieve full multiplexing gain.

4.4.1 RZF-CDA Precoding

Proposition 4.6. *Let $\mathbf{\Theta}_k = \mathbf{I}_M \; \forall k$. Then the CSIT distortion τ^2, such that the rate gap $\Delta R_{k,\mathrm{rzf-cda}}$ of user k between RZF-CDA precoding with perfect CSIT and imperfect CSIT satisfies*

$$\Delta R_{k,\mathrm{rzf-cda}} - \log_2 b \overset{M\to\infty}{\longrightarrow} 0$$

almost surely, has to scale as

$$\tau^2 = \frac{\bar{\phi}_{\mathrm{rzf-cda}}(\rho, b)}{\rho}, \tag{4.49}$$

$$\bar{\phi}_{\mathrm{rzf-cda}}(\rho, b) = \frac{\rho\left[(1+\beta)b + \delta(\beta-1)\right] - \frac{1}{2b}(\delta^2 - b^2)}{(1+\beta)b + \delta(\beta-1) + \frac{1}{2b}(\delta^2 - b^2)}, \tag{4.50}$$

$$\delta = 1 - b + \chi(1) + \rho(\beta - 1),$$

where χ is defined in (4.9)*. With $\beta = 1$, the distortion τ^2 has to scale as*

$$\tau^2 = \frac{1 + 4\rho - \frac{\delta^2}{b^2}}{3 + \frac{\delta^2}{b^2}} \frac{1}{\rho}.$$

Proof of Proposition 4.6. Set $\Delta\bar{R}_{\mathrm{rzf-cda}}$ given in Corollary 4.3 equal to $\log_2 b$ and solve for τ^2. □

Although the proposed scaling of τ^2 in (4.49) converges to zero for asymptotically high SNR, we can approximate the term $\bar{\phi}_{\mathrm{rzf-cda}}(\rho, b)$ in the high SNR regime.

Proposition 4.7. *For asymptotically high SNR, the term* $\bar{\phi}_{\mathrm{rzf-cda}}(\rho, b)$ *defined in* (4.50) *converges to the following limits,*

$$\lim_{\rho\to\infty} \bar{\phi}_{\mathrm{rzf-cda}}(\rho, b) = \begin{cases} b^2 - 1 & \text{if } \beta = 1 \\ b - 1 & \text{if } \beta > 1. \end{cases} \tag{4.51}$$

Proof of Proposition 4.7. For $\beta = 1$ observe that δ scales as $2\sqrt{\rho}$. Thus, for $\rho \to \infty$, (4.50) converges to $b^2 - 1$. If $\beta > 1$, the term δ takes the form

$$\delta = 1 - b + (\beta - 1)\rho + |1 - \beta|\rho\,(1 + o(1)) \overset{\rho\to\infty}{\longrightarrow} 2\rho(\beta - 1) + 1 - b.$$

Therefore, for $\rho \to \infty$, (4.50) converges to $b - 1$, which completes the proof. □

Remark 4.2. *Note that* $\lim_{\rho\to\infty} \frac{\bar{\phi}_{\mathrm{rzf-cda}}(\rho,b)}{\rho} = 0$ *and thus, we require* $\beta > 1$ *to ensure that the limit* $\rho \to \infty$ *of the deterministic equivalent is well defined, see Remark 4.1. However, for finite SNR with the approximation in Proposition 4.7, we have* $\tau^2 > 0$ *and the scaling result holds true.*

To compare Proposition 4.6 to [35, Theorem 3], we use the upper bound on the quantization distortion (4.47), i.e., $\tau^2 = 2^{-\frac{\bar{B}_{\mathrm{rzf-cda}}}{M-1}}$, where $\bar{B}_{\mathrm{rzf-cda}}$ is the number of feedback bits per user under RZF-CDA precoding. Thus, (4.49) can be rewritten as

$$\bar{B}_{\mathrm{rzf-cda}} = (M - 1)\log_2 \rho - (M - 1)\log_2 \bar{\phi}_{\mathrm{rzf-cda}}(\rho, b). \tag{4.52}$$

4.4.2 RZF-CDU Precoding

Although the RZF-CDU precoder is suboptimal under imperfect CSIT, the results are useful to compare to the work in [35].

Proposition 4.8. *Let* $\mathbf{\Theta}_k = \mathbf{I}_M\ \forall k$. *Then the CSIT distortion* τ^2, *such that the rate gap* $\Delta R_{k,\mathrm{rzf-cdu}}$ *with* $\alpha = 1/(\beta\rho)$ *of user* k *between RZF-CDU precoding with perfect CSIT and imperfect CSIT satisfies*

$$\Delta R_{k,\mathrm{rzf-cdu}} - \log_2 b \overset{M\to\infty}{\longrightarrow} 0$$

almost surely, has to scale as

$$\tau^2 = \frac{\bar{\phi}_{\mathrm{rzf-cdu}}(\rho, b)}{\rho},$$
$$\bar{\phi}_{\mathrm{rzf-cdu}}(\rho, b) = \frac{(b - 1 - e)[\rho + (1 + e)^2] + be[\rho + (1 + e)^2]}{(b - 1 - e)[1 - (1 + e)^2] + be[1 + \frac{1}{\rho}(1 + e)^2]},$$

where e *is defined in* (3.84).

Proof of Proposition 4.8. Set $\Delta R_{k,\mathrm{rzf-cdu}}$ from Corollary 3.13 equal to $\log_2 b$ and solve for τ^2. □

An approximation of the term $\bar{\phi}_{\mathrm{rzf-cdu}}(\rho, b)$ at high SNR is given in the following proposition

Proposition 4.9. *For asymptotically high SNR, $\bar{\phi}_{\mathrm{rzf-cdu}}(\rho, b)$ converges to the following limits,*

$$\lim_{\rho\to\infty} \bar{\phi}_{\mathrm{rzf-cdu}}(\rho, b) = \begin{cases} 2(b-1) & \text{if } \beta = 1 \\ b-1 & \text{if } \beta > 1. \end{cases} \tag{4.53}$$

Proof od Proposition 4.9. For $\beta = 1$ and ρ large, e scales as $\sqrt{\rho}$. Therefore, $\lim_{\rho\to\infty} \bar{\phi}_{\mathrm{rzf-cdu}}(\rho, b) = 2(b-1)$. If $\beta > 1$, for large ρ, the term e scales as $\rho(\beta - 1)$. With this approximation we obtain $\lim_{\rho\to\infty} \bar{\phi}_{\mathrm{rzf-cdu}}(\rho, b) = b - 1$, which completes the proof. □

Applying the upper bound on the CSIT distortion under RVQ (4.47) with $\bar{B}_{\mathrm{rzf-cdu}}$ bits per user, we obtain

$$\bar{B}_{\mathrm{rzf-cdu}} = (M-1)\log_2 \rho - (M-1)\log_2 \bar{\phi}_{\mathrm{rzf-cdu}}(\rho, b). \tag{4.54}$$

4.4.3 ZF Precoding

The following results are only valid for $\beta > 1$ and thus, they cannot be compared to [35, Theorem 3] which are derived under the assumption $M = K$. However, for high SNR the results for the RZF-CDU precoder are a good approximation for the ZF precoder as well, even for $\beta = 1$.

Proposition 4.10. *Let $\beta > 1$ and $\mathbf{\Theta}_k = \mathbf{I}_M \ \forall k$, to maintain a rate offset $\Delta R_{k,\mathrm{zf}}$ such that*

$$\Delta R_{k,\mathrm{zf}} - \log_2 b \overset{M\to\infty}{\longrightarrow} 0$$

almost surely, the distortion τ^2 has to scale according to

$$\tau^2 = \frac{\bar{\phi}_{\mathrm{zf}}(\rho, b)}{\rho},$$
$$\bar{\phi}_{\mathrm{zf}}(\rho, b) = \frac{(b-1)[1+\rho(\beta-1)]}{1-b+(\beta-1)[\rho+b]}. \tag{4.55}$$

Proof of Proposition 4.10. From Corollary 3.14 Set $\Delta\bar{R}_{\mathrm{zf}} = \log_2 b$ and solve for τ^2. □

Proposition 4.11. *For asymptotically high SNR, $\bar{\phi}_{\mathrm{zf}}(\rho, b)$ in (4.55) converges to*

$$\lim_{\rho\to\infty} \bar{\phi}_{\mathrm{zf}}(\rho, b) = b - 1. \tag{4.56}$$

Proof of Proposition 4.11. From (4.55), the result is immediate. □

Under RVQ with $\bar{B}_{\mathrm{zf}}$ feedback bits per user, we have

$$\bar{B}_{\mathrm{zf}} = (M-1)\log_2 \rho - (M-1)\log_2 \bar{\phi}_{\mathrm{zf}}(\rho, b). \tag{4.57}$$

4.4.4 Discussion and Numerical Results

At this point, we can draw the following conclusions. The optimal scaling of the CSIT distortion τ^2 is lower for $\beta = 1$ compared to $\beta > 1$. For $\beta = 1$, the optimal scaling of the feedback bits $\bar{B}_{\mathrm{rzf-cda}}$, $\bar{B}_{\mathrm{rzf-cdu}}$ and B for ZF in [35, Theorem 3] are different, even at high SNR. In fact, for large M, under RZF-CDU precoding and ZF precoding, the upper bound in [35, Theorem 3] appears to be too pessimistic in the scaling of the feedback bits. From (4.54) and (4.53), a more accurate choice may be

$$\bar{B}_{\mathrm{rzf-cdu}} = (M-1)\log_2 \rho - (M-1)\log_2(2(b-1)), \tag{4.58}$$

i.e., $M-1$ bits less than proposed in [35, Theorem 3]. However, recall that (4.58) becomes an upper bound for large M and a rate gap of at least $\log_2 b$ bits/s/Hz cannot be guaranteed for small values of M. Moreover, for high SNR, $\beta = 1$ and large M, to maintain a rate offset of $\log_2 b$, the RZF-CDA precoder requires $(M-1)\log_2(\frac{b+1}{2})$ bits *less* than the RZF-CDU and ZF precoder and $(M-1)\log_2(b+1)$ bits *less* than the scaling proposed in [35, Theorem 3].

In contrast, for $\beta > 1$ and high SNR, we have $\bar{B}_{\mathrm{rzf-cda}} = \bar{B}_{\mathrm{rzf-cdu}} = \bar{B}_{\mathrm{zf}}$. Intuitively, the reason is that, for $\beta > 1$, the channel matrix is well conditioned and the RZF and ZF precoders perform similarly. Therefore, both schemes are equally sensitive to imperfect CSIT and thus the scaling of τ^2 is the same for high SNR.

Note that our model comprises a generic distortion of the CSIT. That is, the distortion can be a combination of different additional factors, e.g. channel estimation at the receivers, channel mismatch due to feedback delay or feedback errors (see [32]) as long as they can be modeled as additive noise (1.14). Moreover, we consider i.i.d. block-fading channels, which can be seen as a worst case scenario in terms of feedback overhead. It is possible to exploit channel correlation in time, frequency and space to refine the CSIT or to reduce the amount of feedback.

Figures 4.14 and 4.15 depict the ergodic sum rate of RZF precoding under RVQ and the corresponding number of feedback bits per user B, respectively. To avoid an infinitely high regularization term $\bar{\alpha}^\star$, the minimum number of feedback bits is set to one.

In Figure 4.14, we plot the ergodic sum rate for RZF precoding under perfect CSIT with total power constraint (red solid lines) and unit norm constraint on the precoding vectors (red dashed line). We observe, that the sum rate under unit norm constraint is slightly larger at high SNR, suggesting that our scaling results for RZF precoding derived under a total power constraint become inaccurate under the unit norm constraint at high SNR. Hence, one has to be cautious when comparing the scaling in [35, Theorem 3] directly to the scaling derived with the large system approximations at high SNR. From Figure 4.14, we further observe that (i) the desired sum rate offset of 10 bits/s/Hz is approximately maintained over the given SNR range when B is chosen according to (4.52) and the high SNR approximation in (4.54) under RZF-CDA and RZF-CDU precoding, respectively, (ii) given an equal number of feedback bits (4.52),

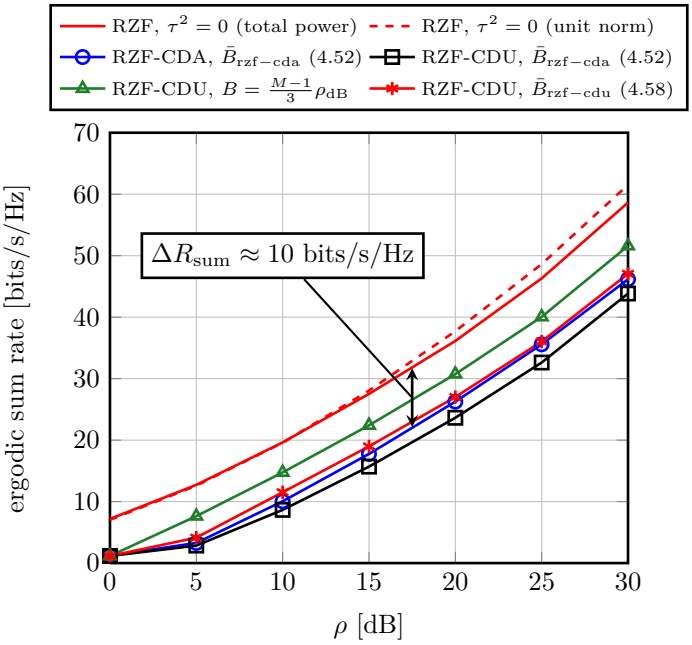

Figure 4.14: RZF, ergodic sum rate vs. SNR under RZF precoding and RVQ with B feedback bits per user, where B is chosen to maintain a sum rate offset of $K \log_2 b = 10$, $\boldsymbol{\Theta}_k = \mathbf{I}_M \ \forall k$ and $M = K = 10$.

the RZF-CDA precoder achieves a significantly higher sum rate compared to RZF-CDU for medium and high SNR, e.g., about 2.5 bits/s/Hz at 20 dB and (iii) to maintain a sum rate offset of K bits/s/Hz, the proposed feedback scaling of $B = \frac{M-1}{3}\rho_{\mathrm{dB}}$ for unit norm precoding vectors [35] is very pessimistic, since the sum rate offset to RZF with total power constraint and unit norm constraint is about 6 bits/s/Hz and 7 bits/s/Hz at 20 dB, respectively.

We conclude that the proposed RZF-CDA precoder significantly increases the sum rate for a given feedback rate or equivalently significantly reduces the amount of feedback given a target rate. Moreover, the scaling of the number of feedback bits under RZF-CDU precoding proposed in [35, Theorem 3] appears to be less accurate under a total power constraint than our large system approximation in (4.52).

4.4.5 Comparison of Digital Feedback to Analog Feedback

Instead of quantizing the channel direction, the users can also directly feedback their estimated channel coefficients by modulating the carrier with their channel estimate. Such a scheme is called analog feedback and has been studied in [72, 73]. Similar to the work in [32], we will compare the performance of analog feedback to channel quantization under RVQ (referred to as digital feedback)

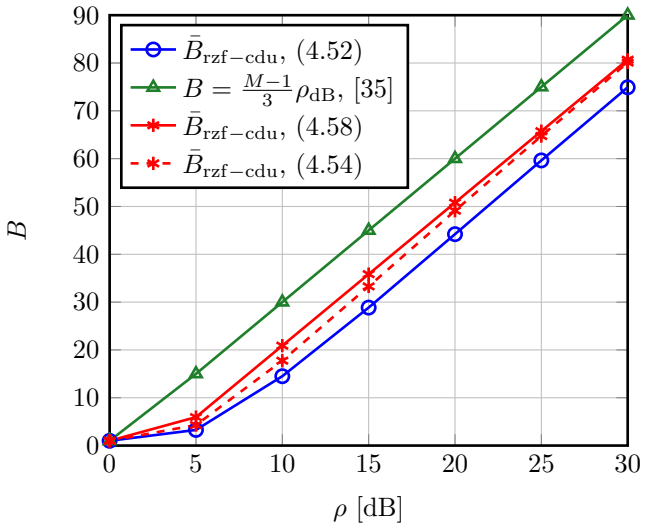

Figure 4.15: RZF, B feedback bits per user vs. SNR, with B to maintain a sum rate offset of $K \log_2 b = 10$ and $\mathbf{\Theta}_k = \mathbf{I}_M \ \forall k$, $M = K = 10$.

for an error-free, zero-delay AWGN feedback link. The analysis in [32] has been carried out for ZF precoding with $M = K$ and *unit norm* precoding vectors using bounds on the ergodic per-user rate (similar to [35]). In our case, we apply the large system rate approximations derived under a *total power constraint* which are almost surely exact as $M \to \infty$. Furthermore, we study MF, ZF and RZF precoding.

Assuming perfect CSIR, the signal $\mathbf{r}_k$ observed by the transmitter is given by

$$\mathbf{r}_k = \sqrt{\eta P_{ul}}\mathbf{h}_k + \mathbf{n}_k, \tag{4.59}$$

where P_{ul} is the available transmit power of the users, η is the number of channel users per channel coefficient, i.e., to estimate the channel coefficient $h_{kj} \sim \mathcal{CN}(0,1)$, $j = 1, \ldots, M$, at least $\eta \geq 1$ channel uses are required. Moreover, we assume that the noise level in the uplink is the same as in the downlink, i.e., $\mathbf{n}_k \sim \mathcal{CN}(\mathbf{0}, \sigma^2\mathbf{I}_M)$. Similar to the case of pilot signaling, the transmitter is performing MMSE estimation of the channel coefficients h_{kj}. Therefore, the estimated channel coefficients $\hat{h}_{kj}$ can be written as

$$\hat{h}_{kj} = \sqrt{1 - \tau_{\mathrm{af}}^2}h_{kj} + \tau_{\mathrm{af}}e_{kj}, \tag{4.60}$$

where $e_{kj} \sim \mathcal{CN}(0,1)$ is independent of h_{kj} and τ_{af}^2 is given by

$$\tau_{\mathrm{af}}^2 = \frac{1}{1 + \eta\rho_{ul}}, \tag{4.61}$$

where we defined the uplink SNR $\rho_{ul} \triangleq P_{ul}/\sigma^2$. Substituting (4.61) into the deterministic equivalents of the per-user rate gap under the various precoding

schemes yields an approximation of the per-user rate gap under analog feedback. To compare to digital feedback, we make the same assumptions as in [32], i.e., we suppose an error-free AWGN feedback link operating at capacity $\log_2(1+\rho_{ul})$ bits per symbol. Furthermore, since analog feedback estimates also the channel magnitude, whereas digital feedback only quantizes the channel direction, we assume that ηM feedback symbols correspond to $\eta(M-1)$ feedback symbols in the digital feedback scheme.[3] Therefore, under RVQ the number of feedback bits per user B becomes $B = \eta(M-1)\log_2(1+\rho_{ul})$ resulting in an upper bound of the quantization error of

$$\tau^2_{\mathrm{df}} < \frac{1}{(1+\eta\rho_{ul})^{\eta}}. \tag{4.62}$$

From (4.62) and (4.61) it is clear that for $\eta = 1$, the approximated rates of analog feedback and digital feedback are identical and both schemes perform equally well. We will see that, except under MF precoding, for $\eta > 1$ analog feedback is strictly sub-optimal and is outperformed by the digital feedback scheme. The same conclusions have been drawn in [32] for ZF precoding.

In what follows, we compute a deterministic equivalent of the per-user rate gap under analog feedback $\Delta\bar{R}^{\mathrm{af}}$ for different precoders and compare it to the corresponding per-user rate gap under RVQ $\Delta\bar{R}^{\mathrm{df}}$ at asymptotically high SNR, i.e., uplink SNR ρ_{ul} and downlink SNR $\rho_{dl} \triangleq P/\sigma^2$ go jointly to infinity with finite ratio $c \triangleq \rho_{dl}/\rho_{ul}$. The approximated per-user rate gaps $\Delta\bar{R}^{\mathrm{af}}$ and $\Delta\bar{R}^{\mathrm{df}}$ are obtained by substituting τ^2 by (4.61) and (4.62), respectively, into the deterministic equivalent of the per-user rate gap $\Delta\bar{R}$.

MF Precoding

From Corollary 3.12, the approximated per-user rate gap under MF precoding $\Delta\bar{R}_{\mathrm{mf}}$ converges for asymptotically high SNR to the following limit.

$$\lim_{\rho_{dl}\to\infty} \Delta\bar{R}^{\mathrm{af}}_{\mathrm{mf}} = \Delta\bar{R}^{\mathrm{df}}_{\mathrm{mf}} = 0. \tag{4.63}$$

Thus, under MF precoding the approximated per-user rate gap vanishes for both analog feedback and digital feedback. Both schemes perform equally well since the rate of user k saturates at $\log_2(1+\beta(1-\tau^2))$ and for both schemes the error τ^2 goes to zero as $\rho_{ul} \to \infty$, although for $\eta > 1$ the convergence under digital feedback is faster than under analog feedback, cf. Figure 4.19.

RZF-CDA Precoding

The approximated per-user rate gap under RZF-CDA precoding $\bar{R}_{\mathrm{rzf-cda}}$ is given in Corollary 4.3.

[3] One symbol could be used to feedback the channel magnitude information.

Proposition 4.12. *For asymptotically high SNR, the rate gap of RZF-CDA precoding under analog feedback converges to the following limits,*

$$\lim_{\rho_{dl}\to\infty} \Delta\bar{R}^{\mathrm{af}}_{\mathrm{rzf-cda}} = \begin{cases} \frac{1}{2}\log_2\left(1+\frac{c}{\eta}\right) & \text{if } \beta = 1 \\ \log_2\left(1+\frac{c}{\eta}\right) & \text{if } \beta > 1. \end{cases} \tag{4.64}$$

Proof of Proposition 4.12. For $\beta = 1$, from Corollary 4.3, $\Delta\bar{R}^{\mathrm{af}}_{\mathrm{rzf-cda}}$ reads

$$\Delta\bar{R}^{\mathrm{af}}_{\mathrm{rzf-cda}} = \log_2\left(\frac{1+\sqrt{4\rho_{dl}+1}}{1+\sqrt{4\omega\rho_{dl}+1}}\right), \tag{4.65}$$

where $\omega = \frac{\eta\rho_{ul}}{1+\rho_{dl}+\eta\rho_{ul}}$. Noting that $\lim_{\rho_{dl}\to\infty}\omega = \eta/(c+\eta)$, $\Delta\bar{R}^{\mathrm{af}}_{\mathrm{rzf-cda}}$ converges to (4.64). If $\beta > 1$, from Corollary 4.2, the approximated SINR $\bar{\gamma}_{\mathrm{rzf-cda}}$ under imperfect CSIT scales as $2\omega\rho_{dl}(\beta-1)$ and we obtain (4.64), which completes the proof. □

For $\beta > 1$ and $c = 1$, the same limit has been obtained in [32] for $M = K$ under ZF precoding. On the contrary if $\beta = 1$, the rate gap is only half as large as for $\beta > 1$ under RZF-CDA precoding or as the bound in [32] for ZF precoding with $M = K$. Therefore, optimal regularization reduces the rate gap (sum rate gap or per-user rate gap) by half.

Under digital feedback for $\eta > 1$ we have $\lim_{\rho_{dl}\to\infty}\Delta\bar{R}^{\mathrm{df}}_{\mathrm{rzf-cda}} = 0$ since $\lim_{\rho_{dl}\to\infty}\omega = 1$, i.e., the rate gap vanishes at asymptotically high SNR.

RZF-CDU Precoding

The approximated per-user rate gap $\Delta\bar{R}_{\mathrm{rzf-cdu}}$ is given in Corollary 3.13. Under analog feedback $\Delta\bar{R}^{\mathrm{af}}_{\mathrm{rzf-cdu}}$ converges to the following limits.

Proposition 4.13. *For asymptotically high SNR, the rate gap of RZF-CDU precoding under analog feedback converges to the following limits,*

$$\lim_{\rho_{dl}\to\infty} \Delta\bar{R}^{\mathrm{af}}_{\mathrm{rzf-cdu}} = \begin{cases} \log_2\left(1+\frac{c}{2\eta}\right) & \text{if } \beta = 1 \\ \log_2\left(1+\frac{c}{\eta}\right) & \text{if } \beta > 1. \end{cases} \tag{4.66}$$

Proof of Proposition 4.13. For analog feedback $\tau^2 \sim \frac{c}{\eta\rho_{dl}}$, if $\beta = 1$, e in Corollary 3.13 scales as $e \sim \sqrt{\rho_{dl}}$ and thus the approximated SINR of RZF-CDU precoding under imperfect CSIT scales as $2\sqrt{\rho_{dl}}/(2+c/\eta)$ and we obtain the result in (4.66). In the case $\beta > 1$, $e \sim \rho_{dl}(\beta-1)$ and the approximated SINR under analog feedback scales as $\frac{\rho_{dl}(\beta-1)}{1+c/\eta}$ yielding (4.66), which completes the proof. □

Therefore, $\Delta\bar{R}^{\mathrm{af}}_{\mathrm{rzf-cdu}} > \Delta\bar{R}^{\mathrm{af}}_{\mathrm{rzf-cda}}$ for $\beta = 1$ and both are equal for $\beta > 1$. Similar to RZF-CDA precoding, for $\eta > 1$, the per-user rate gap under digital feedback $\Delta\bar{R}^{\mathrm{df}}_{\mathrm{rzf-cdu}}$ vanishes at high SNR.

ZF Precoding

The approximated per-user rate gap $\Delta\bar{R}_{\mathrm{zf}}$ is given in Corollary 3.14. Under analog feedback $\Delta\bar{R}_{\mathrm{zf}}^{\mathrm{af}}$ converges to the following limit.

Proposition 4.14. *Let $\beta > 1$, then for asymptotically high SNR, the rate gap of ZF precoding under analog feedback converges to the following limit,*

$$\lim_{\rho_{dl}\to\infty} \Delta\bar{R}_{\mathrm{zf}}^{\mathrm{af}} = \log_2\left(1 + \frac{c}{\eta}\right). \tag{4.67}$$

Proof of Proposition 4.14. From Corollary 3.14 together with (4.61), we have $\omega = \frac{\eta\rho_{ul}}{1+\rho_{dl}+\eta\rho_{ul}}$ and therefore $\lim_{\rho_{dl}\to\infty}\omega = \eta/(c+\eta)$. Substituting into $\Delta\bar{R}_{\mathrm{zf}}^{\mathrm{af}}$ and taking the limit $\rho_{dl}\to\infty$ yields (4.67), which completes the proof. □

Since ZF precoding and RZF-CDU precoding are identical for asymptotically high SNR, we have $\lim_{\rho_{dl}\to\infty}\Delta\bar{R}_{\mathrm{zf}}^{\mathrm{af}} = \log_2(1+\frac{c}{2\eta})$ if $\beta = 1$.

Numerical Results

In Figures 4.16 and 4.17 we plot the ergodic sum rate under RZF-CDA and RZF-CDU precoding, respectively. To compare analog and digital feedback, we choose $\eta = 2$, since for $\eta = 1$ both schemes perform equally. As expected for $\eta > 1$, for both precoders it can be observed that digital feedback outperforms analog feedback and the rate-gap vanishes as the SNR grows large. Furthermore, the approximated sum rate gaps under RZF-CDA and RZF-CDU precoding, given by Propositions 4.12 and 4.13, are 8.8 bits/s/Hz and 9.7 bits/s/Hz, respectively, which are very close to the true rate gaps 8.3 bits/s/Hz and 9.6 bits/s/Hz, respectively. Hence, the approximations are very accurate for both schemes. RZF-CDA precoding achieves a smaller rate gap since it takes the quantization error into account.

The same observations and conclusions for the RZF precoders also hold for the ZF precoder in Figure 4.18. From Proposition 4.14, the approximated sum rate gap is 8.8 bits/s/Hz which is also very accurate compared to the true sum rate gap of 8.1 bits/s/Hz. The ergodic sum rate gap under MF precoding in Figure 4.19 vanishes for both analog feedback and digital feedback at high SNR but digital feedback outperforms analog feedback at low and medium SNR. Both schemes perform equally at high SNR since the sum rate under MF precoding saturates at high SNR even under perfect CSIT due to the inter-user interference. The sum rate loss caused by the interference is significantly larger than any loss due to limited feedback. Therefore, the performance of the MF precoder is interference-limited and not feedback-limited.

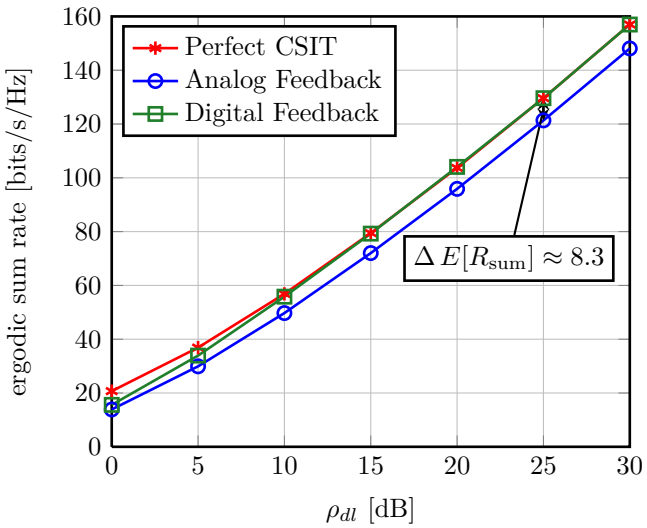

Figure 4.16: RZF-CDA, $M = K = 30$, $\mathbf{\Theta}_k = \mathbf{I}_M$, $\mathbf{P} = \frac{1}{K}\mathbf{I}_K$, $\rho_{dl} = \rho_{ul}$ and $\eta = 2$.

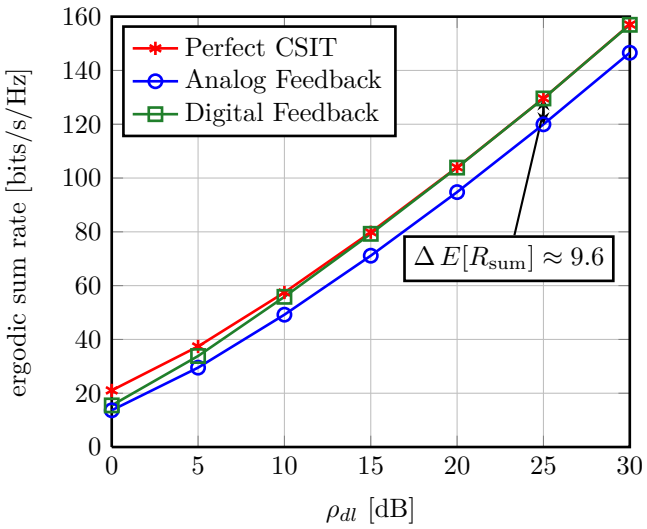

Figure 4.17: RZF-CDU, $M = K = 30$, $\mathbf{\Theta}_k = \mathbf{I}_M$, $\mathbf{P} = \frac{1}{K}\mathbf{I}_K$, $\rho_{dl} = \rho_{ul}$ and $\eta = 2$.

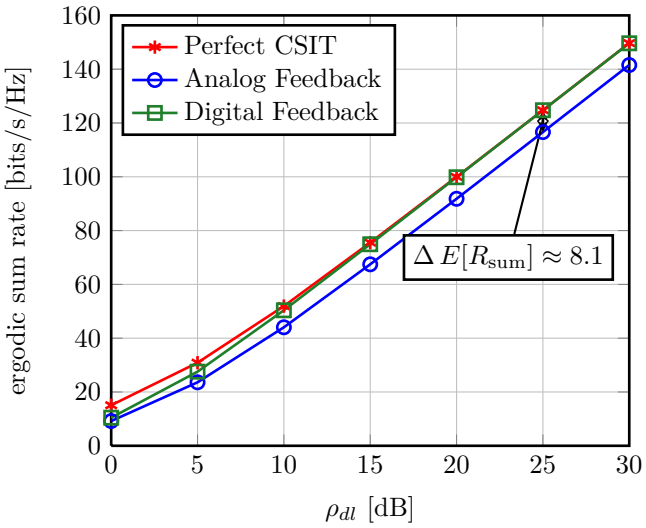

Figure 4.18: ZF, $M = 30$, $K = 15$, $\mathbf{\Theta}_k = \mathbf{I}_M$, $\rho_{dl} = \rho_{ul}$ and $\eta = 2$.

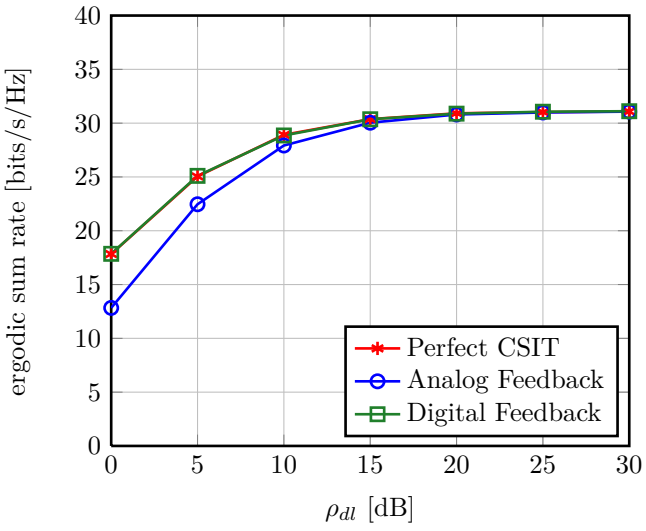

Figure 4.19: MF, $M = K = 30$, $\mathbf{P} = \frac{1}{K}\mathbf{I}_K$,$\mathbf{\Theta}_k = \mathbf{I}_M$, $\rho_{dl} = \rho_{ul}$ and $\eta = 2$.

Chapter 5

Unitary Precoding with Constant Modulus Constraint

In this chapter, we study a precoder that takes the practical constraints on the transmit RF power amplifiers into account and allows for *exact* SINR computation at the receivers. From a practical point of view, additional fluctuations in the signal amplitude caused by the precoding operation decrease the efficiency of the RF power amplifiers which is undesired. Furthermore, in the current LTE standard the users have no possibility to estimate the multi-user interference. That information could be exploited in the receive algorithm resulting in higher supportable rates and an improved user scheduling. Unlike the previously discussed precoding techniques, the unitary precoder with constant modulus elements, studied in this chapter, alleviates these drawbacks. In particular, it only applies phase changes to the transmit signal and thus does not lead to any additional fluctuations in the instantaneous transmit power. Moreover, the property of orthogonal precoding vectors enables each user to exactly compute the multi-user interference power and hence the SINR.

The chapter is structured as follows: In Section 5.1, we discuss the motivation behind the constraints and their practical implications. Section 5.2 discusses the unitary precoder. In Section 5.3, we analyze the unitary precoder with constant modulus constraint. In Section 5.4, we propose an algorithm to compute the sum rate maximizing constraint unitary precoder. Finally, in Section 5.5, we carry out simulations and discuss the results.

5.1 Introduction and Motivation

The constrained unitary beamforming (CUBF) technique is motivated by practical constraints in the radio front-end and improved user scheduling. It is more efficient to have balanced transmit powers, since all power amplifiers can be designed for the same dynamic range. Different additional amplitude variations of the transmit signal due to the precoding operation require a larger linearity region of the power amplifiers which renders them inefficient and more expensive. Moreover, the unitarity of the precoding matrix enables the users to compute the multi-user interference power accurately. The information about the MU interference power can be used in the receiver to enhance the decoding capability and thus higher rates can be supported. Moreover, an accurate SINR estimation at the receiver leads to a better performance of the user scheduling algorithm. For instance in [74], the authors proposed to exploit the MU interference in the receiver to increase the performance. These are two reasons why codebooks containing unitary constant modulus matrices are chosen for MU-MIMO precoding, for instance in the LTE and LTE-A standards [75].

The problem of designing optimal unitary codebooks for MU-MISO has been addressed in [76]. However, in this thesis, we assume that the transmitter computes the optimal unitary precoder based on the available CSIT. A closed form solution for the sum rate maximizing unitary precoder for $M = 2$ has been derived in [77]. For arbitrary M, the authors in [78] proposed an iterative algorithm based on successive Givens rotations to compute the optimal unitary precoder. This algorithm is rather complex. Therefore, we propose to apply an efficient steepest descent algorithm in Riemannian space from [79, 80] to compute the sum rate maximizing unitary precoder. Introducing the additional constraint of a constant magnitude of the precoder entries significantly reduces the degrees of freedom for the precoder optimization. We address the problem of finding the sum rate maximizing CUBF matrix by exploiting a description of complex Hadamard matrices based on an equivalence relation [81].

5.2 Unitary Precoding

Consider $M = K$ and let the entries of the channel matrix $\mathbf{H}$ be i.i.d. Gaussian distributed with zero mean and unit variance. Denote the *unitary* beamforming matrix as $\mathbf{G}_{\text{ubf}} = [\mathbf{g}_1, \ldots, \mathbf{g}_K] \in \mathbb{C}^{M \times K}$, $\mathbf{G}_{\text{ubf}}^{\mathsf{H}}\mathbf{G}_{\text{ubf}} = \mathbf{G}_{\text{ubf}}\mathbf{G}_{\text{ubf}}^{\mathsf{H}} = \mathbf{I}$. Under this assumption and with equal power allocation ($p_k = P/K \ \forall k$) the SINR $\gamma_{k,\text{ubf}}$ of user k takes the form [82]

$$\gamma_{k,\text{ubf}} = \frac{\nu_k^2}{\xi_k + 1 - \nu_k^2}, \tag{5.1}$$

where $\xi_k = \frac{K\sigma^2}{P\|\mathbf{h}_k\|_2^2}$, $\nu_k = |\bar{\mathbf{h}}_k^{\mathsf{H}}\mathbf{g}_k| \in [0, 1]$ is the alignment between the channel direction $\bar{\mathbf{h}}_k = \frac{\mathbf{h}_k}{\|\mathbf{h}_k\|}$ and the precoding vector $\mathbf{g}_k$ of user k. The sum rate

maximizing unitary precoding matrix $\mathbf{G}_{\text{ubf}}^{\star}$ is the solution of the following optimization problem.

$$\mathbf{G}_{\text{ubf}}^{\star} = \arg\max_{\mathbf{G}_{\text{ubf}}} \{R_{\text{sum}}\} \tag{5.2}$$

$$\text{s.t.} \quad \mathbf{G}_{\text{ubf}}^{\mathsf{H}}\mathbf{G}_{\text{ubf}} = \mathbf{I}_K, \tag{5.3}$$

where R_{sum} is given in (1.7). This is a nonconvex optimization problem with nonlinear constraints. A closed form solution for $M = 2$ has been derived in [77]. In [78] this problem has been approached via an iterative algorithm based on successive Givens rotations. In contrast, we use the *self-tuning Riemannian steepest descent algorithm* [79, Table II], given in Table 5.1, to solve the optimization problem in (5.2). Define the element (i, j) of the gradient matrix $\mathbf{\Gamma} = \nabla_{\mathbf{G}_{\text{ubf}}} R_{\text{sum}}$ as

$$[\mathbf{\Gamma}]_{ij} = \frac{\partial R_{\text{sum}}}{\partial [\mathbf{G}_{\text{ubf}}^{*}]_{ij}}. \tag{5.4}$$

The gradient matrix $\mathbf{\Gamma}$ of the cost function in (1.7) is given by

$$\mathbf{\Gamma} = [c_1\mathbf{h}_1\mathbf{h}_1^{\mathsf{H}}\mathbf{g}_1, \ldots, c_K\mathbf{h}_K\mathbf{h}_K^{\mathsf{H}}\mathbf{g}_K] \tag{5.5}$$

$$\text{with} \quad c_k = \left(\xi_k + 1 - \nu_k^2\right)^{-1}. \tag{5.6}$$

The gradient direction in Riemannian space Φ is defined as [79]

$$\Phi = \mathbf{\Gamma}\mathbf{G}_{\text{ubf}}^{\mathsf{H}} - \mathbf{G}_{\text{ubf}}\mathbf{\Gamma}^{\mathsf{H}}. \tag{5.7}$$

Following the gradient Φ the algorithm in Table 5.1 guaranties to converge to a local maximum. If only an imperfect channel estimate $\hat{\mathbf{H}}$ is available at the transmitter, then the optimization algorithm takes $\hat{\mathbf{H}}$ as an input instead of $\mathbf{H}$. We will use this algorithm to compare unitary precoding to unitary precoding with constant modulus constraint. The unitary precoder with constant modulus elements is the subject of the next section.

5.3 Unitary Precoder with Constant Modulus Elements

This section describes the CUBF matrices by applying a framework for the description of complex Hadamard matrices.

5.3.1 Description of Complex Hadamard Matrices

In this section, we provide the mathematical framework for the construction of unitary beamforming matrices with constant modulus entries $\mathbf{G}_{\text{cubf}}$. We first introduce various definitions that we will use later to parametrize $\mathbf{G}_{\text{cubf}}$.

Definition 5.1. *A square matrix* $\mathbf{A}$ *of size* M *where the entries are of equal modulus* $|a_{ij}|^2 = \frac{1}{M}$; $i, j = 1, \ldots, M$, *is called normalized Hadamard matrix if*

$$\mathbf{A}\mathbf{A}^{\mathsf{H}} = \mathbf{I}_M. \tag{5.8}$$

INPUT:	$\mathbf{H}$, P, σ^2
OUTPUT:	$\mathbf{G}_{\text{ubf}}^{\star}$

Step 1: `# Initialization`
$j = 0$, $\mathbf{G}_{\text{ubf}}^{(j)} = \mathbf{I}_M$ and $\mu = 1$
Step 2: `# Gradient of sum rate on Euclidean space`
$\mathbf{\Gamma}^{(j)} = [c_1 \mathbf{h}_1 \mathbf{h}_1^{\mathsf{H}} \mathbf{g}_1^{(j)}, \ldots, c_K \mathbf{h}_K \mathbf{h}_K^{\mathsf{H}} \mathbf{g}_K^{(j)}]$ with
$c_k^{(j)} = \left(\xi_k + 1 - (\nu_k^{(j)})^2 \right)^{-1}$
Step 3: `# Gradient direction in Riemannian space`
$\Phi^{(j)} = \mathbf{\Gamma}^{(j)} (\mathbf{G}_{\text{ubf}}^{(j)})^{\mathsf{H}} - \mathbf{G}_{\text{ubf}}^{(j)} (\mathbf{\Gamma}^{(j)})^{\mathsf{H}}$
Step 4:
Evaluate $\frac{1}{2} \Re(\text{tr} \Phi^{(j)} (\Phi^{(j)})^{\mathsf{H}})$ if small enough, then STOP and
$\mathbf{G}_{\text{ubf}}^{\star} = \mathbf{G}_{\text{ubf}}^{(j)}$
Step 5: `# Determine the rotation matrices`
$\mathbf{R}^{(j)} = \exp(\mu \Phi^{(j)})$, $\mathbf{T}^{(j)} = \mathbf{R}^{(j)} \mathbf{R}^{(j)}$
Step 6:
while $|R_{\text{sum}}(\mathbf{G}_{\text{ubf}}^{(j)}) - R_{\text{sum}}(\mathbf{T}^{(j)} \mathbf{G}_{\text{ubf}}^{(j)})| \geq \frac{\mu}{2} \Re(\text{tr} \Phi^{(j)} (\Phi^{(j)})^{\mathsf{H}})$
do
  $\mathbf{R}^{(j)} = \mathbf{T}^{(j)}$, $\mathbf{T}^{(j)} = \mathbf{R}^{(j)} \mathbf{R}^{(j)}$, $\mu = 2\mu$
end while
Step 7:
while $|R_{\text{sum}}(\mathbf{G}_{\text{ubf}}^{(j)}) - R_{\text{sum}}(\mathbf{R}^{(j)} \mathbf{G}_{\text{ubf}}^{(j)})| < \frac{\mu}{4} \Re(\text{tr} \Phi^{(j)} (\Phi^{(j)})^{\mathsf{H}}))$
do
  $\mathbf{R}^{(j)} = \exp(\mu \Phi^{(j)})$, $\mu = \frac{\mu}{2}$
end while
Step 8: `# Update`
$\mathbf{G}_{\text{ubf}}^{(j+1)} = \mathbf{R}^{(j)} \mathbf{G}_{\text{ubf}}^{(j)}$, $j = j + 1$, go to **Step 2**

Table 5.1: Self-tuning Riemannian steepest descent algorithm from [79, Table II] applied to compute sum rate maximizing unitary precoder $\mathbf{G}_{\text{ubf}}^{\star}$.

The set of normalized complex Hadamard matrices of size M is denoted $\mathcal{H}_M$. In the unnormalized case: $\mathbf{A}\mathbf{A}^{\mathsf{H}} = M \mathbf{I}_M$.

Definition 5.2. *[81, Definition 2.2] The complex Hadamard matrices $\{\mathbf{A}, \tilde{\mathbf{A}}\} \in \mathcal{H}_M$ are equivalent, written $\mathbf{A} \cong \tilde{\mathbf{A}}$, if there exist diagonal unitary matrices $\mathbf{D}_{\text{r}}, \mathbf{D}_{\text{c}}$ and permutation matrices $\mathbf{P}_{\text{r}}, \mathbf{P}_{\text{c}}$ such that*[1]

$$\mathbf{A} = \mathbf{D}_{\text{r}} \mathbf{P}_{\text{r}} \tilde{\mathbf{A}} \mathbf{P}_{\text{c}} \mathbf{D}_{\text{c}}. \tag{5.9}$$

There are $M!$ row and column permutation matrices $\mathbf{P}_{\text{r}}$ and $\mathbf{P}_{\text{c}}$, respectively. The equivalence class of $\mathbf{A} \in \mathcal{H}_M$ under the equivalence relation (5.9) is

$$\mathbf{Q}_M(\mathbf{A}) = \{\mathbf{B} \in \mathcal{H}_M | \mathbf{A} \cong \mathbf{B}\}. \tag{5.10}$$

[1] In this definition transposition and complex conjugate are excluded since they are meaningless in the application of precoding.

We denote $\mathcal{G}_M = \mathcal{H}_M/\cong$, the set of equivalence classes $\mathcal{G}_M$.

In the next section, we will present the set $\mathcal{G}_M$ of equivalence classes for several dimensions M.

5.3.2 Equivalence Classes

Interestingly, the complete set of equivalence classes $\mathcal{G}_M$ is only known for $M < 6$. The problem of finding *all* equivalence classes for dimensions $M \geq 6$ remains unsolved and a catalog of known equivalence classes can be found in [81]. In the following we give a short overview of the (unnormalized) equivalence classes for $M = 2, \ldots, 5$.

$M = 2$

There is only one equivalence class $\mathcal{G}_2 = \{\mathbf{Q}_2(\mathbf{F}_2)\}$ with

$$\mathbf{F}_2 = \begin{bmatrix} 1 & 1 \\ 1 & -1 \end{bmatrix} \tag{5.11}$$

The real Hadamard matrix coincides with the discrete Fourier transform (DFT) matrix $\mathbf{F}_2$, where $\mathbf{F}_M$ of size M is defined as

$$\mathbf{F}_M(m,n) = e^{-\mathbf{i}\frac{2\pi}{M}(m-1)(n-1)} \;;\; m,n = 1,2,\ldots,M. \tag{5.12}$$

$M = 3$

There exists only one equivalence class $\mathcal{G}_3 = \{\mathbf{Q}_3(\mathbf{F}_3)\}$ equal to the DFT matrix $\mathbf{F}_3$ defined in (5.12).

$M = 4$

Here, there exists a *continuous* family of equivalence classes with one free parameter $\mathcal{G}_4 = \{\mathbf{Q}_4(\mathbf{Q}_4^o(\theta));\ \theta \in [\frac{\pi}{2}, \frac{3}{2}\pi)\}$, where $\mathbf{Q}_4^o(\theta)$ is defined as

$$\mathbf{Q}_4^o(\theta) = \begin{bmatrix} 1 & 1 & 1 & 1 \\ 1 & -1 & e^{\mathbf{i}\theta} & -e^{\mathbf{i}\theta} \\ 1 & 1 & -1 & -1 \\ 1 & -1 & -e^{\mathbf{i}\theta} & e^{\mathbf{i}\theta} \end{bmatrix}. \tag{5.13}$$

Note that the real Hadamard matrix $\mathbf{Q}_4^o(\pi)$ and the DFT matrix $\mathbf{F}_4 \cong \mathbf{Q}_4^o(\frac{\pi}{2})$ are special cases of (5.13).

$M = 5$

All complex Hadamard matrices are equivalent to the DFT matrix, i.e., $\mathcal{G}_5 = \{\mathbf{Q}_5(\mathbf{F}_5)\}$.

In the next section, we will apply the framework of describing all complex Hadamard matrices through the equivalence relation (5.9) to parametrize the CUBF matrices which are a special case of complex Hadamard matrices.

5.3.3 Parametrization of CUBF Matrices in MISO BC

In general, the set of CUBF matrices is equal to the set of normalized complex Hadamard matrices $\mathcal{H}_M$. The description of $\mathcal{H}_M$ is solely given by the equivalence relation (5.9) and the equivalence classes (5.10) and can be used to parametrize the CUBF. However, depending on the objective function, some parameters in the general description become obsolete. If the beamforming matrix $\mathbf{G}_{\text{cubf}}$ is intended to modify the SINR of each user in (5.1) (and hence the sum rate) the diagonal unitary matrix $\mathbf{D}_{\text{c}}$ in (5.9) can be omitted since it does not affect the SINR (5.1). Consequently, the diagonal unitary matrix $\mathbf{D}_{\text{r}}$ in (5.9) takes the form

$$\mathbf{D}_{\text{r}} = \text{diag}([1, e^{\mathbf{i}\varphi_1}, \ldots, e^{\mathbf{i}\varphi_{M-1}}]) \tag{5.14}$$

with $\varphi_i \in [0, 2\pi),\ i = 1, 2, \ldots, M-1$.

Remark 5.1. *One may remark that the equivalence relations in* (5.9) *involve continuous parameters (phases in the diagonals) and discrete parameters (permutations). One may think of counting the number of continuous parameters by subtracting from the* $2M^2$ *real entries the number of real constraints imposed by CUBF:* M^2 *due to unitarity,* $(M-1)^2$ *for the constant element magnitudes (suffices to apply to a* $(M-1) \times (M-1)$ *sub-matrix), and* M *(for a first row of all 1's). One ends up with* $M-1$ *degrees of freedom, which correspond to the matrix* $\mathbf{D}_{\text{r}}$*. The curiosity is the unexpected appearance of* θ *in* $\mathbf{Q}_4^o(\theta)$*. The explanation is that counting the obvious constraints must lead to redundancies. The appearance of the additional free parameters can be explained as follows. (Unnormalized) complex Hadamard matrices can in fact be constructed recursively as follows: [83]* $\mathbf{V}(\mathbf{A}, \mathbf{B}) = \begin{bmatrix} \mathbf{A} & \mathbf{B} \\ \mathbf{A} & -\mathbf{B} \end{bmatrix}$ *where* $\mathbf{A}$ *and* $\mathbf{B}$ *are itself complex Hadamard and hence allow equivalence transformations as in* (5.9)*. Now, for* $\mathbf{A}$ *they do not need to be applied since they can equivalently be applied to* $\mathbf{V}$*. However, since* $\mathbf{B}$ *appears both as* $\mathbf{B}$ *and* $-\mathbf{B}$*, not all equivalences on* $\mathbf{B}$ *appear in* $\mathbf{V}$*. At* $M = 4$*, we can take* $\mathbf{A} = \mathbf{B} = \mathbf{F}_2$*, but the one such equivalence that needs to be allowed at the level of* $\mathbf{B}$ *is* $\mathbf{DB}$ *with* $\mathbf{D} = \text{diag}([1\ e^{\mathbf{i}\theta}])$*. So we obtain for* $M = 4$*:* $\mathbf{V}(\mathbf{F}_2, \mathbf{DF}_2)$*.*

If $M = 4$ another construction of CUBF matrices via the Householder transformation exists which is used in 3GPP LTE [75]. The set $\mathcal{V}$ of all CUBF matrices generated by the Householder transformation is

$$\mathcal{V} = \left\{ \mathbf{V} = \mathbf{I}_M - 2\frac{\mathbf{u}\mathbf{u}^{\mathsf{H}}}{\mathbf{u}^{\mathsf{H}}\mathbf{u}} \;\middle|\; \mathbf{u} \in \mathbf{C}^{M\times 1};\ |u_i| = 1;\ u_1 = 1 \right\}. \tag{5.15}$$

The construction of a CUBF matrix via the Householder transformation describes only a subset of all possible CUBF matrices. In fact, $\mathcal{V} \subset \mathbf{Q}_4^o(\pi) \subset \mathcal{H}_4$. To prove $\mathcal{V} \subset \mathbf{Q}_4^o(\pi) \subset \mathcal{H}_4$, observe that $\mathbf{V} \cong \mathbf{Q}_4^o(\pi)$ since we have $\mathbf{Q}_4^o(\pi) = 2\mathbf{P}_{\text{r}}\mathbf{D}_1\mathbf{D}^{\mathsf{H}}\mathbf{V}\mathbf{D}\mathbf{D}_1\mathbf{P}_{\text{c}}$ with $\mathbf{D} = \text{diag}(\mathbf{u})$, $\mathbf{D}_1 = \text{diag}([1, -1, -1, -1])$, $\mathbf{P}_{\text{c}} = [\mathbf{e}_1, \mathbf{e}_2, \mathbf{e}_4, \mathbf{e}_3]$ and $\mathbf{P}_{\text{r}} = [\mathbf{e}_1, \mathbf{e}_3, \mathbf{e}_2, \mathbf{e}_4]$, where $\mathbf{e}_i$ is the ith column of $\mathbf{I}_M$. Hence, $\mathcal{V}$ is the subset of $\mathcal{H}_4$ that stems from the unique real equivalence class

$d_0(k,m) = \lvert a_{km}\rvert^2 + \lvert b_{km}\rvert^2$
$d_1(k,m) = 2\lvert a_{km}\rvert \cdot \lvert b_{km}\rvert$
$\delta_{km} = \angle b_{km} - \angle a_{km}$
$d_2(k,m) = d_1(k,m)\cos\delta_{km}$
$d_3(k,m) = 2d_1(k,m)\sin\delta_{km}$

Table 5.2: Auxiliary Variables

$\mathbf{Q}_4^o(\pi)$. Thus, restricting $\mathbf{G}_{\text{cubf}} \in \mathcal{V}$ leads to a significant performance loss as we show by simulation in Section 5.5.

In the next Section, we derive an optimization algorithm that computes the sum rate maximizing CUBF matrix $\mathbf{G}_{\text{cubf}}^{\star}$.

5.4 Optimization of the CUBF Matrices

Under the assumption that there are always $K = M$ users available for transmission and that the transmit power is equally divided among them, we can formulate the optimization criterion as follows

$$\{\mathbf{D}_{\text{r}}^{\star}, \mathbf{Q}_M^{\star}, \mathbf{P}_c^{\star}, \mathbf{P}_r^{\star}\} = \underset{\mathbf{D}_{\text{r}}, \mathbf{Q}_M \in \mathcal{G}_M, \mathbf{P}_c, \mathbf{P}_r}{\arg\max} \left\{ \sum_{k=1}^{K} \log\left(1+\gamma_k\right) \right\} \tag{5.16}$$

where γ_k is defined in (5.1). The diagonal unitary matrix $\mathbf{D}_{\text{r}}$ contains $M-1$ angles. The optimal permutation matrices $\mathbf{P}_r^{\star}, \mathbf{P}_c^{\star}$ have to be found by exhaustive search. Similarly, all equivalence classes $\mathbf{Q}_M \in \mathcal{G}_M$ have to be tried to determine the optimal one $\mathbf{Q}_M^{\star}$. Consequently, the optimal CUBF matrix $\mathbf{G}_{\text{cubf}}^{\star}$ is given by

$$\mathbf{G}_{\text{cubf}}^{\star} = \frac{1}{\sqrt{M}} \mathbf{D}_{\text{r}}^{\star} \mathbf{P}_r^{\star} \mathbf{Q}_M^{\star} \mathbf{P}_c^{\star}. \tag{5.17}$$

Denote $\mathcal{A} = \{\varphi_1, \ldots, \varphi_{M-1}, \theta\}$ the set of angles to be optimized. Note that only for $M = 4$ the set $\mathcal{A}$ contains the additional angle θ. After some algebraic manipulation (5.16) takes the form

$$\{\mathbf{D}_{\text{r}}^{\star}, \mathbf{Q}_M^{\star}, \mathbf{P}_c^{\star}, \mathbf{P}_r^{\star}\} = \underset{\mathbf{D}_{\text{r}}, \mathbf{Q}_M \in \mathcal{G}_M, \mathbf{P}_c, \mathbf{P}_r}{\arg\min} \left\{ \prod_{k=1}^{K} \left(1 + \xi_k - \nu_k^2\right) \right\}. \tag{5.18}$$

This is still a non-convex optimization and the global optimum can only be found by exhaustive search. Subsequently, we present an iterative algorithm to calculate the optimal set of angles $\mathcal{A}^{\star}$. However, this algorithm cannot be guaranteed to converge to the global optimum.

5.4.1 Iterative Optimization Algorithm

A joint optimization of the angles in $\mathcal{A}$ is too involved, therefore we optimize the angles one by one while the others are fixed (i.e., alternating maximization)

for given permutation matrices $\mathbf{P}_c$ and $\mathbf{P}_r$ and equivalence class $\mathbf{Q}_M \in \mathcal{G}_M$. Denote $\mathbf{W} \triangleq \frac{1}{\sqrt{M}}\mathbf{P}_r\mathbf{Q}_M\mathbf{P}_c = [\mathbf{w}_1, \ldots, \mathbf{w}_M]$. We write

$$\nu_k(\varphi_m) = |\bar{\mathbf{h}}_k^{\mathsf{H}}\mathbf{g}_k| = |\bar{\mathbf{h}}_k^{\mathsf{H}}\mathbf{D}_{\mathrm{r}}\mathbf{w}_k| \tag{5.19}$$

$$= |\bar{h}_{k1}^* w_{k1} + \bar{h}_{k2}^* w_{k2} e^{\mathbf{i}\varphi_1} + \cdots + \bar{h}_{kM}^* w_{kM} e^{\mathbf{i}\varphi_{M-1}}| \tag{5.20}$$

$$= |a_{km} + b_{km} e^{\mathbf{i}\varphi_m}|, \tag{5.21}$$

where $\varphi_m \in \mathcal{A}$ and both $b_{km} = \bar{h}_{km+1}^* w_{km+1}$ and $a_{km} = \nu_k - b_{km}$ are independent of φ_m. With the auxiliary variables in Table 5.2, we obtain

$$\nu_k^2(\varphi_m) = d_0(k,m) + d_1(k,m)\cos(\delta_{km} - \varphi_m). \tag{5.22}$$

With the substitution

$$s_m = \tan\frac{\varphi_m}{2}, \tag{5.23}$$

we have $\cos\varphi_m = \frac{1-s_m^2}{1+s_m^2}$ and $\sin\varphi_m = \frac{2s_m}{1+s_m^2}$. Together with $\cos(\delta_{km} - \varphi_m) = \cos\delta_{km}\cos\varphi_m - \sin\delta_{km}\sin\varphi_m$, (5.22) takes the form

$$\nu_k^2(s_m) = d_0(k,m) - \frac{1}{1+s_m^2}\left[d_2(k,m)s_m^2 - d_3(k,m)s_m - d_2(k,m)\right]. \tag{5.24}$$

From (5.18) we have the objective function

$$F_m(s_m) = \prod_{k=1}^{M}\left(1 + \xi_k - \nu_k^2(s_m)\right) \tag{5.25}$$

$$= \prod_{k=1}^{M}\frac{c_2(k,m)s_m^2 + c_1(k,m)s_m + c_0(k,m)}{1+s_m^2}, \tag{5.26}$$

where

$$c_2(k,m) = 1 + \xi_k - d_2(k,m) - d_0(k,m) \tag{5.27}$$

$$c_1(k,m) = d_3(k,m) \tag{5.28}$$

$$c_0(k,m) = 1 + \xi_k + d_2(k,m) - d_0(k,m). \tag{5.29}$$

Define $P_1(s_m) = \prod_{k=1}^{M} c_2(k,m)s_m^2 + c_1(k,m)s_m + c_0(k,m)$ and $P_2(s_m) = (1 + s_m^2)^M$. To solve $\frac{dF_m(s_m)}{ds_m} = 0$, we have to find the real roots of the polynomial $G(s_m)$ of order $2(2M-1)$ given as

$$G_m = \frac{dP_1(s_m)}{ds_m}P_2(s_m) - P_1(s_m)\frac{dP_2(s_m)}{ds_m}. \tag{5.30}$$

Once the real roots have been found, we undo the substitution in (5.23), i.e., $s_m = 2\arctan\varphi_m$, and evaluate (5.18) for every solution to obtain the optimal solution $\varphi_m^\star$. If $M = 4$, there is an additional angle θ in $\mathbf{Q}_4^o$. To find the optimal angle $\theta^\star$, we can apply the same approach as for φ_m. The algorithm to compute

INPUT:	$\mathbf{H}$, σ^2, $\mathbf{P}_\mathrm{r}$, $\mathbf{P}_\mathrm{c}$, $\mathbf{Q}_M$, $\mathcal{A}_\mathrm{init}$ N_iter
OUTPUT:	$\mathcal{A}^\star$

$\mathbf{W} = \frac{1}{\sqrt{M}}\mathbf{P}_r\mathbf{Q}_M\mathbf{P}_c$
$\mathcal{A} = \mathcal{A}_\mathrm{init}$
for $n = 1, 2, \ldots, N_\mathrm{iter}$ **do**
  for $m = 1, 2, \ldots, M-1$ **do**
    Compute G_m in (5.30).
    Compute real roots of G_m and find $\varphi_m^\star$.
    $\varphi_m \in \mathcal{A} = \varphi_m^\star$
  end for
end for
$\mathcal{A}^\star = \mathcal{A}$

Table 5.3: Alternating optimization to compute the set of optimal angles $\mathcal{A}^\star$.

the optimal set of angles $\mathcal{A}^\star$ is given in Table 5.3. The number of iterations N_iter has to be chosen large enough for the algorithm to converge, which is usually the case after a few iterations. In addition to the exhaustive search over the permutation matrices $\mathbf{P}_\mathrm{r}$ and $\mathbf{P}_\mathrm{c}$ as well as $\mathbf{Q}_M \in \mathcal{G}_M$, the algorithm can be carried out for multiple sets of initial angles $\mathcal{A}_\mathrm{init}$ to increase the probability of finding the global optimum.

5.5 Numerical Results

In this section, we compare the CUBF with the codebooks of CUBF matrices (called CB-CUBF) defined in 3GPP LTE [75]. In case of $M = 2$ the codebook contains the identity matrix and two rotations of the DFT matrix according to (5.9) with $\varphi_1 = \{0, \frac{\pi}{2}\}$ and $\mathbf{P}_\mathrm{r} = \mathbf{P}_\mathrm{c} = \mathbf{I}_2$. The codebook for 4 transmit antennas is a subset of $\mathcal{V}$ defined in (5.15) generated by 16 vectors $\mathbf{u}$ where the elements of $\mathbf{u}$ are taken from a 8-PSK constellation and $u_1 = 1$. The optimal CB-CUBF is computed at the transmitter by exhaustive search based on the available CSIT. The performance metric is the ergodic sum rate $E[R_\mathrm{sum}]$. Throughout this section we average our results over 10 000 independent uncorrelated ($\mathbf{\Theta}_k = \mathbf{I}_K \ \forall k$) Rayleigh fading channel realizations.

Figure 5.1 shows the sensitivity of CUBF, CB-CUBF and ZF precoding to erroneous CSIT $\hat{\mathbf{h}}_k$ which is model similar to (1.14) as $\hat{\mathbf{h}}_k = \sqrt{1-\tau^2}\mathbf{z}_k + \tau\mathbf{e}_k$, where both $\mathbf{z}_k$ and $\mathbf{e}_k$ have i.i.d. Gaussian entries of zero mean and unit variance. From Figure 5.1 it can be observed that CUBF and CB-CUBF outperform ZF precoding starting from $\tau^2 \approx 0.22$ and $\tau^2 \approx 0.5$, respectively. ZF precoding, that achieves high sum rates under the assumption of perfect CSIT, experiences a severe performance loss as soon as the CSIT is erroneous. In practical systems such a scheme is not attractive since it requires highly accurate CSIT which entails an enormous feedback overhead.

Figures 5.2 and 5.3 present the ergodic sum rate performance for $M = K = 2$

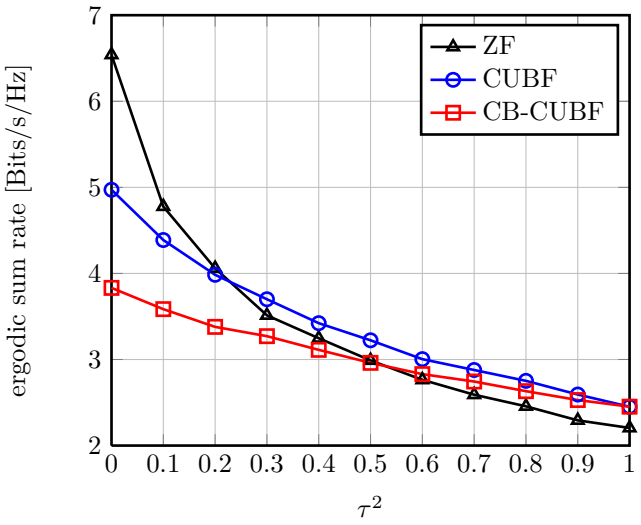

Figure 5.1: $M = K = 2$, impact of erroneous CSIT on ergodic sum rate, SNR = 15 dB.

and $M = K = 4$ system, respectively. We observe that the CUBF significantly outperforms the CB-CUBF in both configurations. At an SNR of 20 dB the gain is about 40 % and 30 %, respectively. Furthermore, it can be observed that UBF significantly outperforms CUBF which suggests that the constant modulus constraint is a severe restriction resulting in a large performance loss. Indeed, the sum rate performance under UBF does not saturate, since under UBF the precoding vector $\mathbf{g}_k$ can always be perfectly aligned to the channel $\mathbf{h}_k$, i.e., $\nu_k = 1$ and therefore the interference for user k is zero. Moreover, the sum rate saturation level of CUBF is lower for $M = 4$ than for $M = 2$. This is due to the fact that the number of degrees of freedom (the number of angles to be optimized) of CUBF scales significantly slower with M than the number of channel coefficients. Thus, the CUBF is increasingly maladjusted to the channel and consequently the interference level is rising resulting in a lower sum rate saturation level. Also note that the rather poor performance of the CUBF scheme may be significantly increased if it is applied in conjunction with an appropriate scheduling techniques or an advanced (interference-aware) receive algorithm. However, to cancel the multi-user interference, the receiver requires knowledge of the precoding vectors and modulation scheme of the interfering users. In the current LTE-A standard, this information is not signaled to the users, which makes it difficult to obtain. Under unitary precoding, the multi-user interference power can be computed without the knowledge of the other precoding vectors but still the modulation scheme has to be estimated. Indeed, the results in [74] show that the system performance increases significantly if the receiver accounts for the interference even under false assumptions on the

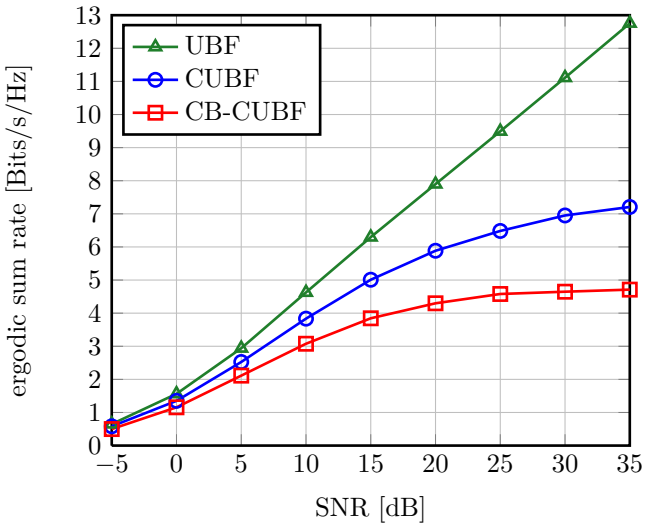

Figure 5.2: $M = K = 2$, ergodic sum rate vs. SNR.

interfering modulation scheme.

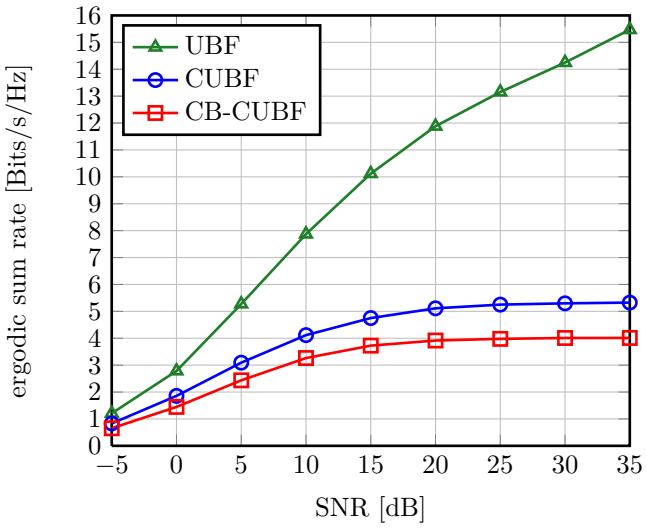

Figure 5.3: $M = K = 4$, ergodic sum rate vs. SNR.

Chapter 6

Conclusion and Perspectives

This dissertation studied large MU-MISO systems under various linear precoding techniques and imperfect CSIT.

Conclusion

In this thesis, we considered the MU-MISO downlink under linear precoding and imperfect CSIT and analyzed the system behavior for large numbers of transmit antennas and users. We presented a consistent framework for the study of several linear precoding schemes based on the theory of large dimensional random matrices. The tools from large RMT allowed us to consider a very realistic channel model accounting for per-user channel correlation as well as individual channel gains for each link. The system performance under this general type of channel is extremely difficult to study for finite dimensions but becomes feasible by assuming large system dimensions. Thanks to large RMT, the system performance (i.e., SINR or rate) can be approximated by a deterministic equivalent (independent of the channel realizations) that is almost surely exact as the system dimensions grow asymptotically large with bounded ratio. Simulation results showed that these approximations are very accurate even for small system dimensions and reveal the deterministic dependence of the system performance on several important system parameters, such as the transmit correlation, signal powers, SNR and CSIT quality. Applied to practical optimization problems, the deterministic approximations lead to important insights into the system behavior, which are consistent with previous results, but

go further and extend them to more realistic channel models and other linear precoding techniques. Furthermore, the proposed channel-independent performance approximations can be used to simulate the system behavior without having to carry out extensive Monte-carlo simulations. Although not yet practical, large numbers of transmit antennas are expected to be widely deployed in the future, at which point the results in this dissertation may prove all the more relevant. Moreover, since practical considerations often limit the choices for a precoding technique, we studied the precoding scheme adopted in the 3GPP LTE standard and developed an algorithm to evaluate the performance of such precoding schemes.

Perspectives

From a mathematical point of view, the deterministic equivalent of the empirical Stieltjes transform under the generalized variance profile is a general result and may have applications outside the field of mobile communications.

The proposed framework considered a single isolated cell but is the foundation for the study of more complex multi-cell systems. For instance, recently, the results in this thesis have been applied to study the effect of pilot contamination on the system performance in large multi-cell networks. But other scenarios can be considered as well, for example the impact of inter-cell interference can be included in the system model. Moreover, our analysis can be extended to multi-cell systems with different levels of base station cooperation (coordinated beamforming), with imperfect CSIT at the base stations due to limited back haul capacity. Furthermore, it is possible to extend this framework to MU-MIMO with a single stream per user by considering linear receive filters. On the contrary, an extension to MU-MIMO with multiple streams per user is very involved and requires the development of more advanced random matrix theory tools. But the application of the presented results is not limited to broadcast channels. The proposed framework can be extended to linearly precoded multi-user MISO *amplify-and forward* downlink channels, where the signal is linearly processed at the transmitter and the relay before being received by the users. Lastly, the proposed methodology may also be applied to interference channels with linear transmit and receive filters.

Appendix

A Proof of Proposition 2.3

The proof is based on the matrix inequalities in Lemmas F.8, F.10, F.11, F.12. F.9 and F.13.

Applying Lemma F.9, $|d_i^{(1)}|$ can be upper-bounded as

$$|d_i^{(1)}| = \left| \frac{\mathbf{y}_i^{\mathsf{H}} \mathbf{\Psi}_i^{\mathsf{H}} \left(\mathbf{B}_{[i]} - z\mathbf{I}_N\right)^{-1} \left[\mathbf{D}_{[i]}^{-1} - \mathbf{D}^{-1}\right] \mathbf{\Psi}_i \mathbf{y}_i}{1 + \mathbf{y}_i^{\mathsf{H}} \mathbf{\Psi}_i^{\mathsf{H}} \left(\mathbf{B}_{[i]} - z\mathbf{I}_N\right)^{-1} \mathbf{\Psi}_i \mathbf{y}_i} \right| \tag{A.1}$$

$$\leq \frac{|z|}{\Im z} \left| \mathbf{y}_i^{\mathsf{H}} \mathbf{\Psi}_i^{\mathsf{H}} \left(\mathbf{B}_{[i]} - z\mathbf{I}_N\right)^{-1} \left[\mathbf{D}_{[i]}^{-1} - \mathbf{D}^{-1}\right] \mathbf{\Psi}_i \mathbf{y}_i \right|. \tag{A.2}$$

We further bound $|d_i^{(1)}|$ by applying Lemmas F.10, F.12 and the fact that $\| \left(\mathbf{B}_{[i]} - z\mathbf{I}_N\right)^{-1} \| \leq \frac{1}{\Im z}$. We obtain

$$|d_i^{(1)}| \leq \frac{|z| \|\mathbf{\Theta}_i\|}{(\Im z)^2} \|\mathbf{y}_i\|_2^2 \|\mathbf{D}_{[i]}^{-1} - \mathbf{D}^{-1}\|. \tag{A.3}$$

In order to bound $\|\mathbf{D}_{[i]}^{-1} - \mathbf{D}^{-1}\|$ we apply Lemma F.1 and Lemma F.12

$$\|\mathbf{D}_{[i]}^{-1} - \mathbf{D}^{-1}\| \tag{A.4}$$

$$= \| - \mathbf{D}_{[i]}^{-1} \left[\mathbf{D}_{[i]} - \mathbf{D}\right] \mathbf{D}^{-1}\| \tag{A.5}$$

$$= \| - \mathbf{Q}_N \left(\mathbf{R}_{[i]} + \mathbf{S}_N - z\mathbf{I}_N\right)^{-1} \left[\mathbf{R}_{[i]} - \mathbf{R}\right] \left(\mathbf{R} + \mathbf{S}_N - z\mathbf{I}_N\right)^{-1} \| \tag{A.6}$$

$$\leq \|\mathbf{Q}_N\| \| \left(\mathbf{R}_{[i]} + \mathbf{S}_N - z\mathbf{I}_N\right)^{-1} \| \|\mathbf{R}_{[i]} - \mathbf{R}\| \| \left(\mathbf{R} + \mathbf{S}_N - z\mathbf{I}_N\right)^{-1} \|, \tag{A.7}$$

where $\mathbf{R}_{[i]} = \frac{1}{N} \sum_{i=1}^n \frac{\mathbf{\Theta}_i}{1 + \frac{1}{N} \mathrm{tr} \mathbf{\Theta}_i \left(\mathbf{B}_{[i]} - z\mathbf{I}_N\right)^{-1}}$. First we have

$$\|(\mathbf{R} - z\mathbf{I}_N + \mathbf{S}_N)^{-1}\| = \left\| \frac{1}{N} \sum_{i=1}^n \frac{\mathbf{\Theta}_i [1 + \frac{1}{N} \mathrm{tr} \mathbf{\Theta}_i \left(\mathbf{B}_N - z\mathbf{I}_N\right)^{-1}]^*}{|1 + \frac{1}{N} \mathrm{tr} \mathbf{\Theta}_i \left(\mathbf{B}_N - z\mathbf{I}_N\right)^{-1}|^2} + \mathbf{S}_N - z\mathbf{I}_N \right\| \tag{A.8}$$

$$\overset{(a)}{\leq} \frac{1}{\Im z}, \tag{A.9}$$

where (a) follows from the observation that (A.8) can be written as $\|(\mathbf{R}-z\mathbf{I}_N+\mathbf{S}_N)^{-1}\| = \mathbf{A}-\mathbf{i}\mathbf{B}-\Im z\mathbf{I}_N$, where $\mathbf{B}$ is nonnegative-definite, since the $\mathbf{\Theta}_i$ are nonnegative-definite and $\Im[\frac{1}{N}\mathrm{tr}\mathbf{\Theta}_i\left(\mathbf{B}_N-z\mathbf{I}_N\right)^{-1}]$ is always positive as it is the Stieltjes transform of a nonnegative finite measure. Therefore, we apply Lemma F.13 and obtain (A.9). Similarly to (A.8) we have

$$\|(\mathbf{R}_{[i]}-z\mathbf{I}_N+\mathbf{S}_N)^{-1}\| \leq \frac{1}{\Im z}. \tag{A.10}$$

The term $\|\mathbf{R}_{[i]}-\mathbf{R}\|$ takes the form

$$\|\mathbf{R}_{[i]}-\mathbf{R}\| = \left\| \frac{1}{N}\sum_{i=1}^{n}\mathbf{\Theta}_i \frac{\frac{1}{N}\mathrm{tr}\mathbf{\Theta}_i\left[\left(\mathbf{B}_N-z\mathbf{I}_N\right)^{-1}-\left(\mathbf{B}_{[i]}-z\mathbf{I}_N\right)^{-1}\right]}{\left[1+\frac{1}{N}\mathrm{tr}\mathbf{\Theta}_i\left(\mathbf{B}_{[i]}-z\mathbf{I}_N\right)^{-1}\right]\left[1+\frac{1}{N}\mathrm{tr}\mathbf{\Theta}_i\left(\mathbf{B}_N-z\mathbf{I}_N\right)^{-1}\right]} \right\|. \tag{A.11}$$

Applying Lemma F.12 together with the rank-1 perturbation Lemma F.8, the numerator in (A.11) can be bounded as

$$\left|\frac{1}{N}\mathrm{tr}\mathbf{\Theta}_i\left[\left(\mathbf{B}_N-z\mathbf{I}_N\right)^{-1}-\left(\mathbf{B}_{[i]}-z\mathbf{I}_N\right)^{-1}\right]\right| \leq \frac{\|\mathbf{\Theta}_i\|}{N\Im z}. \tag{A.12}$$

Since $\frac{1}{N}\mathrm{tr}\mathbf{\Theta}_i\left(\mathbf{B}_{[i]}-z\mathbf{I}_N\right)^{-1}$ is the Stieltjes transform of a nonnegative finite measure, we apply [19, Corollary 3.1] and (2.20) to upper bound (A.11) as

$$\|\mathbf{R}_{[i]}-\mathbf{R}\| \leq \frac{T|z|^2}{N^2(\Im z)^3}\sum_{j=1}^{n}\|\mathbf{\Theta}_j\|. \tag{A.13}$$

Substituting (A.9), (A.13) and (A.11) into (A.7) yields

$$\|\mathbf{D}_{[i]}^{-1}-\mathbf{D}^{-1}\| \leq \frac{T\|\mathbf{Q}_N\||z|^2}{N^2(\Im z)^5}\sum_{j=1}^{n}\|\mathbf{\Theta}_j\|. \tag{A.14}$$

Therefore, with (A.14) the upper bound of $|d_i^{(1)}|$ in (A.3) becomes

$$|d_i^{(1)}| \leq \|\mathbf{y}_i\|_2^2\frac{T\|\mathbf{\Theta}_i\|\|\mathbf{Q}_N\||z|^3}{N^2(\Im z)^7}\sum_{j=1}^{n}\|\mathbf{\Theta}_j\|. \tag{A.15}$$

Before considering the pth order moment of $|d_i^{(1)}|$, we proceed with bounding the remaining terms $|d_i^{(2)}|$, $|d_i^{(3)}|$ and $|d_i^{(4)}|$.

Applying Lemma F.9, the term $|d_i^{(2)}|$ is bounded as

$$|d_i^{(2)}| \leq \frac{|z|}{\Im z}\left|\frac{1}{N}\mathrm{tr}\mathbf{\Theta}_i\left(\mathbf{B}_{[i]}-z\mathbf{I}_N\right)^{-1}\mathbf{D}_{[i]}^{-1}-\mathbf{y}_i^{\mathsf{H}}\mathbf{\Psi}_i^{\mathsf{H}}\left(\mathbf{B}_{[i]}-z\mathbf{I}_N\right)^{-1}\mathbf{D}_{[i]}^{-1}\mathbf{\Psi}_i\mathbf{y}_i\right| \tag{A.16}$$

Again, using Lemma (F.9), $|d_i^{(3)}|$ is bounded as

$$|d_i^{(3)}| \leq \frac{|z|}{\Im z}\left|\frac{1}{N}\mathrm{tr}\boldsymbol{\Theta}_i\left(\mathbf{B}_N - z\mathbf{I}_N\right)^{-1}\mathbf{D}^{-1} - \frac{1}{N}\mathrm{tr}\boldsymbol{\Theta}_i\left(\mathbf{B}_{[i]} - z\mathbf{I}_N\right)^{-1}\mathbf{D}_{[i]}^{-1}\right|. \tag{A.17}$$

Applying the triangle inequality, we obtain

$$\begin{aligned}&\left|\frac{1}{N}\mathrm{tr}\boldsymbol{\Theta}_i\left(\mathbf{B}_N - z\mathbf{I}_N\right)^{-1}\mathbf{D}^{-1} - \frac{1}{N}\mathrm{tr}\boldsymbol{\Theta}_i\left(\mathbf{B}_{[i]} - z\mathbf{I}_N\right)^{-1}\mathbf{D}_{[i]}^{-1}\right| \leq \\ &\left|\frac{1}{N}\mathrm{tr}\boldsymbol{\Theta}_i\left[\left(\mathbf{B}_N - z\mathbf{I}_N\right)^{-1} - \left(\mathbf{B}_{[i]} - z\mathbf{I}_N\right)^{-1}\right]\mathbf{D}^{-1}\right| \\ &+ \left|\frac{1}{N}\mathrm{tr}\boldsymbol{\Theta}_i\left(\mathbf{B}_{[i]} - z\mathbf{I}_N\right)^{-1}\left[\mathbf{D}_{[i]}^{-1} - \mathbf{D}^{-1}\right]\right|. \end{aligned}\tag{A.18}$$

With Lemma F.12 together with (A.12) and $\|\mathbf{D}^{-1}\| \leq \frac{\|\mathbf{Q}_N\|}{\Im z}$, the first term on the RHS of (A.18) can be bounded as

$$\left|\frac{1}{N}\mathrm{tr}\boldsymbol{\Theta}_i\left[\left(\mathbf{B}_N - z\mathbf{I}_N\right)^{-1} - \left(\mathbf{B}_{[i]} - z\mathbf{I}_N\right)^{-1}\right]\mathbf{D}^{-1}\right| \leq \frac{\|\boldsymbol{\Theta}_i\|\|\mathbf{Q}_N\|}{N(\Im z)^2}. \tag{A.19}$$

Similarly with Lemma F.11, F.12 and (A.5), we have

$$\left|\frac{1}{N}\mathrm{tr}\boldsymbol{\Theta}_i\left(\mathbf{B}_{[i]} - z\mathbf{I}_N\right)^{-1}\left[\mathbf{D}_{[i]}^{-1} - \mathbf{D}^{-1}\right]\right| \leq \frac{\|\boldsymbol{\Theta}_i\|^2\|\mathbf{Q}_N\||z|^2}{N^2(\Im z)^6}\sum_{j=1}^{n}\|\boldsymbol{\Theta}_j\|. \tag{A.20}$$

Therefore

$$|d_i^{(3)}| \leq \frac{|z|}{N\Im z}\left[\frac{\|\boldsymbol{\Theta}_i\|\|\mathbf{Q}_N\|}{(\Im z)^2} + \frac{\|\boldsymbol{\Theta}_i\|^2\|\mathbf{Q}_N\||z|^2}{N^2(\Im z)^6}\sum_{j=1}^{n}\|\boldsymbol{\Theta}_j\|\right]. \tag{A.21}$$

Applying the Cauchy-Schwarz inequality, Lemmas F.9, F.11 and F.12 we have

$$|d_i^{(4)}| \leq \frac{\|\boldsymbol{\Theta}_i\|\|\mathbf{Q}_N\||z|^2}{(\Im z)^4}\left[\mathbf{y}_i^{\mathsf{H}}\boldsymbol{\Psi}_i^{\mathsf{H}}\left(\mathbf{B}_{[i]} - z\mathbf{I}_N\right)^{-1}\boldsymbol{\Psi}_i\mathbf{y}_i - \frac{1}{N}\mathrm{tr}\boldsymbol{\Theta}_i\left(\mathbf{B}_N - z\mathbf{I}_N\right)^{-1}\right]. \tag{A.22}$$

Adding and subtracting $\frac{1}{N}\mathrm{tr}\boldsymbol{\Theta}_i\left(\mathbf{B}_{[i]} - z\mathbf{I}_N\right)^{-1}$ from the term in brackets and applying the triangle inequality together with the bound in (A.12) we obtain

$$\begin{aligned}|d_i^{(4)}| \leq &\frac{\|\boldsymbol{\Theta}_i\|\|\mathbf{Q}_N\||z|^2}{(\Im z)^4}\left[\left|\mathbf{y}_i^{\mathsf{H}}\boldsymbol{\Psi}_i^{\mathsf{H}}\left(\mathbf{B}_{[i]} - z\mathbf{I}_N\right)^{-1}\boldsymbol{\Psi}_i\mathbf{y}_i - \frac{1}{N}\mathrm{tr}\boldsymbol{\Theta}_i\left(\mathbf{B}_{[i]} - z\mathbf{I}_N\right)^{-1}\right|\right. \\ &\left. + \frac{\|\boldsymbol{\Theta}_i\|}{N\Im z}\right],\end{aligned}\tag{A.23}$$

The pth order moment of $|d_i^{(1)}|$ can be bounded as

$$E\left[|d_i^{(1)}|^p\right] \leq \left[\frac{\|\boldsymbol{\Theta}_i\|^2\|\mathbf{Q}_N\||z|^3}{N(\Im z)^7}\sum_{j=1}^{n}\|\boldsymbol{\Theta}_j\|\right]^p\frac{1}{N^p}E\left[\left|\mathbf{y}_i^{\mathsf{H}}\mathbf{y}_i\right|^p\right]. \tag{A.24}$$

Applying the inequality $|x+y|^p \leq 2^{p-1}(|x|^p + |y|^p)$ yields

$$E\left[|d_i^{(1)}|^p\right] \leq 2^{p-1}\left(\frac{\beta T^3 Q|z|^3}{(\Im z)^7}\right)^p \frac{1}{N^p}\left(E\left[\left|\mathbf{y}_i^{\mathsf{H}}\mathbf{y}_i - 1\right|^p\right] + 1\right) \tag{A.25}$$

If the moments $E[|d_i^{(1)}|^4]$ and $E[|d_i^{(1)}|^{2p}]$ exist and are bounded, we apply Lemma F.3, and obtain

$$E\left[|d_i^{(1)}|^p\right] \leq 2^{p-1}\left(\frac{\beta T^3 Q|z|^3}{(\Im z)^7}\right)^p \frac{1}{N^p}\left(\frac{C_p^{(1)}}{N^{p/2}} + 1\right) \tag{A.26}$$

where $C_p^{(1)}$ is some constant depending only on p. Similarly, applying Lemma F.3 yields

$$E\left[|d_i^{(2)}|^p\right] \leq \frac{|z|^4}{(\Im z)^4}\frac{C_p^{(2)}}{N^{p/2}}, \tag{A.27}$$

$$E\left[|d_i^{(3)}|^p\right] \leq \left(\frac{|z|TQ}{N(\Im z)^3}\right)^p \left[1 + \frac{\beta T^2|z|^2}{(\Im z)^4}\right]^p, \tag{A.28}$$

$$E\left[|d_i^{(4)}|^p\right] \leq 2^{p-1}\left(\frac{TQ|z|^2}{(\Im z)^4}\right)^p \left[\frac{C_p^{(4)}}{N^{p/2}} + \frac{T^p}{N^p(\Im z)^p}\right], \tag{A.29}$$

which completes the proof.

B Deterministic Equivalents for Precoders with RZF Structure

This section provides three lemmas that are applied in the derivation of a deterministic equivalent of the SINR for WSR maximizing precoding in Section 3.3 and RZF precoding in Section 3.4. We remind that the kth column $\hat{\mathbf{h}}_k$ of $\hat{\mathbf{H}}^{\mathsf{H}}$ is defined in (1.14), $\hat{\mathbf{H}}_{[k]} = [\hat{\mathbf{h}}_1, \ldots, \hat{\mathbf{h}}_{k-1}, \hat{\mathbf{h}}_{k+1}, \ldots, \hat{\mathbf{h}}_K]^{\mathsf{H}}$, $\alpha > 0$ and the power allocation matrix $\mathbf{P} = \mathrm{diag}(p_1, \ldots, p_K)$. The subsequent lemmas make use of the following definitions.

$$\boldsymbol{\Gamma}_{[k]} \triangleq \frac{1}{M}\hat{\mathbf{H}}_{[k]}^{\mathsf{H}}\hat{\mathbf{H}}_{[k]} \tag{B.1}$$

$$\mathbf{C}_{[k]} \triangleq \boldsymbol{\Gamma}_{[k]} + \alpha\mathbf{I}_M \tag{B.2}$$

$$\hat{\mathbf{W}} \triangleq \left(\hat{\mathbf{H}}^{\mathsf{H}}\hat{\mathbf{H}} + M\alpha\mathbf{I}_M\right)^{-1}. \tag{B.3}$$

B.1 Deterministic Equivalent for $\Psi = \mathrm{tr}\mathbf{P}\hat{\mathbf{H}}\hat{\mathbf{W}}^2\hat{\mathbf{H}}^{\mathsf{H}}$

Lemma B.1. *Let* $\Psi = \mathrm{tr}\mathbf{P}\hat{\mathbf{H}}(\hat{\mathbf{H}}^{\mathsf{H}}\hat{\mathbf{H}} + M\alpha\mathbf{I}_M)^{-2}\hat{\mathbf{H}}^{\mathsf{H}}$ *and let Assumption 3.1 hold true. Then, a deterministic equivalent* $\bar{\Psi}$ *such that* $\Psi - \bar{\Psi} \overset{M\to\infty}{\longrightarrow} 0$, *almost*

surely, is given by

$$\bar{\Psi} = \frac{1}{M}\sum_{k=1}^{K}\frac{p_k e_k'}{(1+e_k)^2}, \tag{B.4}$$

where the $e_1, \ldots, e_K$ *form the unique positive solutions of*

$$e_i = \frac{1}{M}\mathrm{tr}\boldsymbol{\Theta}_i\mathbf{T}, \tag{B.5}$$

$$\mathbf{T} = \left(\frac{1}{M}\sum_{j=1}^{K}\frac{\boldsymbol{\Theta}_j}{1+e_j} + \alpha\mathbf{I}_M\right)^{-1} \tag{B.6}$$

and $\mathbf{e}' = [e_1', \ldots, e_K']^{\mathsf{T}}$ *reads*

$$\mathbf{e}' = (\mathbf{I}_K - \mathbf{J})^{-1}\mathbf{v}, \tag{B.7}$$

$$[\mathbf{J}]_{ij} = \frac{\frac{1}{M}\mathrm{tr}\boldsymbol{\Theta}_i\mathbf{T}\boldsymbol{\Theta}_j\mathbf{T}}{M(1+e_j)^2}, \tag{B.8}$$

$$\mathbf{v} = \left[\frac{1}{M}\mathrm{tr}\boldsymbol{\Theta}_1\mathbf{T}^2, \ldots, \frac{1}{M}\mathrm{tr}\boldsymbol{\Theta}_K\mathbf{T}^2\right]^{\mathsf{T}}. \tag{B.9}$$

Proof of Lemma B.1. Ψ can be rewritten as

$$\Psi = \sum_{k=1}^{K} p_k \hat{\mathbf{h}}_k^{\mathsf{H}}\left(\hat{\mathbf{H}}^{\mathsf{H}}\hat{\mathbf{H}} + M\alpha\mathbf{I}_M\right)^{-2}\hat{\mathbf{h}}_k \overset{(a)}{=} \frac{1}{M}\sum_{k=1}^{K} p_k \frac{\hat{\mathbf{z}}_k^{\mathsf{H}}\boldsymbol{\Theta}_k^{1/2}\mathbf{C}_{[k]}^{-2}\boldsymbol{\Theta}_k^{1/2}\hat{\mathbf{z}}_k}{\left(1+\hat{\mathbf{z}}_k^{\mathsf{H}}\boldsymbol{\Theta}_k^{1/2}\mathbf{C}_{[k]}^{-1}\boldsymbol{\Theta}_k^{1/2}\hat{\mathbf{z}}_k\right)^2}, \tag{B.10}$$

where we used the definitions (B.2) and (B.1) and in (a) we applied Lemma F.1 twice together with (1.14). For M large and under Assumptions 3.1, we apply Lemma F.4 and obtain

$$\Psi - \frac{1}{M}\sum_{k=1}^{K} p_k \frac{\frac{1}{M}\mathrm{tr}\boldsymbol{\Theta}_k\mathbf{C}_{[k]}^{-2}}{\left(1+\frac{1}{M}\mathrm{tr}\boldsymbol{\Theta}_k\mathbf{C}_{[k]}^{-1}\right)^2} \overset{M\to\infty}{\longrightarrow} 0$$

$$\overset{(b)}{\Leftrightarrow} \Psi - \frac{1}{M}\sum_{k=1}^{K} p_k \frac{m'_{\boldsymbol{\Gamma},\boldsymbol{\Theta}_k}(-\alpha)}{\left(1+m_{\boldsymbol{\Gamma},\boldsymbol{\Theta}_k}(-\alpha)\right)^2} \overset{M\to\infty}{\longrightarrow} 0,$$

almost surely, where in (b) we applied Lemma F.6, the definition (2.7) and denoted $m'_{\boldsymbol{\Gamma},\boldsymbol{\Theta}_k}(-\alpha)$ the derivative of $m_{\boldsymbol{\Gamma},\boldsymbol{\Theta}_k}(z)$ along z at $z=-\alpha$. Applying Theorem 2.1 to $m_{\boldsymbol{\Gamma},\boldsymbol{\Theta}_k}(z)$, we obtain

$$m_{\boldsymbol{\Gamma},\boldsymbol{\Theta}_k}(-\alpha) - \frac{1}{M}\mathrm{tr}\boldsymbol{\Theta}_k\mathbf{T} \overset{M\to\infty}{\longrightarrow} 0, \tag{B.11}$$

almost surely, and further

$$m'_{\boldsymbol{\Gamma},\boldsymbol{\Theta}_k}(-\alpha) - \frac{1}{M}\mathrm{tr}\boldsymbol{\Theta}_k\mathbf{T}' \overset{M\to\infty}{\longrightarrow} 0, \tag{B.12}$$

almost surely, where $\mathbf{T}$ is defined in (3.77) and $\mathbf{T}'$ is given by

$$\mathbf{T}' = \mathbf{T}\left[\frac{1}{M}\sum_{j=1}^{K}\frac{\boldsymbol{\Theta}_j e_j'}{(1+e_j)^2} + \mathbf{I}_M\right]\mathbf{T}. \tag{B.13}$$

Define $\mathbf{e}' = [e_1', \ldots, e_K']^{\mathsf{T}}$ with $e_i' = \frac{1}{M}\mathrm{tr}\boldsymbol{\Theta}_i\mathbf{T}'$. The system of K equations formed by the e_i' takes the form $\mathbf{e}' = \mathbf{J}\mathbf{e}' + \mathbf{v}$ and the explicit solution $\mathbf{e}'$ is given in (B.7). Substituting $m_{\mathbf{\Gamma},\boldsymbol{\Theta}_k}(-\alpha)$ and $m'_{\mathbf{\Gamma},\boldsymbol{\Theta}_k}(-\alpha)$ by their respective deterministic equivalents e_k and e_k', we obtain $\bar{\Psi}$ in (B.1) such that $\Psi - \bar{\Psi} \overset{M\to\infty}{\longrightarrow} 0$, almost surely, which completes the proof. □

B.2 Deterministic Equivalent for $\mathbf{h}_k^{\mathsf{H}}\hat{\mathbf{W}}\hat{\mathbf{h}}_k$

Lemma B.2. *Let $\Phi_k = \mathbf{h}_k^{\mathsf{H}}\hat{\mathbf{W}}\hat{\mathbf{h}}_k$ and let Assumption 3.1 hold true. Then, a deterministic equivalent $\bar{\Phi}_k$ such that $\Phi_k - \bar{\Phi}_k \overset{M\to\infty}{\longrightarrow} 0$, almost surely, is given by*

$$\bar{\Phi}_k = \sqrt{1-\tau_k^2}\frac{e_k}{1+e_k}, \tag{B.14}$$

where e_k is given in (3.76).

Proof of Lemma B.2. Similar to the derivations in the proof of Lemma B.1, we have

$$\begin{aligned}\Phi_k &= \frac{\mathbf{z}_k^{\mathsf{H}}\boldsymbol{\Theta}_k^{1/2}\mathbf{C}_{[k]}^{-1}\boldsymbol{\Theta}_k^{1/2}\hat{\mathbf{z}}_k}{1+\hat{\mathbf{z}}_k^{\mathsf{H}}\boldsymbol{\Theta}_k^{1/2}\mathbf{C}_{[k]}^{-1}\boldsymbol{\Theta}_k^{1/2}\hat{\mathbf{z}}_k} \\ &= \frac{\sqrt{1-\tau_k^2}\mathbf{z}_k^{\mathsf{H}}\boldsymbol{\Theta}_k^{1/2}\mathbf{C}_{[k]}^{-1}\boldsymbol{\Theta}_k^{1/2}\mathbf{z}_k}{1+\hat{\mathbf{z}}_k^{\mathsf{H}}\boldsymbol{\Theta}_k^{1/2}\mathbf{C}_{[k]}^{-1}\boldsymbol{\Theta}_k^{1/2}\hat{\mathbf{z}}_k} + \frac{\tau_k\hat{\mathbf{z}}_k^{\mathsf{H}}\boldsymbol{\Theta}_k^{1/2}\mathbf{C}_{[k]}^{-1}\boldsymbol{\Theta}_k^{1/2}\mathbf{e}_k}{1+\hat{\mathbf{z}}_k^{\mathsf{H}}\boldsymbol{\Theta}_k^{1/2}\mathbf{C}_{[k]}^{-1}\boldsymbol{\Theta}_k^{1/2}\hat{\mathbf{z}}_k}.\end{aligned}$$

Since $\mathbf{e}_k$ and $\mathbf{z}_k$ are independent, we apply Lemma F.5 together with Lemma F.4 and F.6 and obtain $\bar{\Phi}_k$, such that $\Phi_k - \bar{\Phi}_k \overset{M\to\infty}{\longrightarrow} 0$, almost surely, as

$$\bar{\Phi}_k = \sqrt{1-\tau_k^2}\frac{e_k}{1+e_k},$$

which completes the proof. □

B.3 Deterministic Equivalent for $\mathbf{h}_k^{\mathsf{H}}\hat{\mathbf{W}}\hat{\mathbf{H}}_{[k]}^{\mathsf{H}}\mathbf{P}_{[k]}\hat{\mathbf{H}}_{[k]}\hat{\mathbf{W}}\mathbf{h}_k$

Lemma B.3. *Let $P_{I,k} = \mathbf{h}_k^{\mathsf{H}}\hat{\mathbf{W}}\hat{\mathbf{H}}_{[k]}^{\mathsf{H}}\mathbf{P}_{[k]}\hat{\mathbf{H}}_{[k]}\hat{\mathbf{W}}\mathbf{h}_k$ and let Assumptions 3.1 and 3.4 hold true and let $\|\mathbf{P}\| < \infty$ uniformly on M. Then, a deterministic equivalent $\bar{P}_{I,k}$ such that $P_{I,k} - \bar{P}_{I,k} \overset{M\to\infty}{\longrightarrow} 0$, almost surely, is given by*

$$\bar{P}_{I,k} = \frac{\bar{\Upsilon}_k\left[1-\tau_k^2\left(1-(1+e_k)^2\right)\right]}{(1+e_k)^2}, \tag{B.15}$$

where e_k *is defined in* (3.76) *and* $\bar{\Upsilon}_k$ *reads*

$$\bar{\Upsilon}_k = \frac{1}{M} \sum_{j=1, j\neq k}^{K} \frac{p_j e'_{j,k}}{(1+e_j)^2} \tag{B.16}$$

with e_i *defined in* (3.76) *and* $\mathbf{e}'_k = [e'_{1,k}, \ldots, e'_{K,k}]^{\mathsf{T}}$ *reads*

$$\mathbf{e}'_k = (\mathbf{I}_K - \mathbf{J})^{-1} \mathbf{v}_k, \tag{B.17}$$

$$\mathbf{v}_k = \left[\frac{1}{M} \mathrm{tr} \boldsymbol{\Theta}_1 \mathbf{T} \boldsymbol{\Theta}_k \mathbf{T}, \ldots, \frac{1}{M} \mathrm{tr} \boldsymbol{\Theta}_K \mathbf{T} \boldsymbol{\Theta}_k \mathbf{T} \right]^{\mathsf{T}}, \tag{B.18}$$

where $\mathbf{J}$ *and* $\mathbf{T}$ *are defined in* (B.8) *and* (B.6)*, respectively.*

Proof of Lemma B.3. With (1.8) and $\mathbf{C} \triangleq \boldsymbol{\Gamma} + \alpha \mathbf{I}_M$, $\boldsymbol{\Gamma} \triangleq \frac{1}{M} \hat{\mathbf{H}}^{\mathsf{H}} \hat{\mathbf{H}}$, we have

$$\begin{aligned} P_{I,k} &= \frac{1}{M} \mathbf{z}_k^{\mathsf{H}} \boldsymbol{\Theta}_k^{1/2} \mathbf{C}^{-1} \hat{\mathbf{H}}_{[k]}^{\mathsf{H}} \mathbf{P}_{[k]} \hat{\mathbf{H}}_{[k]} \mathbf{C}^{-1} \boldsymbol{\Theta}_k^{1/2} \mathbf{z}_k \\ &= \frac{1}{M} \mathbf{z}_k^{\mathsf{H}} \boldsymbol{\Theta}_k^{1/2} \mathbf{C}_{[k]}^{-1} \hat{\mathbf{H}}_{[k]}^{\mathsf{H}} \mathbf{P}_{[k]} \hat{\mathbf{H}}_{[k]} \mathbf{C}^{-1} \boldsymbol{\Theta}_k^{1/2} \mathbf{z}_k \\ &+ \frac{1}{M} \mathbf{z}_k^{\mathsf{H}} \boldsymbol{\Theta}_k^{1/2} \left[\mathbf{C}^{-1} - \mathbf{C}_{[k]}^{-1} \right] \hat{\mathbf{H}}_{[k]}^{\mathsf{H}} \mathbf{P}_{[k]} \hat{\mathbf{H}}_{[k]} \mathbf{C}^{-1} \boldsymbol{\Theta}_k^{1/2} \mathbf{z}_k. \end{aligned} \tag{B.19}$$

Substituting $\mathbf{C}^{-1} - \mathbf{C}_{[k]}^{-1} = -\mathbf{C}^{-1}(\mathbf{C} - \mathbf{C}_{[k]})\mathbf{C}_{[k]}^{-1}$ with $\mathbf{C} - \mathbf{C}_{[k]} = \boldsymbol{\Theta}_k^{1/2}(c_0 \mathbf{z}_k \mathbf{z}_k^{\mathsf{H}} + c_1 \mathbf{e}_k \mathbf{e}_k^{\mathsf{H}} + c_2 \mathbf{z}_k \mathbf{e}_k^{\mathsf{H}} + c_2 \mathbf{e}_k \mathbf{z}_k^{\mathsf{H}}) \boldsymbol{\Theta}_k^{1/2}$, where $c_0 \triangleq 1 - \tau_k^2$, $c_1 \triangleq \tau_k^2$ and $c_2 \triangleq \tau_k \sqrt{1-\tau_k^2}$ into (B.19), we obtain a sum of five terms

$$\begin{aligned} P_{I,k} =& \frac{1}{M} \mathbf{z}_k^{\mathsf{H}} \mathbf{B}_k \mathbf{z}_k - \frac{c_0}{M} \mathbf{z}_k^{\mathsf{H}} \mathbf{A}_k \mathbf{z}_k \mathbf{z}_k^{\mathsf{H}} \mathbf{B}_k \mathbf{z}_k - \frac{c_1}{M} \mathbf{z}_k^{\mathsf{H}} \mathbf{A}_k \mathbf{e}_k \mathbf{e}_k^{\mathsf{H}} \mathbf{B}_k \mathbf{z}_k \\ &- \frac{c_2}{M} \mathbf{z}_k^{\mathsf{H}} \mathbf{A}_k \mathbf{z}_k \mathbf{e}_k^{\mathsf{H}} \mathbf{B}_k \mathbf{z}_k - \frac{c_2}{M} \mathbf{z}_k^{\mathsf{H}} \mathbf{A}_k \mathbf{e}_k \mathbf{z}_k^{\mathsf{H}} \mathbf{B}_k \mathbf{z}_k \end{aligned} \tag{B.20}$$

with $\mathbf{A}_k \triangleq \boldsymbol{\Theta}_k^{1/2} \mathbf{C}^{-1} \boldsymbol{\Theta}_k^{1/2}$ and $\mathbf{B}_k \triangleq \boldsymbol{\Theta}_k^{1/2} \mathbf{C}_{[k]}^{-1} \hat{\mathbf{H}}_{[k]}^{\mathsf{H}} \mathbf{P}_{[k]} \hat{\mathbf{H}}_{[k]} \mathbf{C}^{-1} \boldsymbol{\Theta}_k^{1/2}$. Noting that $c_0 + c_1 = 1$ and $c_0 c_1 - c_2^2 = 0$, we apply Lemma F.7 to each of the four quadratic forms in (B.20). Under Assumption 3.1, we obtain

$$\mathbf{z}_k^{\mathsf{H}} \mathbf{A}_k \mathbf{z}_k - \frac{u(1+c_1 u)}{1+u} \overset{M\to\infty}{\longrightarrow} 0, \quad \text{and} \quad \mathbf{z}_k^{\mathsf{H}} \mathbf{A}_k \mathbf{e}_k - \frac{-c_2 u^2}{1+u} \overset{M\to\infty}{\longrightarrow} 0,$$

almost surely, where $u = \frac{1}{M} \mathrm{tr} \boldsymbol{\Theta}_k \mathbf{C}_{[k]}^{-1}$. Moreover, under Assumptions 3.1, 3.4 and $\|\mathbf{P}\| < \infty$ uniformly on M, we have

$$\mathbf{z}_k^{\mathsf{H}} \mathbf{B}_k \mathbf{z}_k - \frac{u'(1+c_1 u)}{1+u} \overset{M\to\infty}{\longrightarrow} 0, \quad \text{and} \quad \mathbf{e}_k^{\mathsf{H}} \mathbf{B}_k \mathbf{z}_k - \frac{-c_2 u u'}{1+u} \overset{M\to\infty}{\longrightarrow} 0,$$

almost surely, where $u' = \frac{1}{M}\text{tr}\mathbf{P}_{[k]}\hat{\mathbf{H}}_{[k]}\mathbf{C}_{[k]}^{-1}\mathbf{\Theta}_k\mathbf{C}_{[k]}^{-1}\hat{\mathbf{H}}_{[k]}^{\mathsf{H}}$. Substituting the random terms in (B.20) by their respective deterministic equivalents yields

$$P_{I,k} - \Bigg[\frac{1}{M}\frac{u'(1+c_1u)}{1+u} - \frac{1}{M}\frac{c_0(1+c_1u)^2 - c_1c_2^2u^2 - 2c_2^2u}{(1+u)^2}uu'\Bigg] \overset{M\to\infty}{\longrightarrow} 0 \tag{B.21}$$

almost surely. The second term in brackets of (B.21) reduces to $\frac{1}{M}\frac{1-\tau_k^2}{(1+u)^2}uu'$ and we obtain

$$\mathbf{h}_k^{\mathsf{H}}\hat{\mathbf{W}}\hat{\mathbf{H}}_{[k]}^{\mathsf{H}}\mathbf{P}_{[k]}\hat{\mathbf{H}}_{[k]}\hat{\mathbf{W}}\mathbf{h}_k - \frac{1}{M}\frac{1-\tau_k^2\left[1-(1+u)^2\right]}{(1+u)^2}u' \overset{M\to\infty}{\longrightarrow} 0 \tag{B.22}$$

almost surely. From Lemma F.6 we have

$$u - m_{\mathbf{\Gamma},\mathbf{\Theta}_k}(-\alpha) \overset{M\to\infty}{\longrightarrow} 0 \quad \text{and} \quad \frac{1}{M}u' - \Upsilon_k \overset{M\to\infty}{\longrightarrow} 0,$$

almost surely, where $m_{\mathbf{\Gamma},\mathbf{\Theta}_k}(-\alpha) = \frac{1}{M}\text{tr}\mathbf{\Theta}_k\mathbf{C}^{-1}$ and

$$\Upsilon_k = \frac{1}{M^2}\text{tr}\mathbf{P}_{[k]}\hat{\mathbf{H}}_{[k]}\mathbf{C}^{-1}\mathbf{\Theta}_k\mathbf{C}^{-1}\hat{\mathbf{H}}_{[k]}^{\mathsf{H}}.$$

Note that we choose not to approximate $\mathbf{P}_{[k]}$ by $\mathbf{P}$ since the power p_k can be significant. Therefore, (B.22) becomes

$$P_{I,k} - \frac{\Upsilon_k\left[1-\tau_k^2\left(1-(1+m_{\mathbf{\Gamma},\mathbf{\Theta}_k}(-\alpha))^2\right)\right]}{(1+m_{\mathbf{\Gamma},\mathbf{\Theta}_k}(-\alpha))^2} \overset{M\to\infty}{\longrightarrow} 0,$$

almost surely. We rewrite Υ_k as

$$\Upsilon_k = \frac{1}{M}\sum_{j=1,j\neq k}^{K} p_j\hat{\mathbf{z}}_j^{\mathsf{H}}\mathbf{\Theta}_j^{1/2}\mathbf{C}^{-1}\mathbf{\Theta}_k\mathbf{C}^{-1}\mathbf{\Theta}_j^{1/2}\hat{\mathbf{z}}_j.$$

Applying Lemmas F.1, F.4 and F.6, we obtain almost surely

$$\Upsilon_k - \frac{1}{M}\sum_{j=1,j\neq k}^{K} p_j\frac{\frac{1}{M}\text{tr}\mathbf{\Theta}_j\mathbf{C}^{-1}\mathbf{\Theta}_k\mathbf{C}^{-1}}{\left[1+\frac{1}{M}\text{tr}\mathbf{\Theta}_j\left(\mathbf{\Gamma}+\alpha\mathbf{I}_M\right)^{-1}\right]^2} \overset{M\to\infty}{\longrightarrow} 0.$$

A deterministic equivalent e_i of $m_{\mathbf{\Gamma},\mathbf{\Theta}_i}(-\alpha) = \frac{1}{M}\text{tr}\mathbf{\Theta}_i\left(\mathbf{\Gamma}+\alpha\mathbf{I}_M\right)^{-1}$ such that $m_{\mathbf{\Gamma},\mathbf{\Theta}_i}(-\alpha) - e_i \overset{M\to\infty}{\longrightarrow} 0$, almost surely is given in (3.76). To derive a deterministic equivalent for $\frac{1}{M}\text{tr}\mathbf{\Theta}_j\mathbf{C}^{-1}\mathbf{\Theta}_k\mathbf{C}^{-1}$ define $m'(\mathbf{A}) \triangleq \frac{1}{M}\text{tr}\mathbf{D}\mathbf{C}^{-1}\mathbf{A}\mathbf{C}^{-1}$ and initially assume that $\mathbf{A}$ is invertible. Denoting $\bar{\mathbf{C}} \triangleq \mathbf{A}^{-1/2}\mathbf{\Gamma}\mathbf{A}^{-1/2} + \alpha\mathbf{A}^{-1}$, we have

$$m'(\mathbf{A}) = \frac{1}{M}\text{tr}\mathbf{D}\mathbf{C}^{-1}\mathbf{A}\mathbf{C}^{-1} = \frac{1}{M}\text{tr}\mathbf{A}^{-1/2}\mathbf{D}\mathbf{A}^{-1/2}\bar{\mathbf{C}}^{-2} \tag{B.23}$$

$$= \frac{d}{dz}\frac{1}{M}\text{tr}\mathbf{D}(\mathbf{\Gamma}+\alpha\mathbf{I}_M - z\mathbf{A})^{-1} \tag{B.24}$$

at $z = 0$. Applying Theorem 2.1, we obtain

$$\frac{1}{M}\text{tr}\mathbf{D}(\mathbf{\Gamma} + \alpha\mathbf{I}_M - z\mathbf{A})^{-1} - \frac{1}{M}\text{tr}\mathbf{D}\mathbf{T}(\mathbf{A}) \overset{M\to\infty}{\longrightarrow} 0, \tag{B.25}$$

almost surely, where $\mathbf{T}(\mathbf{A})$ is given by

$$\mathbf{T}(\mathbf{A}) = \left(\frac{1}{M}\sum_{j=1}^{K}\frac{\mathbf{\Theta}_j}{1+e_j} + \alpha\mathbf{I}_M - z\mathbf{A}\right)^{-1} \tag{B.26}$$

and the $e_1, \ldots, e_K$ are the unique positive solution of $e_i = \frac{1}{M}\mathbf{\Theta}_i\mathbf{T}(\mathbf{A})$. By differentiating along z we have

$$\frac{1}{M}\text{tr}\mathbf{D}\mathbf{C}^{-1}\mathbf{A}\mathbf{C}^{-1} - \frac{1}{M}\text{tr}\mathbf{D}\mathbf{T}'(\mathbf{A}) \overset{M\to\infty}{\longrightarrow} 0, \tag{B.27}$$

almost surely, where $\mathbf{T}'(\mathbf{A}) = \frac{d}{dz}\mathbf{T}(\mathbf{A})$ is given by

$$\mathbf{T}'(\mathbf{A}) = \mathbf{T}(\mathbf{A})\left[\frac{1}{M}\sum_{j=1}^{K}\frac{\mathbf{\Theta}_j e_j'}{(1+e_j)^2} + \mathbf{A}\right]\mathbf{T}(\mathbf{A}) \tag{B.28}$$

and the $e_1', \ldots, e_K'$ are the unique positive solution of $e_i' = \frac{1}{M}\mathbf{\Theta}_i\mathbf{T}'(\mathbf{A})$. Define $\mathbf{e}' = [e_1', \ldots, e_K']^{\mathsf{T}}$ and $\mathbf{J}(\mathbf{A})$ and $\mathbf{v}(\mathbf{A})$ as

$$[\mathbf{J}(\mathbf{A})]_{ij} = \frac{\frac{1}{M}\text{tr}\mathbf{\Theta}_i\mathbf{T}(\mathbf{A})\mathbf{\Theta}_j\mathbf{T}(\mathbf{A})}{M(1+e_j)^2} \tag{B.29}$$

$$\mathbf{v}(\mathbf{A}) = \left[\frac{1}{M}\text{tr}\mathbf{\Theta}_1\mathbf{T}(\mathbf{A})\mathbf{A}\mathbf{T}(\mathbf{A}), \ldots, \frac{1}{M}\text{tr}\mathbf{\Theta}_K\mathbf{T}(\mathbf{A})\mathbf{A}\mathbf{T}(\mathbf{A})\right]^{\mathsf{T}}. \tag{B.30}$$

Therefore, $\mathbf{e}'$ is given explicitly as

$$\mathbf{e}' = (\mathbf{I}_K - \mathbf{J}(\mathbf{A}))^{-1}\mathbf{v}(\mathbf{A}). \tag{B.31}$$

Note that $\mathbf{I}_K - \mathbf{J}(\mathbf{A})$ is always invertible since $\mathbf{e}'$ is a unique positive solution. The authors in [28] proved that the convergence in (B.27) also holds for non-invertible matrices $\mathbf{A}$. The proof unfolds as follows: $\mathbf{A} + \mathbf{I}_M$ is always invertible and from (B.27) we have

$$m'(\mathbf{A} + \mathbf{I}_M) - \frac{1}{M}\text{tr}\mathbf{D}\mathbf{T}'(\mathbf{A} + \mathbf{I}_M) \overset{M\to\infty}{\longrightarrow} 0, \tag{B.32}$$

almost surely. It is easy to show that

$$m'(\mathbf{A} + \mathbf{I}_M) - m'(\mathbf{A}) = m'(\mathbf{I}_M) \tag{B.33}$$

$$\frac{1}{M}\text{tr}\mathbf{D}\mathbf{T}'(\mathbf{A} + \mathbf{I}_M) - \frac{1}{M}\text{tr}\mathbf{D}\mathbf{T}'(\mathbf{A}) = \frac{1}{M}\text{tr}\mathbf{D}\mathbf{T}'(\mathbf{I}_M). \tag{B.34}$$

Therefore

$$m'(\mathbf{A}) - \frac{1}{M}\mathrm{tr}\mathbf{D}\mathbf{T}'(\mathbf{A}) \tag{B.35}$$

$$= m'(\mathbf{A}+\mathbf{I}_M) - \frac{1}{M}\mathrm{tr}\mathbf{D}\mathbf{T}'(\mathbf{A}+\mathbf{I}_M) - \left[m'(\mathbf{I}_M) - \frac{1}{M}\mathrm{tr}\mathbf{D}\mathbf{T}'(\mathbf{I}_M)\right] \overset{M\to\infty}{\longrightarrow} 0, \tag{B.36}$$

almost surely.

Thus, substituting $\mathbf{D} = \boldsymbol{\Theta}_i$ and $\mathbf{A} = \boldsymbol{\Theta}_k$ we have,

$$\frac{1}{M}\mathrm{tr}\boldsymbol{\Theta}_j\mathbf{C}^{-1}\boldsymbol{\Theta}_k\mathbf{C}^{-1} - \frac{1}{M}\mathrm{tr}\boldsymbol{\Theta}_i\mathbf{T}'(\boldsymbol{\Theta}_k) \overset{M\to\infty}{\longrightarrow} 0, \tag{B.37}$$

almost surely. For $z = 0$, we obtain $\mathbf{T}(\boldsymbol{\Theta}_k) = \mathbf{T}$ defined in (B.6), it follows that $\mathbf{J}(\boldsymbol{\Theta}_k) = \mathbf{J}$ in (B.8) and $\mathbf{v}(\boldsymbol{\Theta}_k) = \mathbf{v}_k$ in (B.18). Moreover, defining $e'_{i,k} = \frac{1}{M}\mathrm{tr}\boldsymbol{\Theta}_i\mathbf{T}'(\boldsymbol{\Theta}_k)$, the $\mathbf{e}'_k = [e'_{1,k}, \ldots, e'_{K,k}]^{\mathsf{T}}$ are given in (B.17). Finally, substituting $m_{\boldsymbol{\Gamma},\boldsymbol{\Theta}_j}(-\alpha)$ and $\frac{1}{M}\mathrm{tr}\boldsymbol{\Theta}_j\mathbf{C}^{-1}\boldsymbol{\Theta}_k\mathbf{C}^{-1}$ by their respective deterministic equivalents e_j and $e'_{j,k}$, we obtain $\bar{\Upsilon}_k$ in (B.16) such that $\Upsilon_k - \bar{\Upsilon}_k \overset{M\to\infty}{\longrightarrow} 0$, almost surely, which completes the proof. □

C Proof of Theorem 3.4

We bound $|\gamma_{k,\mathrm{zf}} - \bar{\gamma}_{k,\mathrm{zf}}|$ by adding and subtracting $\gamma_{k,\mathrm{rzf}}(\alpha)$ and $\bar{\gamma}_{k,\mathrm{rzf}}(\alpha)$ and applying the triangle inequality. We obtain

$$|\gamma_{k,\mathrm{zf}} - \bar{\gamma}_{k,\mathrm{zf}}| \leq |\gamma_{k,\mathrm{zf}} - \gamma_{k,\mathrm{rzf}}(\alpha)| + |\gamma_{k,\mathrm{rzf}}(\alpha) - \bar{\gamma}_{k,\mathrm{rzf}}(\alpha)| + |\bar{\gamma}_{k,\mathrm{rzf}}(\alpha) - \bar{\gamma}_{k,\mathrm{zf}}|. \tag{C.1}$$

To show that $|\gamma_{k,\mathrm{zf}} - \bar{\gamma}_{k,\mathrm{zf}}| \to 0$ almost surely as $M, K \to \infty$, take $\varepsilon > 0$ arbitrarily small. For $\alpha > 0$ small enough, we will demonstrate that $|\gamma_{k,\mathrm{zf}} - \gamma_{k,\mathrm{rzf}}(\alpha)| < \frac{\varepsilon}{3}$ almost surely and $|\bar{\gamma}_{k,\mathrm{rzf}}(\alpha) - \bar{\gamma}_{k,\mathrm{zf}}| < \frac{\varepsilon}{3}$ independently of M and K. Furthermore, we show that for M, K large enough, $|\gamma_{k,\mathrm{rzf}}(\alpha) - \bar{\gamma}_{k,\mathrm{rzf}}(\alpha)| < \frac{\varepsilon}{3}$ almost surely, from which we conclude that (C.1) can be made as small as desired.

In order to prove that $|\gamma_{k,\mathrm{zf}} - \gamma_{k,\mathrm{rzf}}(\alpha)| < \frac{\varepsilon}{3}$ for α small enough, it suffices to study the matrices $\hat{\mathbf{W}} = (\hat{\mathbf{H}}^{\mathsf{H}}\hat{\mathbf{H}} + M\alpha\mathbf{I}_M)^{-1}$ and $\underline{\hat{\mathbf{W}}} = \hat{\mathbf{H}}^{\mathsf{H}}(\hat{\mathbf{H}}\hat{\mathbf{H}}^{\mathsf{H}})^{-2}\hat{\mathbf{H}}$ in the SINR of RZF precoding (3.74) and ZF precoding (3.85). Applying the matrix inversion lemma, $\hat{\mathbf{W}}$ takes the form

$$\hat{\mathbf{W}} = \hat{\mathbf{H}}^{\mathsf{H}}(\hat{\mathbf{H}}\hat{\mathbf{H}}^{\mathsf{H}} + M\alpha\mathbf{I}_K)^{-2}\hat{\mathbf{H}} + M\alpha(\hat{\mathbf{H}}^{\mathsf{H}}\hat{\mathbf{H}} + M\alpha\mathbf{I}_M)^{-2}.$$

Under Assumption 3.5, $\lambda_{\min}(\hat{\mathbf{H}}\hat{\mathbf{H}}^{\mathsf{H}}) > \varepsilon > 0$ and, since $\lambda_{\max}(\hat{\mathbf{H}}\hat{\mathbf{H}}^{\mathsf{H}})$ is almost surely bounded for all large M, K, for any continuous functional $f(\hat{\mathbf{W}})$ we have $|f(\hat{\mathbf{W}}) - f(\underline{\hat{\mathbf{W}}})| \overset{\alpha\to 0}{\longrightarrow} 0$ with probability one. Therefore, $|\gamma_{k,\mathrm{zf}} - \gamma_{k,\mathrm{rzf}}(\alpha)| \overset{\alpha\to 0}{\longrightarrow} 0$ uniformly on M, K almost surely.

From Theorem 3.3, we have immediately that for any $\alpha > 0$, $|\gamma_{k,\mathrm{rzf}}(\alpha) - \bar{\gamma}_{k,\mathrm{rzf}}(\alpha)| \overset{M\to\infty}{\longrightarrow} 0$ almost surely.

In order to prove $|\bar{\gamma}_{k,\mathrm{rzf}}(\alpha) - \bar{\gamma}_{k,\mathrm{zf}}| < \frac{\varepsilon}{3}$ for α small enough, uniformly on M, rewrite $\bar{\gamma}_{k,\mathrm{rzf}}(\alpha)$ as

$$\bar{\gamma}_{k,\mathrm{rzf}}(\alpha) = \frac{p_k(1-\tau_k^2)\left(\alpha e_k\right)^2}{\bar{\Upsilon}_{k,\mathrm{rzf}}(\alpha^2 - \tau_k^2[\alpha^2 - (\alpha+\alpha e_k)^2]) + \frac{\bar{\Psi}_{\mathrm{rzf}}}{\rho}(\alpha+\alpha e_k)^2}. \tag{C.2}$$

To show that $\bar{\gamma}_{k,\mathrm{zf}} = \lim_{\alpha\to 0}\bar{\gamma}_{k,\mathrm{rzf}}(\alpha)$, we need to verify that the limit $\alpha \to 0$ of both numerator and denominator in (C.2) exists and that the denominator is uniformly bounded away from zero. Define $\underline{e}_i = \lim_{\alpha\to 0}\alpha e_i(\alpha)$. Under Assumption 3.6, all $\underline{e}_i$ exist and are strictly positive. Since $\alpha e_i(\alpha)$ is holomorphic for $\alpha > 0$, and is bounded away from zero in a neighborhood of zero, by continuity extension in $\alpha = 0$, we obtain the limit $\alpha \to 0$ as

$$\begin{aligned}
\underline{e}_i &= \lim_{\alpha\to 0}\left\{\frac{1}{M}\mathrm{tr}\boldsymbol{\Theta}_i\left(\frac{1}{M}\sum_{j=1}^{K}\frac{\boldsymbol{\Theta}_j}{\alpha+\alpha e_j(\alpha)} + \mathbf{I}_M\right)^{-1}\right\} \\
\underline{e}_i &= \frac{1}{M}\mathrm{tr}\boldsymbol{\Theta}_i\underline{\mathbf{T}},
\end{aligned} \tag{C.3}$$

where $\underline{\mathbf{T}}$ is given in (3.90). It is easy to verify that $\underline{e} \triangleq \sup_i \underline{e}_i$ is uniformly bounded on M. We have

$$|\underline{e}| \le \sup_i \|\boldsymbol{\Theta}_i\|. \tag{C.4}$$

Define $\underline{\mathbf{e}} \triangleq [\underline{e}_1, \ldots, \underline{e}_K]^{\mathsf{T}}$, $f_i : \underline{\mathbf{e}} \mapsto \frac{1}{M}\mathrm{tr}\boldsymbol{\Theta}_i\underline{\mathbf{T}}(\underline{\mathbf{e}})$ and $\mathbf{f}(\underline{\mathbf{e}}) = [f_1(\underline{\mathbf{e}}), \ldots, f_K(\underline{\mathbf{e}})]^{\mathsf{T}}$. Under Assumption 3.6, there exists a fixed point $\mathbf{f}(\underline{\mathbf{e}}^*) = \underline{\mathbf{e}}^*$, where $\underline{\mathbf{e}}^* \triangleq [\underline{e}_1^*, \ldots, \underline{e}_K^*]^{\mathsf{T}}$ with $\underline{e}_i^* > 0\ \forall i$. In this case, we can extend the results in [55][1] and show that the iterative fixed point algorithm defined by $\underline{\mathbf{e}}^{(n+1)} = \mathbf{f}(\underline{\mathbf{e}}^{(n)})$, $(n \ge 0)$, converges to the unique positive solution $\underline{\mathbf{e}}^*$ for any initial point $\underline{\mathbf{e}}^{(0)}$, $\underline{e}_i^{(0)} > 0\ \forall i$.

Furthermore, we need to show that both $\bar{\Upsilon}_{k,\mathrm{zf}} = \lim_{\alpha\to 0}\bar{\Upsilon}_{k,\mathrm{rzf}}$ and $\bar{\Psi}_{\mathrm{zf}} = \lim_{\alpha\to 0}\bar{\Psi}_{\mathrm{rzf}}$ exist and are uniformly bounded on M. Observe that

$$\lim_{\alpha\to 0}\alpha^2 e_i' = \underline{e}_i \tag{C.5}$$

and we obtain

$$\bar{\Psi}_{\mathrm{zf}} = \lim_{\alpha\to 0}\frac{1}{M}\sum_{j=1}^{K} p_j\frac{\alpha^2 e_j'}{(\alpha+\alpha e_j)^2} = \frac{1}{M}\sum_{j=1}^{K}\frac{p_j}{\underline{e}_j}. \tag{C.6}$$

[1]Since $\mathbf{f}(\underline{\mathbf{e}})$ can be extended by continuity in zero, where it satisfies $\mathbf{f}(0) = 0$, the positivity property of $\mathbf{f}(\underline{\mathbf{e}})$, defined in [55], does not hold. We precisely need to show that $\underline{\mathbf{e}}^{(n+1)} = \mathbf{f}(\underline{\mathbf{e}}^{(n)})$ can not converge to the fixed point 0, which unfolds from Assumption 3.6 with similar arguments as in [55].

Therefore, $0 < \bar{\Psi}_{\mathrm{zf}} < \infty$ for all $\underline{e}_i > 0$. Similarly, define $\underline{e}'_{j,k} = \lim_{\alpha\to 0} \alpha^2 e'_{j,k}$ given in (3.91) and thus

$$\bar{\Upsilon}_{k,\mathrm{zf}} = \lim_{\alpha\to 0} \frac{1}{M} \sum_{j=1, j\neq k}^{K} p_j \frac{\alpha^2 e'_{j,k}}{(\alpha + \alpha e_j)^2} = \frac{1}{M} \sum_{j=1, j\neq k}^{K} p_j \frac{\underline{e}'_{j,k}}{\underline{e}_j^2},$$

satisfying $0 < \bar{\Upsilon}_{k,\mathrm{zf}} < \infty$ for all $\underline{e}_i > 0$. To fulfill the constraints $\underline{e}_i > 0$, we have to evoke Assumption 3.5. The limit $\bar{\gamma}_{k,\mathrm{zf}} = \lim_{\alpha\to 0} \bar{\gamma}_{k,\mathrm{rzf}}(\alpha)$ is given by (3.87), which completes the proof.

D Proof of Proposition 4.1

The proof is inspired by [27] with adaptations to account for imperfect CSIT. From Corollary 3.7 with $p_k = P/K \ \forall k$ and $\tau_k = \tau \ \forall k$, for large M, K, the SINR $\bar{\gamma}_{\mathrm{rzf}}$ takes the form

$$\bar{\gamma}_{\mathrm{rzf}} = \rho\beta e(1-\tau^2)\Gamma,$$

where

$$\Gamma = \frac{\frac{1}{\beta} e_{22} + \alpha(1+e)^2 e_{12}}{\rho e_{22}(1-\tau^2) + \tau^2\rho(1+e)^2 e_{22} + (1+e)^2 e_{12}}$$

with e and e_{ij} defined in (3.79) and (3.81), respectively. Taking the derivative along α, we obtain

$$\frac{\partial \bar{\gamma}_{\mathrm{rzf}}}{\partial \alpha} = \rho\beta e(1-\tau^2)\Gamma \left[\frac{e'}{e} + \frac{\Gamma'}{\Gamma}\right], \tag{D.1}$$

where

$$e' = -\frac{(1+e)^2 e_{12}}{1 - \frac{e_{22}}{\beta}}. \tag{D.2}$$

and thus, together with (3.82), we have

$$\frac{e'}{e} = -\frac{(1+e)^2 e_{12}}{\frac{1}{\beta} e_{22} + \alpha(1+e)^2 e_{12}}.$$

Therefore, (D.1) becomes

$$\begin{aligned}
\frac{\partial \bar{\gamma}_{\mathrm{rzf}}}{\partial \alpha} &= \rho\beta e(1-\tau^2)\Gamma \\
&\quad \times \left[\frac{2\alpha(1+e)e' e_{12} + \alpha(1+e)^2 e'_{12} + \frac{1}{\beta} e'_{22}}{\frac{1}{\beta} e_{22} + \alpha(1+e)^2 e_{12}}\right. \\
&\quad - \frac{[1-\tau^2+\tau^2(1+e)^2]\rho e'_{22} + 2\tau^2\rho(1+e)e' e_{22}}{[1-\tau^2+\tau^2(1+e)^2]\rho e_{22} + (1+e)^2 e_{12}} \\
&\quad \left. - \frac{2(1+e)e' e_{12} + (1+e)^2 e'_{12}}{[1-\tau^2+\tau^2(1+e)^2]\rho e_{22} + (1+e)^2 e_{12}}\right].
\end{aligned} \tag{D.3}$$

Denoting $\chi \triangleq (1+e)^2 e_{12}$, $\psi \triangleq 2(1+e)e'e_{12}+(1+e)^2 e'_{12}$ and $\phi \triangleq 1-\tau^2+\tau^2(1+e)^2$, (D.3) takes the form

$$\begin{aligned}\frac{\partial \bar{\gamma}_{\mathrm{rzf}}}{\partial \alpha} &= \rho\beta e(1-\tau^2)\Gamma \\ &\quad \times \left[\frac{\frac{1}{\beta}e'_{22}+\alpha\psi}{\frac{1}{\beta}e_{22}+\alpha\chi} - \frac{\rho\phi e'_{22}+\psi+2\tau^2\rho(1+e)e'e_{22}}{\rho\phi e_{22}+\chi}\right] \\ &= \frac{\phi\rho^2\beta e(1-\tau^2)\Gamma}{Z}\left[\left(\alpha-\frac{1}{\beta\rho\phi}\right)(e_{22}\psi - e'_{22}\chi)\right. \\ &\quad \left. - \frac{2\tau^2(1+e)e'e_{22}[\frac{e_{22}}{\beta}+\alpha\chi]}{\phi}\right],\end{aligned}$$

where $Z = (\frac{1}{\beta}e_{22}+\alpha\chi)(\rho\phi e_{22}+\chi)$. Denoting

$$\begin{aligned}\Omega &\triangleq \frac{2\phi\rho^2\beta e(1-\tau^2)(1+e)e'e_{12}e_{22}\Gamma}{Z} \\ \nu &\triangleq \frac{(1+e)^2[e'_{12}e_{22}-e_{12}e'_{22}]}{2(1+e)e'e_{12}e_{22}},\end{aligned} \tag{D.4}$$

we obtain

$$\frac{\partial \bar{\gamma}_{\mathrm{rzf}}}{\partial \alpha} = \Omega\left[\left(\alpha-\frac{1}{\beta\rho\phi}\right)(1+\nu) - \frac{\tau^2[\frac{e_{22}}{\beta}+\alpha\chi]}{\phi e_{12}}\right]. \tag{D.5}$$

Rewriting the term in brackets in (D.5), we have

$$\frac{\partial \bar{\gamma}_{\mathrm{rzf}}}{\partial \alpha} = \Omega\left[\alpha - \frac{[1+\nu+\tau^2\rho\frac{e_{22}}{e_{12}}]\frac{1}{\beta\rho}}{(1-\tau^2)(1+\nu)+\tau^2\nu(1+e)^2}\right] = 0.$$

Since $\Omega \neq 0$ for $\rho > 0$ and $\tau^2 < 1$, the optimal regularization parameter $\bar{\alpha}^\star$ is given by (4.2). Substituting (D.2) into (D.4), the term ν takes the form

$$\nu = \frac{1-\frac{e_{22}}{\beta}}{2(1+e)e_{12}}\frac{e'_{12}}{e_{22}}\left[\frac{e'_{22}}{e'_{12}} - \frac{e_{22}}{e_{12}}\right]. \tag{D.6}$$

With (3.82) and (D.2), we obtain $e'_{12} = \frac{-2e_{13}}{1-e_{22}/\beta}$ and $e'_{22} = \frac{-2e_{23}}{1-e_{22}/\beta}$. Substituting these terms into (D.6) yields (4.3), which completes the proof.

E Alternative Proof of Proposition 4.1 for Uncorrelated Channels

For $\mathbf{\Theta}_k = \mathbf{I}_M$, e in (3.84) is the Stieltjes transform of the Marčenko-Pastur law[2] in $z = -\alpha$ and reads [20, Example 2.8]

$$e = \frac{\beta(1-\alpha) - 1 + \sqrt{\alpha^2\beta^2 + 2\alpha\beta(1+\beta) + (1-\beta)^2}}{2\alpha\beta}. \tag{E.1}$$

Furthermore, for $p_k = P/K \ \forall k$, from Corollary 3.7 we have $e_{11} = e_{22} = \frac{(1+e)^2}{e^2}$ and therefore

$$\bar{\Psi}_{\mathrm{rzf}} = \bar{\Upsilon}_{k,\mathrm{rzf}} = \frac{\frac{P}{K}e^2}{\beta(1+e)^2 - e^2}. \tag{E.2}$$

Substituting (E.1) and (E.2) into the SINR (3.75) with $\tau_k = \tau \ \forall k$, we obtain

$$\bar{\gamma}_{k,\mathrm{rzf}} = \bar{\gamma}_{\mathrm{rzf}} = (1-\tau^2)\frac{\beta(1+e)^2 - e^2}{1 - \tau^2 + (1+e)^2\left[\tau^2 + \frac{1}{\rho}\right]}. \tag{E.3}$$

The derivative of (E.3) with respect to α reads

$$\frac{\partial\bar{\gamma}_{\mathrm{rzf}}}{\partial\alpha} = \frac{\partial\bar{\gamma}_{\mathrm{rzf}}}{\partial e}\frac{\partial e}{\partial\alpha} = -2\frac{\left[\tau^2 + \frac{1}{\rho}\right]e^2 + \left[1 + \frac{1}{\rho} - \beta(1-\tau^2)\right]e - \beta(1-\tau^2)}{\left[1 - \tau^2 + (1+e)^2\left(\tau^2 + \frac{1}{\rho}\right)\right]^2}\frac{\partial e}{\partial\alpha}. \tag{E.4}$$

Since e is a Stieltjes transform in $z = -\alpha$, its derivative $\frac{\partial e}{\partial\alpha}$ is always nonzero for all $\alpha > 0$. Therefore, maximizing (E.3) is equivalent to solving

$$e^2 + \frac{1 + \frac{1}{\rho} - \beta(1-\tau^2)}{\tau^2 + \frac{1}{\rho}}e - \frac{\beta(1-\tau^2)}{\tau^2 + \frac{1}{\rho}} = 0. \tag{E.5}$$

As the coefficients of the quadratic polynomial in e are independent of α, we solve (E.5) for e and subsequently find the maximizing α. The only positive solution $e^\star$ to (E.5) is given by

$$e^\star = -\frac{1}{2}\frac{1 + \frac{1}{\rho} - \beta(1-\tau^2)}{\tau^2 + \frac{1}{\rho}} + \sqrt{\frac{1}{4}\left[\frac{1 + \frac{1}{\rho} - \beta(1-\tau^2)}{\tau^2 + \frac{1}{\rho}}\right]^2 + \frac{\beta(1-\tau^2)}{\tau^2 + \frac{1}{\rho}}}. \tag{E.6}$$

Setting $e^\star$ in (E.6) equal to e in (E.1) and after tedious algebraic calculus, we obtain

$$\frac{\alpha^2\beta}{(\tau^2\rho + 1)^2}\left[\alpha\beta\rho(\tau^2 - 1) + \tau^2\rho + 1\right]^2 = 0. \tag{E.7}$$

Since $\alpha > 0$, we only need to consider the term in brackets. This quadratic equation has exactly one distinct real root (4.4), which completes the proof.

[2] Of the random matrix $\mathbf{X}^{\mathsf{H}}\mathbf{X}$, where $\mathbf{X} \in \mathbb{C}^{K\times M}$ has i.i.d. entries of zero mean and variance $1/M$.

F Important Lemmas

Lemma F.1 (Matrix Inversion Lemma)**.** *[53, Lemma 2.2] Let* $\mathbf{U}$ *be an* $N \times N$ *invertible matrix and* $\mathbf{x} \in \mathbb{C}^N$*,* $c \in \mathbb{C}$ *for which* $\mathbf{U} + c\mathbf{x}\mathbf{x}^{\mathsf{H}}$ *is invertible. Then*

$$\mathbf{x}^{\mathsf{H}} \left(\mathbf{U} + c\mathbf{x}\mathbf{x}^{\mathsf{H}}\right)^{-1} = \frac{\mathbf{x}^{\mathsf{H}}\mathbf{U}^{-1}}{1 + c\mathbf{x}^{\mathsf{H}}\mathbf{U}^{-1}\mathbf{x}}.$$

Lemma F.2 (Resolvent Identity)**.** *Let* $\mathbf{U}$ *and* $\mathbf{V}$ *be two invertible complex matrices of size* $N \times N$*. Then*

$$\mathbf{U}^{-1} - \mathbf{V}^{-1} = -\mathbf{U}^{-1}(\mathbf{U} - \mathbf{V})\mathbf{V}^{-1}. \tag{F.1}$$

Lemma F.3. *[51, Lemma B.26] Let* $\mathbf{A} \in \mathbb{C}^{N \times N}$ *be a deterministic matrix and* $\mathbf{x} \in \mathbb{C}^N$ *have i.i.d. complex entries of zero mean, variance* $1/N$ *and bounded* l*th order moment* $E\left|x_i\right|^l \leq \nu_l$*. Then for any* $p \geq 1$

$$E\left|\mathbf{x}^{\mathsf{H}}\mathbf{A}\mathbf{x} - \frac{1}{N}\mathrm{tr}\mathbf{A}\right|^p \leq \frac{C_p}{N^{p/2}}\left(\frac{1}{N}\mathrm{tr}\mathbf{A}\mathbf{A}^{\mathsf{H}}\right)^{p/2}\left[\nu_4^{p/2} + \nu_{2p}\right], \tag{F.2}$$

where C_p *is a constant solely depending on* p*.*

Lemma F.4. *[19, Lemma 14.2] Let* $\mathbf{A}_1, \mathbf{A}_2, \ldots$*, with* $\mathbf{A}_N \in \mathbb{C}^{N \times N}$*, be a series of random matrices generated by the probability space* $(\Omega, \mathcal{F}, P)$ *such that, for* $\omega \in A \subset \Omega$*, with* $P(A) = 1$*,* $\|\mathbf{A}_N(\omega)\| < K(\omega) < \infty$*, uniformly on* N*. Let* $\mathbf{x}_1, \mathbf{x}_2, \ldots$*, with* $\mathbf{x}_N \in \mathbb{C}^N$*, be random vectors of i.i.d. entries with zero mean, variance* $1/N$ *and eighth order moment of order* $O(1/N^4)$*, independent of* $\mathbf{A}_N$*. Then*

$$\mathbf{x}_N^{\mathsf{H}}\mathbf{A}_N\mathbf{x}_N - \frac{1}{N}\mathrm{tr}\mathbf{A}_N \overset{N\to\infty}{\longrightarrow} 0,$$

almost surely.

Proof. The proof unfolds from a direct application of the Tonelli theorem, [50, Theorem 18.3]. Denoting $(X, \mathcal{X}, P_X)$ the probability space that generates the series $\mathbf{x}_1, \mathbf{x}_2, \ldots$, we have that for every $\omega \in A$ (i.e., for every realization $\mathbf{A}_1(\omega), \mathbf{A}_2(\omega), \ldots$), the trace lemma, [19, Theorem 3.4], holds true. From [50, Theorem 18.3], the space B of couples $(x, \omega) \in Y \triangleq X \times \Omega$ for which the trace lemma holds, satisfies

$$\int_Y 1_B(x,\omega) dP_Y(x,\omega) = \int_\Omega \int_X 1_B(x,\omega) dP_X(x) dP_\Omega(\omega).$$

If $\omega \in A$, then $1_B(x, \omega) = 1$ on a subset of X of probability one. Therefore, the inner integral equals one whenever $\omega \in A$. As for the outer integral, since $P(A) = 1$, it also equals one, and the result is proved. □

Lemma F.5. *Let* $\mathbf{A}_N$ *be as in Lemma F.4 and* $\mathbf{x}_N, \mathbf{y}_N \in \mathbb{C}^N$ *be random, mutually independent with standard i.i.d. entries of zero mean, variance* $1/N$ *and eighth order moment of order* $O(1/N^4)$*, independent of* $\mathbf{A}_N$*.*

$$\mathbf{y}_N^{\mathsf{H}}\mathbf{A}_N\mathbf{x}_N \overset{N\to\infty}{\longrightarrow} 0,$$

almost surely.

Proof. Remark that $E\,|\mathbf{y}_N^{\mathsf{H}}\mathbf{A}_N\mathbf{x}_N|^4 < c/N^2$ for some constant $c > 0$ independent of N. The result then unfolds from the Markov inequality the Borel-Cantelli Lemma [50] and the Tonelli Theorem [50, Theorem 18.3]. □

Lemma F.6. *[19, Lemma 14.3] Let $\mathbf{A}_1, \mathbf{A}_2, \ldots$, with $\mathbf{A}_N \in \mathbb{C}^{N\times N}$, be deterministic with uniformly bounded spectral norm and $\mathbf{B}_1, \mathbf{B}_2, \ldots$, with $\mathbf{B}_N \in \mathbb{C}^{N\times N}$, be random Hermitian, with eigenvalues $\lambda_1^{\mathbf{B}_N} \leq \ldots \leq \lambda_N^{\mathbf{B}_N}$ such that, with probability one, there exist $\varepsilon > 0$ for which $\lambda_1^{\mathbf{B}_N} > \varepsilon$ for all large N. Then for $\mathbf{v}\in\mathbb{C}^N$*

$$\frac{1}{N}\mathrm{tr}\mathbf{A}_N\mathbf{B}_N^{-1} - \frac{1}{N}\mathrm{tr}\mathbf{A}_N(\mathbf{B}_N + \mathbf{v}\mathbf{v}^{\mathsf{H}})^{-1} \overset{N\to\infty}{\longrightarrow} 0$$

almost surely, where $\mathbf{B}_N^{-1}$ and $(\mathbf{B}_N + \mathbf{v}\mathbf{v}^{\mathsf{H}})^{-1}$ exist with probability one.

Proof. The proof unfolds similarly as above, with some particular care to be taken. For $\omega \in B$, the smallest eigenvalue of $\mathbf{B}_N(\omega)$ is uniformly greater than $\varepsilon(\omega)$. Therefore, with $\mathbf{B}_N(\omega)$ and $\mathbf{B}_N(\omega) + \mathbf{v}\mathbf{v}^{\mathsf{H}}$ invertible and, taking $z = -\varepsilon(\omega)/2$, we can write

$$\frac{1}{N}\mathrm{tr}\mathbf{A}_N\mathbf{B}_N^{-1}(\omega) = \frac{1}{N}\mathrm{tr}\mathbf{A}_N\left(\left[\mathbf{B}_N(\omega) - \frac{\varepsilon(\omega)}{2}\mathbf{I}_N\right] + \frac{\varepsilon(\omega)}{2}\mathbf{I}_N\right)^{-1}$$

and

$$\begin{aligned}&\frac{1}{N}\mathrm{tr}\mathbf{A}_N\left(\mathbf{B}_N(\omega) + \mathbf{v}\mathbf{v}^{\mathsf{H}}\right)^{-1}\\ &= \frac{1}{N}\mathrm{tr}\mathbf{A}_N\left(\left[\mathbf{B}_N(\omega) + \mathbf{v}\mathbf{v}^{\mathsf{H}} - \frac{\varepsilon(\omega)}{2}\mathbf{I}_N\right] + \frac{\varepsilon(\omega)}{2}\mathbf{I}_N\right)^{-1}.\end{aligned}$$

Under these notations, $\mathbf{B}_N(\omega) - \varepsilon(\omega)/2\mathbf{I}_N$ and $\mathbf{B}_N(\omega) + \mathbf{v}\mathbf{v}^{\mathsf{H}} - \varepsilon(\omega)/2\mathbf{I}_N$ are still nonnegative definite for all N. Therefore, the rank-1 perturbation lemma, [84, Lemma 2.1], can be applied for this ω. But then, from the Tonelli theorem again, in the space that generates the couples $((\mathbf{x}_1, \mathbf{x}_2, \ldots), (\mathbf{B}_1, \mathbf{B}_2, \ldots))$, the subspace where the rank-1 perturbation lemma applies has probability one, which is what needed to be proved. □

Lemma F.7. *Let $\mathbf{U}, \mathbf{V}, \mathbf{\Theta} \in \mathbb{C}^{N\times N}$ be of uniformly bounded spectral norm with respect to N and let $\mathbf{V}$ be invertible. Further, define $\mathbf{x} \triangleq \mathbf{\Theta}^{1/2}\mathbf{z}$ and $\mathbf{y} \triangleq \mathbf{\Theta}^{1/2}\mathbf{q}$ where $\mathbf{z}, \mathbf{q} \in \mathbb{C}^N$ have i.i.d. complex entries of zero mean, variance $1/N$ and finite 8th order moment and be mutually independent as well as independent of $\mathbf{U}, \mathbf{V}$. Define $c_0, c_1, c_2 \in \mathbb{R}^+$ such that $c_0c_1 - c_2^2 \geq 0$ and let $u \triangleq \frac{1}{N}\mathrm{tr}\mathbf{\Theta}\mathbf{V}^{-1}$ and $u' \triangleq \frac{1}{N}\mathrm{tr}\mathbf{\Theta}\mathbf{U}\mathbf{V}^{-1}$. Then we have*

$$\begin{aligned}&\mathbf{x}^{\mathsf{H}}\mathbf{U}\left(\mathbf{V} + c_0\mathbf{x}\mathbf{x}^{\mathsf{H}} + c_1\mathbf{y}\mathbf{y}^{\mathsf{H}} + c_2\mathbf{x}\mathbf{y}^{\mathsf{H}} + c_2\mathbf{y}\mathbf{x}^{\mathsf{H}}\right)^{-1}\mathbf{x}\\ &- \frac{u'(1 + c_1u)}{(c_0c_1 - c_2^2)u^2 + (c_0 + c_1)u + 1} \overset{N\to\infty}{\longrightarrow} 0,\end{aligned}$$

almost surely. Furthermore

$$\mathbf{x}^{\mathsf{H}}\mathbf{U}\left(\mathbf{V}+c_0\mathbf{x}\mathbf{x}^{\mathsf{H}}+c_1\mathbf{y}\mathbf{y}^{\mathsf{H}}+c_2\mathbf{x}\mathbf{y}^{\mathsf{H}}+c_2\mathbf{y}\mathbf{x}^{\mathsf{H}}\right)^{-1}\mathbf{y} - \frac{-c_2uu'}{(c_0c_1-c_2^2)u^2+(c_0+c_1)u+1} \overset{N\to\infty}{\longrightarrow} 0,$$

almost surely.

Proof. Denote $\mathbf{V} = \left(\mathbf{A}+c_0\mathbf{x}\mathbf{x}^{\mathsf{H}}+c_1\mathbf{y}\mathbf{y}^{\mathsf{H}}+c_2\mathbf{x}\mathbf{y}^{\mathsf{H}}+c_2\mathbf{y}\mathbf{x}^{\mathsf{H}}\right)^{-1}$. Now $\mathbf{x}^{\mathsf{H}}\mathbf{U}\mathbf{V}\mathbf{x}$ can be resolved using Lemma F.2

$$\begin{aligned}\mathbf{x}^{\mathsf{H}}\mathbf{U}\mathbf{V}\mathbf{x}-\mathbf{x}^{\mathsf{H}}\mathbf{U}\mathbf{A}^{-1}\mathbf{x} &= \mathbf{x}^{\mathsf{H}}\mathbf{U}\mathbf{V}\left(\mathbf{V}^{-1}-\mathbf{A}\right)\mathbf{A}^{-1}\mathbf{x}\\ &= -\mathbf{x}^{\mathsf{H}}\mathbf{U}\mathbf{V}(c_0\mathbf{x}\mathbf{x}^{\mathsf{H}}+c_1\mathbf{y}\mathbf{y}^{\mathsf{H}}+c_2\mathbf{x}\mathbf{y}^{\mathsf{H}}+c_2\mathbf{y}\mathbf{x}^{\mathsf{H}})\mathbf{A}^{-1}\mathbf{x}. \qquad \text{(F.3)}\end{aligned}$$

Equation (F.3) can be rewritten as

$$\mathbf{x}^{\mathsf{H}}\mathbf{U}\mathbf{V}\mathbf{x} = \frac{\mathbf{x}^{\mathsf{H}}\mathbf{U}\mathbf{A}^{-1}\mathbf{x}-\mathbf{x}^{\mathsf{H}}\mathbf{U}\mathbf{V}\mathbf{y}(c_1\mathbf{y}^{\mathsf{H}}\mathbf{A}^{-1}\mathbf{x}+c_2\mathbf{x}^{\mathsf{H}}\mathbf{A}^{-1}\mathbf{x})}{1+c_0\mathbf{x}^{\mathsf{H}}\mathbf{A}^{-1}\mathbf{x}+c_2\mathbf{y}^{\mathsf{H}}\mathbf{A}^{-1}\mathbf{x}}.$$

Similarly to (F.3), we apply Lemma F.2 to $\mathbf{x}^{\mathsf{H}}\mathbf{U}\mathbf{V}\mathbf{y}$. Thus, we obtain an expression involving the terms $\mathbf{x}^{\mathsf{H}}\mathbf{U}\mathbf{A}^{-1}\mathbf{x}$, $\mathbf{y}^{\mathsf{H}}\mathbf{A}^{-1}\mathbf{y}$, $\mathbf{x}^{\mathsf{H}}\mathbf{U}\mathbf{A}^{-1}\mathbf{y}$ and $\mathbf{y}^{\mathsf{H}}\mathbf{A}^{-1}\mathbf{x}$. To complete the proof, we apply Lemma F.4 and Lemma F.5, with $u = \frac{1}{N}\mathrm{tr}\boldsymbol{\Theta}\mathbf{A}^{-1}$ and $u' = \frac{1}{N}\mathrm{tr}\boldsymbol{\Theta}\mathbf{U}\mathbf{A}^{-1}$ and we have

$$\mathbf{x}^{\mathsf{H}}\mathbf{U}\mathbf{V}\mathbf{x} - \frac{u'(1+c_1u)}{(c_0c_1-c_2^2)u^2+(c_0+c_1)u+1} \overset{N\to\infty}{\longrightarrow} 0, \qquad \text{(F.4)}$$

almost surely. Similarly we have

$$\mathbf{x}^{\mathsf{H}}\mathbf{U}\mathbf{V}\mathbf{y} - \frac{-c_2uu'}{(c_0c_1-c_2^2)u^2+(c_0+c_1)u+1} \overset{N\to\infty}{\longrightarrow} 0, \qquad \text{(F.5)}$$

almost surely. Note that as $c_0, c_1, c_2 \in \mathbb{R}^+$ and $c_0c_1 \geq c_2^2$, equations (F.4) and (F.5) hold since $(c_0c_1-c_2^2)u^2+(c_0+c_1)u+1$ is bounded away from zero, which completes the proof. □

Lemma F.8. *[84, Lemma 2.1] Let $\zeta > 0$, $\mathbf{B}, \mathbf{A} \in \mathbb{C}^{N\times N}$ with $\mathbf{B}$ Hermitian nonnegative definite, $\tau \in \mathbb{R}$ and $\mathbf{q} \in \mathbb{C}^N$. Then*

$$\left|\mathrm{tr}\mathbf{A}\left[(\mathbf{B}+\zeta\mathbf{I}_N)^{-1}-(\mathbf{B}+\tau\mathbf{q}\mathbf{q}^{\mathsf{H}}+\zeta\mathbf{I}_N)^{-1}\right]\right| \leq \frac{\|\mathbf{A}\|}{\zeta}.$$

Lemma F.9. *[19, Corollary 3.2] Let $z \in \mathbb{C}^+$, $t > 0$, $\mathbf{q} \in \mathbb{C}^N$ and $\mathbf{B} \in \mathbb{C}^{N\times N}$ Hermitian nonnegative definite. Then*

$$\left|\frac{1}{1+t\mathbf{q}^{\mathsf{H}}\left(\mathbf{B}+z\mathbf{I}_N\right)^{-1}\mathbf{q}}\right| \leq \frac{|z|}{\Im z}.$$

Lemma F.10. *Let* $\mathbf{q} \in \mathbb{C}^N$ *and* $\mathbf{A} \in \mathbb{C}^{N \times N}$ *Hermitian nonnegative definite, then*

$$\mathbf{q}^{\mathsf{H}} \mathbf{A} \mathbf{q} \leq \|\mathbf{A}\| \|\mathbf{q}\|_2^2. \tag{F.6}$$

Proof. Let $\mathbf{A} = \mathbf{U} \mathbf{\Lambda} \mathbf{U}^{\mathsf{H}}$ be the spectral decomposition of $\mathbf{A}$ and $\mathbf{y} \triangleq \mathbf{U}^{\mathsf{H}} \mathbf{q}$, then

$$\mathbf{q}^{\mathsf{H}} \mathbf{A} \mathbf{q} = \mathbf{y}^{\mathsf{H}} \mathbf{\Lambda} \mathbf{y} = \sum_{i=1}^{N} \lambda_i |y_i|^2 \leq \lambda_{\max} \sum_{i=1}^{N} |y_i|^2 = \|\mathbf{A}\| \|\mathbf{y}\|_2^2. \tag{F.7}$$

Since multiplication by a unitary matrix does not change the norm we obtain (F.6). □

Lemma F.11. *Let* $\mathbf{A} \in \mathbb{C}^{N \times N}$ *be Hermitian nonnegative-definite, then*

$$\frac{1}{N} \mathrm{tr} \mathbf{A} \leq \|\mathbf{A}\|. \tag{F.8}$$

Proof. The result is immediate by bounding the eigenvalues of $\mathbf{A}$ as $\lambda_i \leq \lambda_{\max}$. □

Lemma F.12. *Let* $\mathbf{A}, \mathbf{B} \in \mathbb{C}^{N \times N}$ *Hermitian nonnegative-definite, then*

$$\|\mathbf{A}\mathbf{B}\| \leq \|\mathbf{A}\| \|\mathbf{B}\|. \tag{F.9}$$

Proof. The result immediately follows from the spectral decomposition of $\mathbf{A}$ or $\mathbf{B}$ as $\mathbf{U} \mathbf{\Lambda} \mathbf{U}^{\mathsf{H}}$ and by subsequently upper bounding all eigenvalues $\lambda_i \leq \lambda_{\max}$. □

Lemma F.13. *Let* $v > 0$, $\mathbf{A}, \mathbf{B} \in \mathbb{C}^{N \times N}$ *Hermitian and* $\mathbf{B}$ *nonnegative-definite. Denote* $\mathbf{D} = \mathbf{A} - \mathbf{i}\mathbf{B} - \mathbf{i}v\mathbf{I}_N$, *then*

$$\|\mathbf{D}^{-1}\| \leq \frac{1}{v}. \tag{F.10}$$

Proof. We have $\mathbf{D}\mathbf{D}^{\mathsf{H}} = (\mathbf{A} - \mathbf{i}\mathbf{B})(\mathbf{A} + \mathbf{i}\mathbf{B}) + 2v\mathbf{B} + v^2\mathbf{I}_N$. Therefore, the eigenvalues of $\mathbf{D}\mathbf{D}^{\mathsf{H}}$ are greater than or equal to v^2. Thus the singular values (equivalently the eigenvalues, since $\mathbf{D}$ is Hermitian) of $\mathbf{D}^{-1}$ are greater than or equal to $1/v$. □

List of Publications

Conference Publications

- S. Wagner and D. T. M. Slock "Weighted Sum Rate Maximization of Correlated MISO Broadcast Channels under Linear Precoding: A Large System Analysis", *Proc. IEEE 12th International Workshop on Signal Processing Advances in Wireless Communications (SPAWC'11)*, San Francisco, USA, 26-29 Jun. 2011.

- S. Wagner, R. Couillet, M. Debbah, D. T. M. Slock, "Deterministic Equivalent for the SINR of Regularized Zero-forcing Precoding in Correlated MISO Broadcast Channels with Imperfect CSIT", *Proc. IEEE International Conference on Communications (ICC'11)*, Kyoto, Japan, 5-9 Jun. 2011.

- S. Wagner, R. Couillet, M. Debbah, D. T. M. Slock, "Optimal Training in Large TDD Multi-user Downlink Systems under Zero-forcing and Regularized Zero-forcing Precoding", *Proc. IEEE Global Communications Conference (GC'10)*, Miami, USA, 6-10 Dec. 2010.

- S. Wagner, R. Couillet, D. T. M. Slock, M. Debbah "Large System Analysis of Zero-Forcing Precoding in MISO Broadcast Channels with Limited Feedback", *Proc. IEEE 11th International Workshop on Signal Processing Advances in Wireless Communications (SPAWC'10)*, Marrakech, Morocco, 20-23 Jun. 2010.

- S. Wagner, S. Sesia, D. T. M. Slock, "On Unitary Beamforming for MIMO Broadcast Channels", *Proc. IEEE International Conference on Communications (ICC'10)*, Cape Town, South Africa, 23-27 May. 2010.

- S. Wagner, S. Sesia, D. T. M. Slock, "Unitary Beamforming under Constant Modulus Constraint in MIMO Broadcast Channels", *Proc. IEEE 10th Workshop on Signal Processing Advances in Wireless Communications (SPAWC'09)*, Perugia, Italy, 21-24 Jun. 2009.

- R. Couillet, S. Wagner, M. Debbah, "Asymptotic Analysis of Correlated Multi-Antenna Broadcast Channels", *Proc. of the IEEE Wireless Communications & Networking Conference (WCNC'09)*, Budapest, Hungary, 5-8 Apr. 2009.

- R. Couillet, S. Wagner, M. Debbah, A. Silva, "The Space Frontier: Physical Limits of Multiple Antenna Information Transfer", *Proc. of the 3rd ACM International Conference on Performance Evaluation Methodologies and Tools (VALUETOOLS'08)*, Athens, Greece, 20-24 Oct. 2008, no. 84. **BEST STUDENT PAPER AWARD**

Journal Publications

- S. Wagner, R. Couillet, M. Debbah, D. T. M. Slock "Large System Analysis of Linear Precoding in Correlated MISO Broadcast Channels under Limited Feedback", *to appear in IEEE Trans. Inf. Theory*, arXiv Preprint 0906.3682.

Patents owned by ST-Ericsson

- R. Couillet, S. Wagner, **Application no. WO2010EP04427 20100720** "Precoding process for a transmitter of a MU-MIMO communication system"

- S. Sesia, D. Slock. S. Wagner, **Application no. WO2010EP00246 20100118** "Process for beamforming data to be transmitted by a base station in a MU-MIMO system and apparatus for performing the same"

Bibliography

[1] G. J. Foschini and M. J. Gans, "On Limits of Wireless Communications in a Fading Environment when Using Multiple Antennas," *Wireless Personal Communications*, vol. 6, no. 3, pp. 311–335, Mar. 1998.

[2] E. Telatar, "Capacity of Multi-antenna Gaussian Channels," *European Transactions on Telecommunications*, vol. 10, no. 6, pp. 585–595, Feb. 1999.

[3] D. Gesbert, M. Kountouris, R. W. Heath, Jr., C. B. Chae, and T. Sälzer, "From Single User to Multiuser Communications: Shifting the MIMO Paradigm," *IEEE Signal Process. Mag.*, vol. 24, no. 5, pp. 36–46, May 2007.

[4] M. H. Costa, "Writing on dirty paper," *IEEE Trans. Inf. Theory*, vol. IT-29, no. 3, pp. 439–441, May 1983.

[5] G. Caire and S. Shamai, "On the Achievable Throughput of a Multiantenna Gaussian Broadcast Channel," *IEEE Trans. Inf. Theory*, vol. 49, no. 7, pp. 1691–1706, Jul. 2003.

[6] P. Viswanath and D. N. C. Tse, "Sum Capacity of the Vector Gaussian Broadcast Channel and Uplink-Downlink Duality," *IEEE Trans. Inf. Theory*, vol. 49, no. 8, pp. 1912–1921, Aug. 2003.

[7] W. Yu and J. M. Cioffi, "Sum Capacity of Gaussian Vector Broadcast Channels," *IEEE Trans. Inf. Theory*, vol. 50, no. 9, pp. 1875–1892, Sep. 2004.

[8] S. Vishwanath, N. Jindal, and A. Goldsmith, "Duality, Achievable Rates, and Sum-Rate Capacity of Gaussian MIMO Broadcast Channels," *IEEE Trans. Inf. Theory*, vol. 49, no. 10, pp. 2658–2668, Oct. 2003.

[9] H. Weingarten, Y. Steinberg, and S. Shamai, "The Capacity Region of the Gaussian Multiple-Input Multiple-Output Broadcast Channel," *IEEE Trans. Inf. Theory*, vol. 52, no. 9, pp. 3936–3964, Sep. 2006.

[10] C. B. Peel, B. M. Hochwald, and A. L. Swindlehurst, "A Vector-Perturbation Technique for Near-Capacity Multiantenna Multiuser Communication–Part I: Channel Inversion and Regularization," *IEEE Trans. Commun.*, vol. 53, no. 1, pp. 195–202, Jan. 2005.

[11] T. Yoo and A. Goldsmith, "On the Optimality of Multiantenna Broadcast Scheduling Using Zero-Forcing Beamforming," *IEEE J. Sel. Areas Commun.*, vol. 24, no. 3, pp. 528–541, Mar. 2006.

[12] A. Wiesel, Y. C. Eldar, and S. Shamai, "Zero-Forcing Precoding and Generalized Inverses," *IEEE Trans. Signal Process.*, vol. 56, no. 9, pp. 4409–4418, Sep. 2008.

[13] S. Christensen, R. Agarwal, and J. M. Cioffi, "Weighted Sum-Rate Maximization using Weighted MMSE for MIMO-BC Beamforming Design," *IEEE Trans. Wireless Commun.*, vol. 7, no. 12, pp. 4792–4799, Dec. 2008.

[14] S. Shi, M. Schubert, and H. Boche, "Rate Optimization for Multiuser MIMO Systems With Linear Processing," *IEEE Trans. Signal Process.*, vol. 56, no. 8, pp. 4020–4030, Aug. 2008.

[15] C. Guthy, W. Utschick, R. Hunger, and M. Joham, "Efficient weighted sum rate maximization with linear precoding," *IEEE Trans. Signal Process.*, vol. 58, no. 4, pp. 2284–2297, 2010.

[16] Q. Spencer, A. Swindlehurst, and M. Haardt, "Zero-forcing methods for downlink spatial multiplexing in multiuser mimo channels," *IEEE Trans. Signal Process.*, vol. 52, no. 2, pp. 461–471, Feb. 2004.

[17] M. Joham, K. Kusume, M. H. Gzara, W. Utschick, and J. A. Nossek, "Transmit Wiener Filter for the Downlink of TDD DS-CDMA Systems," in *Proc. IEEE International Symposium on Spread Spectrum Techniques and Applications (ISSSTA'02)*, vol. 1, Prague, Czech Republic, Sep. 2002, pp. 9–13.

[18] D. J. Love, R. W. Heath, Jr., V. K. N. Lau, D. Gesbert, B. D. Rao, and M. Andrews, "An Overview of Limited Feedback in Wireless Communication Systems," *IEEE J. Sel. Areas Commun.*, vol. 26, no. 8, pp. 1341–1365, Oct. 2008.

[19] R. Couillet and M. Debbah, *Random Matrix Methods for Wireless Communications*, 1st ed. Cambridge, UK: Cambridge University Press, 2011.

[20] A. M. Tulino and S. Verdú, *Random Matrix Theory and Wireless Communications*. Delft, Netherlands: Now Publishers Inc., 2004.

[21] Technical Specification Group Radio Access Network; Evolved Universal Terrestrial Radio Access (E-UTRA), "Further advancements for E-UTRA physical layer aspects (Release 9)," 3GPP TR 36.814 V9.0.0, Tech. Rep., Mar. 2010.

[22] B. Hochwald and S. Vishwanath, "Space-Time Multiple Access: Linear Growth in the Sum Rate," in *Proc. IEEE Annual Allerton Conference on Communication, Control, and Computing*, Monticello, Illinois, Oct. 2002, pp. 387–396.

[23] D. Hwang, B. Clercks, and G. Kim, "Regularized Channel Inversion with Quantized Feedback in Down-link Multiuser Channels," *IEEE Trans. Wireless Commun.*, vol. 8, no. 12, pp. 5785–5789, Dec. 2009.

[24] R. Couillet, S. Wagner, M. Debbah, and A. Silva, "The Space Frontier: Physical Limits of Multiple Antenna Information Transfer," in *Proceedings of the 3rd ACM International Conference on Performance Evaluation Methodologies and Tools (VALUETOOLS'08)*, no. 84, Athens, Greece, Oct. 2008.

[25] V. K. Nguyen and J. S. Evans, "Multiuser Transmit Beamforming via Regularized Channel Inversion: A Large System Analysis," in *Proc. IEEE Global Communications Conference (GC'08)*, New Orleans, LO, Dec. 2008, pp. 1–4.

[26] R. Muharar and J. Evans, "Downlink beamforming with transmit-side channel correlation: A large system analysis," in *Proc. IEEE International Conference on Communications (ICC'11)*, Kyoto, Japan, Jun. 2011.

[27] ——, "Downlink Beamforming with Transmit-side Channel Correlation: A Large System Analysis," *unpublished*, 2009. [Online]. Available: http://www.cubinlab.ee.unimelb.edu.au/~rmuharar/doc/techRepCorr.pdf

[28] J. Hoydis, S. ten Brink, and M. Debbah, "How many Antennas are needed for Massive MIMO," *unpublished*, 2011.

[29] A. Wiesel, Y. C. Eldar, and S. Shamai, "Linear Precoding via Conic Optimization for Fixed MIMO Receivers," *IEEE Trans. Signal Process.*, vol. 54, no. 1, pp. 161–176, Jan. 2006.

[30] R. Zakhour and S. V. Hanly, "Base station cooperation on the downlink: Large system analysis," *IEEE Trans. Inf. Theory*, Jun. 2010. [Online]. Available: http://arxiv.org/abs/1006.3360

[31] W. Hachem, P. Loubaton, and J. Najim, "Deterministic Equivalents for Certain Functionals of Large Random Matrices," *Annals of Applied Probability*, vol. 17, no. 3, pp. 875–930, Jun. 2007.

[32] G. Caire, N. Jindal, M. Kobayashi, and N. Ravindran, "Multiuser MIMO Achievable Rates With Downlink Training and Channel State Feedback," *IEEE Trans. Inf. Theory*, vol. 56, no. 6, pp. 2845–2866, Jun. 2010.

[33] U. Salim and D. Slock, "How much Feedback is Required for TDD Multi-Antenna Broadcast Channels with User Selection?" *EURASIP Journal on Advances in Signal Processing*, 2010.

[34] J. Jose, A. Ashikhmin, P. Whiting, and S. Vishwanath, "Linear Precoding for Multi-User Mulitple Antenna TDD Systems," *IEEE Trans. Inf. Theory*, submitted for publication. [Online]. Available: http://arxiv.org/abs/0812.0621

[35] N. Jindal, "MIMO Broadcast Channels With Finite-Rate Feedback," *IEEE Trans. Inf. Theory*, vol. 52, no. 11, pp. 5045–5060, Nov. 2006.

[36] P. Ding, D. J. Love, and M. D. Zoltowski, "Multiple Antenna Broadcast Channels With Shape Feedback and Limited Feedback," *IEEE Trans. Signal Process.*, vol. 55, no. 7, pp. 3417–3428, Jul. 2007.

[37] T. M. Cover and J. A. Thomas, *Elements of Information Theory*, 2nd ed. Hoboken, NJ: Wiley & Sons, 2006.

[38] B. Nosrat-Makouei, J. G. Andrews, and R. W. Heath, Jr., "MIMO Interference Alignment Over Correlated Channels With Imperfect CSIT," *IEEE Trans. Signal Process.*, vol. 59, no. 6, pp. 2783–2794, Jun. 2011.

[39] M. Ding and S. D. Blostein, "MIMO Minimum Total MSE Transceiver Design With Imperfect CSI at Both Ends," *IEEE Trans. Signal Process.*, vol. 57, no. 3, pp. 1141–1150, Mar. 2009.

[40] C. Wang and R. D. Murch, "Adaptive Downlink Multi-User MIMO Wireless Systems for Correlated Channels with Imperfect CSI," *IEEE Trans. Wireless Commun.*, vol. 5, no. 9, pp. 2453–2446, Sep. 2006.

[41] T. Yoo and A. Goldsmith, "MIMO Capacity with Channel Uncertainty: Does Feedback Help?" in *Proc. IEEE Global Communications Conference (GC'04)*, Dallas, USA, Dec. 2004, pp. 96–100.

[42] W. Hachem, P. Loubaton, and J. Najim, "A CLT For Information-theoretic Statistics of Gram Random Matrices with a Given Variance Profile," *Annals of Applied Probability*, vol. 18, no. 6, pp. 2071–2130, Dec. 2009.

[43] V. L. Girko, *Theory of Stochastic Canonical Equations*, 1st ed. Boston, MA: Dordrecht, 2001.

[44] J. Wishart, "The generalized product moment distribution in samples from a normal multivariate population," *Biometrika*, vol. 20, no. 1-2, pp. 32–52, dec 1928.

[45] R. A. Fisher, "The sampling distribution of some statistics obtained from non-linear equations." *Annals of Human Genetics*, vol. 9, no. 3, pp. 238–249, 1939.

[46] M. A. Girshick, "On the sampling theory of roots of determinantal equations," *The Annals of Mathematical Statistics*, vol. 10, no. 3, pp. 203–224, 1939.

[47] P. L. Hsu, "On the distribution of roots of certain determinantal equations," *Annals of Human Genetics*, vol. 9, no. 3, pp. 250–258, 1939.

[48] S. N. Roy, "p-statistics or some generalisations in analysis of variance appropriate to multivariate problems," *Sankhyā: The Indian Journal of Statistics*, vol. 4, no. 3, pp. 381–396, 1939.

[49] V. A. Marčenko and L. A. Pastur, "Distribution of eigenvalues for some sets of random matrices," *Mathematics of the USSR-Sbornik*, vol. 1, no. 4, pp. 457–483, apr 1967.

[50] P. Billingsley, *Probability and Measure*, 3rd ed. Hoboken, NJ: John Wiley & Sons, Inc., 1995.

[51] Z. Bai and J. W. Silverstein, *Spectral Analysis of Large Dimensional Random Matrices*, 2nd ed. Spring Street, NY: Springer, 2010.

[52] J. Hoydis, R. Couillet, and M. Debbah, "Iterated Deterministic Equivalents for the Capacity Analysis of Communication Systems," *IEEE Trans. Inf. Theory*, 2011, to be submitted.

[53] J. W. Silverstein and Z. D. Bai, "On the Empirical Distribution of Eigenvalues of a Class of Large Dimensional Random Matrices," *Journal of Multivariate Analysis*, vol. 54, no. 2, pp. 175–192, Aug. 1995.

[54] J. Hoydis, M. Kobayashi, and M. Debbah, "Asymptotic moments for interference mitigation in correlated fading channels," in *Proc. IEEE International Symposium on Information Theory (ISIT'11)*, Saint-Petersburg, Russia, Jul. 2011.

[55] R. D. Yates, "A Framework for Uplink Power Control in Cellular Radio Systems," *IEEE J. Sel. Areas Commun.*, vol. 13, no. 7, pp. 1341–1347, Sep. 1995.

[56] R. Couillet, J. Hoydis, and M. Debbah, "Random Beamforming over Quasi-Static and Fading Channels: A Deterministic Equivalent Approach," *IEEE Trans. Inf. Theory*, 2012, to appear.

[57] R. Couillet, M. Debbah, and J. W. Silverstein, "A Deterministic Equivalent for the Capacity Analysis of Correlated Multi-user MIMO Channels," *IEEE Trans. Inf. Theory*, submitted for publication. [Online]. Available: http://arxiv.org/abs/0906.3667v3

[58] F. Dupuy and P. Loubaton, "On the Capacity Achieving Covariance Matrix for Frequency Selective MIMO Channels Using the Asymptotic Approach," unpublished. [Online]. Available: http://arxiv.org/abs/1001.3102

[59] Technical Specification Group Radio Access Network; Evolved Universal Terrestrial Radio Access (E-UTRA), "User Equipment (UE) Radio Transmission and Reception," 3GPP TR 36.101 V10.3.0, Tech. Rep., Jun. 2011.

[60] Z. D. Bai and J. W. Silverstein, "No Eigenvalues Outside the Support of the Limiting Spectral Distribution of Large Dimensional Sample Covariance Matrices," *Annals of Probability*, vol. 26, no. 1, pp. 316–345, Jan. 1998.

[61] T. L. Marzetta, "How Much Training Is Required For Multiuser MIMO?" in *Proc. IEEE Conference Record of the Asilomar Conference on Signals, Systems, and Computers ACSSC'06*, Pacific Grove, CA, Oct. 2006, pp. 359–363.

[62] ——, "Noncooperative Cellular Wireless with Unlimited Numbers of Base Station Antennas," *IEEE Trans. Wireless Commun.*, vol. 9, no. 11, pp. 3590–3600, Nov. 2010.

[63] W. C. Jakes and D. C. Cox, *Microwave Mobile Communications*. Hoboken, NJ: Wiley-IEEE Press, 1994.

[64] A. D. Dabbagh and D. J. Love, "Multiple Antenna MMSE Based Downlink Precoding with Quantized Feedback or Channel Mismatch," *IEEE Trans. Commun.*, vol. 56, no. 11, pp. 1859–1868, Nov. 2008.

[65] D. P. Palomar and J. R. Fonollosa, "Practical Algorithms for a Family of Waterfilling Solutions," *IEEE Trans. Signal Process.*, vol. 53, no. 2, pp. 686–695, Feb. 2005.

[66] N. Jindal, A. Lozano, and T. L. Marzetta, "What is the value of joint processing of pilots and data in block-fading channels," in *Proc. IEEE International Symposium on Information Theory (ISIT'09)*, Seoul, South Korea, Jun. 2009, pp. 2189–2193.

[67] H. V. Poor, *An Introduction to Signal Detection and Estimation*, 2nd ed. Springer, 1994.

[68] S. Boyd and L. Vandenberghe, *Convex Optimization*, 6th ed. New York, USA: Cambridge University Press, 2008.

[69] M. Kobayashi, G. Caire, and N. Jindal, "How Much Training and Feedback are Needed in MIMO Broadcast Channels?" in *Proc. IEEE International Symposium on Information Theory (ISIT'08)*, Toronto, Canada, Jul. 2008, pp. 2663–2667.

[70] M. Kobayashi, N. Jindal, and G. Caire, "Optimized Training and Feedback for MIMO Downlink Channels," in *Proc. IEEE Information Theory Workshop on Networking and Information Theory (ITW'09)*, Volos, Greece, Jun. 2009, pp. 226–230.

[71] D. Marco and D. L. Neuhoff, "The validity of the additive noise model for uniform scalar quantizers," *IEEE Trans. Inf. Theory*, vol. 51, no. 5, pp. 1739–1755, May 2005.

[72] T. L. Marzetta and B. M. Hochwald, "Fast Transfer of Channel State Information in Wireless Systems," *IEEE Trans. Signal Process.*, vol. 54, no. 4, pp. 1268–1278, Apr. 2006.

[73] D. Samardzija and N. Mandayam, "Unquantized and Uncoded Channel State Information Feedback in Multiple-Antenna Multiuser Systems," *IEEE Trans. Commun.*, vol. 54, no. 7, pp. 1335–1345, Jul. 2006.

[74] R. Ghaffar and R. Knopp, "Interference Sensitivity for Multiuser MIMO in LTE," in *Proc. IEEE International Workshop on Signal Processing Advances for Wireless Communications (SPAWC'11)*, San Francisco, CA, Jun. 2011.

[75] S. Sesia, I. Toufik, and B. Matthew, Eds., *LTE, The UMTS Long Term Evolution: From Theory to Practice.* Wiley & Sons, February, 2009.

[76] I. H. Kim, S. Y. Park, D. J. Love, and S. J. Kim, "Improved Multiuser MIMO Unitary Precoding Using Partial Channel State Information and Insights from the Riemannian Manifold," *IEEE Trans. Wireless Commun.*, vol. 8, no. 8, pp. 4014–4023, 2009.

[77] A. Jalali and D. J. Love, "Closed-form expression for optimal two-user mimo unitary precoding," *IEEE Commun. Lett.*, vol. 13, no. 4, pp. 251–253, Apr. 2009.

[78] R. de Francisco and D. T. Slock, "An iterative Optimization Method for Unitary Beamforming in MIMO Broadcast Channels," in *Proceedings of the 45th Allerton Conf. on Commun., Control and Comput.*, Sep. 2007, pp. 360–367.

[79] T. Abrudan, J. Eriksson, and V. Koivunen, "Steepest descent algorithms for optimization under unitary matrix constraint," *IEEE Trans. Signal Process.*, vol. 56, no. 3, pp. 1134–1147, Mar. 2008.

[80] ——, "Conjugate gradient algorithm for optimization under unitary matrix constraint," *Signal Processing*, vol. 89, no. 9, pp. 1704–1714, 2009.

[81] W. Tadej and K. Życzkowski, "A Concise Guide to Complex Hadamard Matrices," *Open Systems & Information Dynamics*, vol. 13, no. 2, pp. 133–177, 2006.

[82] R. de Francisco, M. Kountouris, D. T. M. Slock, and D. Gesbert, "Orthogonal Linear Beamforming in MIMO Broadcast Channels," in *Proc. IEEE Wireless Communications & Networking Conference (WCNC'07)*, Hong Kong, China, Jun. 2007, pp. 1210–1215.

[83] P. Dita, "Some results on the parametrization of complex Hadamard matrices," *Journal of Physics A: Mathematical and General*, vol. 37, pp. 5355–5374, 2004.

[84] Z. D. Bai and J. W. Silverstein, "On the Signal-to-Interference Ratio of CDMA Systems in Wireless Communications," *Annals of Applied Probability*, vol. 17, no. 1, pp. 81–101, Feb. 2007.